Effects of High Energy Mechanical Milling on the Kinetics of Solid State Reactions

A thesis submitted in partial fulfilment
of the requirements for the degree of

Ph.D.

in Materials and Process Engineering

by

Danyang Ying

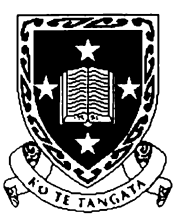

The
University
of Waikato
*Te Whare Wānanga
o Waikato*

Hamilton, New Zealand
2000

To my family

for their love and support

Abstract

The effects of high energy mechanical milling on the kinetics of solid state reactions in two binary metallic systems, Al-Ni and Cu-Al, and two metal-oxide systems, Al-TiO_2 and Cu(Al)-CuO, have been investigated by using X-ray diffractometry (XRD), differential thermal analysis (DTA), differential scanning calorimetry (DSC), optical microscopy, scanning electron microscopy (SEM) and transmission electron microscopy (TEM).

A quantitative analysis of the Ni/Al system was performed to gain an understanding of the reaction behaviour during heating of the high energy mechanically milled powders. Results showed that nucleation and lateral growth along the interface region occurred at different temperatures from the diffusion controlled transverse growth. The amount of new phase formed through nucleation and lateral growth along the interface region increased in proportion to the interface area.

A two-step model for describing new phase nucleation and growth along the interface and transverse growth perpendicular to the interface was developed from the principles of classic heterogeneous nucleation and growth theories and the one-dimensional diffusion equation. The model was verified against the experimental results of Ni/Al system. It was found that the interface area, activation energy and pre-exponential factor are the major parameters affecting the kinetics of the solid state reactions of the powders.

It was found that, in the Cu/Al system, Cu(Al) solid solution or γ-Cu_9Al_4 intermetallic compound could form after the powder mixture was milled for up to 8 hours. Upon heating the powder mixtures milled for shorter times, γ-Cu_9Al_4 formed first in the powder with a nominal composition of Cu-14at%Al, and then, γ-Cu_9Al_4 dissolved into Cu forming Cu(Al) solid solution. Whereas, θ-$CuAl_2$ formed first for the powder with a nominal composition of Cu-37at%Al, and then, θ-$CuAl_2$ reacted with Cu forming γ-Cu_9Al_4 intermetallic compound. The solid

solution or intermetallic compound formed by heating the powders milled for shorter times is the same as that produced by mechanical alloying.

In the Al/TiO_2 system, the effects of high energy milling on the phase formation and reaction kinetics was studied. It was found that the reaction between Al and TiO_2 also followed a two step reaction mechanism: interfacial reaction and bulk diffusional reaction. The first phase formed by the interfacial reaction was always Al_3Ti irrespective of the initial composition of the powder mixture. The reaction product for the subsequent reaction depends on the composition of the powder mixture. α-Ti phase could form at a higher temperature. The formation of α-Al_2O_3 phase is highly dependent on the reaction kinetics. It requires higher temperature or longer time to form detectable amount.

In the case of Cu(Al)-CuO system, two reactions occurred sequentially: Reaction 1, forming Cu_2O from the reaction between CuO and Cu-Al powders and Reaction 2, forming Cu from the reaction between Cu_2O and Cu-Al powders. High energy mechanical milling enhanced both reactions leading to a substantial decrease in the reaction temperatures.

Overall, high energy mechanical milling enhances the solid state reactions by establishing and refining composite microstructures of the powder particles. The reaction temperature could be substantially decreased. Prolonged mechanical alloying process can be replaced by a short time mechanical milling plus a well controlled heat treatment process.

Acknowledgements

I would like to thank my supervisor Dr. Deliang Zhang for taking me into this wonderful materials world and guiding me through every single step towards my thesis work. Thanks to my co-supervisor Associate Prof. Alan Langdon for helpful advice.

I owe my wife and my family for their support from every aspect. Without their support, I won't be able to finish my thesis.

Thanks to Janis and the smile of Lesley and the helpful hands whenever asked. Many thanks to the technical support from Jijian, Yuanji, Alf and David.

Many thanks to Martin Newby for critical reading my thesis and many constructive suggestions.

Thanks to fellow students, Georgees, Garry, Xiong, Zhihong, Conrad, Rob, Matt, Yanhai, Geoff and Michael for their help and valuable discussions. Special thanks to Garry for sending me his first chapter of his PhD thesis as a template to allow me to get the thesis assembly started.

Many thanks to Prof. Brian Cantor from University of Oxford, UK, Prof. Lu Li from National University of Singapore, Prof. F.H (Sam) Froes from University of Idaho, USA, Prof. Ian Brown from Industrial Research Limited, NZ, Prof. Evan Ma from Johns Hopkins University, USA, Prof. Wei Gao from University of Auckland, NZ, Prof. Laszlo Takacs from University of Maryland, USA, Prof. Bernard Kear from Rutgers University, USA, Prof. Alain Reza Yavari from LTPCM-ENSEEG, France, Prof. Livio Battezzati from Universita Di Torino, Italy, Prof. Michael Atzmon from The University of Michigan, USA, Prof. Niels Hansen from Riso National Laboratory, Denmark, for many helpful discussions and communications.

Special thanks to the partial financial support from the Foundation for Research, Science and Technology, New Zealand, and Titanox Development limited.

Table of Contents

List of Figures

List of Tables

Glossary

Abbreviations used in this text:

MM	Mechanical milling
MA	Mechanical alloying
CR	Charge ratio
XRD	X-ray diffractometry
SEM	Scanning electron microscope
TEM	Transmission electron microscope
EDAX	Energy dispersive X-ray analysis
DTA	Differential thermal analysis
DSC	Differential scanning calorimeter
PCAs	Process control agents
ODS	Oxide dispersion strengthened materials
SHS	Self-propagating high energy synthesis
CAS	Combustion-assisted synthesis
SSA	Solid state amorphisation
RSP	Rapid solidification process

SI units have been used throughout this thesis. However, °C has been retained where appropriate as a convenient unit. The most common units used in this thesis are listed below:

Length:	mm (10^{-3} m); μm (10^{-6} m); nm (10^{-9} m); Å (10^{-10} m)
Time:	h. (hour) and min. (minute)
Activation energy:	kJ/mol and eV
Density:	g/cm^3

Chapter One

Introduction and Literature Review

1.1 Introduction

For most solid state reactions the formation of reaction products spatially separate the reactants, causing reaction kinetics to be dependent on product size and morphology and limited by diffusion rates through the product phases. As a consequence high temperature is required to achieve a sufficiently high reaction rate.[1] Whereas, if one can design a process that can continuously break the product barriers and bring the reactants into constant intimate contact, the reaction could be substantially accelerated. A process known as high energy mechanical milling is one of such processes.

High energy mechanical milling is a powder metallurgy process in which reactant powders are milled under inert atmosphere and are subjected to repetitive severe plastic deformation, fracturing and cold welding due to the high energy impact of the milling media, such as balls, rods, or split discus. As a consequence, the reaction kinetics can be substantially enhanced. In many cases, reactions, which normally require high temperatures, occur at low temperatures during mechanical milling. Even in the cases where reactions do not occur during milling, the reduction of the size of the reaction couples caused by microstructural refinement accompanying the mechanical milling process also significantly reduces the reaction temperature.[2,3]

Because high energy mechanical milling is a versatile and promising solid state materials processing technique of technological significance, continually increasing interest has been paid to this process in the international research

communities in the last two to three decades.[4] Of particular interest is the effect of high energy mechanical milling on solid-state reaction kinetics.

The purpose of this thesis is to study the fundamental aspects of solid-state reactions in high energy mechanically milled powders and understand the underlying mechanisms that contribute to the enhanced reaction kinetics. This work has three aspects: (1) Study the microstructural evolution of powder particles during mechanical milling and the effects of the microstructure of powder particles on the reaction kinetics during subsequent heat treatment of the milled powders; (2) Simulate the solid state reactions of the high energy mechanically milled powders during subsequent heat treatment; (3) Demonstrate that a combination of high energy mechanical milling and heat treatment is an efficient technique of processing some advanced materials, such as *in-situ* metal or intermetallic matrix composite materials.

This thesis has eight chapters. The remaining part of the first chapter serves as a literature review on high energy mechanical milling, mechanical alloying, effect of milling on solid-state reactions and processing of *in-situ* metal matrix composites. Chapter two describes the experimental methods used in this work. Chapter three presents and discusses the results of a study of solid-state reactions in Al-Ni and Cu-Al systems. Chapter four presents a kinetic model which simulates the solid state reactions that occur during heating the high energy mechanically milled powders. Chapter five presents and discusses the results for a study of the reactions between TiO_2 and Al. Chapter six presents and discusses the results of a study of the reactions between CuO and Cu-Al alloy powders and of the processing of in-situ Cu matrix nanocomposite materials. Chapter seven is devoted to a general discussion. Finally, in Chapter eight a number of conclusions are drawn and recommendations are made for the future work. At the end of the thesis, in Appendix A, the publications produced as a result of this thesis work are listed.

1.2 High Energy Mechanical Milling

Milling process has long been used to prepare materials. However, it was only after Benjamin and his group[5] reported the successful production of oxide

dispersion strengthened Ni-base super alloys in 1966 that mechanical milling (MM) started a new era marked with a new name "mechanical alloying" (MA). It is worthwhile to clarify two confusing terms: "Mechanical Milling" (MM) and "Mechanical Alloying" (MA), for the start. In Mechanical Milling (MM), a single powder or a powder mixture experiences a series intermixing, deformation, fracturing and cold welding without reactions at atomic level. The process is more physical than chemical. In Mechanical Alloying (MA), the process is identical to MM but, in addition, atomic level reactions do occur forming new phases, i.e. in MA the process is not only physical but also chemical. In this section, the review will be focused on mechanical milling. Mechanical alloying and/or mechanochemical reactions will be reviewed in section 1.3.

1.2.1 High Energy Milling Devices

The most commonly used high energy mills include attritor mills (e.g. Szegvari attritor), tumbler mills, shaker mills (e.g. SPEX 8000 mixer/mill from USA), planetary mills (e.g. Fritsch and Retsch mills from Germany), and discus mills (Rocklab "Split Discus" mill from New Zealand). The energy transfer to the powder particles in these mills takes place by impacts between fast moving media such as balls, discus, or rods, or between moving media and container wall. The attritor was invented in 1922 by Szegvari for a quick dispersion of fine sulphur particles during the vulcanization of rubber.[6] The attritor has a vertical cylindrical tank in which the powder and balls are charged. The movement of the balls and powder is achieved by the horizontal impellers attached to a vertical shaft, which is made to rotate (Figure 1-1(a)). Placed consecutively at right angles to each other, the impellers drive the movement of the balls causing the impacts with powder. Due to the high capacity of these attritor mills (Table 1-1),[7] they are usually preferred in industry.

The tumbler mills, which are traditionally used in mineral processing, can also be used as high energy mill if the diameters of the container are sufficiently large (in the order of meters) and the mills are operated below the critical speed. This is the speed beyond which the balls are pinned to the inner wall of the container. For large scale production, tumbler mills are more economical than attritor and other high energy ball mills.[8]

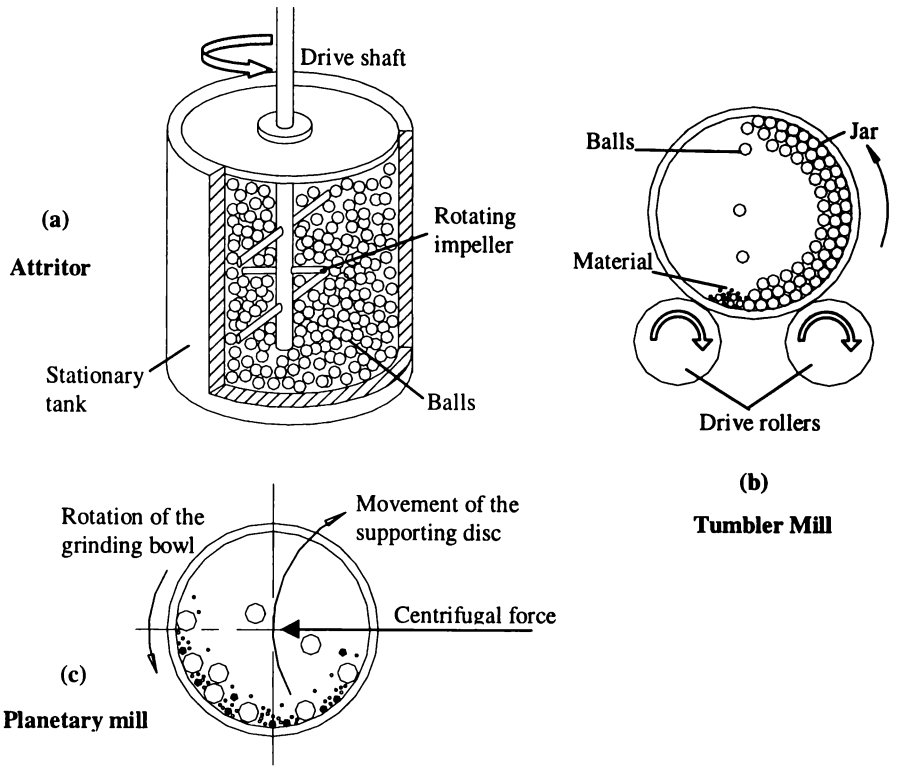

Figure 1-1. Schematic of ball movement in typical ball mills used for MM/MA.[4]

Table 1-1. Comparison of various high energy mills (based on Murty and Ranganathan.[4])

Type of mill	Capacity	Ball velocity, m/s
SPEX Mill	Up to 2~20g	<3.9
Planetary	Up to 4~250g	<11.24
Attritor	0.5~100kg	<0.8
Discus mill	500~1000g	Not known

Laboratory scale mills having smaller capacity achieve higher ball velocities.[9-11] The capacity and ball velocity of various high energy mills are compared in Table 1-1. Among the laboratory scale mills, the SPEX 8000 mills and Fritsch planetary mill are most widely used. In the SPEX mill, most widely used in USA, the vial containing a charge of balls and powder vibrate in three dimensions with amplitude of 50 mm and a frequency of approximately 25 Hz. In the Fritsch planetary mill, commonly used in European countries, the disc on which the vial is mounted rotates in the opposite direction to that of the vial rotation. This gives a centrifugal force to the balls (Figure 1-1(c)). Even though the ball velocity in the Fritsch planetary mill is higher than that in the SPEX mill, the frequency of

impacts is much greater in the SPEX mill.[9,10] This makes the SPEX mill a higher energy mill in comparison with the Fritsch planetary mill. Due to low mill energy, it takes longer to achieve alloying when an attritor mill is used. It has been shown in the Ti-Mg system[12] that alloying takes place after 16 hours in the SPEX mill, while the attritor took 100 hours to achieve the same result.

The discus mill has been used for rock crushing for a long time. Only recently it has been used for the purpose of mechanical alloying in the University of Waikato. The discus mill is constructed of a pair of hardened steel discus with a diameter varies from 100 to 200 mm which are vibrated in a hardened steel bowl causing shearing and impacting. The current model of discus mill has a capacity of handling 100 to 1000 grams of powder.

1.2.2 Mill Set-ups and Parameters Affecting Milling

The milling effect depends largely on the energy transferred to the powder from the moving media during milling. The energy transfer is governed by many parameters such as the type of mill, milling speed, the type, size and size distribution of the balls, ball/powder weight ratio, and temperature of milling. The kinetic energy of the balls is higher with higher speeds of milling and with heavier balls. A number of investigators have reported an increase in the glass forming composition range with an increase in milling speeds. Joardar *et al.*[13] have shown that NiAl formation and its disordering tendency during MM are enhanced with increasing milling density. It has also been reported[14] that the reaction rate for the formation of TiC during MM increases exponentially with the density of balls. The size and size distribution and the number of balls should be chosen so as to achieve optimum occupation of the space in the vial. If too much space is taken by the balls, the mean free path of the ball movement would be too small, while a too small number of balls in the vial means the collision frequency might be too low. Ball/powder weight ratios in the range 5:1-10:1 are widely used and is effective.

High energy mechanical milling is characterised by repeated welding and fracturing of the powder. The extent of welding and fracturing is decided by the deformation behaviour of the powder and the temperature of milling. Thus the nature of phase transitions during milling is, to a large extent, a function of the

temperature of milling. Lee *et al.*[15] have shown that the rate of amorphization increases with milling temperature. Klassen *et al.*[16] have reported alloying in the Ag-Cu system was achieved with a low milling temperature. During milling, a fraction of the kinetic energy of balls is dissipated as heat, which raises the temperature of the powder. This aspect will be discussed in detail in the section 1.3.2.

MM is usually carried out in a dry condition under an inert atmosphere to prevent oxidation of powders. Process control agents (PCAs) are used to prevent excessive welding of powder particles to the balls and the inner wall of the vial and to achieve proper balance between welding and fracture in the case of milling ductile materials such as Al and Sn. The PCAs are mostly organic materials such as stearic acid, methanol, and toluene. Radlinski *et al.*[17] have shown that milling in presence of PCAs can largely affect the microstructure development of the powder particles in the Al-Mg system. In certain cases milling is performed in a wet condition in order to avoid excessive welding and oxidation.[18] Excessive welding can also be prevented by carrying out the MM at sub-zero temperature where the fracturing of the particles is more pronounced.[19]

1.2.3 Microstructural Evolutions

The MM process is characterised by repeated deformation, fracturing and cold welding of powder particles trapped between the colliding balls during milling. The extent of these individual microprocesses depends mainly on the mechanical behaviour of the powder components. Hence, the powder components are usually classified as (a) ductile/ductile, (b) ductile/brittle, and (c) brittle/brittle systems.

1.2.3.1 Ductile/Ductile Systems

The mechanism of microstructural evolution when both components of a blend are ductile was first studied by Benjamin and Volin[20] and was explained in more detail by Benjamin in later reports.[5,21-25] According to these, the MM process can be conveniently divided into five stages based on optical microscopy observations.

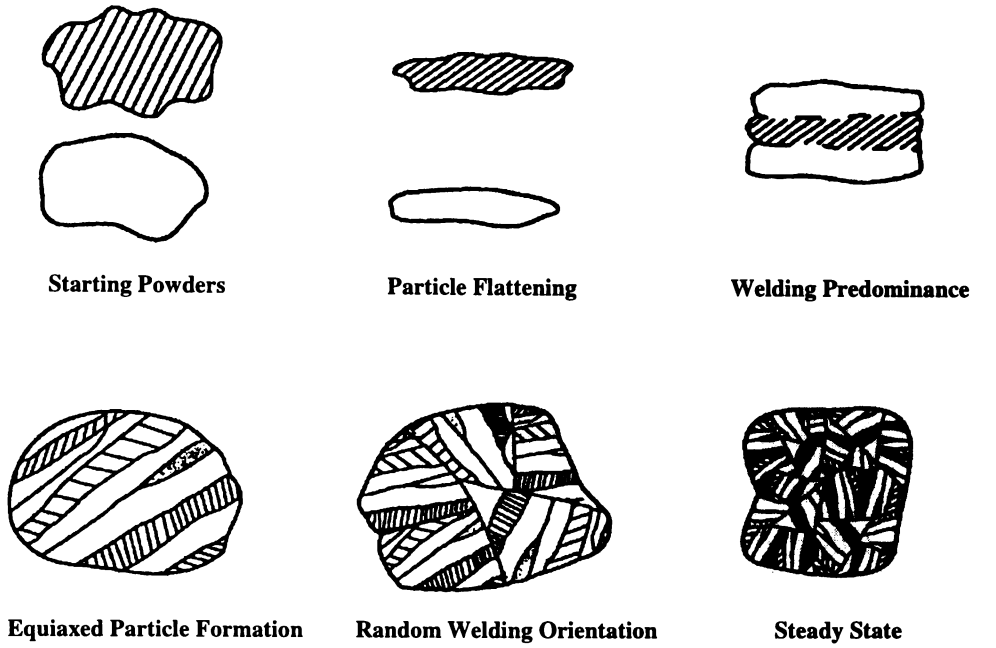

Figure 1-2. The five stages of microstructural evolution as described by Benjamin and Volin.[20]

Figure 1-2 shows schematically the microstructural evolution of powder particles during MM. In the initial stage of MM, the equiaxed ductile particles are flattened and forged resulting in plate-like particles. The second stage is the period of welding predominance. A multilayered composite structure formed in the coarser particles. The finer particles remain elemental with flake-shape. The third stage is the period of equiaxed particle formation. The particle size decreases because of further fracturing. The fourth stage is characterised by cold welding in random directions leading to formation of a number of lamellar colonies of random orientation in each composite powder particle. In the fifth stage, there is a reasonable balance between the welding and fracturing of the particles and thus, the average particle size does not change much. However, the composite microstructure becomes finer and finer with milling and eventually the lamellae become unresolveable under an optical microscope.

1.2.3.2 Ductile/Brittle Systems

The ODS alloys, which Benjamin and his group[21,22] worked on in the early stage, are typical examples of ductile/brittle systems. In such systems, the ductile metallic particles such as Ni or Al are flattened and welded to each other during

milling, while the brittle phase such as oxide particles is fragmented and embedded in the layers of the ductile phase. As milling proceeds, the layers of the ductile phase come closer and ultimately become unresolveable, while the brittle phase is uniformly distributed as fine particles in the matrix of the ductile phase.

1.2.3.3 Brittle/Brittle Systems

The microstructural evolution in brittle/brittle system differs markedly from that described previously for ductile systems. Davis and Koch[43] made an interesting observation while characterising particle morphology of brittle components during MM. In these systems, such as Si-Ge, Mn-Bi, and alpha quartz, numerous cases of interparticle necking were observed. They also found that the mechanically milled powders did not appear to have homogeneous particles, rather they appeared to be composed of smaller particles cold-welded together.

1.2.4 Modelling of Milling Process

In MM, the phase formation is quite sensitive to the milling conditions. This has led many researchers to study the physics/mechanisms of MM in order to predict the outcome of an MM process. Benjamin and Volin[20] were the first to attempt to develop a semi-empirical model to predict the time required for forming a particular microstructure during MM. Based on microhardness measurements of the particles at various milling times, they worked out an expression for the layer thickness of the composite powder particle as a function of milling time. Their analysis was based on the assumption that the rate of energy input and the rate at which material is trapped between colliding balls during MM are independent of milling time and that the energy required per unit strain is a linear function of instantaneous hardness of the powder particle. The time at which the layer thickness reached the resolving limit of the optical microscope was considered to be the time required for "alloying." Since this work, more sophisticated attempts[26,27] have been made to gain a deeper understanding of MM. Six main research groups have been involved in this modelling work. They are, Hashimoto and Watanabe[28] from Japan, Maurice and Courtney[29,30,31] and Koch *et al.* from USA, Magini *et al.*[32] from Italy, Gaffet *et al.*[33] from France, and Wang and Zhang[34] from New Zealand.

Modelling efforts can be classified as local and global modelling. In local modelling, the extent of plastic deformation, frequency of welding, and fracturing during collision are estimated. The impact velocities, frequencies, and angle of impacts are mill dependent, so global modelling is essential to predict them for a specific milling device. A combination of local and global models can give a more complete picture of what goes on during high-energy ball milling.[4]

Local Modelling

Maurice and Courtney[25] were the first to made the attempt to develop local model. They considered collision involving powder entrapped between milling media. Bhattacharya and Arzt[35] took an alternative approach and modelled the response of a porous compact and predicted the change in the dislocation density as a function of milling time and intensity. Maurice and Courtney[36] have also attempted a more rigorous treatment of the single collision, developed criteria for welding and fracturing, and developed two computer programs.[37] The programs describe the changes in the powder size, hardness, and microstructural scale during MM. The programs predict[38] several stages of the MM process described originally by Benjamin and Volin.[20] The predicted particle sizes are in reasonable agreement with the measured ones.[20,39]

Aikin *et al.*[40-42] used kinetic principles to study the fracture and coalescence events. The model predicts the welding and fracturing probabilities and the particle size distribution[40,41] during MM. They showed[40] that the fracturing and welding probabilities scale directly with ball/powder weight ratio and vary almost linearly with mill power.

Global Modelling

Davis and Koch[43] were the first to model the kinetics of ball milling in a Spex mill. The study showed that the majority of the impacts have an energy dissipation of 10^{-3}-10^{-2} J. The impact velocity was predicted to be less than 6 m/s. The model also predicts that the majority of the impacts are glancing in nature and not head-on. This result was later confirmed by the modelling studies of Maurice and Courtney.[25] Maurice and Courtney[44] have also modelled the milling dynamics in a SPEX mill and a hypothetical one-dimensional ball mill. They suggested that

most of the collisions result in a modest energy loss, while only 4-7% of the collisions result in an appreciable energy transfer. In an experiment, Basset *et al.*[45] have estimated the impact velocities from the indentation on a Cu plate fixed at one end of the vial in a SPEX mill. Their estimated velocities in the mill were in the range of 1.8-3.3 m/s and found to be strongly dependent on the ball size.

Hashimoto and Watanabe[46-49] have also simulated one, two and three dimensional ball motion in three types of mill, namely, vibratory, tumbler and planetary mills. The whole motion of the balls could be determined step by step. The simulation result for tumbler mills compares quite closely with video observations.

Le Brun *et al.*[50] studied ball motion in a planetary mill. They concluded that attrition and wear are more pronounced than impact in the MM process in planetary mill. Dallimore and McCormick[51] have developed a two-dimensional model to predict the motion of balls in a planetary mill. From the study of reaction between CuO and Ni during ball milling they concluded that the distribution of impact energies does not significantly affect reaction kinetics.

Observation of ball motion plays an important role in the model development. Rydin *et al.*[52] have used high speed cinematography to study the ball motion and the behaviour of the milling media in a transparent attritor. They suggested many ways of improving the efficiency of the attritor. A study with a mixture of different size balls[53] has shown that both welding and fracturing rates are enhanced.

Wang and Zhang[34] developed a 3-dimensional model to simulate the head-on impact process between two balls or between a ball and vial wall with powder in between by considering the elastic deformation of impact objects, and the visco-plastic flow and elastic deformation of the powder compact. The movement of balls considering the effects of powder, ball spinning, oblique impact of balls, and multi-ball impacts were also considered. They also developed a 3-dimensional global model for the SPEX-8000 Mixer/Mill based on the mechanics of the machine. By using this model, the motion of the vial was numerically determined. Then the global model was coupled with the models for the impacts in order to predict the dynamics of milling process.

1.3 Mechanical Alloying

Mechanical Alloying (MA) process differs from Mechanical Milling (MM) in that the former involves alloying or reactions at atomic levels. In other words, MA process is an extension of the MM process although the alloying or reaction could occur simultaneously from the start of MM.

The first work that addressed the issue as to whether the MA process results in only a fine mixture of the constituents of the elemental blend, or forms true alloys, was that of Benjamin[21] and Koch *et al.*[54]. Benjamin demonstrated from magnetic measurements that the behaviour of a Ni-Cr alloy prepared by MA was exactly the same as the alloy produced by ingot metallurgy route. Once a sufficient amount of Cr is dissolved in Ni, the later loses its ferromagnetic property and becomes paramagnetic. This would not happen if Ni and Cr remained as a mixture of individual elemental phases. Independently, Koch *et al.*[54] had demonstrated this by formation of an amorphous phase by mechanical milling a mixture of Ni and Nb powders. This has proved that alloying at the atomic level occurs during high energy ball milling, which is true mechanical alloying. Subsequently, reports on formation of intermetallic compounds by mechanical alloying of elemental powder mixtures also appeared.[22,43] A typical example is the formation of β-brass (bcc) during the MA of an elemental blend of Cu (fcc) and Zn (hcp)[55,56].

The process of applying mechanical energy to activate chemical reaction has been recorded way back to fourth century B.C.[57] Native cinnabar (mercuric sulphide, HgS) was ground with vinegar in a copper mortar to produce liquid metal, Hg. This process was also called "mechanochemical reaction". Whatever name is given to the process, the basic idea is to mill a powder mixture to achieve alloying at the atomic level or to mechanically activate the reactions. In addition to elemental powder mixtures, prealloyed powders and ceramics, such as oxides, nitrides, etc., can also be used to produce alloys and composites. Mechanical alloying has established itself as a viable solid state processing route for the synthesis of a variety of equilibrium and non-equilibrium phases and phase mixtures.[4,58] They are a number of general reviews on MA,[7,59-63] and reviews on specific aspects such as, oxide dispersion strengthened (ODS) alloys,[21,22,64-67] amorphisation,[68-78] disordering,[79] quasicrystals,[80] intermetallic compounds,[81,82]

nanocrystals,[33,83,84] reactive milling/combustion synthesis,[29,32,85-89] and modelling of energy transfer during milling[90]. A book by Lu and Lai[58] on mechanical alloying was published in 1998. Murty and Ranganathan[4] have made a comprehensive review on the materiels synthesised by MA. In the following sections, I will very briefly go through MA process with a focus on the works relating to the solid state reaction kinetics in MA.

1.3.1 History of MA

As early as 1930, Hoyt[91] used high-energy ball milling to coat WC with Co in order to achieve better mechanical properties of Wc/Co cermet. In 1966, Benjamin and his co-workers used high-energy ball mill to produce oxide dispersion strengthened (ODS) Ni-base super alloys for gas turbine applications. The success of their work led to the first patent on this process. The process was initially referred to as 'milling/mixing'. The term 'mechanical alloying' was given by Ewan C. McQueen, a Patent Attorney for Inco.[92]

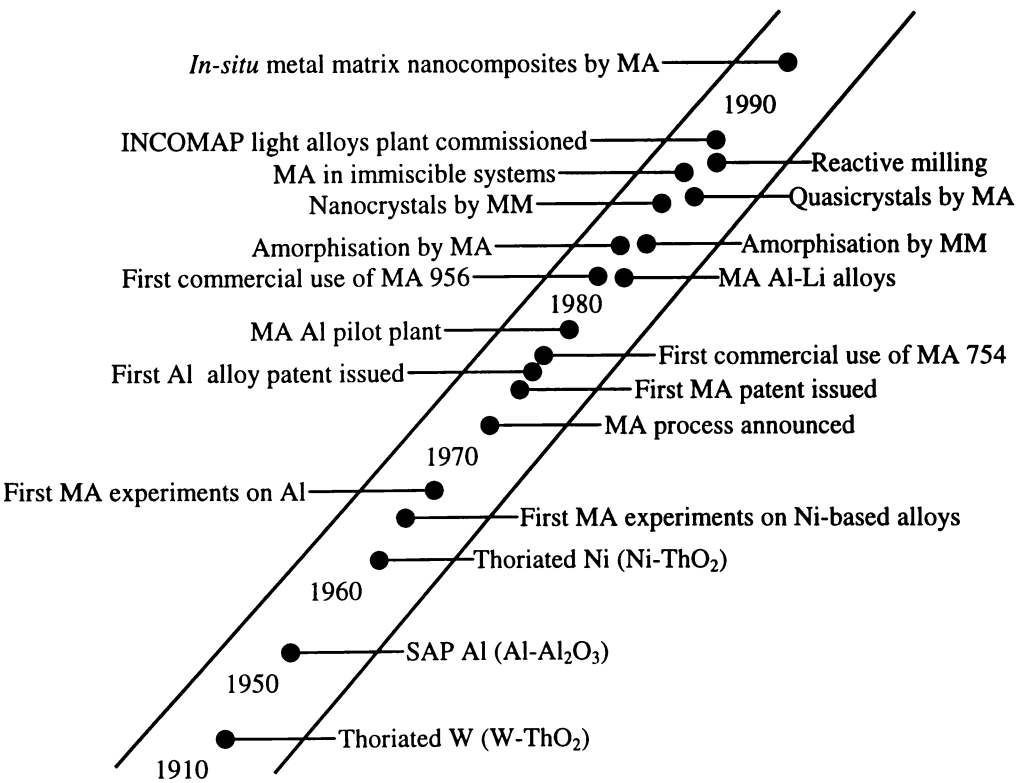

Figure 1-3. Chronological evolution of MA process (Modified from Murty and Ranganathan's review.[4])

Figure 1-3 shows the chronological evolution of the MA process modified from Murty and Ranganathan's review[4]. Most of the work on MA before the early 1980s was focused on ODS super alloys (Ni- and Fe-base) and Al alloys.[93] In 1983, Koch and his group reported the formation of an amorphous phase by milling a mixture of Ni and Nb powders.[54] In the same year two more papers appeared on amorphisation by low temperature diffusion annealing of multilayers of Au and La[94] and that of Zr_3Rh by hydrogenation.[95] Codeformation (rolling) of pure metal foils of Ni and Zr followed by low temperature annealing was also reported to result in the formation of an amorphous alloys.[96,97] Therefore, 1983 was considered as the birth year of solid state amorphisation (SSA) in the review by Murty and Ranganathan.[4] In the same article Benjamin was regarded as the pioneer of MA and Koch as the father of present face of MA.

Mechanical alloying has also been widely used for the synthesis of nanocrystalline metals, alloys, intermetallic compounds, ceramics, and nanocomposites in recent years[83]. In addition, quasicrystalline phases have also been synthesised in many metallic systems by MA[91]. A new area that started in late 1980s is reactive milling/combustion synthesis. Following the success of Schaffer and McCormick in reduction of CuO by Ca using high energy milling,[98] a large amount of work has been carried out to check the feasibility of applying high-energy milling to chemical refining.

1.3.2 Temperature Increase During Milling and its Effect on MA

Part of the milling energies is used in increasing the temperature of the powder and the milling media.[99] The temperature during milling depends on the kinetic energy of milling media and the material characteristics of the powder charge. The temperature of the powder influences the diffusivity and defect concentration in the powder and thus influences the phase transformations induced by milling.

Davis[100] and McDermont[101] have measured the maximum temperature of a SPEX mill to be 50°C (40°C without balls) and concluded that most of the heat comes from the motor and bearings. Kimura[102] reported a maximum macroscopic

temperature of 172°C in the attritor. Borzov and Kaputkin[103] have determined the temperature to be in the range 100-215°C for an attritor. Kuhn *et al.*[104] reported a substantial temperature rise of 120 K in vibratory mills. The macroscopic temperature during milling appears to be low and sensitive to the mill design.[4,99,105]

The local temperature of the powder trapped at impact points during impact can be quite high. Yermakov *et al.*[106,107] have attributed amorphisation during milling to the local melting and rapid solidification of the powders. Because it is hard to measure the local temperature during milling, two approaches were used to estimate the temperature rise. One is to calculate this temperature by using appropriate models and the other is to infer the temperature from the structural/microstructural changes during milling.

Schwarz and Koch[9] estimated a local temperature rise of about 40 K for $Ni_{32}Ti_{68}$ and $Ni_{45}Nb_{55}$ powders in a SPEX mill by assuming that particles trapped between colliding balls deform by localised shear. Davis and Koch[43] calculated the ball velocities and used the expression and materials of Schwardz and Koch[9] to predict a rise in temperature (ΔT) of about 112 K. They also calculated the maximum ΔT to be about 350 K. Maurice and Courtney[25] developed an expression for the adiabatic temperature rise during milling. They assumed that the material was in the cold working regime. Magini *et al.*[108] calculated the adiabatic temperature in a planetary mill and reported the maximum temperature of 400 K during a Hertzian collision. Bhattacharya and Arzt[109] calculated the temperature of impacting surfaces and calculated that the temperature was approximately 350°C. Davis and Koch[43] found the ΔT due to sliding friction to be very low (=<10 K). Miller *et al.*[110] used microsecond time resolved radiometry to observe a temperature rise during impact on various materials. They observed a ΔT of about 400 K.

The observation of deformation bands and slip lines by optical microscopy and the high dislocation densities and deformation bands seen in transmission electron microscopy[111] indicate that the local temperature is lower than the recrystallisation temperature. In some cases, it is reported[71,102] that the temperature is above the crystallisation temperature of the amorphous phase. Davis and Koch[43] studied the tempering of martensite in an Fe-1.2C steel during ball milling and concluded the

maximum local temperature to be about 275°C. Davis and Koch[43] have also milled Bi powder and concluded that the temperature of milling is below the melting point of Bi (271°C). The milling temperatures obtained by both calculation and experiment suggest that there is only a moderate temperature rise during milling and that the possibility of local melting can be ruled out.

1.3.3 Phase Formation during Mechanical Alloying

1.3.3.1 Extension of Solid Solubility

Many studies have shown that high energy mechanical milling can extend the terminal solid solubility. The formation of solid solution in the entire composition range in the eutectic Ag-Cu system[112] has highlighted the potential of MA in achieving large extensions of terminal solid solubility even in systems with positive enthalpies of mixing in the solid state. Suryanarayana and Froes[12] achieved a terminal solid solubility of 6at% of Mg in Ti by MA though these elements are immiscible in solid state under equilibrium conditions. Suryanarayana and Froes attributed this extension of solid solubility to the nanocrystalline structure formed during MA. The large volume fraction of grain boundaries present in the nanocrystalline state is expected to enhance the solid solubility in these materials. Murty *et al.*[113] showed that in the Ti-Ni and Ti-Cu systems, only amorphisation could limit the extension of solid solubility. Thus MA can be used very effectively to extend the solid solubility.

1.3.3.2 Alloying in Immiscible Systems

High energy mechanical milling has also achieved alloying in immiscible systems. There have been efforts to understand the driving force for such a behaviour during high energy ball milling. Yavari *et al.*[114,115] have attributed this to the capillarity effect. Yavari *et al.* argued that high energy ball milling results in the formation of small fragments with tip radii of the order of 1 nm. The capillarity pressure at these tips forces the atoms on these fragments to dissolve. But Ma *et al.*[116,117] argued that such a mechanism would only lead to spheroidisation. Ma *et al.* believed that the high interfacial energy associated with a fine-structured two-phase domain mixture created by ball milling is likely to be

a key factor that drives homogenisation and constrains the system in a single-phase metastable state. Gente *et al.*[118] and Huang *et al.*[119] have proposed that formation of homogeneous solid solution is energetically more favoured when the crystallite size of the constituents is reduced below a critical size which is of the order of 1-2 nm. Huang *et al.*[120-122] have shown that nanocrystallisation is a prerequisite for alloying during MA.

1.3.3.3 Formation of Amorphous Phases

Koch *et al.*[54] was the first to report the formation of amorphous phase by MA. During milling a Ni-Nb elemental powder mixture, they observed a continuous broadening and shifting of the major X-ray diffraction peaks, which was interpreted as a continuous decrease in crystallite size. This mechanism has been categorized as type I amorphisation reaction in the review by Weeber and Bakker.[73] For this type, there is a continuous broadening and shifting of the Bragg peaks of the elements in X-ray diffraction pattern as a function of milling time until an amorphous phase eventually results. The system Zr-Al, first studied using ball milling by Fecht *et al.*[123], apparently also belongs to this category.

It was reported that the amorphisation reaction behaviour might vary even in the same powder system if the powder mixture was milled under different milling conditions associated with different milling process parameters or different milling equipment. As observed by Petzoldt[73] during MA of a Ni-Nd powder mixture, the peaks of the elements became slightly broader and their intensity decreases continuously, same as the reaction type found by Schwarz *et al.*[124] for amorphisation of Ni-Ti. This type was categorised as type II amorphisation reaction in the review by Weeber and Bakker.[73] In this type, the amorphisation occurs by interdiffusion during the process. The amorphisation process during milling is similar to the amorphisation in multilayered structures during heating. The amorphous parts grow by cold welding of the amorphous layers formed by interdiffusion. The eventual homogenization takes place by cold welding combined with further diffusion.

A third type of amorphisation reaction, as categorized by Weeber and Bakker[73] in their review is the formation of crystalline intermetallic intermediate products and

further milling resulting in the transformation of these products into a homogeneous amorphous phases.

MM of crystalline alloy powders has also been reported to form amorphous phases with much shorter time than that required for MM elemental powder mixtures.[73] A competition between the tendency to go to the thermodynamically stable situation and the enthalpy increase due to the energy transferred from the balls to the material to be milled. This depends on the local conditions during milling. The local conditions are determined by the milling equipment used. This implies that different milling equipments can result in different glass forming ranges. Furthermore, the local conditions determine the amorphisation reaction path.

Zhang and Massalski[125] reported an amorphous phase formed during MA in the copper-cadmium system by reaction between the equilibrium δ phase and one of the constituent metals (copper). By contrast, such an amorphous phase can neither be formed by a direct reaction of copper and cadmium powders nor by milling a powder consisting of only δ phase. They considered three possibilities that can raise the energy of a mixture of copper and the δ-phase powders to a sufficiently high value to provide a driving force for amorphisation: (1) an accumulation of structural defects during milling; (2) a change of composition of the δ phase; and (3) a contribution of copper/δ interfacial free energy. They believed that the contribution of copper/δ interfacial free energy plays the major role in providing this needed driving force.

Ma *et al.*[116,117] reviewed the amorphization mechanisms by MA reported by several authors. Amorphisation by ball milling was first hypothesized to result from rapid quenching of local melts produced by mechanical impacts. Latter studies suggest that melting is unlikely and solid-state processes are most likely to be responsible for vitrification. For milling of intermetallic compounds, it is suggested that the amorphisation is due to the accumulation of deformation-generated defects, which raise the free energy of the compound to above that of the amorphous phase. For milling of elemental powder mixtures it has been proposed and widely accepted that an amorphous phase nucleates at interfaces and grows by interdiffusion reaction under interfacial metastable equilibrium

analogous to that in thin-film diffusion couples and in co-deformed metal foils. Ball milling facilitates such reactions by fracturing and cold-welding crystalline particles to create alternating layers with fresh interfaces, and by generating a high density of defects. Many experimental observations, reported for a number of binary systems, are consistent with this picture. In some alloy systems consisting of ductile elements, multilayer structures produced by the milling process have been observed. Amorphous interlayers sandwiched between crystalline layers have been observed under TEM in the Ni-Nb and Ni-Zr systems.[73] It has also been reported that as ball milling of elemental powders proceeds, the X-ray diffraction peaks of the constituent elements remain at the same position but decreases in intensity, and separately, a broad peak of amorphous phase appears with increasing intensity. Moreover, alloys in the central composition range transform into an amorphous single phase and a terminal solid solution, presumably under metastable equilibrium. These features correspond well with those observed for amorphisation by interdiffusion reactions. Such a mechanism of interdiffusion under metastable equilibrium has been categorized as amorphisation reaction type II in the review by Weeber and Bakker.[73] Well studied examples that apparently belong to this category include easy glass forming systems such as Zr-Fe and Ti-Ni.

Lu *et al.*[126] observed an amorphous-nanocrystalline-amorphous phase transformation in element selenium during ball-milling a melt-quenched amorphous Se. They found that during the major amorphization process, the crystallite size keeps unchanged at about 13 nm. This phenomenon is in conflict with the 'skin' model that proposed the amorphous phase nucleated at grain boundaries and grew into the grains by gradually consuming the crystalline phase, resulting in shrinking of remaining crystallite size. The observed constant grain size during amorphisation process implies that the grains smaller than a certain grain size (say 13 nm) may be transferred into amorphous completely while those larger than 13 nm remain crystalline. They also proposed that the driving force contribution from the lattice distortion might be significant for the amorphisation process in the small crystallites below the critical grain size.

The formation of amorphous interlayer (a-interlayer) by solid-state diffusion in diffusion couples has been one of the most challenging problems in condensed

matter physics in recent years. The a-interlayer has been found to occur in all refractory metal/Si and a number of rare-earth (RE) metal and platinum group metal and crystalline silicon systems. Chen[127] reviewed the solid state amorphization in metal/Si systems. He showed that, (1) a negative heat of mixing provides the driving force for the reaction and fast diffusion of one component into the other pre-empts the formulation of crystalline compounds, (2) the growth follows a linear law at the initial stage with activation energy around 1-1.5 eV for refractory metal/Si systems and 0.5 eV for RE metal/Si systems, (3) the dominant diffusing species is Si, (4) the stability of amorphous interlayer depends on the composition, (5) simultaneous presence of multiphases in the initial stage of metal/Si interaction, and (6) good correlations between physical parameters and kinetic data.

Liu and co-workers[128-130] studied the formation of metastable and amorphous phase in Ni-Nb, Ni-Zr, Y-Zr systems by annealing multilayer thin-films and ion mixing. Grushko and Shechtman[131] proposed a model of metastable phase formation by a diffusion process. Gosele and Tu[132] applied the "critical thickness" concept to the amorphous phase formation in binary diffusion couples.

1.3.4 Reactive Milling and Mechanochemical Processing

The milling process during which chemical reactions take place leading to the metallothermic reduction and/or resulting in the formation of compounds is termed "reactive milling". If the reactions are highly exothermic, combustive reaction may occur.[98,133] Schaffer and McCormick[98,134] were the first to report the reduction of metal oxide by reactive metals. They have shown that reduction of CuO by Ca is feasible by ball milling the powders together. An exothermic reaction resulted in an abrupt rise in the temperature of the vial by 140 K during dry milling. They calculated the adiabatic rise in the temperature from the enthalpy change of the reaction (~ 473 kJ/mol) and the heat capacities of the reactants to be 4000 K. This is much above that required for self-sustaining combustion (~2300 K). They have also shown[134] the formation of β-CuZn phase by the simultaneous reduction of CuO and ZnO with Ca. Schaffer and McCormick, in their subsequent publications[2,135-137] have shown similar

metallothermic reduction reactions in a number of systems. Schaffer and McCormick[2] have studied the kinetics of these reactions and showed an increase in the rates of the reaction at higher milling energies. Yang and McCormick[138,139] reported combustion reaction of zinc oxide with magnesium and reduction of tantalum chloride by magnesium during mechanical milling. They studied the mechanochemical reduction of V_2O_5 using Mg, Al and Ti,[140] and reduction of NiO using graphite.[141] Lu *et al.*[142] have reported the reduction of Fe_3O_4 with Al during milling which resulted in the formation of ferromagnetic Fe and superparamagnetic Fe particles. Nasu *et al.*[143] reported reduction of Fe_2O_3 using Al and Mg in a planetary mill. El-Eskandarany[144] has reported the formation of nanocrystalline Cu and TiO_2 particles by the reduction of Cu_2O with Ti. Xi *et al.*[145] reported forming Cu and SiO_2 nanocomposite by high energy ball milling CuO and Si.

McCormick *et al.*[146] have also shown the reduction of $TiCl_4$ with Mg and formation of not only Ti but also alloys such as Ti-3Al, Ti-6Al-4V, TiAl, and Ti_3Al by changing the proportions of the constituents. Ding *et al.*[147] have shown the reduction of $FeCl_3$ and $CuCl_2$ with Na and Ca which has led to the formation of nanocrystalline Cu and Fe powders. Suryanarayana *et al.*[148] have shown the formation of TiAl by the reactions between Al_3Ti and TiH_2.

There have been a number of reports describing the formation of nitrides and oxynitrides by milling elemental powders in liquid nitrogen (LN_2). Perez *et al.*[149] have produced nanodispersions of Al_2O_3 and AlN in Fe-10wt.%Al alloys by the cryomilling of Fe and Al together. Huang *et al.*[150] have obtained a similar dispersion in NiAl by the MA of Ni and Al in LN_2. Aikin *et al.*[151] have produced AlN by the cryomilling of NiAl. Ball milling of metals by sealing the vial with nitrogen gas has also led to the formation of various nitride such as Fe_2N, NbN, Ti_2N, TiN, Si_3N_4, TaN, ZrN, and (Ti,Al)N. Nitrides have also been produced by milling the elemental powders in an ammonia atmosphere.[4]

Takacs[86] reviewed the literature on the mechanism of reactive milling with particular attention to the initiation of combustion. He argued that the gradual or combustive nature of the reaction depends on thermodynamic parameters, the microstructure of the reaction mixture, and the way they develop during the

milling process. He pointed out that our current understanding of the reaction milling process is qualitative. Especially little is known about the significance of the mechanical properties of the reactants, the role of diffusion, and the nucleation of product particle at the interface.

Ma and Aztmon[116] suggested that self-sustained reaction are a common mechanism of mechanical alloying in alloy systems with a large negative heat of mixing when subjected to high-energy ball milling. They argued that such reactions may escape detection when only bulk-averaged analysis is used as these reactions may not necessarily propagate through the entire powder mixture, and instead, may occur locally at the ignition (collision) spot, such that the entire sample reacts gradually on a particle-by-particle basis.

1.3.5 Simulation of MA Process

Pabi *et al.*[152] have developed a rigorous mathematical model based on the modified isoconcentration contour migration method to predict the kinetics of diffusive intermixing during MA. They have successfully correlated the kinetics of alloying to the melting temperature in the Cu-Ni system. Courtney *et al.*[153] developed a simplified interdiffusion model to predict the time scale needed for the formation of homogeneous solid solution by mechanical alloying. In their model the periodical temperature rise caused by the high speed impacts was considered as the major contribution to the enhancement of the interdiffusion process. In both of the above models, effect of deformation caused by the impacts was considered by taking the thickness reduction as an exponential function of strain accumulation. But their models did not take the new phase formation into consideration.

1.3.6 Materials Synthesised by MA

A wide range of materials have been synthesized by MA. Among them, oxide dispersion strengthened (ODS) materials were the first success. Following that, other equilibrium and non-equilibrium materials, nanocrystallines and a range of intermetallics were successfully produced by MA.

1.3.6.1 ODS Alloys by Mechanical Alloying

The development of strong ODS alloys has been the prime goal of Benjamin's group, which invented the MA technique. Very fine microstructures and fine dispersion of oxides of Ni- and Fe-base superalloys and Al alloys produced by MA have yielded materials with superior mechanical properties over the conventional alloys. Some of these MA ODS alloys have been commercially produced despite strong competition from conventional ODS alloys. The ODS alloys produced by MA can be classified based mainly on the matrix materials as ODS superalloys, Al alloys, Ti alloys, and ODS intermetallics.[4]

1.3.6.2 Intermetallic Compounds

The intermetallics constitute some of the most technologically promising engineering materials. This stems from their unique attributes such as excellent high temperature strength, and thermal stability apart from the high corrosion/oxidation resistance and unique electrical and magnetic properties. The high melting point and the poor formability of the intermetallics, however, poses major impediments to their conventional processing. Under this perspective, MA has been regarded as an extremely promising solution. Over the past decade, a considerable volume of work has been reported on the synthesis of a large number of intermetallic compounds via MA. The bulk of these efforts has been on the aluminides and to some extent on the silicides.[4]

Overwhelming interest in the MA of aluminides has been instigated by their possible applications in aerospace and automotive industries owing to their high specific strength at elevated temperatures. Among all aluminides, the MA of Ni, Ti, and Fe aluminides have so far received major attention. Apart from Ni, Ti, and Fe aluminides, the versatility of MA has been demonstrated in the synthesis of several other aluminides such as Al-Nb, Al-Mo, Al-Zr, including ternary aluminides such as Al-Ni-Fe, etc.[4]

The MA of silicides has gained significant interest in recent years,[154] particularly because of their potential applications as structural materials in the field of microelectronics and electrical technology. Among silicides, the MA of Fe, Ti, and Mo silicides have so far received major attention.

Although the aluminides and silicides are the major focus of MA research in the field of intermetallics, several other intermetallics are also important because of fundamental aspects as well as technological importance. The formation of various compounds in the Cu-Zn system through MA has been extensively studied over the past decade.[55,56,155] Various other intermetallic phases are also known to have been produced by MA. A list of non-aluminide and non-silicide intermetallics produced by MA is presented in Table 1-2.

Table 1-2. Intermetallic compounds synthesised by mechanical alloying other than aluminides and silicides[4]

Phase	Structure	ΔHf, kJ/mol	Synthesis route
Co_3C	Hexagonal	+6	MA
Cr_7C_3	Hexagonal	-13	MA + HT
Cr_3C_2	Orthorhombic	-16	MA + HT
Cr_2Nb	C15	-10	MA
β-CuZn	B2	-8	MA
γ-Cu_5Zn_8	$D8_2$	-4	MA
ε-$CuZn_4$	Hexagonal	-2	MA
Fe_3C	Orthorhombic	-25	MA
$FeSn_2$	C16	-1	MA
Fe_3Sn_2	Monoclinic	-2	MA + HT
FeSn	B35	-2	MA + HT
Fe_3Sn	DO_{19}	-2	MA
Fe_3Si	DO_3	-21	MA
FeTi	B2	-25	MA
Fe_3Zn	$D8_2$	-2	MA
Mg_2Ge	C1	-115	MA
Mg_2Ni	Hexagonal	-52	MA + HT
Mg_2Si	C1	-79	MA
Mg_2Sn	C1	-80	MA
Nb_3Ge	A15	-28	MA
Nb_5Ge	Orthorhombic	-19	MA
$NbGe_2$	C40	-29	MA
Nb_3Sn	A15	-16	MA
Nb_3B	Cubic	-21	MA
Ni_3C	Cubic	+7	MA
$Ni3Sn_2$	Hexagonal	-24	MA
TiB_2	Hexagonal	-74	MA
TiC	$L1_2$	-77	MA
TiNi	B2	-52	MA

HT: heat treatment

1.4 Effect of Milling on Solid State Reactions During Heat Treatment

Combining heat treatment with MM has been proven to be an effective technique for advanced materials processing.[81,141,156-160] In some reaction systems, solid state

reactions can not be achieved solely by mechanical milling, so subsequent heat treatment is necessary. MM has not only enhanced the solid state reaction kinetics but also affected phase formation.

The solid state reactions in high energy milled powders during heating are often comparable with that of multilayer thin films. It is known from the literature that a metal in the form of a thin layer was first obtained in 1857.[161] Thin metal layers have since been gradually establishing their place in science and technology. In the 1940s and 1950s an explosive development of thin-film preparation and application technologies has taken place, these being a prerequisite of the development of certain important branches of technology, especially military. Thin films are increasingly employed in optics, micro- and opto-electronics, sensor and computation technologies. They are used as mirrors with front-reflecting surfaces, conduction paths, contact and barrier layers, antireflection and anticorrosion layers, *etc.* With the continuing drive toward greater device densities and finer dimensions in the microelectronics industry, the required properties of the metallization layers have become increasingly stringent. The phase formation in thin film systems is unique. Unlike the bulk diffusion couples in which all the phases appeared to form simultaneously, only one phase is usually observed during phase formation in thin films. Therefore, the thin film geometries are particularly useful for studying the earliest stages of solid state reactions in metals as well as oxides.

1.4.1 On the Reaction Temperature

MM can establish and refine composite powder particle microstructure, consequently the reaction temperature can be decreased substantially.[156] Welham[156] studied the solid state reactions between Al and TiO_2 and found that the unmilled powders were incompletely reacted even after 1 hour at 1200°C whereas the milled powders were fully reacted after 1 hour at 600°C. He attributed these improvements to the enhanced mixing of the components leading to shortened diffusion paths.

Yang and McCormick[141] studied the solid-state reactions between NiO and graphite during high energy ball milling and subsequent heat treatment. They

found that the reduction of NiO to Ni did not occur during milling with graphite at ambient temperatures due to insufficient storage of internal energy in the NiO and temperature rises accompanying collision events. Reduction of NiO to Ni occurred during milling at elevated temperatures. The decrease in particle size from ~200 μm to ~5 μm during milling caused a significant reduction in reaction temperature during subsequent heating.

1.4.2 On the Phase Formation

Due to the large interface area created by MM through a refined composite powder particle microstructure, interfacial reaction tends to dominate the reaction process. Therefore, the phase forming sequence may differ from that of conventional powder blending or bulk diffusion couples.[162-165]

In contrast to the later stages of phase reactions that are solely determined by the thermodynamics of the alloy system, the phase reaction in the early stages is mainly governed by the kinetics of the reaction process. By choosing appropriate reaction conditions this often results in a distinct phase selection in the early stages of phase reaction. Thereby only one of the possible intermetallic compounds or even a metastable phase, which does not exist in the equilibrium phase diagram, is formed. Bormann[166] summarized the quantitative understanding of the kinetics of interface reactions including nucleation and growth kinetics with a particular focus on the mechanisms causing the distinct phase selection occurring during the early stages. He also discussed the influence of microstructures of the parent phases and new phases formed on the phase selection. He concluded that the phase selection during initial stage of interface reactions could be caused by differences in the nucleation rates as well as by the growth kinetics of the competing phases. Due to interdiffusion preceding the nucleation of a new phase, a nucleation barrier can exist even in systems with large free energy of formation for intermetallic compounds. Therefore, heterogeneous nucleation at defects along the interface has to be taken into account, and the microstructure of the parent phase can influence the phase selection. Besides the nucleation barrier that can be significantly decreased by preferred heterogeneous nucleation sites, the nucleation rate is substantially

determined by the activation energy of growth. As energy difference in the growth barrier seem to be even larger than differences in the nucleation barrier, the phase selection during nucleation may be completely overridden by the growth barrier of the competing phases, in particular in polycrystalline diffusion couples. The growth kinetics of competing phases is determined by the flux of diffusing species.[166] Thereby phases with high diffusivity are favoured and can suppress other phases in the early stages of interface reaction. As, at low reaction temperature, the activation energy of growth is again the dominant factor, this turns out to be one of the key parameters determining the phase selection in the early stages of interface reaction. The microstructure of the parent phases and of the new phases can also substantially influence the activation energies of growth of the new phases.

Morris[167,168] obtained Al_3Fe phase by milling Al-12.5at%Fe blends for 80 hours and then annealing at 773 K. The formation of such non-stoichiometric Al_3Fe may be an indication of an extended Al_3Fe phase composition field. Mechanical alloying of Fe-rich composition, e.g. Al-75at%Fe, which incidentally lies in the $AlFe_3$ phase field, has been found to produce AlFe instead.[169] Subsequent annealing, on the other hand, has led to B2-$AlFe_3$ instead of the usual DO_{23} structure.

1.4.3 On the Reaction Kinetics

MM can substantially enhance the solid state reaction kinetics.[170] Yang and McCormick[141] studied the solid-state reactions kinetics between NiO and graphite during subsequent heat treatment. The kinetics of the reduction reaction has been modelled for spherical NiO particles embedded in a uniform graphite medium. The reduction of NiO was assumed to involve the formation of a Ni layer on the particle surface and the diffusion of carbon through the Ni layer was assumed to be the rate-controlling step. The Carter's solid-state reaction model was satisfactorily employed to describe the reaction kinetics during constant heating the milled powders. Yang and McCormick attribute the two-stage reaction kinetics observed for the intermediate milling times to the bimodal particle size distribution developed during milling.[141]

Investigations on Ti-Al intermetallics have revealed considerable resistance to alloying during MM. For example, prolonged milling for 100 hours in a Fritsch P5 planetary mill at a CR of 10:1 has failed to produce Ti-Al compounds.[157] The formation of Ti-Al intermetallics could be achieved by adopting a two-stage process involving MM and subsequent annealing.[18] This is evidenced by the MM attempts for the synthesis of AlTi and Al_3Ti, which required annealing of the ball milled ingredients at 873 and 813 K, respectively.[158] Several other reports on the production of Al-Ti intermetallics such as Al_3Ti, Al_3Ti_2, AlTi, and $AlTi_3$ through a 'mechanically activated annealing process' involving intense ball milling followed by an annealing process are also available.[159,160] It is however, quite obvious that the annealing temperatures would vary considerably depending on the final grain size which dictate the diffusion distance.

1.4.4 Modelling Efforts

Bormann[166] proposed a heterogeneous nucleation model for solid state reaction in multilayer thin films taking into account of the interdiffusion. His model provided a very meaningful insight into the role that nucleation plays in selecting the first phase to form from the solid solutions. The model explained that in some systems, metastable phase or amorphous phase are more favourable than the stable intermetallic phases because of their lower activation energies. Recently, Zhang and Ying[171] has proposed a heterogeneous nucleation model to explain and predict the selective first phase formation in connection with the progress of mechanical milling. The model explained that with the increase of α/β interface area the reaction path will change and affect first phase formation during subsequent annealing of the mechanically milled powders.

An intriguing observation that was first found by calorimetry and brought a new viewpoint into this field was the fact that the formation of the first product phase in a multilayer film can be a two stage process.[172-178] As an example, two exothermic peaks appeared in the DSC traces of the sputter-deposited Nb/Al multilayer thin films. One appeared at lower temperatures (peak A) and the other appeared at higher temperatures (peak B). Extensive X-ray and electron diffraction studies verified that both exothermic peaks of the DSC trace of the

Nb/Al multilayer thin film were associated with the formation of a single phase, $NbAl_3$.[174] The relative areas of the peaks changed with layer thickness in a systematic way. Peak A dominated for small thickness and peak B became increasingly pronounced for large thickness. Similar two-peaked traces have also been observed for evaporated Nb/Al multilayer thin films,[173,177,179] as well as for other systems such as Ni/Al[172,174,180], Ti/Al[181], Ni/amorphous Si[177] and V/amorphous Si[182]. In all cases the two peaks correspond to the formation of a single phase.

The formation of a single phase in two stages is explained by the model of Coffey *et al.*[177] for a two-stage transformation.[177] In this model, a product phase first nucleates and grows laterally in the plane of the interface and forms a coalesced, contiguous layer in stage one (peak A). In stage two this contiguous layer grows normal to the interface until one or both reactants are consumed (peak B). The transformation associated with peak A (stage one) is described by a Johnson-Mehl-Avrami (JMA) nucleation and growth process which, under isothermal conditions, is given by following equation:

$$X(t) = 1 - \exp\left(-kt^n\right)$$

where, X is the transformed volume fraction, k=k(t) is a temperature-dependent rate constant and n is the Avrami exponent. Application of JMA equation to constant-heating-rate conditions[180] leads to the following equation for the volume fraction transformed:

$$X(T) = 1 - \exp\left[-\left(\frac{k_{i,0}k_bT^2}{\beta E}\right)^n \exp\left(-\frac{nE}{k_bT}\right)\right]$$

where $k_{i,0}$ and E are the pre-exponential factor and the activation energy of the JMA process. DX/dT is then proportional to the heat released in peak A in the DSC traces. Coffey *et al.*[177] assumed that the transformation began with a fixed number which subsequently grew as cylindrical grains. The growth parallel to the interface was taken to be interface controlled and was represented by the JMA equation with n=2. The subsequent thickening of the layer, peak B in the DSC

traces, was modelled by 1D diffusion controlled growth by the following equation:

$$\frac{x^2}{2} = \frac{k_{d,0}}{\beta}\frac{k_B T^2}{E_d}\exp\left(-\frac{E_d}{k_B T}\right)$$

where x is the product phase thickness, β is the heating rate, $k_{d,0}$ and E_d are the pre-exponential factor and the activation energy for diffusion-controlled growth respectively, and k_B is the Boltzmann's constant. The derivative of above equation, dx/dT, was fitted to the experimental data of Ni/Al multilayer thin films and the activation energy E_d and the pre-exponential factor $k_{d,0}$ were calculated from this fitting to be 1.72 eV and $2x10^{-3}$ m^2/s, respectively. Calorimetry experiments (isothermal and constant-heating-rate ones) can be used to determine all the model parameters separately, except for the nucleation site density per unit area, N, and the radial growth prefactor, $k_{i,0}$, which appear as $Nk_{i,0}^2$. Determination of these two parameters requires direct observations of the evolution of the product phase grains by a technique such as transmission electron microscopy.

The simple model of Coffey *et al.* successfully describes the outstanding features, namely, the two peaks of the DSC trace of the multilayer thin films and their systematic dependence on the layer thickness. This model has been successful in describing the behaviour of multilayers of Nb/Al (first studied by Coffey *et al.*[177]), and also in Ni/Al[174], Ni/amorphous Si[177] and V/amorphous Si[182].

However, although the simple model of Coffey *et al.*[177] describes the essential features of DSC traces, the model under-estimates the width of peak A and B in some cases. Under-estimating the width of peak A indicates that n is less than 2, which has been found for several systems using isothermal and constant-heating-rate DSC experiments. From another point of view this might be due to the assumption that the nuclei start to grow at the same time. Underestimating the width of peak B may be attributed to the nonuniformities in layer thickness which have been observed in many multilayer systems. These variations in thickness prevent an abrupt termination of the reaction and an abrupt end to peak B.

1.5 *In-Situ* Metal Matrix Composites

Metal matrix composite (MMC) materials combining the ductility of the matrix metal phase and the stiffness and the hardness of the reinforcements can offer mechanical properties superior to the conventional monolithic materials, and have numerous successful commercial applications. However, it has been reported that nearly all commercially important ceramic reinforcements, including SiC, Al_2O_3, B_4C, *etc.*, exhibit poor wetability by a molten matrix.[183] Molten pure aluminium does not wet Al_2O_3 even at 900°C.[183] *In-situ* formation of the reinforcement phase through chemical reaction during the processing has been reported to be an effective route to solve the wetability problem.[184-186] Recently, attempts have been made to grow second phase reinforcements *in-situ* in the matrix by taking advantage of the heat evolved during reaction.[187] This has paid good dividends in meeting the requirements of a clean interface in the TiAl-TiB_2 system. Using a similar approach of exothermic processing, Al-composite and Ti-composites with particulate reinforcements of alumina, carbides, borides, nitrides and their mixtures have been reported.[184,187-190]

1.5.1 Manufacturing Methods of *In-Situ* MMCs

Most commonly used manufacturing methods for *in-situ* MMCs are solidification processing, combustion synthesis, the exothermic dispersion (XD™) process and combustion-assisted synthesis (CAS). Some other techniques for fabricating metal and intermetallic matrix composites have also been developed, such as direct metal oxidation process (DIMOX™), one of Lanxide processes developed by Lanxide Corporation, self-sustained high temperature synthesis (SHS), *etc.*[191-196]

1.5.1.1 Solidification Processing

Solidification processing routes for particulate-reinforced aluminium and titanium composites have the advantages of simplicity, flexibility, cheapness and ease of production of components with complex shapes.

Maity *et al.*[184,185] reported an attempt to produce Al-Al_2O_3 composite by adding TiO_2 into the molten Al. The Al_2O_3 particles formed by the reaction between molten Al and TiO_2 were more compatible with the matrix and the interfaces were

cleaner as compared to the composites produced conventionally. Peng *et al.*[197] reported synthesis of Al_3Ti-Al_2O_3-Al *in-situ* composites by reactions between TiO_2 powder and molten Al *via* squeeze casting route. In their process, Al-27vol%TiO_2 bulk material was prepared by squeeze casting using anatase (TiO_2) powder and pure Al ingot. The squeeze cast TiO_2/Al bulk material was heat-treated and according to the differential thermal analysis results, the reaction between TiO_2 and Al occurred to form the final Al_3Ti-Al_2O_3-Al *in-situ* composite. Peng *et al.* examined the microstructure of the composite and proposed a two-step microstructure evolution mechanism. They believed that firstly, a reaction between the molten aluminium and TiO_2 producing alumina particulates and liquid Ti. Then, a solidification process of remaining Al and Ti displaced from the reaction with decreasing temperature to produce Al + Al_3Ti blocks and then, the smaller Al_3Ti precipitates formed as the solid cools.

There is very little discussion in the literature of attempts to produce particulate-reinforced Ti-composites through the solidification routes. This is due to the high reactivity of titanium with reinforcements in the liquid state and the problems involved in melting and casting titanium and its alloys. However, a few successful efforts made in recent times are worthy of note.[211]

In one such attempt, composites were produced by induction melting. A Ti-TiC composite was produced by mixing graphite powder with titanium during melting, thus forming TiC particles as a second phase in a Ti matrix.[198] The reinforcement in this case was formed inside the material instead of being inserted into the molten metal. The interface wetability problems of the two materials could thus be avoided. On similar lines, an *in-situ* method was used to produce a hybrid mixture of three dimensional TiC reinforment in a titanium matrix.[199] This *in-situ* solidification of carbide provided morphological control of the structure. The approach was to combine traditional ingot metallurgy plus solidification techniques to produce Ti-TiC composites. In this work, a series of Ti-TiC materials, with or without boron additions, were produced. Blended graphite and TiB_2 or boron powder was packed into holes drilled in the titanium rods which were then placed into graphite crucibles. Tantalum foil was wrapped around the crucible which was contained in a quartz tube to evenly heat the sample by induction. The melting was performed in an argon atmosphere to prevent

oxidation using an induction generator. To promote stirring, an ultrasonic vibrator was used. The crucible was dropped into water for quenching after holding for 1 minute in the molten state thus producing the ingots.[211]

1.5.1.2 Combustion Synthesis and 3A Process

Combustion synthesis is an attractive technique which use the exothermicity of solid state reactions to produce advanced materials.[200,201] It offers several advantages, such as relatively simple equipment, low energy requirements, short processing times, high product purity and the possibility of forming metastable or intermediate phases.[200] In the past, combustion synthesis has been used successfully to produce titanium carbide[202], titanium boride[203,204] , titanium carbide/titanium boride[205] and alumina/titanium diboride composites[206,207]. It is possible to use this process with suitable modifications to produce titanium matrix composites.[4] The number of individual compounds already synthesized by combustion synthesis is reported to be more than 350. Most of these are intermetallic and ceramic composites.[211]

Included under the classification of combustion synthesis are thermite-based reactions, which involve a metal reacting with a metallic or non-metallic oxide to form a more stable oxide of the reactant metal and the corresponding metal or nonmetal of the reactant oxide.[200] Thermite-based reactions have the advantage over many of the combustion synthesis reactions, which start with elemental components. Thermite-based reactions start with naturally occurring oxides, which are less expensive and more readily available than elemental powders. Additionally, the simultaneous production of multiple phases in thermite-based reactions makes it possible to produce composite materials with phases uniformly distributed in the materials.[200]

A recent variation of these classic thermite-based reactions is a novel pressureless reaction sintering process for the fabrication of alumina-aluminium alloys (3A).[200, 208-210] The 3A process involves the reaction sintering of intensively milled metal/Al or metal oxide/Al powder compacts, heat-treated in a nonoxidizing atmosphere, to form dense, interpenetrating alumina/aluminide composites. This exciting, new technique has been extended to the development

of some six or so new "3A materials", including aluminides of Ti, Fe, Nb, Mo, Zr, Ni, *etc.* The general reaction scheme is as follows:

$$\upsilon_A Al + \upsilon_B Me_u O_v \rightarrow \upsilon_C Me_x Al_y + Al_2O_3$$

where there is an initial reaction between the Al and metal oxide, known as an aluminothermic reduction reaction, followed by reaction of the remaining Al with the reduced metal to form the respective aluminide. By adjusting the starting powder composition, it is possible to vary the final composition of 3A materials over a wide compositional and volume fraction range. At intermetallic volume fractions >20%, the phases are continuous and hence exhibit an interpenetrating network.[200,210] The resulting composites exhibit the typical thermomechanical properties of Al_2O_3 (e.g., wear and oxidation resistance and high-temperature strength) along with an enhanced fracture toughness due to the interpenetrating ceramic/intermetallic network. The 3A process is usually carried out in the thermal explosion mode of combustion synthesis where the body is heated in a box furnace and the reaction occurs throughout the sample. The reaction kinetics, the amount of heat generated from the aluminothermic reduction reaction and aluminide synthesis, and final properties depend upon the particular 3A system being investigated.[210] Although this new technique appears to be a promising fabrication route for ceramic-intermetallic composites, a comprehensive understanding of the effects of the processing parameters on the reaction behaviour is lacking.

Gaus, *et al.*[200] have developed a continuum model of the 3A process to investigate the general system behaviour over the parameter ranges. They investigated the general behaviour of 3A process under the thermal explosion mode of synthesis by considering the effect of the dimensionless parameters associated with the rate of local heat generation, the activation energy, the rate of heat redistribution, the rate of heat transfer by convection, and the rate of heat transfer by radiation on the reaction behaviour. They found that, in order to produce high-density final products, uncontrolled reaction with high local temperatures should be avoided and the reaction may be better controlled by reducing the initial reactant concentrations, avoiding melting using small sample sizes, compacting at high pressures, and/or increasing the heat loss by using a high thermal conductivity

inert gas. The model was used to investigate the effects of processing conditions on the TiO_2/Al system. The model predictions indicate that for small samples, the TiO_2/Al process can be easily controlled by reducing the heating rate. For large samples, however, the predictions indicate that self-propagating (SHS) reaction fronts may develop.[201]

1.5.1.3 The XD (Exothermic Dispersion) Process

XD process[187] has been developed by Martin Marietta Corporation, Bethesda, MD, to fabricate *in-situ* ultrafine ceramic particle-reinforced metal matrix composites (MMCs). The basic principle of this technique is that the ultrafine ceramic particles are formed *in-situ* by exothermic reaction between elements or between the elements and the compounds. Using this approach, MMCs with a wide range of matrix materials (including aluminium, iron, copper, lead, nickel and titanium) and second-phase particles (including borides, carbides, nitides, oxides and their mixtures) can be produced.[190] Ma and Tjong[190] reported *in-situ* fabrication of several TiB_2 reinforced Al matrix composites from TiO_2 (Ti)-Al-B (B_2O_3) using XD technique. In their process, the powders with nominal compositions were ball milled in alcohol for 8 hours and then dried. The cold-compacted powder mixture was heated to above 800°C in a vacuum and maintained for 10 minutes, then cooled down to 600°C and hot pressed. The pressed billets were extruded at 420°C. Ma and Tjong investigated the reaction mechanisms for *in-situ* particulate formation and the microstructural aspects and mechanical properties of these composites. They found that TiB_2 particulates were formed *in-situ* in the aluminium matrix through the reaction of Ti and B in Ti-Al-B, TiO_2 and B in TiO_2-Al-B, and TiO_2 and B_2O_3 in TiO_2-Al-B_2O_3 systems. The size and shape of TiB_2 particulates were mainly controlled by the diffusion of Ti in molten aluminium. The formation or elimination of the Al_3Ti was determined by both nucleation of TiB_2 and the diffusion of Ti. The Al_2O_3-TiB_2/Al composite fabricated from the TiO_2-Al-B system exhibited excellent mechanical properties among the Ti-Al-B, TiO_2-Al-B, and TiO_2-Al-B_2O_3 systems due to the elimination of Al_3Ti and to the fine size of *in-situ* particulates. The yielding strength of the composites appeared to increase with increasing TiB_2 content. They also found that the incorporation of CuO into the TiO_2-Al-B system did not affect the

reaction process of the system. The strength of the composite was significantly enhanced due to the matrix strengthening by Al_2Cu precipitates.

Titanium and its alloys are highly susceptible to interstitial oxygen contamination and, therefore, they must be processed under an inert atmosphere or vacuum. Furthermore, secondary processing requires complex canning or pack configuration as well as expensive die materials.[211] These problems can be obviated in the XD process.[211] The patented XD technology is based on sustained high temperature synthesis. The technology when applied to TiAl-TiB_2 composites, requires blending and compacting of elemental powders of boron, titanium and aluminium. When ignited, a flame front passes through and spontaneously forms titanium aluminide and titanium diboride. Because of the *in-situ* development of reinforcements, the process eliminates oxide formation that could weaken the interface between the reinforcement and the matrix.[211] Master alloys with as high as 20-75 vol% of TiB_2 can be added to any compatible matrix material to achieve required levels of reinforcement. Composites containing titanium diboride particles introduced via XD processing offer substantial grain refinement and improved microstructural uniformity compared with un-reinforced TiAl.

The production of a variety of metal matrix composites by the XD process has been reported including matrices of Ti, TiAl and Ti_3Al. The reinforcing phases include borides, nitrides and carbides, some in both particulate or platelet form and also as whiskers produced *in-situ.*[188] Research now in progress is focused on the "designer microstructure" containing hard phases and whiskers for creep resistance. In future, XD titanium MMCs may be considered for a host of applications: structural applications include compressor cases, vanes, missile fins and structural brackets; rotating applications involve turbine disks, shaft housing, compressor vanes and turbocharger wheels.[211]

Even though the XD process is inexpensive, there are some possible limitations with regard to chemical and thermal stability of a dispersed phase.[211] If both elemental constituents of the particulate phase have a high diffusivity in the matrix phase, then particle coarsening may occur at elevated temperatures.[212] Large particles will grow at the expense of small particles leading to an increase

in the average interparticle spacing. The increase in interparticle spacing will then reduce the yielding strength of the composite. Different surface energies in the solid state versus the liquid may lead to changes in particle shape, thus adversely affecting the mechanical properties. Another possible problem may arise when the reaction between composite forming elements are less exothermic. In such cases, efforts to produce composites through this route might be unsuccessful. [211]

1.5.1.4 Combustion-Assisted Synthesis (CAS)

The combustion-assisted synthesis technique is a novel and relatively inexpensive technique for the production of titanium-based composites.[211] This technique involves the usual melting and casting of titanium in association with a combustion synthesis reaction. Using this technique it is possible to produce a "designer microstructure". In CAS the second phase reinforcements are formed *in-situ* and, therefore, the general problems encountered in powder metallurgical approaches and conventional molten metal techniques are avoided.

The CAS process for titanium composites preparation in general, consists of preparing the second phase reinforcements directly in the desired volume fraction in the titanium matrix.[211] The second phase forming constituents are first made into a compact. In the melting unit, when such a compact comes in direct contact with a small pool of liquid titanium, a combustion synthesis reaction is initiated in the compact. As a consequence of this, a very uniform dispersion of second phase particulate is obtained in the titanium matrix.

In CAS, the second phase reinforcements are formed *in-situ* and, therefore, the general problems encountered in powder metallurgical approaches and conventional molten metal techniques, are totally averted. However, the presence of reinforcements can drastically reduce the grain size of the matrix by pinning the grain boundary movement.[213] This *in-situ* process also resulted in a clean matrix/particle interface. The reduction in grain size and a clean matrix/particle interface is bound to influence the stiffness, strength and creep behaviour of the composites.[213]

Recently, Moore and Feng[214] reviewed Combustion (self propagating high temperature) synthesis (SHS) reactions and classified the SHS into (i) simple

reaction systems in which no other processing step, other than the SHS reaction, is considered; (ii) SHS reactions which involve simultaneous and/or subsequent densification process(es); (iii) SHS reactions coupled with vapour transport systems and those which synthesize specific products such as functionally-graded materials (FGM), thin films and coatings, and mechanically alloyed powders or those used to join dissimilar ceramics and/or intermetallics. They also compared the various mathematical models that have been developed to simulate and predict instabilities in propagating combustion synthesis reactions.

1.5.1.5 Other Techniques

In-situ TiB-reinforced Ti alloy composites have also been successfully produced by rapid solidification.[215] An approach has also been developed to fabricate discontinuously reinforced composites with an extremely fine grain size. Specifically, composites have been prepared by plasma melting an agglomerate consisting of two dissimilar powders that react to form a reinforcement within a metal matrix. *In-situ* reinforced Ti-matrix composites were successfully fabricated by plasma melting a powder agglomerate of Ti alloys and Zirconium diboride.[216] Extensive analysis of the microstructure using transmission electron microscopy (TEM) identified that the reinforcement which formed during the plasma melting process was titanium boride (TiB_2) in the form of whiskers generally <100 μm in diameter and with an aspect ratio of 10-50. Using vacuum plasma spray, Ti based composites with SiC, B_4C and TiB_2 reinforcements have been produced.

Takacs *et al.*[217] have reported *in-situ* displacement reaction between a metal oxide (Fe_3O_4) and a more reactive metal (Zn) forming a magnetic nanocomposites of small iron particles embedded in nonmagnetic zinc oxide matrix by using SPEX 8000 mixer mill. Xia *et al.*[218] developed an interlayer *in-situ* reaction process to produce laminated metal-intermetallic materials. They have produced $NiAl_3$ and Ni_2Al_3/Ni composites using this technique.

1.5.2 Various *In-Situ* MMCs

Various *in-situ* particulate reinforced composites have been prepared including aluminium based MMCs such as Al-TiB_2,[194,219] Al-Al_2O_3,[184] Al-TiC[220] and

Mo_2Si-SiC[221] etc, and Ti based MMCs. Feng and Froyen[222] developed Al-(Al_2O_3+TiB_2) composites through ball milling the Al, TiO_2 and B powder for 8 hours, compacting the powder blend followed by reactive sintering at 1100°C. They also studied the reaction mechanism. Chen and Chung[223] have developed an aluminium-matrix composite (or dispersion-strengthened metal) which is both ductile and strong. The tensile strength is even higher than those of aluminium-matrix composites containing SiC whiskers or particles, while the tensile ductility is almost as high as that of pure aluminium. This new composite contained about 5 vol% titanium aluminide ($TiAl_3$) particles of size about 1-2 μm and was formed *in-situ* from aluminium, titanium dioxide (TiO_2) particles and sodium hexafluoroaluminate (Na_3AlF_6). The *in-situ* formation caused the reinforcement ($TiAl_3$) to be fine and well-bonded to the aluminium matrix.

In recent years, there have been considerable efforts to produce *in-situ* nanocomposites by MA. In an interesting report, Naser *et al.*[224] showed that no grain growth occurs in the matrix close to its melting point when Cu and Mg are reinforced with nanocrystalline Al_2O_3 by MA. Wu *et al.*[225] reported the formation of nanocrystalline TiC in an amorphous Ti-Al matrix by MA. A solid state reaction leading to the formation of AlN and AlB_2 was reported by them during further processing of these nanocomposites. TiAl-Ti_5Si_3 nanocomposites have been reported by Liu *et al.*[226] by MA followed by thermal treatment. They attribute the formation of these nanocomposites to the crystallisation of the amorphous phase obtained by MA in the Ti-Al-Si system. These nanocrystalline compounds appear to be quite stable and no significant coarsening was observed even after heat treatment for 1 hour at 1000°C. Similar nanocomposites have been obtained by Senkov *et al.*[227] by MA and subsequent heat treatment of a mixture of TiH_2 and Al-Si alloy powders. Al_3Nb-NbC nanocomposites have been obtained by the MA of Al and Nb powders.[228] Interestingly, NbC in this case appears to have formed by the reaction of Nb with the methanol medium in which the milling was performed.

1.6 Objectives of the Work Undertaken in this Thesis

High energy mechanical milling (MM) or mechanical alloying (MA) have been used extensively in material processing as reviewed in the previous sections. However, the effects of the mechanical milling on the kinetics of solid state reactions has not yet been fully understood. This lack of understanding has been the bottle-neck for the application and further development of high energy milling techniques in a variety of materials processing applications. Although numerous studies have focused on this aspect through the study of ignition of a wide range of combustion reactions[2,4,88] using global/local modelling[36-38], and mathematical/numerical simulations[4,152,184], the results are far from being satisfactory. The objectives of the work undertaken in this study are (1) to establish the linkage between microstructure of mechanically milled powder and the reaction kinetics in metal-metal, and metal-oxide systems, (2) to understand the mechanism of enhancement of reaction kinetics by high energy mechanical milling.

1.7 References

1 H. Schmalzried, *Solid State Reaction*, 1995, Weinheim, Germany.

2 G.B. Schaffer, and McCormick: *Metall. Trans. A*, 1992, **23A,** 1285.

3 D.L. Zhang and D.Y. Ying, *Mater. Sci. Eng. A*, in press

4 B.S. Murty, and S. Ranganathan, *International Mater. Rev.*, 1998, **43(3)**, 101.

5 J.S. Benjamin, *Metall. Trans.*,1970, **1,** 2943.

6 F.H. Froes and I.L. Caolan (eds), *'Titanium '92 science and technology'*; 1993, Warrendale, PA. TMS.

7 C.C. Koch, *Ann. Rev. Mater. Sci.*,1998, **19,** 121.

8 V. Arnhold, J. Baumgarten and H.C. Neubing, *in Proc. 'World conf. On powder metallurgy, PM'90'*, Vol. **2**, 259-264; 1990, London, UK, The Institute of Metals.

9 R.B. Schwarz and C.C. Koch, *Appl. Phys. Lett.*, 1986, **49**, 146.

10 M. Abdellaoui and E. Gaffet, *J. Alloy Comp.*, 1994, **209**, 351.

11 M. Abdellaoui and Gaffet, *Acta Metall. Mater.*, 1995, **43**, 1087.

12 C. Suryanarayana and F.H. Froes: *J. Mater. Res.*, 1990, **5**, 1880.

13 J. Joardar, S.K. Pabi, and B.S. Murty, *in Proc. Int. Conf. On 'Recent advances in metallurgical processes'*, (ed. D.H. Sastry *at al.*), 647-652; 1997, New Delhi, India, New Age Int. Publ.

14 G.B. Schaffer and J.S. Forrester, *J. Mater. Sci.*, 1997, **32**, 3157.

15 C.H. Lee, M.Mori, T. Fukunaga, and U. Mizutani, *Jpn J. Appl. Phys.*, 1990, **29**, 540.

16 T. Klassen, U. Herr, and R.S. Averback, *Acta Mater.*, 1997, **45**, 2921.

17 A.P. Radlinski, A. Calka, B.W. Ninham, and W.A. Kaczmarek, *Mater. Sci. Eng.*, 1991, **A134**, 1346.

18 B.S. Murty, *'Study of amorphous phase formation by mechanical alloying in Ti based systems'*, PhD thesis, Indian Institute of Science, Bangalore, India, 1992.

19 R.L. White, 'The use of mechanical alloying in the manufacture of multifilamentary superconducting wire', PhD thesis, Stanford University, Stanford, CA, 1979.

20 J.S. Benjamin and T.E. Volin, *Metall. Trans.*, 1974, **5**, 1929.

21 J.S. Benjamin, *Sci. Am.*,1976, **234(6)** 40.

22 P.S. Gilman and J.S. Benjamin, *Ann. Rev. Mater. Sci.*, 1983, **13**, 279.

23 J.S. Benjamin, *in 'Modern developments in powder metallurgy'*, (ed. P.U. Gummeson and D.A. Gustafson), Vol. 21, 397-414; 1988, Princeton, NJ, American Powder Metallurgy Institute.

24 J.S. Benjamin, *in 'New materials by mechanical alloying'*, (ed. E. Arzt and L. Schultz), 3-18; 1989, Oberursel, Germany, Deutsche Gesellschaft fur Metallkunde.

25 D.R. Maurice and T.H. Courtney, *Metall. Trans. A*, 1990, **21A**, 289.

26 R.B. Schwarz, *Scr. Mater.*, 1996, **34**, 1.

27 B.B. Khina and F.H. Froes, *J. Met.*, 1992, **48(7)**, 36.

28 R. Watanabe, H. Hashimoto, and G.G. Lee, *Mater. Trans. JIM*, 1995, **36**, 123.

29 T.H. Courtney, *Mater. Trans. JIM*, 1995, **36**, 110.

30 D.R. Maurice and T.H. Courtney, *J. Met.*, 1992, **44(8)**, 10.

31 T.H. Courtney, D.R. Maurice, B.J.M. Aikin, R.W. Rydin, and T. Kosmac: *in 'Mechanical alloying for structural applications'*, (ed. J.J. de Barbadillo *at al.*), 1-13; 1993, Materials Park, OH, ASM International.

32 M. Magini and A. Lasonna, *Mater. Trans. JIM*, 1995, **36**, 123.

33 E. Gaffet, M. Abdellaoui, and N.M. Gaffet: *Mater. Trans. JIM*, 1995, **36**, 198.

34 W. Wang, 'Modeling and simulation of the dynamic process in high energy ball milling of metal powders.' PhD thesis, The University of Waikato, New Zealand, 2000.

35 A.K. Bhattacharya and E. Arzt, *Scr. Metall. Mater.*, 1993, **28**, 395.

36 D.R. Maurice and T.H. Courtney, *Metall. Mater. Trans. A*, 1994, **25A**, 147.

37 D.R. Maurice and T.H. Courtney, *Metall. Mater. Trans. A*, 1995, **26A**, 2431.

38 D.R. Maurice and T.H. Courtney, *Metall. Mater. Trans. A*, 1995, **26A**, 2437.

39 P.S. Gilman and W.D. Nix, *Metall. Trans. A*, 1981, **12A**, 813.

40 B.J.M. Aikin, T.H. Courtney, and D.R. Maurice, *Mater. Sci. Eng.*, 1991, **A147**, 229.

41 B.J.M. Aikin and T.H. Courtney, *Metall. Trans. A*, 1993, **24A**, 647.

42 B.J.M. Aikin and T.H. Courtney, *Metall. Trans. A*, 1993, **24A**, 2465.

43 R.M. Davis and C.C. Koch, *Scr. Metall.*, 1987, **21**, 305.

44 D.R. Maurice and T.H. Coutney, *Metall. Mater. Trans. A*, 1996, **27A**, 1973.

45 D. Basset, P. Matteazzi, and F. Miani, *Mater. Sci. Eng.*, 1994, **A174**, 71.

46 R. Watanabe, H. Hashimoto, and G.G. Lee, *Mater. Trans. JIM*, 1995, **36**, 102.

47 H. Hashimoto and R. Watanabe, *Mater. Trans. JIM*, 1990, **31**, 219.

48 H. Hashimoto and R. Watanabe, *Mater. Sci. Forum*, 1992, **88-90**, 89.

49 H. Hashimoto and R. Watanabe, *Mater. Trans. JIM*, 1994, **35**, 40.

50 P. Le Brun, L. Froyen, and L. Delaey, *Mater. Sci. Eng.*, 1993, **A161**, 75.

51 M.P. Dallimore and P.G. McCormick, *Mater. Trans. JIM*, 1996, **37**, 1091.

52 R.W. Rydin, D.R. Maurice, and T.H. Courtney, *Metall. Trans. A*, 1993, **24A**, 175.

53 T.M. Cook and T.H. Courtney, *Metall. Mater. Trans. A*, 1995, **26A**, 2389.

54 C.C. Koch, O.B. Cavin, C.G. McKamey, and J.O. Scorbrough, *Appl. Phys. Lett.*, 1983, **43**, 1017.

55 B.I. McDermott and C.C. Kock, *Scr. Metall.*, 1986, **20**, 669.

56 S.K. Pabi, J. Joardar, and B.S. Murty, J. Mater. Sci., 1996, 31, 3207.

57 L. Takacs, *JOM*, Jan. 2000, 12.

58 L. Lu and M.O. Lai, Mechanical Alloying, Kluwer Academic Publishers, U.S.A., 1998.

59 C.C. Koch, in 'Processing of metals and alloys, materials science and technology – a comprehensive treatment', (ed. R.W. Cahn), Vol. **15,** 193-245; Weinheim, VCH (1991).

60 E. Gaffet, N. Malhouroux, and M. Abdellaou, *J. Alloy Compd.*,1993, **194,** 339.

61 C.C. Koch, *Mater. Trans. JIM*, 1995, **36,** 85.

62 P.H. Shingu and K.N. Ishihara, *Mater. Trans. JIM*, 1995, **36,** 96.

63 C. Suryanarayana, *Metals and Mater.*, 1996, **2** 195.

64 R.C. Benn, J.S. Benjamin, and C.M. Austin, *in 'High temperature alloys – theory and design'*, (ed. J.O. Stiegler), 419-119; 1984, Warrendale, PA, TMS-AIME.

65 M.J. Fleetwood, *Mater. Sci. Technol.*, 1986, **2,** 1176.

66 R. Sundaresan and F.H. Froes, *J. Met.*, 1987, **39(8),** 22.

67 R.C. Benn and P.K. Mirchandent, *in 'New materials by mechanical alloying'*, (ed. E. Arzt and L. Schultz), 19-38; 1989, Oberursel, Germany, Deutsche Gesellschaft fur Metallkunde.

68 W.L. Johnson, *Prog. Mater. Sci.*, 1986, **30**, 81.

69 W.L. Johnson, *Mater. Sci. Eng.*, 1988, **A97**, 1.

70 K. Samer, *Phys. Rev.*, 1988, 161, 1.

71 L. Schultz, *Mater. Sci. Eng.*, 1984, **A97**, 15.

72 R.B. Schwarz, *Mater. Sci. Eng.*, 1988, **A97**, 71.

73 A.W. Weeber and H. Bakker, *Physica B*, 1988, **153**, 93.

74 C.C. Koch, *J. Non-Cryst. Solids*, 1990, **117/118**, 670.

75 B.S. Murty, *Bull. Mater. Sci.*, 1993, **16**, 1.

76 T. Benameur and A. Inoue, *Mater. Trans. JIM*, 1995, **36**, 240.

77 H.J. Fecht, *Mater. Trans. JIM*, 1995, **36**, 777.

78 C.C. Koch, *Scr. Mater.*, 1996, **34**, 21.

79 H Bakker, G.F. Zhou, and H. Yang, *Prog. Mater. Sci.*, 1995, **39**, 159.

80 J. Eckert, L. Schultz, and K. Urban, *Mater. Sci. Eng.*, 1991, **A133**, 393.

81 A.P. Radlinski and A. Calka, *Mater. Sci. Eng.*, 1991, **A134**, 1376.

82 H.J. Ahn and K.Y. Lee, *Mater. Trans. JIM*, 1995, **36**, 297.

83 C.C. Koch, *Nanostructured Mater.*, 1993, **2**, 109.

84 A.R. Yavari, *Mater. Trans. JIM*, 1995, **36**, 228.

85 A. Calka, *in Proc. 'Powder metallurgy world cong. 1993'*, (ed. Y Bando and K. Kosuge), 90-95; 1993, Kyoto, Japan, Japan Society of Powder and Powder Metallurgy.

86 L. Takacs, *in 'Nanophase and nanocomposite materials'*, (ed. K. Srihhar at al.), Vol. **286**, 413-418; 1993, Pittsburgh, PA, Materials Research Society.

87 G. Cocco, G. Mulas, and L. Schiffini, *Mater. Trans. JIM*, 1995, **36**, 150.

88 P.G. McCormick, *Mater. Trans. JIM*, 1995, **36**, 161.

89 M. Nagumo, *Mater. Trans. JIM*, 1995, **36**, 170.

90 T.H. Courtney and D.R. Maurice, *Scr. Mater.*, 1996, **34**, 5.

91 S.L. Hoyt, *AIME Trans.*, 1930. **89**, 9.

92 F.H. Froes, *J. Met.*, 1990, **42(12),** 24.

93 F.H. Froes, J.J. De Barbadillo, and C.S. Suryanarayana, *in 'Structural Applications of Mechanical Alloying'*, 9ed. F.H. Froes and J.J. de Barbadillo), 1-14; 1990, Materials Park, OH, ASM International.

94 R.B. Schwarz and W.L. Johnson, *Phys. Rev. Lett.*, 1983, **51**, 415.

95 X.L. Yeh, K. samwer, and W.L. Johnson, *Appl. Phys. Lett.*, 1983, **42**, 242.

96 M. Atzmon, J.D. Veerhoven, E.D. Gibson, and W.L. Johnson, *Appl. Phys. Lett.*, 1984, **45**, 1052.

97 L. Schultz, *in 'Rapidly quenched metals V'*, (ed. S. Steeb and H. Warlimon), 1585-1588; 1984, Amsterdam, North-Holland.

98 G.B. Schaffer and P.G. McCormick, *Appl. Phys. Lett.*, 1989, **55**, 45.

99 C.C. Koch, *Int. J. Mech.Chem.*. Mech. Alloy., 1994, **1**, 56.

100 R.M. Davis, MS thesis, North Carolina State University, Raleigh, NC, USA, 1988.

101 B.T. McDermott, MS thesis, North Carolina State University, Raleigh, NC, USA, 1988.

102 H. Kimura and M. Kimura, *in 'Solid state powder processing'*, (ed. A.H. Clauer and J.J. de Barbadillo), 365-377; 1990, Warrendale, PA, TMS-AIME.

103 A.B. Borzov and E.Y. Kaputkin, *in 'Mechanical alloying for structural applications'*, (ed. J.J. de Barbadillo *at al.*), Addendum; 1993, Materials Park, OH, ASM International.

104 W.E. Huhn, I.L. Friedman, W. Summers, and A. Szegvari, *in 'Metals handbook'*, 9th edn, Vol. 7, 56-70; 1984. Metals Park, OH, ASM.

105 E.T.B. Levinson, A.A. Kolesnikov, and I.V. Fine, *Mater. Sci. Forum*, 1992, **88-90**, 113.

106 A.E. Yermakov, E.E. Yurchikov, and V.A. Barinov, *Phys. Met. Metallogr.* (USSR), 1981, **52**, 50.

107 A.E. Yermakov, V.A. Barinov, and E.E. Yurchikov, *Phys. Met. Metallogr.* (USSR), 1982, **54**, 935.

108 M. Magini, N. Burgio, A. Iasonna, S. Martelli, F. Padella, and E. Paradiso, *J. Mater. Synth. Process.*, 1993, **1**, 135.

109 M. Magini, A Iasonna and F. Padella, *Scr. Mater.*, 1996, **34**, 13.

110 P.J. Miller, C.S. Coffey, and V.F. Devost, *J. Appl. Phys.*, 1986, **59**, 913.

111 W. Schlump and H. Grewe, *in 'New materials by mechanical alloying'*, (ed. E. Arzt and L. Schultz), 307-318; 1989, Obrursel, Germany, Deutsche Gesellschaft Fur Metallkunde.

112 K. Uenishi, K.F. Kobayashi, K.N. Ishihara, and P.M. Shingu, *Mater. Sci. Eng.*, 1991, **A134**, 1342.

113 B.S. Murty, M. Mohan Rao, and S. Ranganathan, *Nanostructured Mater.*, 1993, **3**, 459.

114 A.R. Yavari, P.J. Desre, and T. Benameur, *Phys. Rev. Lett.*, 1992, **68**, 2235.

115 A.R. Yavari, *Mater. Sci. Eng.*, 1994, **A179/180**, 20.

116 E. Ma, M. Atzmon, *Materials Chemistry & Physics*, 1995, **39(4)**, 249.

117 E. Ma, H.W. Sheng, J.H. He and P.J. Schilling, *Mater. Sci. Eng.*, 2000, **A286** 48.

118 C. Gente, M. Oehering, and R. Bormann, *Phys. Rev.*, 1993, **48B**, 13244.

119 J.Y. Huang, Y.K. Wu, A.Q. He, and H.Q. Ye, *Nanostructured Mater.*, 1994, **4**, 293.

120 J.Y. Huang, A.Q. He, and Y.K. Wu, *Nanostructured Mater.*, 1994, **4**, 1.

121 B.L. Huang, R.J. Perez, E.J. Lavernia, and M.J. Luton, *Nanostructured Mater.*, 1996, **7**, 69.

122 J.Y. Huang, Y.D. Yu, Y.K. Wu, D.X. Li, and H.Q. Ye, *Acta Mater.*, 1997, **45**, 113.

123 H.J. Fecht, G. Han, Z. Fu and W.L. Johnson, *J. Appl. Phys.*, 1990, **67,** 1744.

124 R.B. Schwarz, P.R. Petrich and C.K. Saw, *J. Non-Cryst. Solids*, 1985, **76**, 281.

125 D.L. Zhang and T.B. Massalski, Metall. Mater. Trans. A, 1998, **29A**, 2425.

126 K. Lu, Guo, F.Q., Zhao, Y.H. and Z.H. Jin, *Mater. Sci. Forum,* 1999, **312-314** 43.

127 L.J. Chen, *Mater. Sci. & Eng. R-Reports.* 2000, **29(5),** 115.

128 B.X. Liu, Z.J. Zhang and O. Jin, *J. Alloys Comp.,* 1998, **270**,186.

129 G.W. Yang, C. Lin, J.B. Liu, B.X. Liu, *J. Phys. D-Appl. Phys.* 1999, **32(2)** 79.

130 W.S. Lai, B.X. Liu, *J. Mater. Res.*, 1998, **13(6),** 1712.

131 B. Grushko, and D. Shechtman, *J. Appl. Phys.*, 1990, **67(6),** 2904.

132 U. Gosele and K.N. Tu, *J. Appl. Phys.*, 1989, **66(6),** 2619.

133 L. Takacs, and M.A. Susol, *J. Solid State Chem.*, 1996, **121**, 394.

134 G.B. Schaffer and P.G. McCormick, *Scr. Metall.*, 1989, **23**, 835.

135 G.B. Schaffer and P.G. McCormick, *J. Mater. Sci. Lett.*, 1990, **9**, 1014.

136 G.B. Schaffer and P.G. McCormick, *Metall. Trans. A*, 1990, **A21**, 2789.

137 G.B. Schaffer and P.G. McCormick, *Metall. Trans. A*, 1991, **A22**, 3019.

138 H. Yang and P.G. McCormick, *J. Solid State Chem.*, 1993, **107**, 258.

139 H. Yang and P.G. McCormick, *J. Mater. Sci. Lett.*, 1993 **12,** 1088.

140 H. Yang and P.G. McCormick, *J. Solid State Chem.*,1994, **110**, 136.

141 H. Yang and P.G. McCormick, *Metall. & Mater. Trans. B*, 1998, **29(2)**,449.

142 Y. Lu, R.C. Reno, and L. Takacs, *in 'Nanophase and nanocomposite materials'*, (ed. S. Komarneni *at al.*). Vol. **286**, 215-220; 1993, Pittsburgh, PA, Materials Research Society.

143 T. Nasu, K. Tokumitsu, K. Miyazawa, A.L. Greer, and K. Suzuki, *Mater. Sci. Forum*, 1999, **312-314,** 185.

144 M.S. El-Eskandarany, *Mater. Trans. JIM*, 1995, **36**, 182.

145 S.Q. Xi, J.E. Zhou, X.T. Wang and D.W. Zhang, *J. Mater. Sci. Lett.*, 1996, **15** 634.

146 P.G. McCormick, V.N. Wharton, M.M. Reyhain, and G.B. Schaffer, *in 'Microcomposites and nanophase materials'*, (ed. D.C.V. Aken *at al.*), 65-79; 1991, Warrandale, PA, TMS.

147 J. Ding, W.F. Miao, T. Truzuki, P.G. McCormick, and R. Street, *in 'Synthesis and processing of nanocrystalline powder'*, (ed. D.L. Bourell), 69-79; 1996, Warrendale, PA, TMS.

148 C. Suryanarayana, R. Sundaresan, and F.H. Froes, *Mater. Sci. Eng.*, 1992, **A150**, 117.

149 R.J. Perez, B. Huang, A.A. ahrif, and E.J. Lanernia, *in 'Synthesis and processing of nanocrystalline powder'*, (ed. D.L. Bourell), 273-280; 1996, Warrendale, PA, TMS.

150 B. Huang, J. Vallone, and M.J. Luton, *Nanostructured Mater.*, 1995, **5**, 631.

151 B.J.M. Aikin, R.M. Dickerson, D.T. Jayne, S. Farmer, and J.D. Whittenberger, *Scr. Metall. Mater.*, 1994, **30**, 119.

152 S.K. Pabi, D. Das, T.K. Mahapatra, and I. Manna, *Acta, Mater.*, 1988, **41**, 3501.

153 T.H. Courtney, J.C. Malzahn Kampe, J.K. Lee, D.R. Maurice, *Diffusion Analysis & Applications*, edited by A.D. Roming, Jr. and M.A. Dayananda, *The Minerals, Metals & Materials Siciety*, 1989, pp. 225-253.

154 R. Radhakrishnan, S. Bhaduri, and C.H. Hanegar, Jr, *J. Met.*, 1997, **49 (1)**, 41.

155 F. Cardellini, V. Contini, G. Mazzone, and M. Vittori, *Scr. Metall. Mater.*, 1993, **28**, 1035.

156 N.J. Welham, *Intermetallics,* 1998, **6(5)**, 363.

157 M. Oehring, Z.H. Yan, K. Hassen, and R. Bormann, *Phys. Stat. Solidi (a),* 1992, **131**, 671.

158 R.C. Baun, P.K. Mirchandani, and A.S. Watwe, *in 'Modern developments in powder metallurgy'*, Vol. **18**, 479-490; 1988, Princeton, NJ, American Powder Metal Industries.

159 K.Y. Lee, H.K. Cho, and J.H. Ahn, *J. Mater. Sci. Lett.*, 1996, **15**, 1324.

160 C. Suryanarayana, G.H. Chen, A. Frefer, and F.H. Froes, *Mater. Sci. Eng.*, 1992, **A158**, 93.

161 V. Simic, Z. Marinkovic, *J. Mater. Sci.*1998, **33,** 561.

162 D.L. Zhang, T.B. Massalski, and M.R. Paruchuri, *Metall. Mater. Trans. A*, 1994, **25A**, 73.

163 D.L. Zhang and D.Y. Ying, 'Formation of FCC titanium during heating high energy ball milled Al-Ti powders,' *Materials Letters*, in press.

164 D.Y. Ying and D.L. Zhang, *J. Alloys Comp.*, 2000, **311**, 275.

165 D.L. Zhang and D.Y. Ying, 'Solid state reaction in nanometer scaled diffusion couples prepared using high energy ball milling.' *Mater. Sci. Eng. A*, in press.

166 R. Bormann, in *MRS Symp. Proc.*, 1994, **343,** 169.

167 M.A. Morris and D.G. Morris, *Mater. Sci. Eng.*, 1991, **A136**, 59.

168 M.A. Morris and D.G. Morris, *Mater. Sci. Forum*, 1992, **88-90**, 529.

169 G.H. Fair and J.V. Wood, *Powder Metall.*, 1993, **36**, 123.

170 D.Y. Ying and D.L. Zhang, 'Effect of high energy ball milling on the solid state reactions in Al-25at%Ni powders,' *J. Mater. Sci. Tech.*, in press

171 D.L. Zhang and D.Y. Ying, *J. Metastable & Nanocrystalline Mater.* in press.

172 K. Barmak, C. Michaelsen, G. Lucadamo, *J. Mater. Res.*, 1997, **12(1)**, 133.

173 K. Barmak, K R Coffey, D A Rudman and S Foner, *J. Appl. Phys.*, 1990, **67**, 7313.

174 E. Ma, C.V. Thompson and L.A. Clevenger, *J. Appl. Phys.*, 1991, **69(4)**, 2211.

175 E. Ma, L.A. Clevenger and C.V. Thompson, *J. Mater. Res.*, 1992, **7**, 1350.

176 L.A. Clevenger and C.V. Thompson, *J. Appl. Phys.*, 1990, **67(3)**, 1325.

177 K.R. Coffey, L.A. Clevenger, K. Barmark, D.A. Rudman and C.V. Thompson, *Appl. Phys. Lett.*, 1989, **55(9)**, 852.

178 L.A. Clevenger, C.V. Thompson and R.C. Cammarata, *Appl. Phys. Lett.* 1988, **52(10)**, 795.

179 K.R. Coffey, K. Barmark, D.A. Rudman and S. Foner, *J. Appl. Phys.*, 1992, **72**, 1341.

180 C. Michaelsen, G. Lucadamo and K. Barmak, *J. Appl. Phys.*, 1996, **80 (12)** 6689.

181 C. Michaelsen, S Wohlert, R Borman and K Barmak, *Mater. Res. Soc. Symp. Proc.*, 1996, **343**, 245.

182 L.A. Clevenger, C.V. Thompson, R.R. de Avillev and E. Ma, *J. Vac. Sci. Technol.*, 1990, **A8**, 1566.

183 J.C. Lee, K.N. Subramanian, and Y. Kim, *J. Mater. Sci.*,1994, **29**, 1983.

184 P.C. Maity, S.C. Panigrahi and P.N. Chakraborty, *Scr. Metall.*, 1993, **28**, 549.

185 P.C. Maity, P.N. Chakraborty and S.C. Panigrahi, *J. Mater. Process. Tech.*, 1995, **53**, 857.

186 T.S. Srivatsan, *J. Mater. Sci.*, 1996, **31**, 1375.

187 A.R.C. Westwood, *Metall. Trans A.*, 1988, **19A**, 749.

188 L. Christodoulou, P.A. Parrish, and C.R. Crowe, *in Mater. Res. Soc. Symp. Proc.*, 1988, **120**, 29.

189 S. Ranganath, *'Process for Producing Particulate-Reinforced Titanium Matrix Composites'*, Patent filed, 22 Sept. 1994, Indian Patent Office (New Delhi), No. 1181/DEL/94.

190 Z.Y. Ma and S.C. Tjong, *Metall. & Mater. Trans. A*, 1997, **28(9)**,1931.

191 K. Subhash and K. Michael, *Mater. Sci. Eng.*, 1993, **A162**, 153.

192 R.W. Rice, *J. Mater. Sci.*, 1991, **26**, 6533.

193 A. Stanislav and A.S. Nagelberg, *J. Am. Ceram. Soc.*, 1992, **75**, 44.

194 A.K. Kuruvilla, K.S. Prasad and Y.R. Mahajan, *Scr. Metall.*, 1990, **24**, 873.

195 I. Gotman and M.J. Koczak, *Mater. Sci. Eng.*, 1994, **A187**, 189.

196 K.M. Lee and I.H. Moon, *Mater. Sci. Eng.*, 1994, **A185**, 165.

197 H.X. Peng, D.Z. Wang, L. Geng and C.K. Yao, *Scr. Materia*, 1997, **37(2)**, 199.

198 J. Chen, Z. Geng and B.A. Chin, *in Mater. Res. Soc. Symp. Proc.*, 1989, **133**, 447.

199 R. Zee, C. Yang, Y. Lin and B. Chin, *J. Mater. Sci.*, 1991, **26**, 3853.

200 S.P. Gaus, M.P. Harmer, H.M. Chan, H.S. Caram, and N. Claussen, *J. Am. Ceram. Soc.*,2000, **83(7)** 1599.

201 S.P. Gaus, M.P. Harmer, H.M. Chan, H.S. Caram, J. Bruhn, and N. Claussen, *J. Am. Ceram. Soc.*,2000, **83(7)** 1606.

202 J.B. Holt and Z.A. Munir, *J. Mater. Sci.*, 1986, **21,** 251.

203 J.W. McCauley, N.D. Corbin, T. Reseter and P. Wong, *Ceram. Eng. Sci. Proc.*, 1982, **3,** 538.

204 P.G. Zavistanos and J.R. Morris, *Ibid*, 1983, **4,** 624.

205 R.W. Rice, *Ibid.*, 1990, **11,** 1203.

206 S. Ranganathan and J. Subrahmanyam, *J. Mater. Sci. Lett.*, 1991, **10,** 1297.

207 S. Ranganathan and J. Subrahmanyam, *'Handbook of Advanced Materials Testing'*, (ed. N.P. Cheremisinoff and P.N. Cheremisinoff), Marcel Dekker Inc., NY, 1995, p.901.

208 N. Claussen, D.E. Garcia, and R. Jassen, *J. Mater. Res.*,1996, **11**, 2884.

209 D.E. Garcia, J. Bruhn, S. Schicker, R. Jassen, and N. Claussen, *Ceram. Trans.*, 1996, **79**, 219.

210 S. Schicker, D.E. Garcia, J. Bruhn, R. Jassen, and N. Claussen, *J. Am. Ceram. Soc.*, 1997, **80(9),** 2294.

211 S. Ranganathan, *J. Mater. Sci.*, 1997, **32,** 1.

212 D. Lewis, *'Metal matrix composites: Processing and interfaces'*, (ed. R.K. Everett and R.J. Arsenault), 1991, Academic Press, NY, p.121.

213 S. Ranganathan, T. Roy and R.S. Mishra, *Mater. Sci. Tech.*, 1996, **12**, 219.

214 J.J. Moore and H.J. Feng, *Prog. in Mater. Sci.*, 1995, **39(4-5),** 275.

215 R.J. Lederich, W.O. Soboyejo and T.S. Srivatasan, *J. Met.*, 1994, **46,** 68.

216 M.S. Thompson and V.C. Nardone, *Mater. Sci. Eng.*, 1991, **A144,** 121.

217 L. Takacs, M. Pardavi-Horvath, *J. Appl. Phys.* 1994, **75(10),** 15.

218 Z.H. Xia, J.H. Liu, S.Q. Zhu, and Y.Z. Zhao, *J. Mater. Sci.*, 1999, **34(15),** 3731.

219 R.M. Aikin, Jr. and L. Christodoulou, *Scr. Met. Mater.*, 1991, **25,** 9.

220 P. Sahoo and M.J. Koczak, *Mater. Sci. Eng.*, 1991, **A144,** 37.

221 C.H. Henager, Jr., J.L. Brimhall, and J.P. Hirth, *Mater. Sci. Eng.*, 1992, **A155,** 109.

222 C.F. Feng and L. Froyen, Composites: Part A, 2000, **31**, 385.

223 Y.Y. Chen, D.L. Chung, *J. Mater. Sci.,* 1995, **30(18),** 4609.

224 J. Naser, W. Reinhemann, and H. Ferkel, *Mater. Sci. Eng.*, 1997, **A234,** 467.

225 N.Q. Wu, J.M. Wu, G.X. Wang, and Z.Z. Li, *Mater. Lett.,* 1997, **32,** 259.

226 K. Liu, J. Zhang, J. Wang, and G. Chen, *Scr. Metall. Mater.*, 1997, **36,** 1113.

227 O.N. Senkov, F.H. Froes, and E.G. Baburai, *Scr. Mater.*, 1997, **37,** 575.

228 T. Kaneyoshi, T. Takahashi, Y. Hayashi, and M. Motayama, *in 'Advances in powder metallurgy and particulate materials'*, (ed. E.D. Capus and R.M. German), Vol. **7**, 421-429; 1992, Princeton, NJ, Metal Powder Industries Federation.

Chapter Two

Methods and Materials

Outlined in this chapter are the materials used, the method used for sample preparation and the techniques employed for analysing the samples during the course of the thesis work.

2.1 Materials and Experiments

2.1.1 Materials

The powder materials used in the experiments are listed in the Table 0-1 below.

Table 0-1. Materials used in the experiments

Materials	Manufacturer	Purity	Particle Size
Al	Johnson Mathey Comapny	99.8%	~ 50μm
Ti	VERAC TM Incorporated	99.5%	~ 150μm
Ni	Johnson Mathey GmbH	99.9%	~ 50μm
Cu	Johnson Mathey GmbH	99.5%	~ 150μm
CuO	Aldrich Chemical Company Inc.	>99 %	< 5 μm
TiO_2	Johnson Mathey Company	99.5%	2.0-3.0 μm

2.1.2 Milling Experiments

Most of the milling was carried out in a SPEX 8000 mill, as shown in Figure 0-1(a). Four stainless steel balls, each with a diameter of 12.8 mm and a mass of 8.25 g, together with 8 g of powder mixture were used in each run. Before milling, the powder mixture and the balls were placed in a hardened steel vial (as shown in Figure 0-1 (b)) which was then put in a glovebox. The glovebox was

firstly evacuated and then filled with high purity argon. About 0.2wt% of isopropyl alcohol was added into the powder mixture as process control agent (PCA) to prevent the powder from being stuck onto the milling balls and the vial wall. The vial was sealed under argon atmosphere. The powder was milled for different durations. The milling machine was fan cooled during milling. After some time of milling, some powders such as Al-TiO_2 powder became highly flammable and so the vial must be opened inside the glovebox filled with argon.

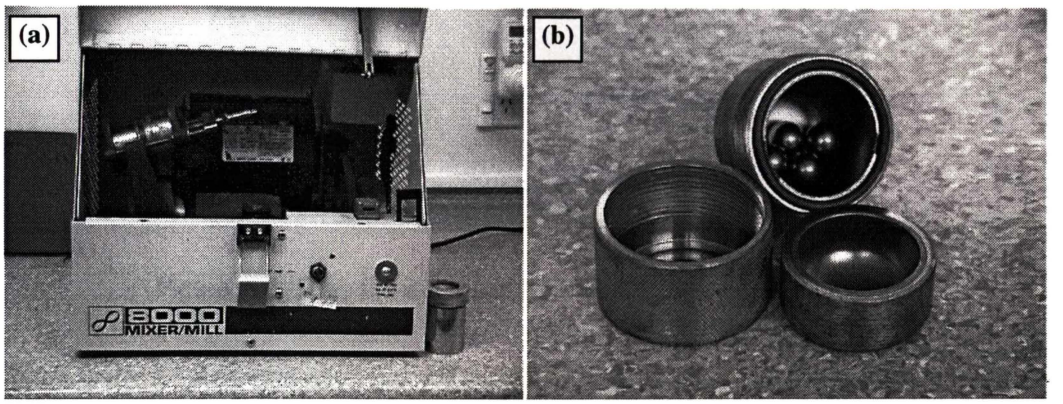

Figure 2-1. (a) SPEX 8000 Mixer/Mill and (b) the vial used in milling experiments.

Part of the powder used in this study was produced by a Split Discus mill, as shown in Figure 2-2. About 600 – 800 grams of powder mixture were used for each run. Before each run, the bowl was evacuated and refilled with argon.

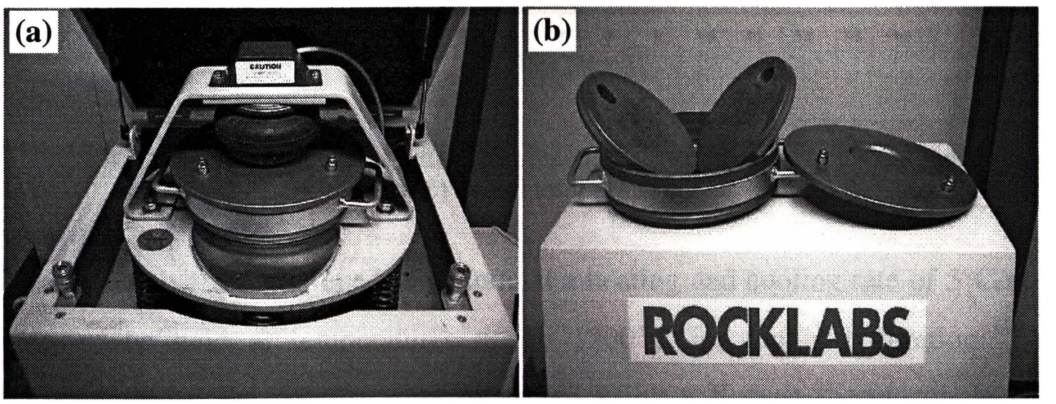

Figure 2-2. (a) Rocklab Split Discus Mill and (b) bowl and discus.

2.1.3 Heat Treatment Experiments

Heat treatment of the powder was carried out in a ceramic tube furnace (Ceramic Engineering, Australia, as shown in Figure 2-3), which was fitted with an

evacuation and argon refill system. The heat treatment was carried out under flowing argon.

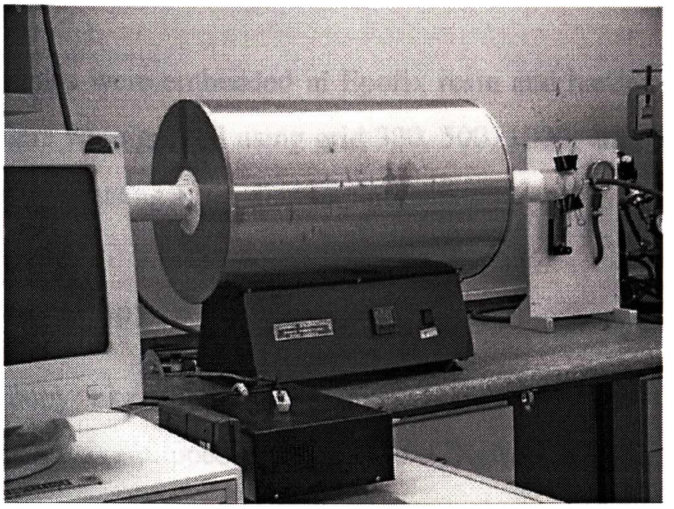

Figure 2-3. Tube furnace used for heat treatment of the powders.

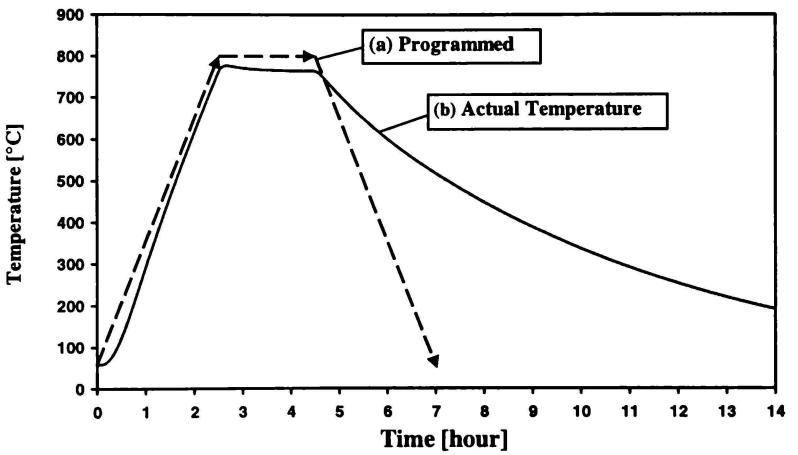

Figure 2-4. Typical furnace temperature-time trace: (a) programmed nominal temperature and (b) actual temperature.

The furnace was programmed to operate at a heating and cooling rate of 5°C/min and can be held at temperatures up to 1200°C for required duration. The temperatures of the powder were measured using a K type thermocouple and recorded by a data acquisition system using a PC. A typical temperature trace is shown in Figure 2-4.

The temperature of the loose powders or cold compacted pellets during heat treatment was monitored by embedding a K type thermocouple in the powder or the pellet, and the temperature history was recorded using a personal computer.

2.2 Microstructure Characterization

2.2.1 Sample Preparation

The powder samples were embedded in Epofix resin and hardened for 24 hours. The resin cylinders were ground using grid 320, 500, 1000, and 4000 SiC papers, followed by polishing using 1 μm diamond polishing powder.

2.2.2 Optical Microscopy

Optical microscopy examination was carried out using an Olympus BX60 microscope, which was equipped with a Polaroid Digital Camera.

2.2.3 Scanning Electron Microscopy and EDAX

Microstructure characterisation of powders was also carried out using a Hitachi S4000 scanning electron microscope (SEM). Energy dispersive x-ray analysis (EDAX) was carried out using a Kevex microanalyser attachment.

2.2.4 Transmission Electron Microscopy

Microstructure characterisation of some metallic powders was also carried out using CM12 Transmission Electron Microscope (TEM) operated at 120 kV. To prepare the TEM samples, the powder samples were mixed with pure Al powder and then cold pressed into a solid pellet. The solid pellet was ground to about 100 μm by using grid 500 and 1000 SiC sand paper and then electrolytically polished using a Tenupol jet polisher.

2.2.5 Image Analysis

Image analysis was carried out using Scion Image, an image processing and analysis program for personal computers. It is based on the NIH Image and can be used to measure area, mean, centroid, perimeter, etc. It can also perform automated particle analysis and provide tools for measuring path lengths and

angles. Spatial calibration was performed to provide real area and length measurements.

2.2.6 X-ray Diffractometry

Powder x-ray diffraction (XRD) was performed using a Philip's X-pert system diffractometer with Cu K_α radiation and a graphite monochromator. The patterns were obtained using a 0.02° step size averaging for 5 seconds per increment. X-ray pattern analysis, α_2 elimination, smoothing and background subtraction were performed using a Philip's software package. Samples were scanned either as finely ground powders pressed into glass holders with sample space dimensions of 2x15x10 mm^3 or 0.2x15x10 mm^3 for small amount of powder samples. For the small quantity of powders collected after thermal analysis, double sided sellotapes were used to mount the powders on to a glass sample holder with a shallow depth of 0.2 mm.

2.3 Thermal Analysis

The thermal analysis was performed in a TA Instruments SDT 2960 Differential Thermal Analyser (DTA) under flowing argon at a rate of 150 ml/sec, and in a TA Instruments DSC 2920 Scanning Differential Calorimeter (DSC) under flowing argon at a rate of 50 ml/sec. The heating rates used was 20 °C/min for normal examination and ranged from 5 to 40 °C/min for the measurement of the activation energies using Kissinger's Method.

Chapter Three

Solid State Reactions in High Energy Milled Metallic Powders

3.1 Introduction

When a mixture of two ductile metal powders is milled using a high energy ball mill, a composite microstructure consisting of alternatively irregular or regular layers of the two metals gradually form in each particle of the powder.[1-3] The thickness of the layers decreases with increasing milling time. Facilitated by the intimate contacts between neighbouring layers, millions of micro-diffusion couples form in each of the powder particles. With continued milling, solid-state reactions may occur during milling at low temperatures as long as thermodynamic principles allow such reactions. It has been established that low temperature reaction is due to the enhancement of the reaction kinetics by introducing a large volume of structural defects such as grain dislocations and grain boundaries. When the solid-state reactions occur at low temperatures, very often they result in formation of metastable phases and amorphous phases. If the milling stops at some point prior to the beginning of the solid state reaction in milling, and the milled powder is heated up in a furnace, the solid state reactions will occur as long as the temperature is high enough and the two metals have a tendency to react. As the diffusion couples established through milling up to this point may have already had very small size and contain a large number of defects, the solid state reactions may be activated thermally at low temperatures as well. If this is the case, the solid-state reactions may again result in formation of metastable phases.[4] Due to the morphological similarity between composite particles produced using high energy ball milling and multilayer thin films produced using sputtering or

vapour deposition, the behaviours of diffusion couples in the two types of carriers are often comparable.[5-7]

Solid-state reactions during heating the ball milled powders are scientifically interesting, and understanding of them is essential in order to combine mechanical milling and thermal treatment effectively in powder material processing. The latter is technologically very important since being able to do so means more opportunities for lowering cost and increasing production rate. It has been reported that a variety of intermetallics[8-12] and metal matrix composites[13] have been obtained by using a combination of high energy milling with thermal treatment. The final products obtained depend largely on the underlying thermodynamics and the kinetics of the reaction system.[6,12]

In order to gain an in depth understanding on the effect of milling on the reaction kinetics, I started by investigating two metallic binary systems: Cu/Al and Ni/Al. For the Cu/Al system, the binary Al-Cu phase diagram shows several equilibrium intermediate phases, such as θ-$CuAl_2$ and γ-Cu_9Al_4, as well as terminal Al(Cu) and Cu(Al) solutions.[14] This means that when a Al/Cu diffusion couple is heated up to activate the solid state reaction between Al and Cu, there are several possibilities in terms of the first phase formed and the sequence of phase formation. Some research has been done to investigate solid-state reactions between Cu and Al under different conditions. Jiang *et. al.*[15] and Liu *et. al.*[16] studied the solid state reactions between Cu and Al during heating of Al/Cu multilayer thin films, and they found that θ-$CuAl_2$ was the first phase formed. The temperature required to activate the reaction in thin films was 157°C. Peng *et. al.*[17] investigated the solid state reactions between Cu and Al in Cu/Al laminate formed by cold rolling and they found that the first phase formed was also θ-$CuAl_2$. The diffusion couples in this case were bulk diffusion couples, and the temperature required to activate the reaction was 300°C. On the other hand, Lima *et. al.*[18] have shown that γ-Cu_9Al_4 intermediate phase can be formed by high energy ball milling of a Cu and Al powder mixture with a normal composition of 33at%Al for sufficiently long time. It was not clear whether this phase was the first phase to be formed during mechanical alloying.

Ni/Al is one of the well studied reaction couples, either in high energy ball milled powders[8-11,19-23] and cold rolled foils[24,25] or multilayer thin films.[26-34] One of the interesting observations made was the formation of Al_3Ni occurred in two separate stages. In the first stage, Al_3Ni nucleates at isolated positions in the interface and the nuclei grow laterally along the interface. In the second stage, the continuous layer of Al_3Ni at the interface grows in the transverse direction.[27,31,33] Experimental evidence for a two-stage process is provided not only by differential scanning calorimetry (DSC) and transmission electron microscopy (TEM), but also by X-ray diffraction (XRD) and electrical resistance measurements.[27,31,33] In the present study, I also select the Ni/Al system to investigate the effect of high energy ball milling on the solid state reaction kinetics with the understanding that the substantial amount of information from literature would allow us to have a greater insight of the relationship between powder milling and the solid state reaction kinetics. Special attention has been paid to the link between microstructure of the milled powder particles and the kinetics of nucleation-and-growth of Al_3Ni along the interface and that of the transverse growth of Al_3Ni into the grains.

The objective of the study in this chapter is to examine the microstructure evolution during high energy milling and the reactions during milling and subsequent heat treatment of Ni/Al and Cu/Al powders.

3.2 Al-Ni System

3.2.1 Microstructural Evolution During Milling

Figure 3-1 shows the SEM back scattered electron micrographs of the cross-sections of the particles in the Al-25at%Ni powders milled for different times. As shown in Figure 3-1 (a), after milling for 0.5 hour, most of the Ni particles were incorporated into the matrix of Al. At this stage of milling, most of the Ni particles still retain the original nearly spherical shapes. Occasionally, elongated Ni particles were also observed. After 2 hours of milling, most of the Ni particles have become elongated as shown in Figure 3-1 (b). At this stage of milling, there still existed a small fraction of free standing Ni particles which were

unincorporated into Al matrix. After 4 hours of milling, Al/Ni multi-layer structure was established with Ni layer thickness ranging from 100 nm to 8.5μm, as shown in Figure 3-1 (c) and Figure 3-2. The average thickness of Ni layers was estimated to be 200 nm. It was observed that the interfaces between Al and Ni were not smooth, and exhibited a saw tooth like morphology, as shown in Figure 3-2.

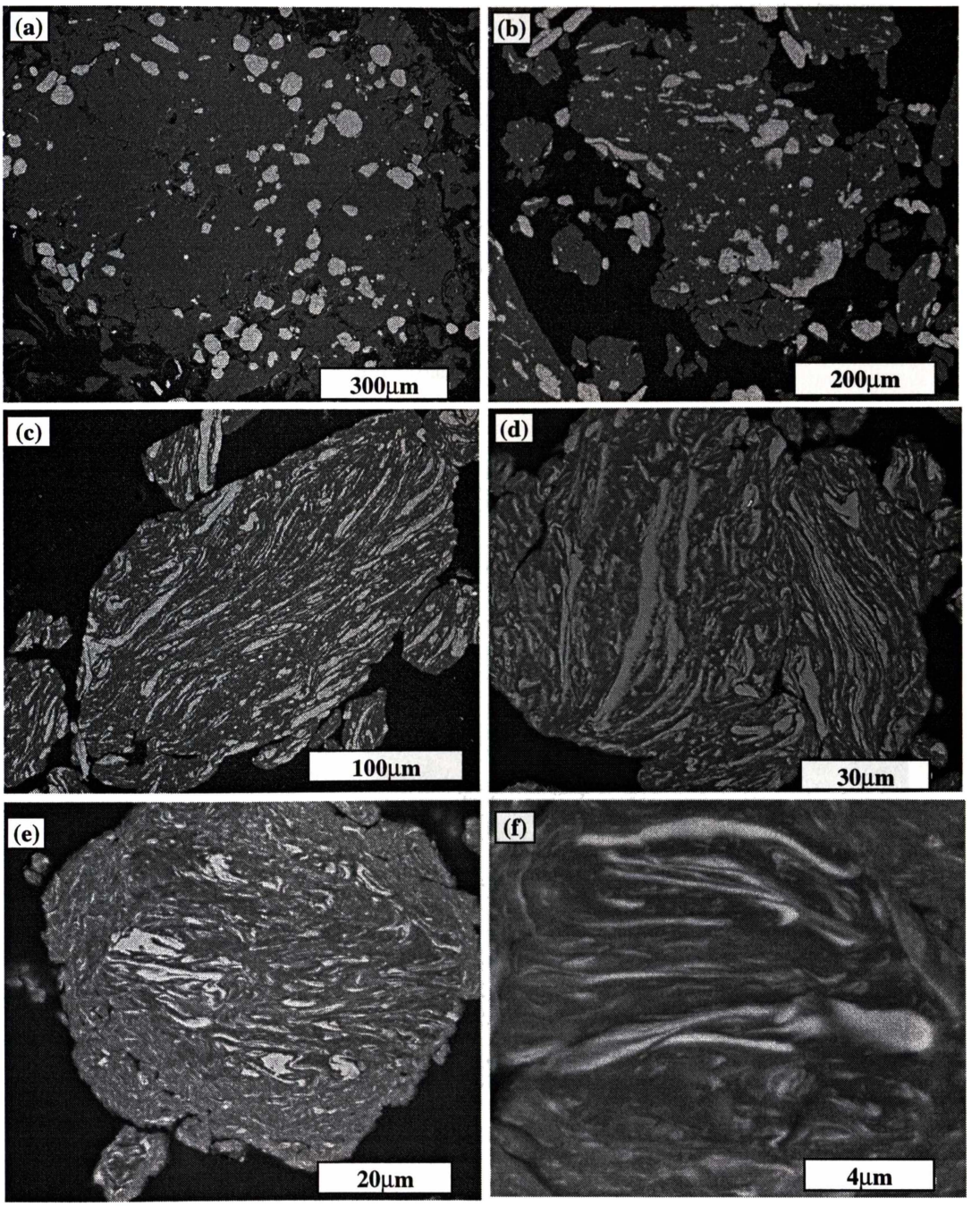

Figure 3-1. SEM back-scattered electron micrographs of the cross-sections of particles in the Al-25at%Ni powders milled for different times: (a) 0.5 hour, (b) 2 hours, (c) 4 hours, (d) 8 hours, (e) 15 hours and (f) 20 hours. The bright phase is Ni, and the dark phase is Al.

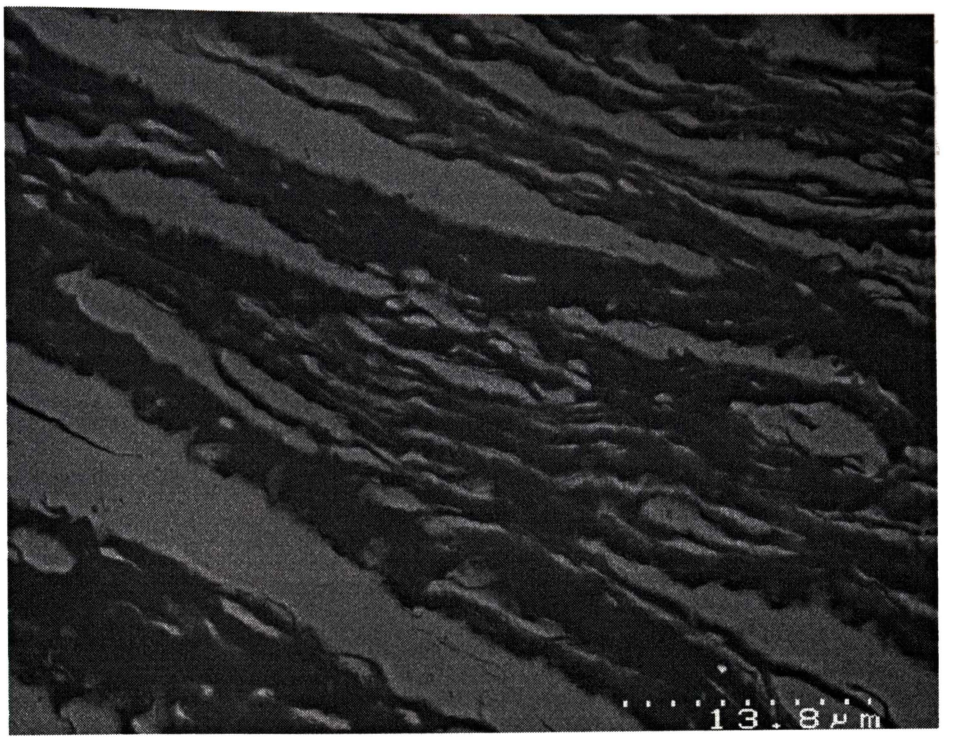

Figure 3-2. SEM back-scattered electron micrograph of the powder particles produced after milling for 4 hours.

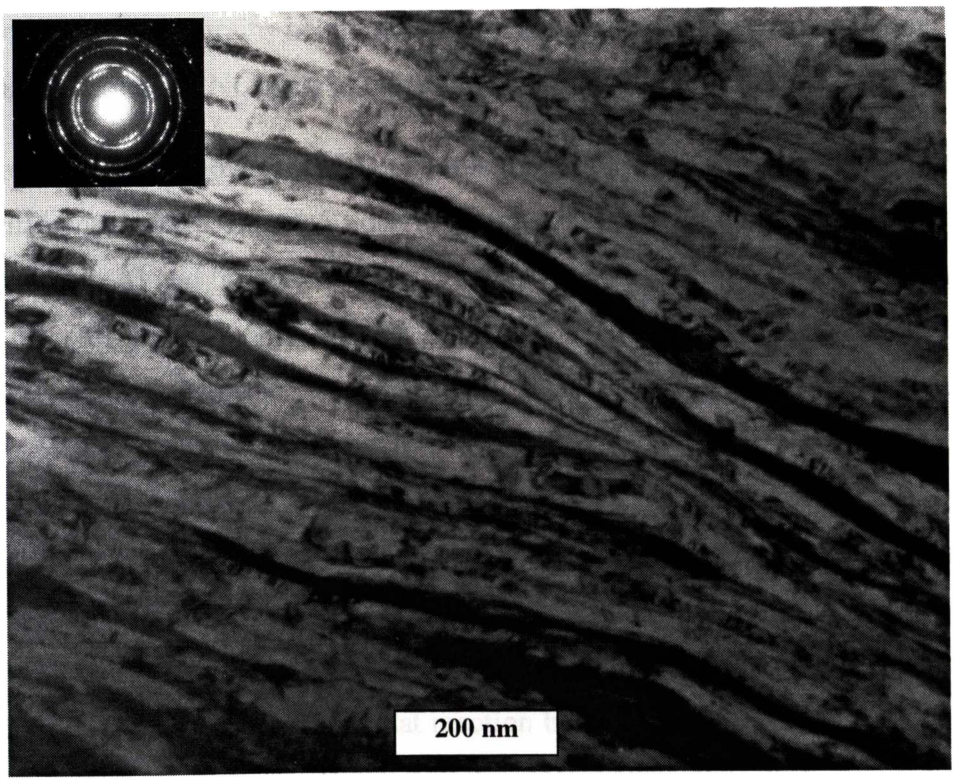

Figure 3-3. TEM bright field image of the cross-section of the 15 hours milled Al-25at%Ni powder particles. The dark phase is Ni and the light phase is Al.

After 8 hours of milling (Figure 3-1(d)), the Al/Ni multi-layer microstructure was refined. The Ni layer thickness ranged from 30 nm to 6.5 μm and the average Ni layer thickness was estimated to be around 70 nm. After 15 hours of milling, as shown in Figure 3-1 (e), the Al/Ni multi-layered structure was further refined. It was interesting to notice that the thickness of the Ni layers in the interior region was much larger than that in the region near the surface of the particles. There were many Ni layers with thickness ranged from 1 to 3 μm in the interior region. TEM observation on the 15 hours milled powder particles revealed that a majority of the powder particle had a multilayer structure with Ni layer thickness ranging from 10 to 30 nm, as shown in Figure 3-3. The average Ni layer thickness was estimated to be around 20 nm. After 20 hours of milling, the microstructure was significantly refined with the majority of Ni layers having a thickness in the sub-micron scale, though a small number of Ni layers having a thickness in the range of 1-2 μm were also observed in the interior region, as shown in Figure 3-1(f). TEM observation on the 20 hours milled powder particles showed that some of the Ni layers were broken into small fragments forming a microstructure of nanometer sized Ni grains being mixed with the grains of Al matrix structure. The average thickness of Ni layers at this point of milling was estimated to be 14 nm.

Figure 3-4 (a)-(e) show the XRD patterns of the powders produced after milling for different times. After 0.5 hour of milling, the XRD pattern (Figure 3-4 (a)) showed only Al and Ni peaks. After 15 hours of milling, the XRD pattern (Figure 3-4 (b)) still showed only Al and Ni peaks. The Ni peaks became relatively stronger than the Al peaks. The Al and Ni peaks also became substantially more wider. When the milling time increased from 15 to 20 hours, the XRD pattern (Figure 3-4 (c)) changed very little, and there was still no sign of extra peaks, indicating that Al and Ni did not react in a significant scale in this stage of milling. However, after 25 hours of milling, the XRD pattern (Figure 3-4 (d)) clearly showed many new peaks which were indexed as peaks of the intermetallic compound Al_3Ni. This indicates that reaction between Al and Ni occurred during milling from 20 to 25 hours, forming Al_3Ni. At this stage of milling, strong Al and Ni peaks were still present in the XRD pattern, indicating that a substantial amount of Al and Ni phases remained unreacted. After 30 hours of milling, the

characteristic peaks of Al and Ni elemental phases had disappeared from the XRD pattern, leaving only the peaks of Al_3Ni, as shown in Figure 3-4 (e).

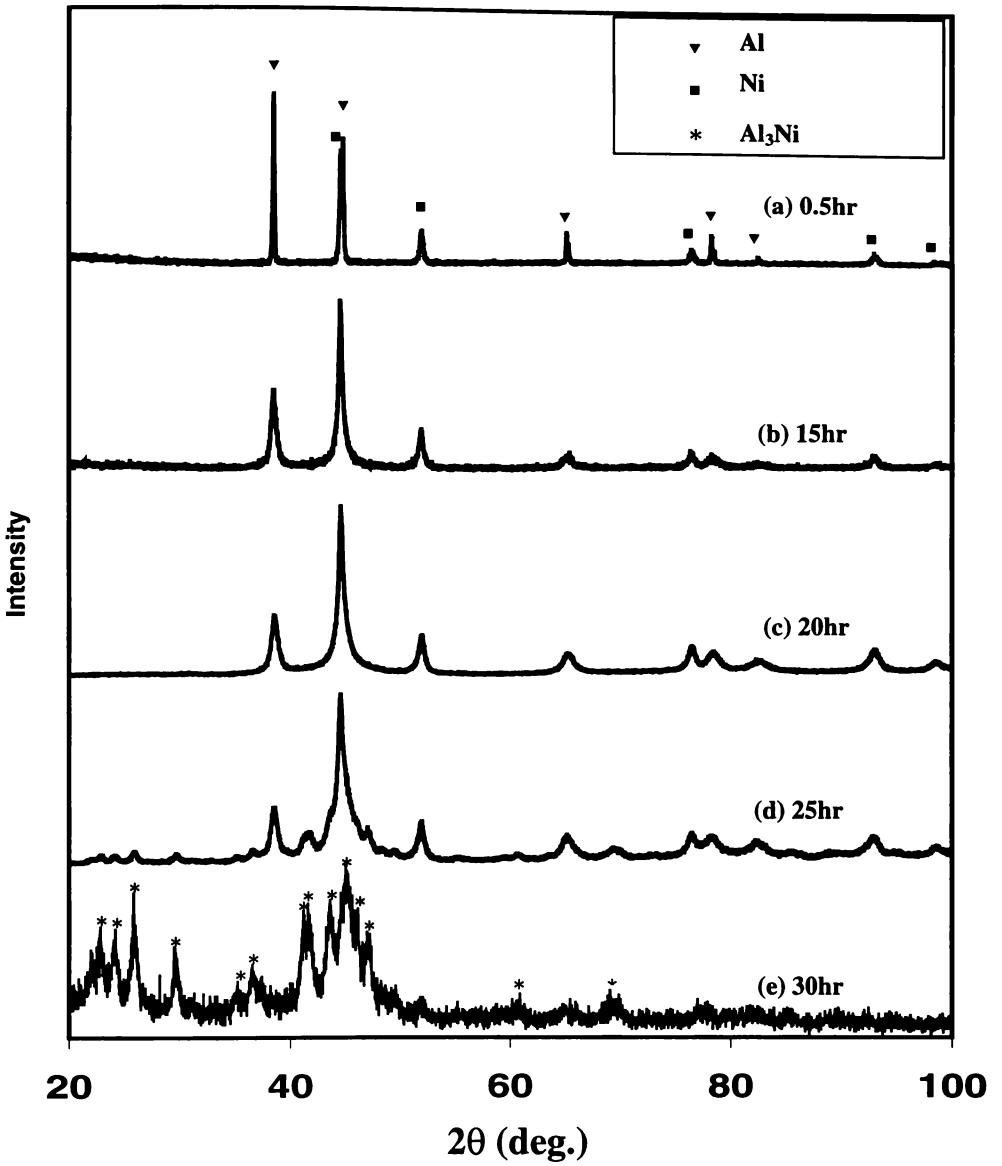

Figure 3-4. XRD patterns of the Al-25at%Ni powders produced after milled for different times: (a) 0.5 hours, (b) 15 hours, (c) 20 hours, (d) 25 hours and (e) 30 hours.

Figure 3-5 shows total area of the Ni/Al interfaces per mole of powder as a function of milling time. The interface area was measured from the cross-section SEM micrographs by using image analysis software. At least 5 typical micrographs were used for one powder sample. The measurement was based on the perimeter and the area fraction of the Ni phase. The total area measured was checked against the nominal volume fraction of Ni in the powder mixture with the intention to eliminate the bias in the selection of the micrographs. The result

showed that the interface area increased almost linearly as the milling time increased from 2 to 20 hours.

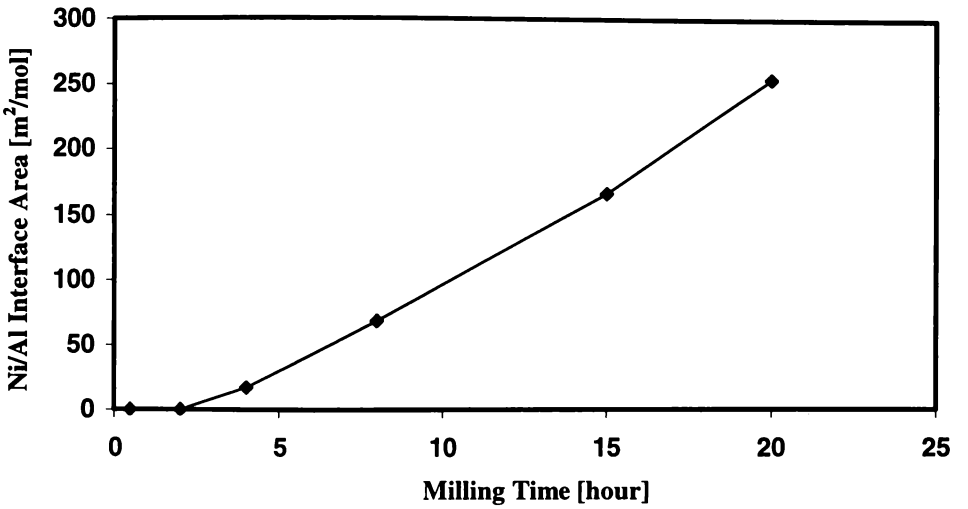

Figure 3-5. Al/Ni interface area as a function of milling time.

3.2.2 Reaction Kinetics During Heating

Figure 3-6 shows the DTA traces of the Al-25at%Ni powders produced by milling the Al and Ni powder mixture for 0.5 hour and 2 hours respectively.

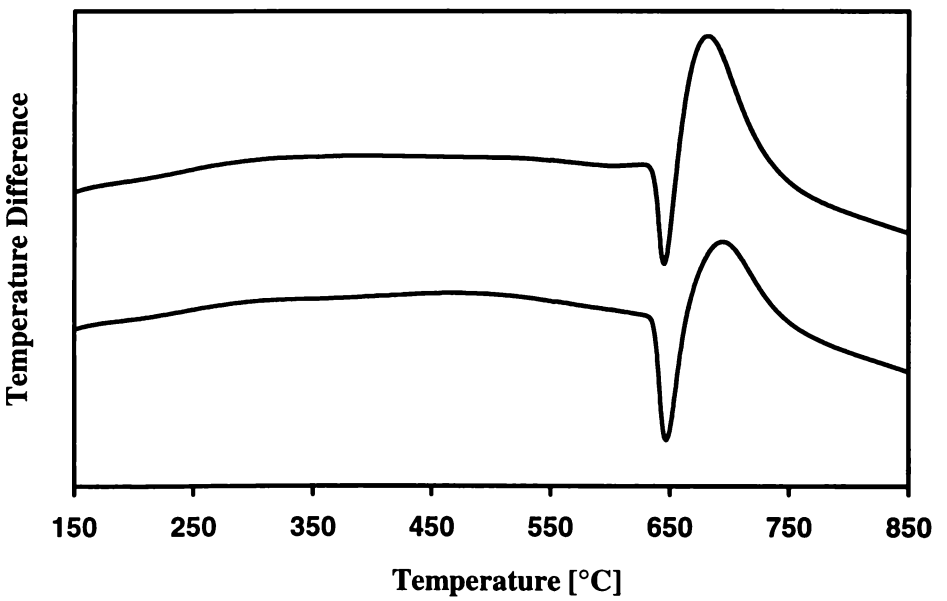

Figure 3-6. DTA traces of the powders produced after ball milling Al-25at%Ni powder mixture for (a) 0.5 hours and (b) 2 hours.

Both of the traces exhibited an endothermic peak and an exothermic peak. The two peaks were overlapped. The onset and peak temperatures of the endothermic peaks were approximately 645°C and 650°C respectively. The endothermic peak was most likely due to the melting of the Al rich phase. The peak temperature of the exothermic peak in trace (a) was 671°C and that in trace (b) was 697°C. XRD analysis of the 0.5 hour and 2 hour milled powders and heated to 800°C showed that all the powder was converted to Al_3Ni . This confirmed that the exothermic peak was due to the reaction between Al and Ni, forming intermetallic compound Al_3Ni.

Figure 3-7 shows DSC traces of the Al-25at%Ni powders produced by milling the Al and Ni powder mixture for different times ranging from 4 to 30 hours. As shown in Figure 3-7 (a), the DSC trace of 4 hours milled powder exhibited two exothermic peaks and an endothermic peak at a higher temperature. The onset and peak temperatures of the first exothermic peak were 230°C and 265°C respectively. The onset and peak temperatures of the second exothermic peak were approximately 360°C and 460°C respectively. The onset and peak temperatures of the endothermic peak were approximately 645°C and 650°C respectively. The endothermic peak was caused by melting of the residual Al rich phase left after the reaction between Al and Ni occurred. This residual Al rich phase was due to inhomogeneous mixing of the Al and Ni phases, as shown in Figure 3-1 (c). After the powder was milled for 8 hours, the exothermic peaks became sharper, and moved to lower temperatures, as shown in Figure 3-7 (b). The onset and peak temperatures of the first peak were lowered to 206°C and 258°C respectively, and its area also increased. The onset and peak temperatures of the second peak were lowered to 330°C and 425°C respectively. There was still a small endothermic peak at 650°C, which corresponded to melting of the residual Al rich phase. This shows that at this point of milling, the mixing was still not completely homogeneous, but much improved from 4 hour milling. After the powder was milled for 15 hours, the first exothermic peak became sharper and stronger, and its onset and peak temperatures were further lowered to 194°C and 218°C respectively, as shown in Figure 3-7 (c). In the mean time, the second exothermic peak became weaker, and its onset and peak temperatures were lowered to 310°C and 388°C respectively. To this point of milling, the

endothermic peak disappeared, indicating that the mixing of Al and Ni was completely homogeneous.

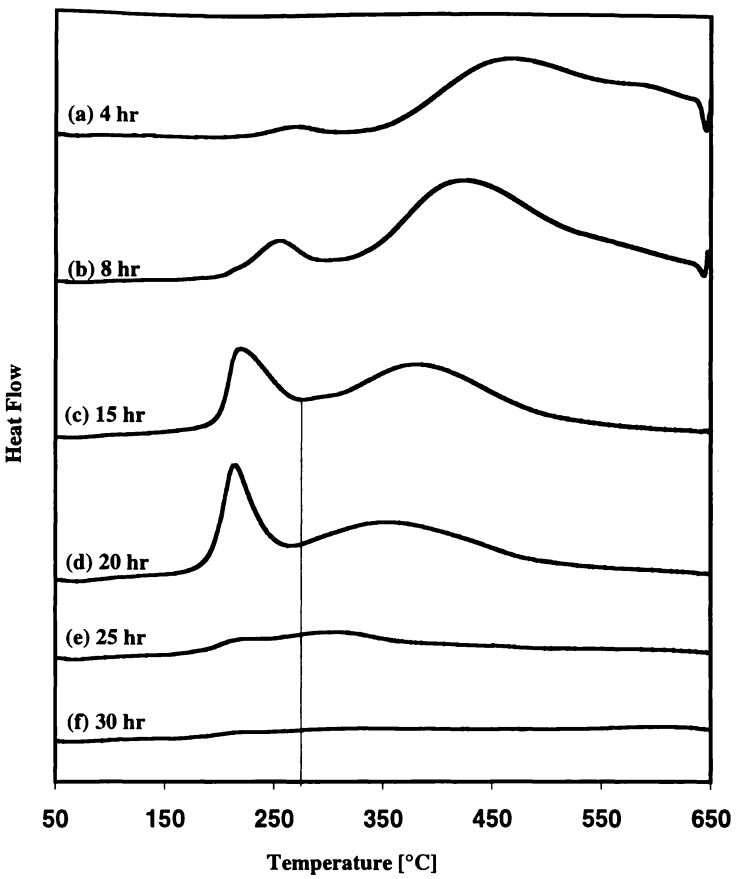

Figure 3-7. DSC traces of the Al-25at%Ni powders produced after milling for different times.

After the powder was milled for 20 hours, as shown in Figure 3-7 (d), the area of the first exothermic peak increased, while the area of the second exothermic peak decreased. The onset and peak temperatures of the first exothermic peak were lowered slightly to 185°C and 215°C respectively. The onset and peak temperatures of the second exothermic peak were lowered to 250°C and 360°C. After the powder was milled for 25 hours, the exothermic peaks became very small, as shown in Figure 3-7 (e). After 30 hours of milling, the DSC trace of the powder did not show any exothermic peaks, as shown in Figure 3-7 (f). This suggests that the majority of Al and Ni reacted during milling from 20 to 25 hours, and the reaction came to completion during milling from 25 to 30 hours.

In order to identify the reactions corresponding to the first and the second exothermic peaks respectively, the powders produced by heating the 15 hours milled powder to 270°C and 650°C respectively were analysed using XRD. Figure 3-8 (a) shows the XRD pattern of the powder produced by heating the 15 hours milled powder to 270°C. Other than strong Al and Ni peaks, this pattern also shows many peaks corresponding to Al_3Ni. This confirms that the first exothermic peak was caused by reaction between Al and Ni, forming Al_3Ni. Figure 3-8 (b) shows the XRD pattern of the powder produced by heating the 15 hour milled powder to 650°C. It shows only Al_3Ni peaks. This confirms that the second peak also corresponded to the reaction between Al and Ni, forming Al_3Ni. Therefore, both of the two exothermic peaks were caused by reaction between Al and Ni, forming Al_3Ni.

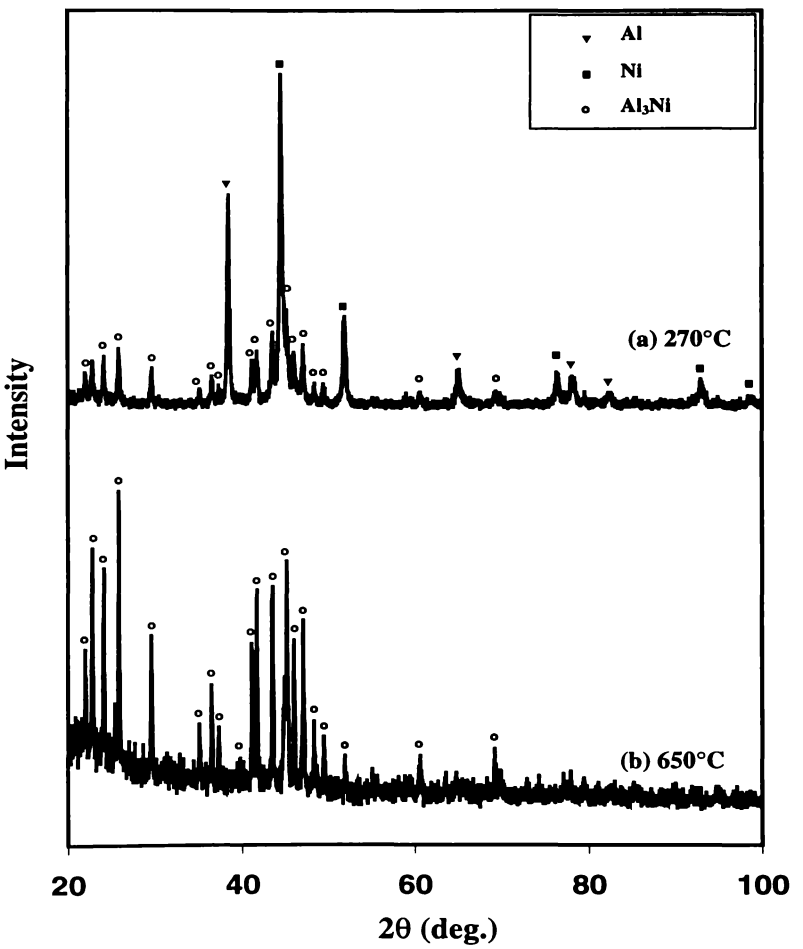

Figure 3-8. XRD patterns of the 15 hours milled powder heated to (a) 270°C and (b) 650°C.

Figure 3-9 shows the peak temperatures of the first and the second exothermic peaks respectively as a function of milling time. After 4 hours of milling, the first peak temperature was quickly lowered to 265°C and the second 460°C. While when the milling time increased from 4 hours to 20 hours, the first peak temperature was lowered to 220°C and the second to 400°C, but much slower.

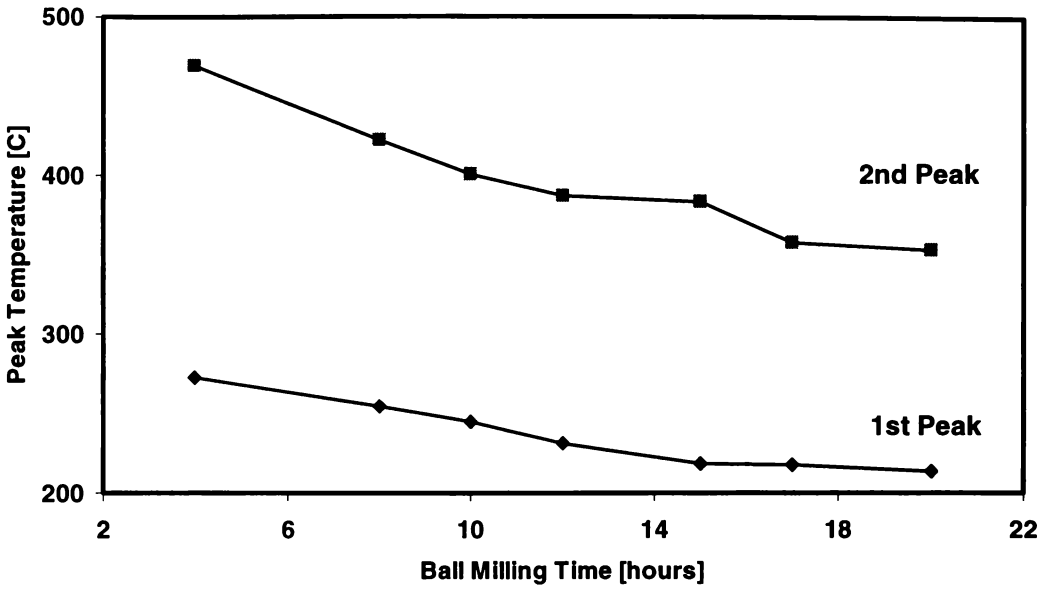

Figure 3-9. The peak temperatures of the first and second exothermic peaks as a function of ball milling time.

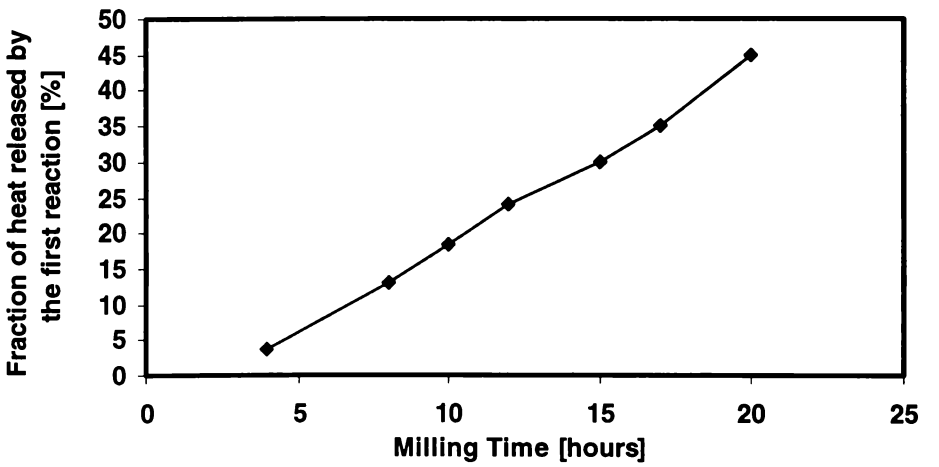

Figure 3-10. Fraction of the heat released by the first reaction as a function of milling time.

Figure 3-10 shows the fraction of heat released by the first reaction, which corresponds to the first peak of the DSC traces as shown in Figure 3-7, as a function of milling time. The first peak did not appear until 4 hours of milling. As shown in Figure 3-10, the fraction of the heat released by the first reaction increased almost linearly from 3% to 45% with increasing milling time from 4 to 20 hours.

The activation energies of the first and second reactions of the powders produced by milling for 4 hour or longer were estimated by studying the peak temperature change with changing heating rate during DSC analysis. The Kissinger plots which represent $\ln\left(\frac{R_t}{T_p^2}\right)$ as a function of $\frac{1000}{T_p}$, were established.[35] Here R_t is heating rate (in K/second), T_p is the peak temperature of the exothermic peak in Kelvin scale. Figure 3-11 shows the Kissinger plots for the first and the second reactions of the 8 hours milled powders. The slope of each Kissinger plot is equal to $\frac{Q}{k}$, where Q is the activation energy of the reaction in eV and k is the Boltzmann constant. Therefore, Q can be estimated by measuring the slopes of the plots.

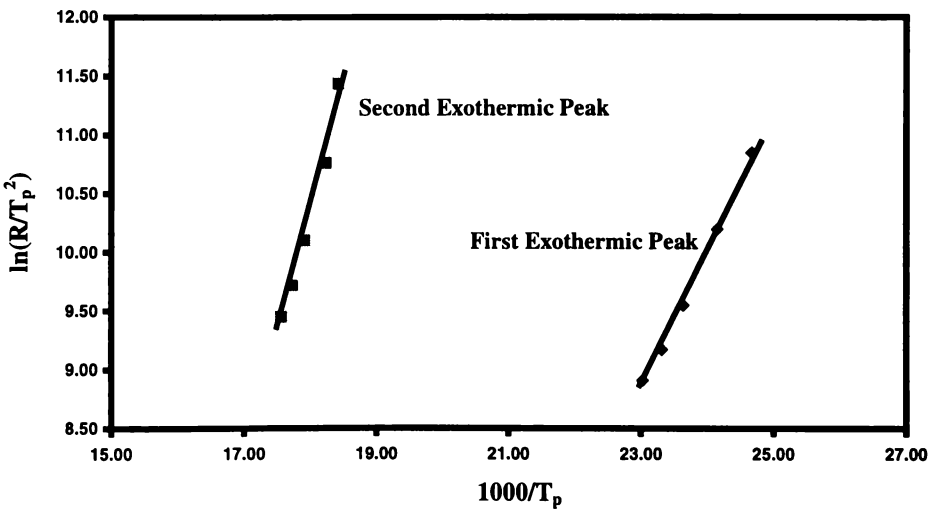

Figure 3-11. Kissinger plots for 8 hours milled Al-25at%Ni powder determined by using heating experiments in DSC.

Figure 3-12 shows the activation energies of the first and second reaction as a function of milling time respectively. It shows that the activation energy of the first reaction remained almost constant with increasing milling time while the activation energy of the second reaction almost linearly decreased with increasing milling time.

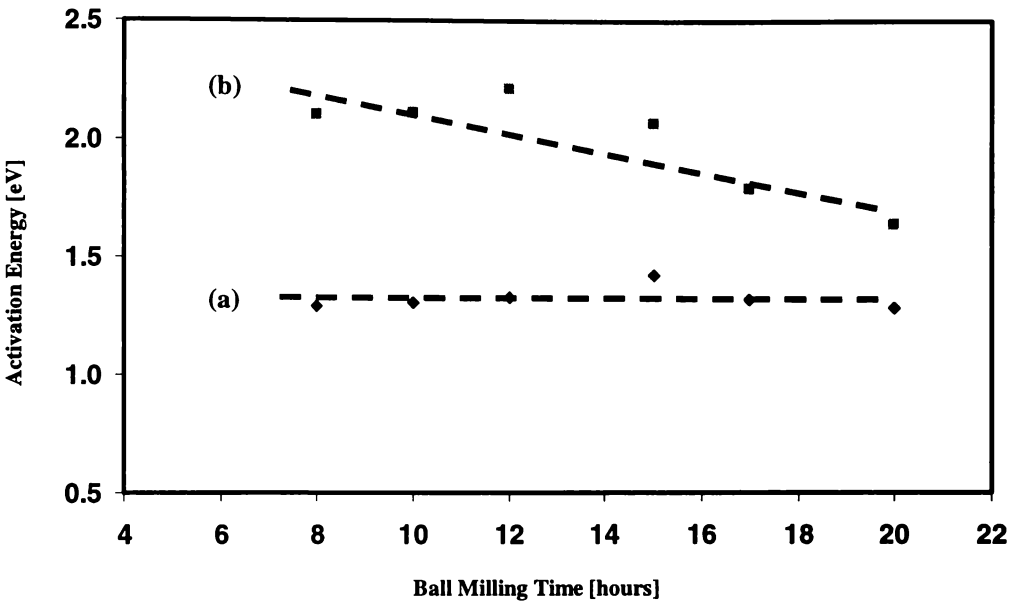

Figure 3-12. Activation energy of the reactions as a function of milling time, estimated by using the Kissinger method. (a) first reaction and (b) second reaction.

3.2.3 Discussions

3.2.3.1 Microstructural Evolution and Reaction Temperatures

Based on the microstructural examination of the milled powder particles, it is clear that the microstructural evolution of the Al/Ni powder particles during high energy milling can be divided into three stages:

- Initial stage (milling time: approximately 0-2 hours): Ni particles are incorporated into the Al matrix, and slightly flattened.
- Intermediate stage (milling time: approximately 2-20 hours): Ni particles are heavily deformed into long and thin plates, leading to the formation of

a multilayer Al/Ni composite structure in each of the powder particles. The layer thickness decreases with increasing milling time.

- Final stage (milling time: approximately 20-30 hours): The solid state reaction between Al and Ni occur in the process of milling, forming Al_3Ni. At the end of this stage, mechanical alloying is complete. Only in this stage, true mechanical alloying eventuates.

This microstructural evolution is very similar to what Aikin and Courtney[2] have observed during milling Cu and Cr and is typical for a ductile/ductile binary system.[1] It appears that the microstructure of the milled Al/Ni powder particles correlated well with the temperature required to activate the reaction, which is measured by using thermal analysis techniques. When the microstructure is in the initial stage, the temperature required to activate the reaction is still high, being higher than the melting temperature of the Al rich phase. This makes one think that melting of Al might be essential to activate the reaction even though the Al/Ni contact is rather intimate. The high reaction temperature can be attributed to the oxide layer present on the surface of as-received Ni powder. This oxide layer prevents reaction to initiate at low temperatures because of the low diffusivity of Al and Ni atoms in it. When the microstructure is in the intermediate stage, the temperature required to activate the reaction is 200°C lower, and melting of Al phase is certainly not a precondition for the activation of reaction. This significant decrease in reaction temperature can be attributed to three important microstructural factors:

- Formation of oxide free Al/Ni interfaces.
- Increase in Al/Ni interfacial area.
- Increase in the amount of structural defects inside Al and Ni phases.

Formation of oxide free Al/Ni interfaces as the powder particle microstructure evolves from the initial stage to intermediate stage is self evident. The Ni particles are heavily flattened while they are embedded in an Al matrix. So the extra area of interfaces is formed without any contamination. With the aspect ratio of Ni particles increasing by many times, the area of newly formed Al/Ni interfaces also increase by many times at the expense of breaking the original oxide layers

covering as-received Ni particles. This means that the presence of oxide phase become insignificant, although they may still decorate the interfaces.

Increase in Al/Ni interface area provides more area for nucleation of Al_3Ni, and thus leads to an increase in nucleation rate at a given temperature. This also causes a decrease of the reaction temperature. When the microstructure of the powder particles is mechanically transformed from the initial stage to the intermediate stage, the amount of plastic deformation of the Ni phase is very large. For Ni, this plastic deformation corresponds to cold working due to its high melting point (~1455°C) and relatively low temperatures at which the deformation occurs in the milling process (typically <350°C).[36,37] This means that a large amount of dislocations, vacancies are introduced in the Ni particles. This enhances the diffusivity of Ni. On the other hand, due to the plastic deformation at low temperatures, fracturing and cold welding, the density of dislocation and the amount of grain boundaries of the Al matrix also increase, leading to enhanced diffusivity of Al. At a given temperature, the enhanced diffusivity of Al and Ni will lead to higher nucleation rate and thus reduce the temperature required for the reaction to occur. It is noticed that within the intermediate microstructure, the reaction temperature decreases more slowly with decreasing the thickness of the Ni layers.

It is interesting to observe that a "core" and "shell" microstructure formed in the powder particles produced after 15 hours of milling, as shown in Figure 3-1(e). It was postulated that the core was formed due to work hardening.[38,39] It could be imagined that after a period of milling, the powder particles become considerably work hardened, and therefore the further plastic deformation is quite difficult unless recovery could occur. The instantaneous temperature increase during powder/ball collisions might permit recovery to occur in the shell region through moving dislocations to form subgrain boundaries and thus allow further plastic deformation to occur in this region. This inhomogeneous deformation of each powder particle would lead to a fine microstructure in the shell region, but a relatively coarser structure in the core region.

3.2.3.2 Nucleation and Growth of Al_3Ni

The most striking feature of the DSC curves obtained by heating the powder milled for more than 4 hours is the presence of two exothermic peaks. It has been determined that both of the peaks correspond to formation of Al_3Ni. Same phenomenon was also observed by Coffey *et al.*[40] while studying multilayer Nb/Al and Ni/amorphous-Si thin films and Ma *et al.*[27] while heating a multilayer Ni/Al thin film in DSC. Through a delicate combination of DSC experiments and transmission electron microscopy examination, Ma *et al.* confirmed that the low temperature peak corresponds to nucleation and lateral growth of Al_3Ni along Ni/Al interfaces, while the higher temperature peak corresponds to growth of the Al_3Ni layer in the transverse direction. It has been well recognized that the multilayer structure established in powder particles is analogous to that of multilayer thin films. Therefore, it can be postulated that the low temperature peak of the DSC trace of 4 or more hours milled powder is caused by nucleation and lateral growth of Al_3Ni at Ni/Al interfaces and the higher temperature one is caused by transverse growth of Al_3Ni. In other words, the first reaction which occurs during heating the milled Ni/Al powder is nucleation and lateral growth of Al_3Ni at Ni/Al interfaces, while the second reaction is transverse growth of the same phase, similar to the postulation made by Atzmon.[19]

It is reasonable to assume that the heat released by formation of a single phase is linearly proportional to the amount of that phase. This means that the fraction of the heat released by the first reaction represents the fraction of the Al_3Ni formed through heterogeneous nucleation and lateral growth. Figure 3-5 and Figure 3-10 show that the increase of the fraction of Al_3Ni formed through nucleation and lateral growth can be correlated with the increase of the total area of the Ni/Al interface. After plotting this fraction as a function of the interface area, as shown in Figure 3-13, it is evident that the fraction of the Al_3Ni is linearly proportional to the area of the Ni/Al interface. This suggests that the thickness of Al_3Ni layer formed in the first reaction is independent of milling time.

It is noticed that the total heat released by the nucleation and growth (including both lateral and transverse) of Al_3Ni in a unit weight of powder clearly decreases with increasing milling time from 4 to 20 hours. Since Al_3Ni is not detected in the

powder milled for up to 20 hours using XRD, formation of Al_3Ni during milling cannot be the primary reason for this decrease of the amount of total heat. The likely cause of this is formation of metastable Al(Ni) and Ni(Al) solid solution in the interface regions. Detailed characterisation of the powder is necessary to confirm the existence of such solid solutions in the as-milled powder.

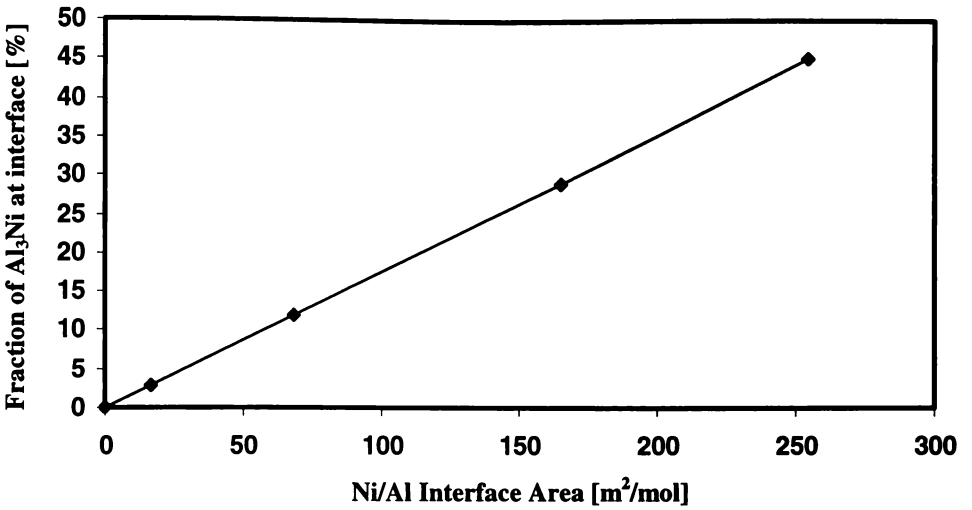

Figure 3-13. Fraction of Al_3Ni formed at the interface as a function of Al/Ni interface area.

Although its reliability and accuracy remains questionable,[41-43] the value of activation energy determined by Kissinger method has been widely used to measure the magnitude of the barrier of a solid state reaction.[30,32,43] The present study has also determined the activation energy of the reactions in the same way. As shown in Figure 3-12 (a), the activation energy of the nucleation and lateral growth of Al_3Ni phase remains approximately 1.32eV with increasing milling time. That is, this activation energy does not change with decreasing the layer thickness of Ni phase. This is hardly surprising, since the activation energy of the reaction at the interfaces is controlled by the state of the interface, not the layer thickness. On the other hand, this observation suggests that the state of Ni/Al interfaces is independent of the milling time. The value of activation energy of nucleation and lateral growth of Al_3Ni in the milled powder is slightly smaller than that in Al/Ni multilayer thin films determined by Ma *et. al.*[27] and Barmak *et al.*[33]. These differences can be attributed to the fact that high energy milling process may introduce more defects at the interfaces.

The activation energy for the transverse growth of the Al_3Ni phase decreases significantly from 2.0 eV to 1.6 eV with the increase of milling time from 4 to 20 hours, as shown in Figure 3-12. Although increase of milling time results in decrease in the thickness of Ni layers, the activation energy should be independent of layer thickness. The factors which influence the activation energy of the transverse growth are likely to be related to the fact that the layers are formed and further thinned by plastic deformation. Bhattacharya and Arzt[44] have demonstrated that plastic deformation played a very important role in controlling the diffusion process during mechanical alloying. Battezzati *et al.*[25] have shown that the activation energy for the reaction in the cold rolled Ni/Al multilayer foils is only 1.2±0.1 eV, clearly lower than that for the multilayer thin films.[27,33] In the present case, since the Ni layers are continuously thinned during milling, the amount of plastic deformation of each layer increases with milling time. It has been well known that the dislocation density in a metal is proportional to the plastic strain.[11,45,46] Therefore, with thinner layers, the activation energy of Ni diffusion becomes lower, leading to lower activation energy of the growth.

3.3 Cu-Al System

3.3.1 Microstructural Evolution During Milling

Figure 3-14(a) and (b) show the typical microstructure of particles in the Cu-14at%Al powder after being milled for 1 hour and 2 hours respectively. It was proved by EDAX analysis that the dark phase was Al and the light phase was Cu. After 1 hour of milling, an irregular multilayer structure consisting of alternating Al and Cu layers was formed in each powder particle as shown in Figure 3-14 (a). The thickness of Al layer ranges from 0.5μm to 5μm. A few thicker elongated pieces of Al phase with a thickness ranging from 10-20μm were also observed. While, after 2 hours of milling, Cu and Al phases were well mixed and the multilayer structure was more clearly defined, as shown in Figure 3-14 (b). The Al rich phase was still present in the microstructure even though the XRD pattern did not show any Al peaks, as will later be shown in Figure 3-16. The thickness of Al layers in 2 hours milled powder ranges from 0.05μm to 0.2μm. After 4 hours

of milling, the microstructure became much finer and could not be resolved using SEM.

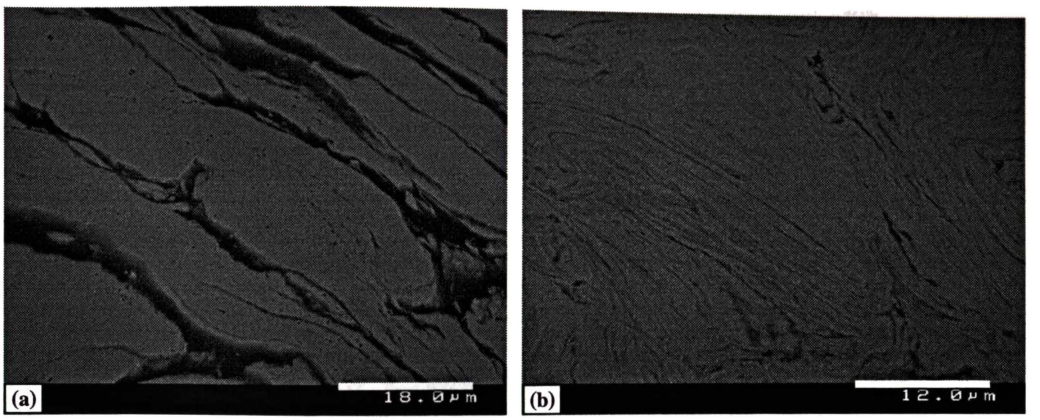

Figure 3-14. SEM micrographs of the cross-sections of powder particles produced by milling Cu-14at%Al powder mixture for (a) 1 hour and (b) 2 hours.

Figure 3-15 (a) and (b) show the typical microstructure of particles in the Cu-37at%Al powder after being milled for 1 hour and 2 hours respectively. Again, the dark phase is Al and the light phase is Cu.

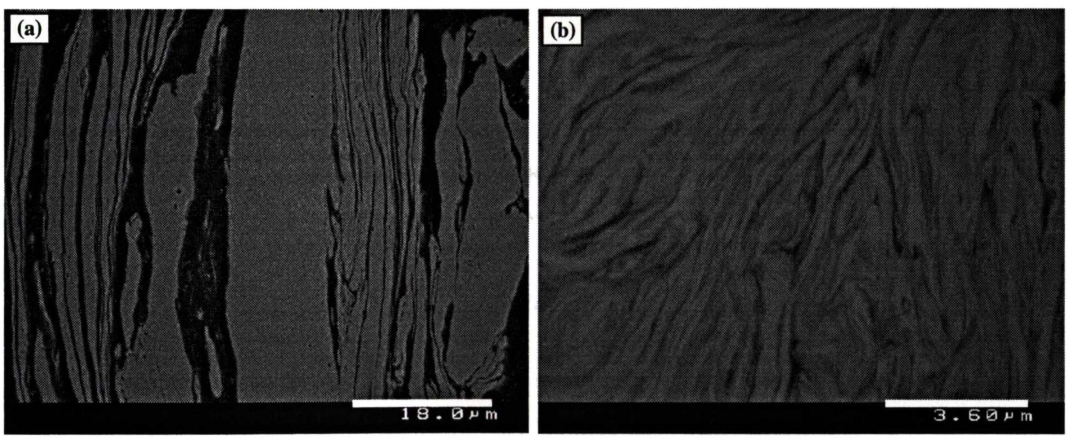

Figure 3-15. SEM micrographs of the cross-sections of powder particles produced by milling Cu-37at%Al powder mixture for (a) 1 hour and (b) 2 hours.

After 1 hour of milling, an irregular multilayer structure consisting of alternating Cu and Al layers formed in each powder particle as shown in Figure 3-15 (a). The layer thickness of Al phase ranged from 1 to 6 μm. A few larger elongated particles of Al with a thickness ranging from 10 to 20μm were also observed. After 2 hours of milling, the Cu and Al phases were well mixed and the multilayer structure was more clearly defined, as shown in Figure 3-15 (b). The thickness of

Al layers ranged from 0.05μm to 0.2μm. After 4 hours of milling, the multilayer structure became significantly finer and could not be clearly resolved using SEM.

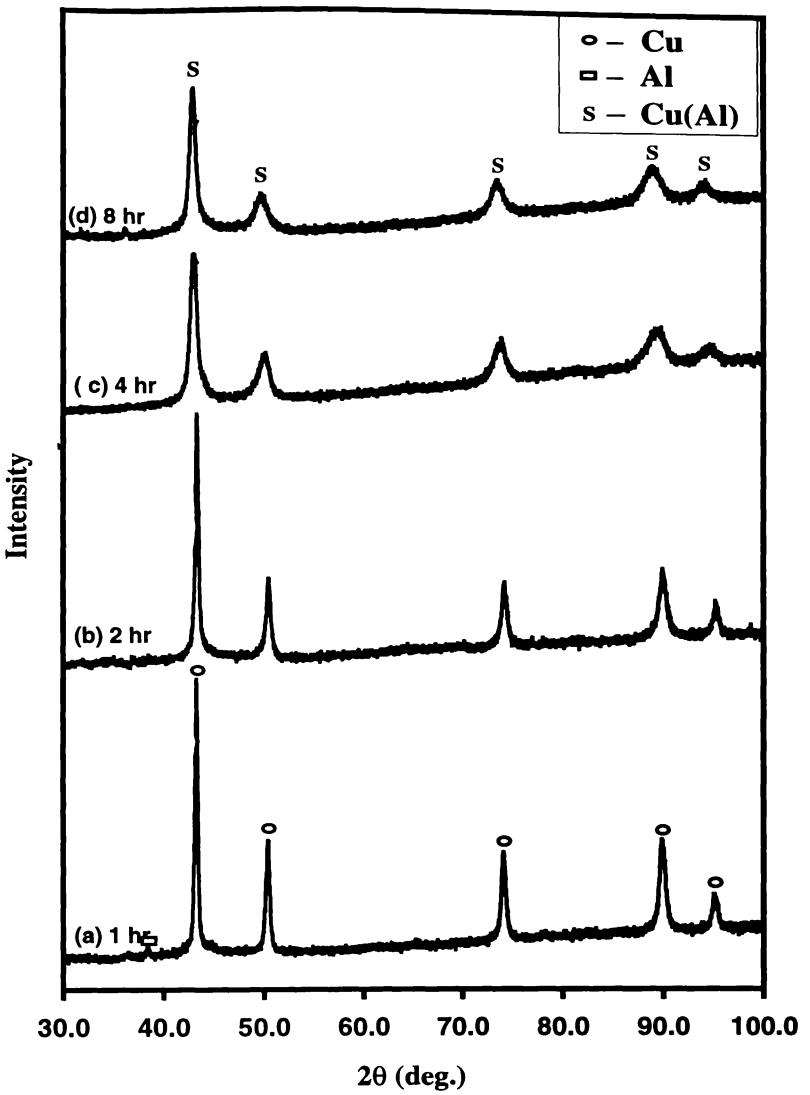

Figure 3-16. XRD patterns of the Cu-14at%Al powders produced after milled for different times.

Figure 3-16 shows the XRD patterns of the powder produced at different stages of milling a Cu/Al powder mixture with a composition of Cu-14at%Al. After 1 hour of milling, the XRD pattern (Figure 3-16 (a)) showed Cu peaks and the Al {111} peak. The positions of Cu and Al peaks remained the same as those of pure Cu and Al peaks, indicating no significant reaction occurred during this initial period of milling. After 2 hours of milling, the Al peak disappeared, and the positions of the Cu peaks still remained unchanged, as shown in Figure 3-16 (b). This indicates that the amount of Al diffusing into the Cu phase is insignificant. After 4

and 8 hours of milling, the position of Cu {111} peak shifted from $2\theta = 43.35°$ to $2\theta = 43.19°$ and $2\theta = 43.07°$ respectively. The final Cu peak shift corresponds to an increase of the Cu lattice parameter from 3.613Å to 3.639Å, i.e. by 0.7%. This lattice parameter increase suggests that a solid solution of Al in Cu forms as a result of mechanical alloying of Cu and Al. It was also noted that with increasing the milling time from 2 hours to 4 hours the Cu peaks became notably broader. The broadening of the XRD peaks was due to residual strain in the Cu rich phase and decrease of grain size. Neglecting the contribution of straining, the average grain size of the Cu rich phase was estimated using the half height width of Cu {111} peak and the Scherrer's equation.[47] The result showed that the average grain size of the Cu rich phase remained in 25 nm as the milling time increased from 1 to 2 hours and decreased substantially from 25 nm to 11 nm as the milling time increased from 2 to 4 hours. However, as the milling time increased from 4 to 8 hours, the average grain size remained almost unchanged.

Figure 3-17 shows the XRD patterns of the powders produced at different stages of milling a Cu/Al powder mixture with a composition of 37at%Al. After milling for 1 hour, the XRD pattern (Figure 3-17 (a)) shows Cu and Al peaks. The positions of the Cu and Al peaks were same as those of pure Cu and Al, indicating no significant reaction occurred during milling. After 2 hours of milling, the Cu and Al peaks remained in the pattern while two new peaks emerged as shown in Figure 3-17 (b). These peaks were indexed as γ-Cu_9Al_4 {330} and {600} peaks. After 4 hours of milling, the γ-Cu_9Al_4 peaks dominated the pattern as shown in Figure 3-17 (c). Although the Cu peaks still remained in the pattern, they became significantly weaker. After 8 hours of milling, the XRD pattern only showed γ-Cu_9Al_4 peaks, as shown in Figure 3-17 (d).

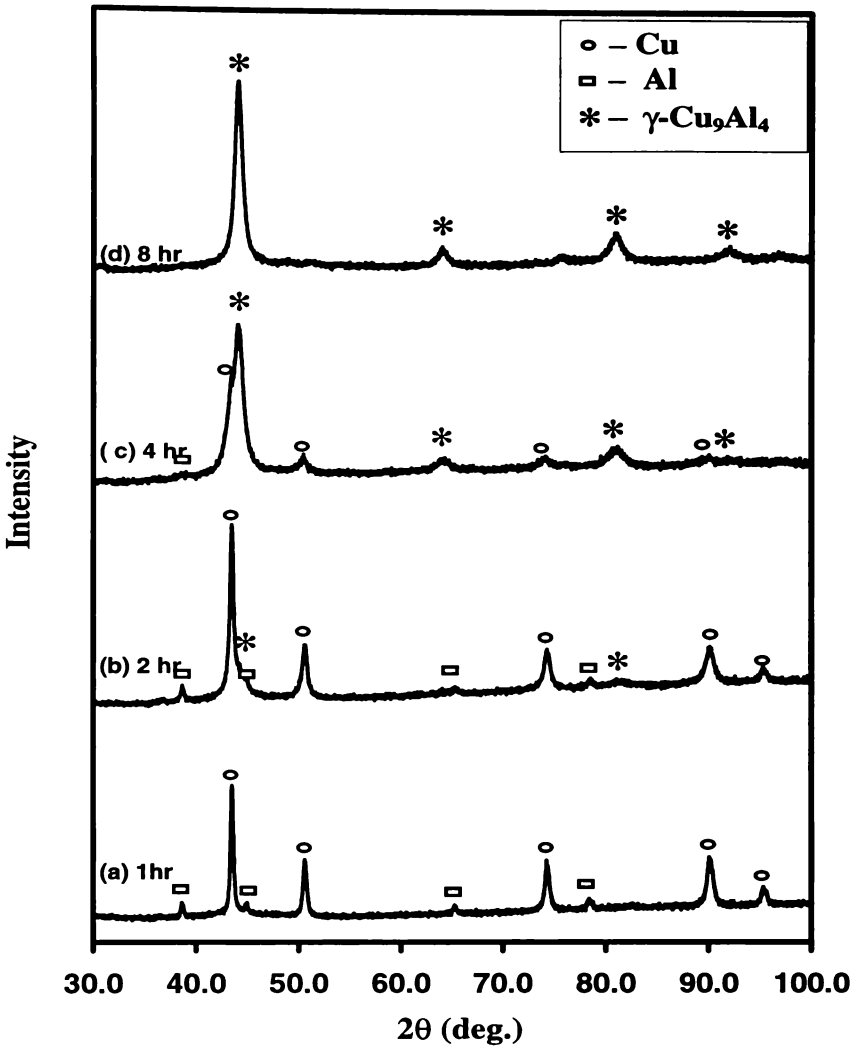

Figure 3-17. XRD patterns of the Cu-37at%Al powders produced after milled for different times.

3.3.2 Reaction Kinetics During Heating

Figure 3-18 shows DSC traces of Cu-14at%Al powders produced after milling for different times. As shown in Figure 3-18 (a), the DSC trace of 1 hour milled powder exhibited two overlapping exothermic peaks and an endothermic peak at high temperatures. The first exothermic peak was rather small and its onset and peak temperatures were approximately 105°C and 150°C respectively. The second exothermic peak was very large and broad, and its onset and peak temperature were approximately 150°C and 300°C respectively. The endothermic peak was small, and its onset and peak temperatures were 550°C and 580°C respectively. It is likely that the endothermic peak was caused by melting of an Al(Cu) solution

with very high Cu content. This solution might be formed during heating due to inhomogeneous distribution of Al and Cu among different powder particles.

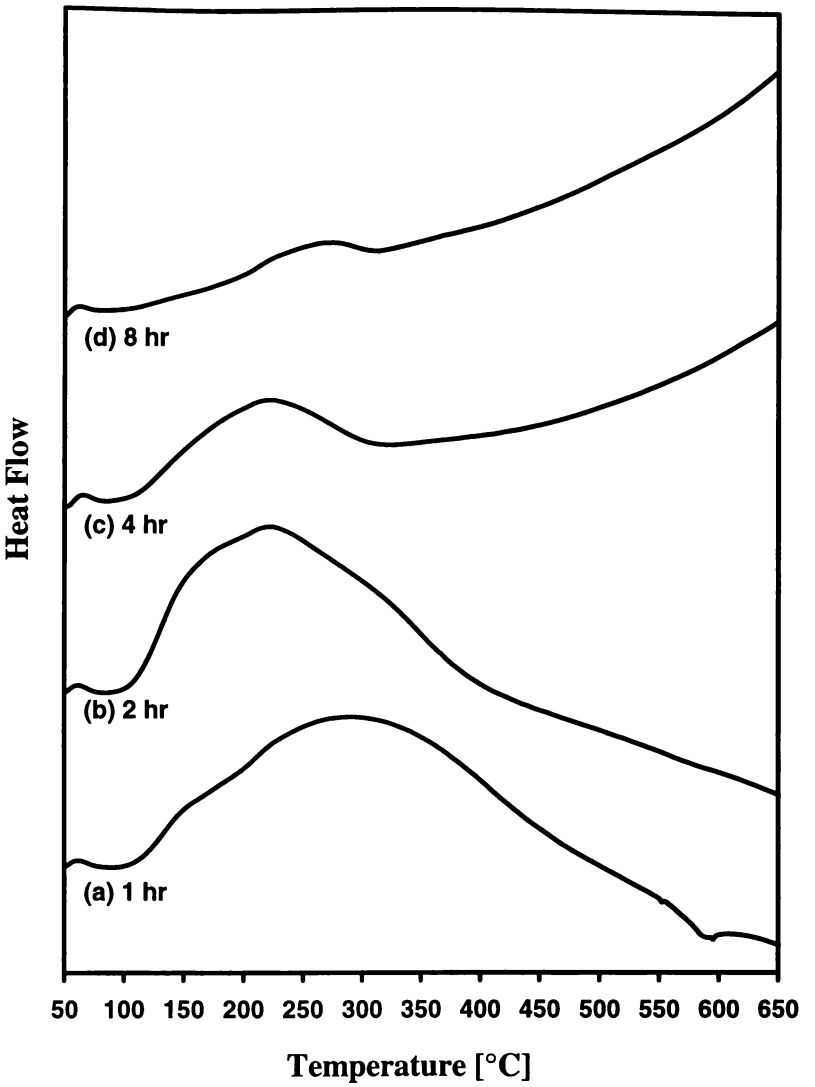

Figure 3-18. DSC traces of the Cu-14at%Al powders produced after milled for different times.

After the powder was milled for 2 hours, the endothermic peak disappeared from the DSC trace. The onset and peak temperatures of the first exothermic peak remained unchanged, but the area clearly increased. The onset temperature of the second exothermic peak also seemed unchanged, but the peak temperature decreased significantly from 300°C to 210°C. The second exothermic peak also became sharper. After the powder was further milled to a total time of 4 hours, the onset and peak temperatures of both exothermic peaks remained unchanged, but their area became substantially smaller. After 8 hours of milling, the first

exothermic peak disappeared, while only a small fraction of the second peak was left.

In order to identify the reactions which caused the first and second exothermic peaks, the 2 hours milled powder was first heated in DSC to 200°C, i.e. just above the peak temperature of the first exothermic peak but below that of the second exothermic peak, and then cooled.

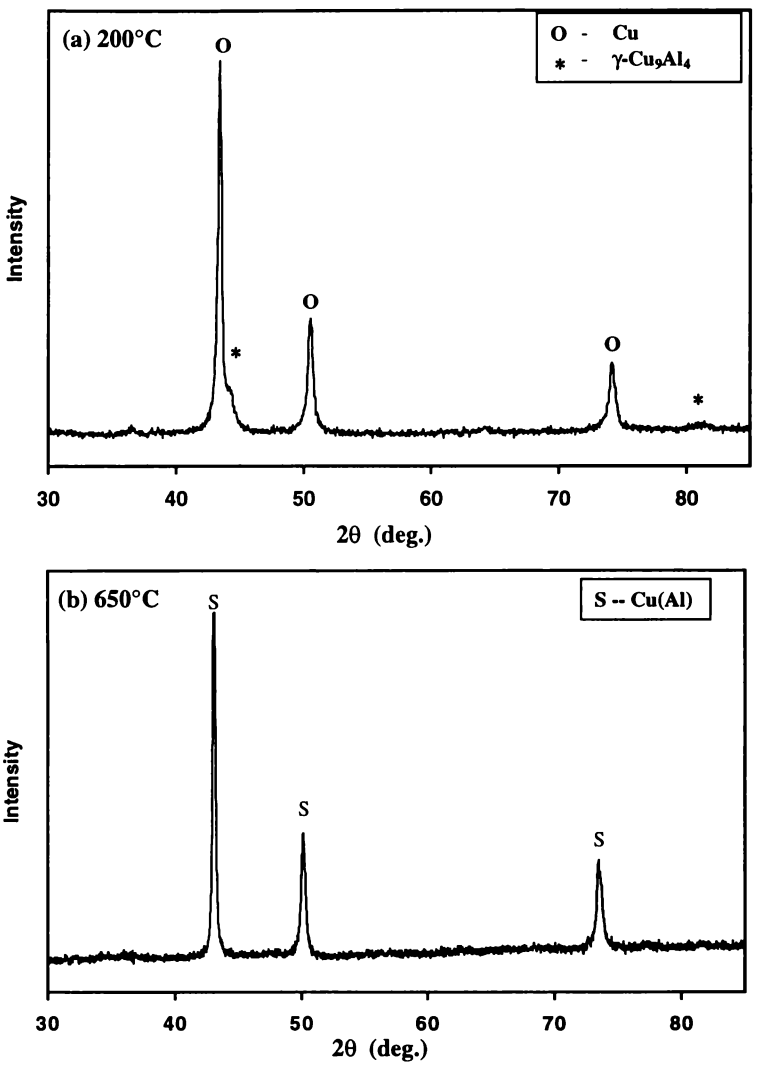

Figure 3-19. XRD patterns of the powders produced after milling a Cu/Al mixture with 14at%Al for 2 hours and then heated to different temperatures.

Figure 3-19 (a) shows the XRD pattern of this powder. It showed strong Cu peaks, weak Al {111} peak and two new peaks which were weak but clear. These two new peaks were indexed as γ-Cu_9Al_4 {330} peak and {600} peak respectively.

This shows that the first exothermic peak was caused by reaction between Al and Cu forming γ-Cu_9Al_4. The position of the Cu {111} peak in this XRD pattern was at $2\theta = 43.4°$, same as that of pure Cu. The 2 hour milled powder heated to 650°C and then cooled to room temperature in DSC was also analysed using XRD. Figure 3-19 (b) shows the XRD pattern of this powder. It showed that all the powder was converted to Cu(Al) solid solution. The position of Cu{111} peak in the XRD pattern is at $2\theta = 43.07°$ which means that the lattice parameter of the fcc phase was a = 3.635Å, almost same as that of the solid solution produced by mechanical alloying.

The heat released during heating the Cu-14at%Al powder as a function of milling time was plotted in Figure 3-20. The heat released from the 1 hour milled Cu-14at%Al powder was 8.72 kJ/mol. The amount of heat released decreases with increase of milling time, and became close to zero after 8 hours milling.

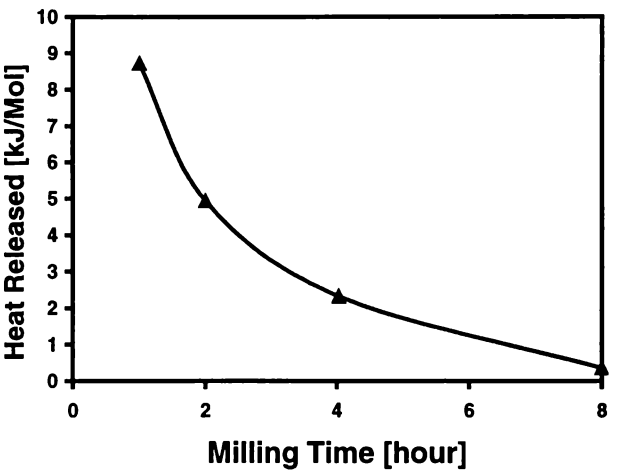

Figure 3-20. The heat released during heating the milled Cu-14at%Al powder as a function of milling time.

Figure 3-21 shows DSC traces of Cu-37at%Al powders produced after milling for different times. As shown in Figure 3-21 (a), the DSC trace of 1 hour milled powder exhibited two overlapping exothermic peaks and 4 endothermic peaks at high temperatures. The first exothermic peak was very small and its onset and peak temperatures were approximately 105°C and 160°C respectively. The second exothermic peak was very large and broad and its onset and peak temperatures were approximately 150°C and 300°C respectively. The endothermic peaks were

in the temperature range of 540-650°C, and they were likely caused by melting of Al rich phases formed through diffusion of Cu into Al during heating.

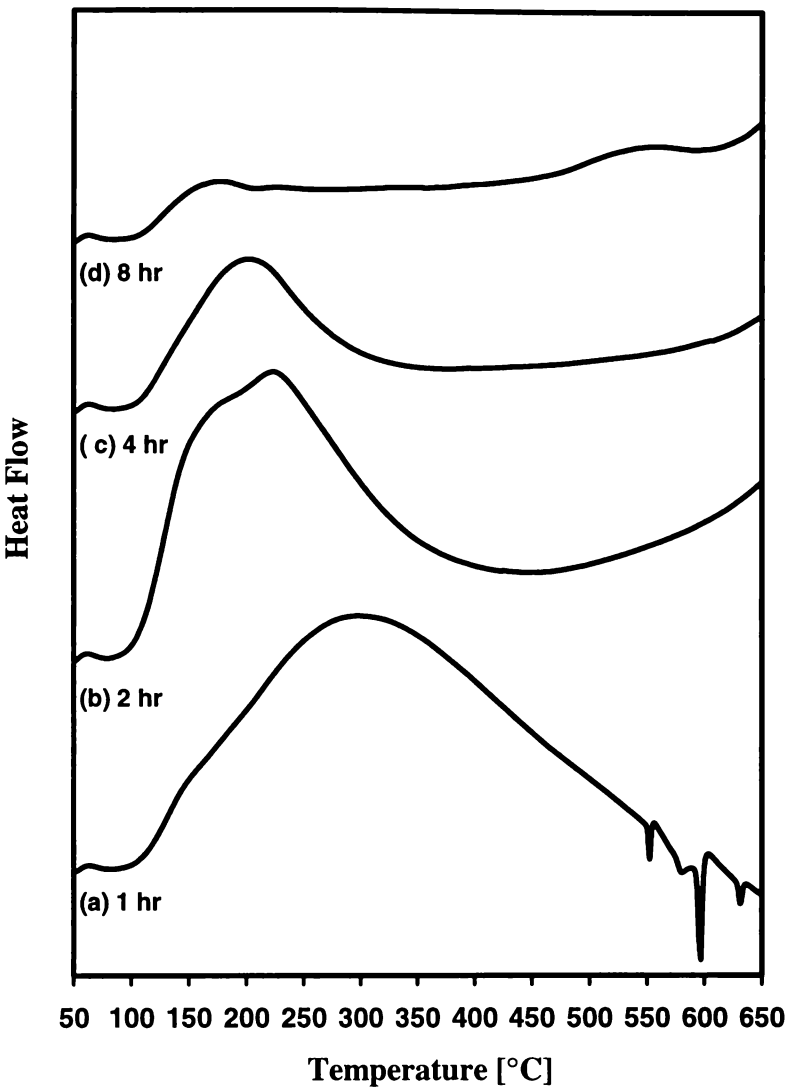

Figure 3-21. DSC traces of the Cu-37at%Al powders produced after milled for different times: (a) 1 hour, (b) 2 hours, (c) 4 hours and (d) 8 hours.

After the powder was milled for 2 hours, the endothermic peaks disappeared from the DSC trace. The first exothermic peak became stronger, and its onset and peak temperatures remained unchanged. The second exothermic peak became much sharper and its onset temperature seemed unchanged. The peak temperature of the second exothermic peak decreased significantly from 300°C to 230°C. After the powder was further milled to a total time of 4 hours, the first exothermic peak almost disappeared, and the second exothermic peak became substantially smaller. The onset temperatures of these peaks seemed unchanged, but the peak

temperature of the second peak decreased to 200°C. This suggests that a substantial fraction of Al phase and Cu phase already reacted during milling from 2 to 4 hours. After 8 hours of milling, the first exothermic peak disappeared, while only a small fraction of the second peak was left. This suggests that almost all of the elemental phases were reacted during 8 hours of milling.

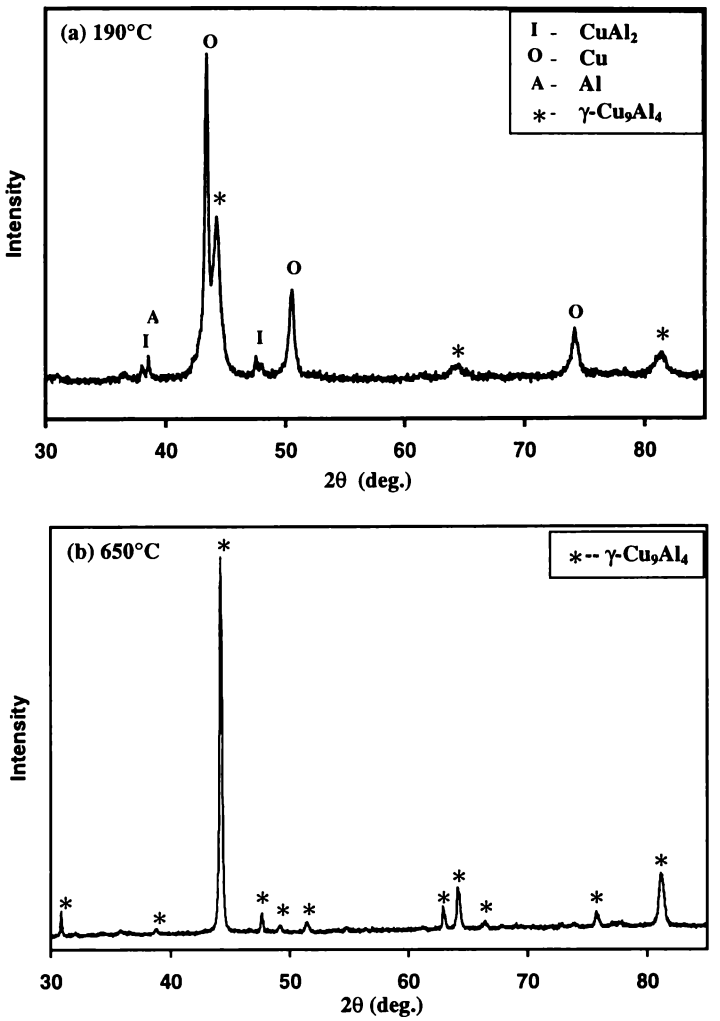

Figure 3-22. XRD patterns of the 2 hours milled Cu-37at%Al powders produced after being heated to (a) 190°C and (b) 650°C.

In order to identify the reactions corresponding to the exothermic peaks, the 2 hour milled powder was heated in DSC to 190°C, i.e. just above the first peak temperature but below the second peak temperature and then cooled. Figure 3-22 (a) shows the XRD pattern of this powder. It showed γ-Cu_9Al_4 peaks, θ-$CuAl_2$ peaks as well as elemental Cu and Al peaks. The 2 hours milled powder heated to 650°C and then cooled to room temperature in DSC was also analysed using

XRD. Figure 3-22 (b) shows the XRD pattern of this powder. It showed only γ-Cu_9Al_4 peaks. This suggests that the first exothermic peak corresponds to reaction between Al and Cu forming θ-$CuAl_2$ while the second peak corresponds to reaction between θ-$CuAl_2$ and Cu forming γ-Cu_9Al_4. The heat released during heating the Cu-37at% as a function of milling time was plotted in Figure 3-23. The reaction heat for the 1 hour milled Cu-37at%Al powder was 15.02 kJ/mol. The amount of heat released decreases with increase of milling time and became close to zero after 8 hour milling.

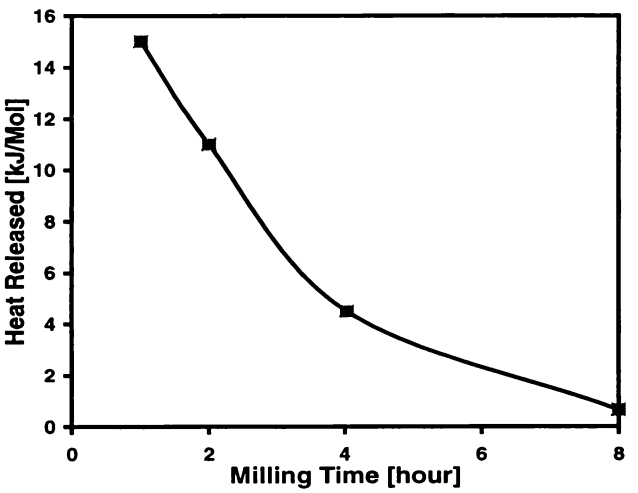

Figure 3-23. The heat released during heating the milled Cu-37at%Al powder as a function of milling time.

3.3.3 Discussion

The present study shows that alloying between Cu and Al can be achieved either mechanically through ball milling of a mixture of Cu and Al elemental powders or thermally through heat treating the short time milled powders. With a low Al composition of 14at%, the mechanical alloying results in formation of a Cu(Al) solid solution. With a high Al composition of 37at%, the mechanical alloying results in formation of γ-Cu_9Al_4. This is in agreement with Lima *at al.*'s observation.[18] Monitoring of the phase development of the process only reveals a progressive conversion of a mixture of elemental phases into a solid solution or an intermediate phase. So it is not clear whether the formation of the final product is preceded by formation of one or more other intermediate phases such as θ-$CuAl_2$.

The mechanical alloying process is slow and progressive, so it is difficult to clarify this issue.

Heating the milled powder in DSC reveals the kinetics of the reactions that are possible in the Cu-Al system. For both compositions, the DSC trace of the milled but not extensively reacted powder show two heavily overlapping exothermic peaks. With a low Al composition, at low temperatures, Cu and Al react forming γ-Cu_9Al_4, while at high temperatures γ-Cu_9Al_4 is dissolved into Cu forming Cu(Al) solid solution. With a high Al composition, at low temperatures, Cu and Al react, forming θ-$CuAl_2$, while at high temperatures $CuAl_2$ and Cu react, forming γ-Cu_9Al_4. It seems that with a low Al composition, the first phase formed by reaction between Cu and Al is γ-Cu_9Al_4, while with high Al composition, the first phase is θ-$CuAl_2$. However, the Al composition in the powder mixture only affects the volume ratio of Al phase and Cu phase in the Cu/Al composite. It would be unlikely for the change of volume ratio of the two elemental phases to alter the formation of the first phase which is controlled by the state of Cu/Al interface. The fact that in the Cu/Al composite powder with high Al volume fraction, formation of $CuAl_2$ precedes formation of γ-Cu_9Al_4 shows that it is easier for θ-$CuAl_2$ to nucleate at the Cu/Al interfaces than γ-Cu_9Al_4. The crystal structure of θ-$CuAl_2$ is also simpler than γ-Cu_9Al_4. This is also a favourable factor to determine that $CuAl_2$ is easier to nucleate. Therefore, it is likely that even with low Al composition, θ-$CuAl_2$ may still be the first phase formed. But since the $CuAl_2$ is Al rich, the amount of $CuAl_2$ may be too small to be revealed by DSC and XRD analysis.

The DSC analysis of the milled powder shows that θ-$CuAl_2$ is the first phase to be formed by reaction between Cu and Al. The θ-$CuAl_2$ phase nucleates and grows at temperatures ranging from 100 to 190°C. This temperature range is very similar to that observed by Jiang *et. al.*[15] during annealing Cu/Al multilayer thin films. The DSC analysis also reveals that γ-Cu_9Al_4 starts to nucleate at about 150°C. This temperature is also similar to those observed by Jiang *et. al.*[15] during annealing of multilayer thin films. These similarities suggest that after sufficient time of milling (1-2 hours in this case), the behaviour of the Cu/Al composite powder

during heating is very much similar to that of the multilayer thin films, even though the layer thickness has not been as small as a few nanometres.

Another aspect of this study is about the effect of Cu/Al composite structure on the reaction kinetics. When the composite structure is refined by increasing milling time from 1 to 2 hours, the onset temperature of the formation of the first phase remains unchanged, as shown in Figure 3-18 (a) and (b) and Figure 3-21 (a) and (b) respectively. However, with the refinement of the composite structure, the fraction of the first phase formed increases and the temperature range for completing formation of the second phase became narrower. It is not difficult to envisage that θ-$CuAl_2$ phase nucleates at Cu/Al interfaces. With refinement of the composite structure, the total area of the interfaces becomes larger, so the number of nucleation sites per unit weight of powder becomes larger. This would increase the nucleation rate. On the other hand, the onset temperature of nucleation is controlled by interface diffusivity rather than the total area. So it is quite understandable that the onset temperature remains unchanged. Likewise, the narrowing of the temperature range for formation of the γ-Cu_9Al_4 phase or the solid solution is caused by decrease of layer thickness. The layer thickness determines the required growth distance. With smaller layer thickness, the required growth distance is smaller, so it is faster for the reaction to come to completion.

3.4 Summary

In this chapter, the microstructural evolution and solid state reactions of Ni-Al and Cu-Al elemental powders during high energy ball milling and subsequent heat treatment were investigated.

In Ni-Al system, the microstructure evolves in three stages during milling. Stage I: formation of entrapped Ni particles in Al matrix structure; Stage II: formation of Ni/Al multilayer structure; Stage III: formation of Al_3Ni single phase. The temperature required to activate the reaction between Al and Ni during heating decreases by more than 200°C as the powder particle microstructure evolves from the entrapped particles to a multilayer structure and then it decreases gradually

with decreasing Ni layer thickness. Similarly to experiments using multilayer Ni/Al thin films, the nucleation and lateral growth of Al_3Ni phase at the Ni/Al interfaces occurred at much lower temperatures than the transverse growth of Al_3Ni. The fraction of Al_3Ni formed through nucleation and lateral growth at the interface is almost linearly proportional to the interface area. The activation energy of the nucleation and lateral growth of Al_3Ni at the Al/Ni interfaces is independent of Ni layer thickness, but the activation energy of the transverse growth of Al_3Ni decreases substantially with decreasing the Ni layer thickness.

It was found that high energy milling of Cu and Al elemental powder mixture can result in formation of solid solution or an intermetallic compound depending on the initial composition of the powder mixture, and that heat treating the shorter time milled powder can achieve the same outcome as that of prolonged milling. During heating the mechanically milled but not extensively reacted powders, the phase transformation developed in stages varies from the nominal compositions of the elemental powder mixtures. With low Al composition, 14at%Al, γ-Cu_9Al_4 forms first at low temperatures, while at high temperatures γ-Cu_9Al_4 is dissolved into Cu forming Cu(Al) solid solution. With high Al composition, 37at%Al Cu and Al react forming θ-$CuAl_2$ at low temperatures, while at high temperatures $CuAl_2$ and Cu react forming γ-Cu_9Al_4. The behaviour of the Cu/Al composite powder produced by high energy milling during heating is very similar to that of the multilayer thin films.

For both Ni/Al and Cu/Al reaction couples, the multilayer composite powder particle microstructure were established. A substantial decrease in reaction temperatures was achieved.

3.5 References

1 J. S. Benjamin and T. E. Vollin, *Met. Trans.* 1974, **5**, 1929.

2 B. J. Aikin and T. H. Courtney, *Met. Trans. A*, 1993, **24A**, 647.

3 D. L. Zhang and D. Y. Ying, *Materials Science and Engineering A*, in press.

4 M. Sherif El-Eshandarany, A. A. Bahgat, N. S. Gomaa, N. A. Eissa, *J. Alloys Comp.*, 1999, **290**, 181.

5 G. B. Schaffer and P. G. McCormick, *Mater. Forum*, 1992, **16**, 91.

6 E. Ma and M. Atzmon, *Mater. Chem. and Phys.*, 1995, **39**, 249.

7 S. K. Pabi and B. S. Murty, *Mater. Sci. Eng. A*, 1996, **214(1-2)**, 146.

8 K. B. Povarova, V. B. Proskurin, V. P. Levin, A. G. Nikolaev, N. K. Kazanskaya and A. I. Firov, *Russian Metallurgy.* 1994, **4**, 59.

9 A. Csanady, A. Csordaspinter, L. Varga, L. Toth and G. Vincze, *Journal de Physique I.* 1996, **6(7)**, 925.

10 W. Guo, M. Magini, F. Padella, L. Battezzati, M. Baricco and F. Fracchia, *International Journal of Mechanochemistry and Mechanical Alloying,* 1994, **1(2)**, 97.

11 F. Cardellini, G. Mazzone, A. Montone and M. V., Antisari, *Acta Metall. Mater.*, 1994, **42(7)**, 2445.

12 N. J. Welham, *Intermetallics,* 1998, **6(5)**, 363.

13 F. Cardellini, V. Contini, R. Gupta, G. Mazzone, A. Montone, A. Perin and G. Principi, *J. Mater. Sci.*, 1998, **33**, 2519-.

14 T.B. Massalski, *Binary Alloy Phase Diagram.* ASM International , 1990, p.142.

15 H.G. Jiang, J.Y. Dai, H.Y. Tong, B.Z. Ding, Q.H. Song, Z.Q. Hu, *J. Appl. Phys.*, 1993, **74(10)**, 6165.

16 X.J. Liu, I. Ohnuma, R. Kainuma, K. Ishida, *J. Alloys & Comp.*, 1998, **264(1-2)**, 201.

17 X.K. Peng, R. Wuhrer, G. Heness, W.Y. Yeung, *J. Mat. Sci.*, 1999, **34(9)**, 2029.

18 J.C. Lima, D.M. de, Triches, V.H.F. dos Santos, and T.A. Grandi, *J. Alloys Comp.*, 1999, **282**, 258.

19 M. Atzmon, *Solid State Powder Processing,* (ed. A.H. Clauer and J.J. DeBardillo), The Minerals, Metals & Materials Society, 1990.

20 M. Atzmon, *The American Physical Society*, 1990, **64(4),** 487.

21 S. K. Pabi, J. Joardar, I. Manna and B. S. Murty, *NanoStructured Materials*, 1997, **9**, 149-152 Elsevier Science Ltd.

22 F. Cardellini, V. Contini, G. Mazzone, *Scr. Metall. et Mater.,* 1995, **32(4)**, 641.

23 S. J. Hwang, *Mater. Sci. Forum*, 1999, **312-314**, 581.

24 L. Battezzati, C. Antonione and F. Fracchia, *Intermetallics.* 1995, **3(1)**, 67.

25 L. Battezzati, P. Pappalepore, F. Durbiano and I. Gallino, *Acta Mater.*, 1999, **47(6)**, 1901.

26 C. Herzig, T. Przeorski and Y. Mishin, *Intermetallics,* 1999, **7**, 389.

27 E. Ma, C. V. Thompson and L. A. Clevenger, *J. Appl. Phys.*, 1991, **69(4)**, 2211.

28 E. Ma, M. A. Nicolet and M. Nathan, *J. Appl. Phys.*, 1989, **65(7)**, 2703.

29 A. S. Edelstein, R. K. Everett, G. Y. Richardson, S. B. Qadri, E. I. Altman, J. C. Foley and J. H. Perepezko, *J. Appl. Phys.*, 1994, **76(12)**, 7850.

30 A. S. Edelstein, R. K. Everett, G. R. Richardson, S. B. Qadri, J. C. Foley and J. H. Perepezko, *Mat. Sci. & Eng.*, 1995, **A195**, 13.

31 C. Michaelsen, G. Lucadamo and K. Barmak, *J. Appl. Phys.*, 1996, **80(12)**, 6689.

32 C. Michaelsen and K. Barmak, *J. Alloys & Comp.*, 1997, **257(1-2)**, 211.

33 K. Barmak, C. Michaelsen and Lucadamo, *J. Mater. Res.*, 1997, **12(1)**, 133.

34 F. Hodaj and L. Dumas, *Metallofiz. Noveishie Tekhnol.*, 1999, **21(1)**, 86.

35 H. E. Kissinger, *Journal of Research of the National Bureau of Standards*, 1956, **57(4)**, 217.

36 D.L. Zhang, T. B. Massalski and M. R. Paruchuri, *Metall. and Mater. Trans. A*, 1994, **25A**, 73.

37 C.C. Koch, *Inetrnational Journal of Mechanochemistry and Mechanical Alloying*, 1994, **1(1)**, 56.

38 P. Schumacher, M. H., Enayati and B. Cantor, *Mater. Sci. Forum*, 1999, **312-314**, 351.

39 R. A. Varin, J. Bystrzycki, A. Calka and D. Wexler, *Mater. Sci. Forum*, 1999, **312-314**, 103.

40 K.R. Coffey, L.A. Clevenger, K. Barmark, D.A. Rudman and C.V. Thompson, *Appl. Phys. Lett.*, 1989, **55(9)**, 852.

41 J. A. Kennedy and S. M. Clark, *Mater. Sci. Forum*, 1996, **228-231**, 423.

42 J. A. Augis and J. E. Bennett, *J. Thermal Analysis*, 1978, **13**, 283.

43 W.L. Gao, Y.W. Du, K.Y. Wang, M.X. Quan and J.T. Wang, *Acta Physica Sinica*, 1995, **4(2)**, 113.

44 A. K. Bhattacharya and E. Arzt, *Scripta Metallurgica et Materialia*, 1993, **28**, 395.

45 M. Angiolini, G. Mazzone, A. Montone, and M. Vittori-Antisari, *Phys. Rev. B*, 1999, **59(18)**, 733.

46 T. H. Courtney, *in "Mechanical Property of Materials"*, McGraw-Hill Publishing Co, New York, 1990, p.128.

47 C.S. Barret, and T.B. Massalski, *Structure of Metals*, 3rd ed. (McGraw-Hill, New York, 1996), p.155.

Chapter Four

Modelling of Solid State Reactions in High Energy Milled Powders

4.1 Introduction

When two phases A and B are in contact, interdiffusion will occur and may result in the formation of solid solution or new phases if A and B have negative or zero enthalpy of mixing. Pabi *et al.*[1] have developed a rigorous interdiffusion model, based on the iso-concentration contour migration method, to predict the intermixing in a binary miscible system during mechanical alloying. Courtney *et al.*[2] developed a simplified interdiffusion model to predict the time scale needed for the formation of homogeneous solid solution by mechanical alloying. In their models the periodic temperature rise caused by the high speed impacts was considered as the major contribution to the enhancement of the interdiffusion process. In both of the above models, effect of deformation caused by the impacts was considered by taking the thickness reduction as an exponential function of strain accumulation. But their models did not take the new phase formation into consideration. Bormann[3] proposed a heterogeneous nucleation model for solid state reaction in multilayer thin films taking account of the interdiffusion. His model provided a very meaningful insight into the role that nucleation plays in selecting the first phase to form from the solid solutions. The model explained that in some systems, because of their lower activation energies, metastable phases such as amorphous phases are more favourable than the stable intermetallic phases. Recently, Zhang and Ying[4] have proposed a heterogeneous nucleation model to explain and predict the selective first phase formation in connection with the progress of mechanical milling. The model explained that with the increase of

α/β interface area the reaction path will change and affect first phase formation during subsequent annealing of the mechanically milled powders.

Coffey *et al.*[5] developed a simplified model for the two-step nucleation and growth process for multilayer Nb/Al and Ni/amorphous-Si thin films. In their model, the first step is taken to be the nucleation and two-dimensional growth to coalescence of the product phase in the plane of the initial interface. But the nucleation was assumed to take no time and the growth took place from a fixed areal density n of pre-existing nucleation sites in the interface. In their model, the nucleation density n is not a separate parameter. Instead, the areal growth rate is described by the composite parameter nK_{io}^2 determined by experiment. Where, K_{io} is the interfacial-limited growth prefactor. The second step is taken to be the one-dimensional diffusion controlled thickening of the product layer perpendicular to the interface.

The following section presents a simplified kinetic model based on the two-step nucleation and growth concept to predict solid state reactions of high energy ball milled powders during the subsequent annealing process. Classical heterogeneous nucleation and growth theory was used to model the first step and the impingement concept was used to treat the varied multilayer thickness in the second transverse growth step. The validity of the model was verified by the experimental data of Al-Ni powders.

4.2 Development of Models

4.2.1 The Physical Model

Consider a binary system A-B, which exhibits an intermediate phase γ, as shown by the schematic phase diagram in Figure 4-1 (a). The free energy (G) of α, β and γ phase as a function of A atoms is shown in Figure 4-1 (b). Assume α and β phases form a diffusion couple and heterogeneous nucleation of γ phase occurs at α/β interface region, as shown in Figure 4-1 (a) and Figure 4-2(a). As has been discussed in the recent paper,[4] if the interdiffusivity in α phase is much greater than in β phase at the temperature of interest, the shape of the nucleus can be

simplified as a spherical cap, as shown in Figure 4-2 (a). After the nucleus reaches a critical size, it is assumed that it first needs to grow to form a cylinder shape with thickness of Z_0, as shown in Figure 4-2 (b) and Figure 4-3 (c), and then grow laterally along the interface until forming a continuous layer with a thickness of Z_0, as shown in Figure 4-2 (c). Here, Z_0 is the thickness of the interface region, which may be significantly greater than Z^*. This is the first step. The next step is transverse growth at the direction perpendicular to the original interface. This process is assumed to be controlled by the bulk diffusion through the γ phase, as shown in Figure 4-2 (d).

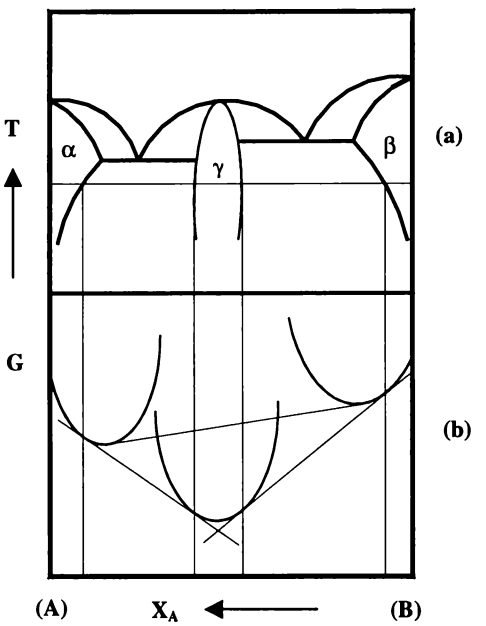

Figure 4-1. Schematic phase diagram and Gibbs energy as a function of X_A.

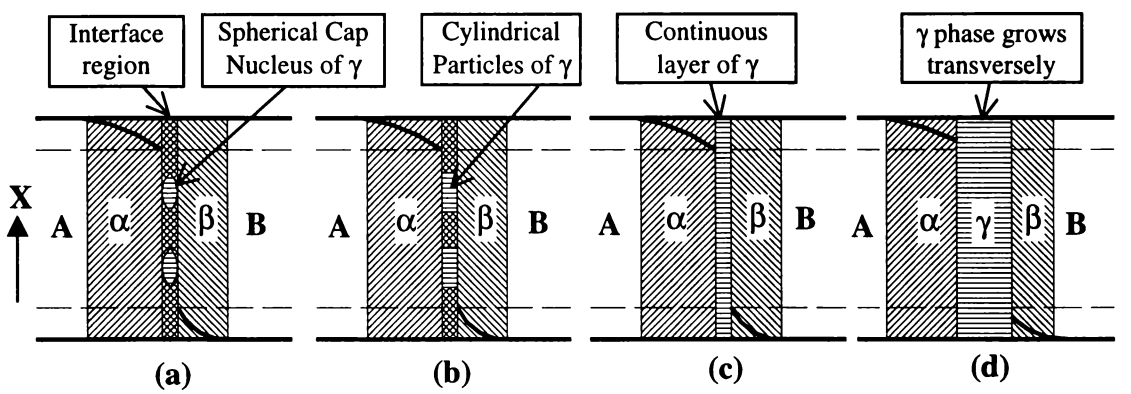

Figure 4-2. Schematic drawing for the interdiffusion-nucleation-growth process. (a) two semi-spherical cap nuclei nucleated at the interface, (b) simplified cylinder shape, (c) nuclei grow along the interface forming a continuous layer of γ, and (d) γ phase grows transversely.

4.2.2 Model for Nucleation and Lateral Growth

The free energy change of the system associated with the nucleation of γ phase with a volume of V and surface area of S includes the following components:

- The decrease of volume free energy, $V\Delta G_v$.
- Increase of surface free energy,

$$S_{\alpha\gamma}\sigma_{\alpha\gamma} + S_{\beta\gamma}\sigma_{\beta\gamma} - S_{\alpha\beta}\sigma_{\alpha\beta} \quad (4\text{-}1)$$

  Where, $S_{\alpha\gamma}$ is the area of α/γ interface, $S_{\beta\gamma}$ is the area of β/γ interface, and $S_{\alpha\beta}$ is the area of interface α/β, consumed by the nucleation of γ phase, and $\sigma_{\alpha\gamma}$, $\sigma_{\beta\gamma}$ and $\sigma_{\alpha\beta}$ are the interfacial energies corresponding to the α/γ, β/γ and α/β interfaces respectively.

- Increase in strain energy caused by the volume change as a result of formation of γ phase $V\Delta G_\varepsilon$.
- Decrease of stored energy (strain, dislocations, defects and grain boundaries, etc.) accumulated through mechanical milling, $V\Delta G_d$.

Summing all these energy changes gives the total free energy change.

$$\Delta G = -V\Delta G_v + V\Delta G_\varepsilon + S_{\alpha\gamma}\sigma_{\alpha\gamma} + S_{\beta\gamma}\sigma_{\beta\gamma} - S_{\alpha\beta}\sigma_{\alpha\beta} - V\Delta G_d \quad (4\text{-}2)$$

To simplify the mathematics, I assume that the spherical cap shaped nucleus takes a radius R and contact angle θ, as shown in Figure 4-3 (c).[4] Taking the equilibrium relationship among the surface tensions, we have $\sigma_{\alpha\beta} = \sigma_{\alpha\gamma}\cos\theta + \sigma_{\beta\gamma}$. Then the total free energy change can be given by[6]

$$\Delta G = \{-\frac{4}{3}\pi R^3(\Delta G_v - \Delta G_\varepsilon + \Delta G_d) + 4\pi R^2\sigma_{\alpha\gamma}\}f(\theta) \quad (4\text{-}3)$$

Where,

$$f(\theta) = \frac{(2+\cos\theta)(1-\cos\theta)^2}{4} \quad (4\text{-}4)$$

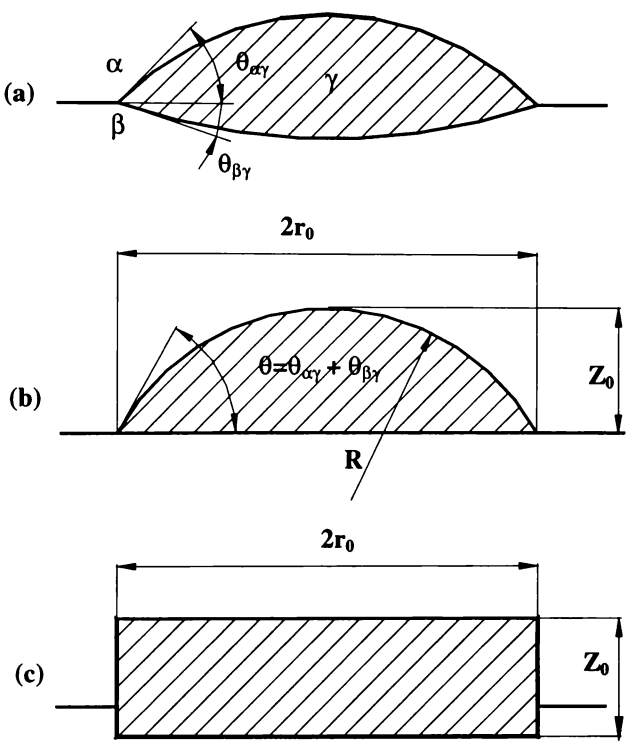

Figure 4-3. Nucleus shape (a) two semi-spherical cap, (b) simplified spherical cap, and (c) simplified cylindrical model.

The critical radius R^* and free energy barrier for the nucleation, ΔG^*, are given by:

$$R^* = \frac{2\sigma_{\alpha\gamma}}{\Delta G_v - \Delta G_s + \Delta G_d} \tag{4-5}$$

and

$$\Delta G^* = \frac{16\pi\sigma_{\alpha\gamma}^3}{3(\Delta G_v - \Delta G_\varepsilon + \Delta G_d)^2} f(\theta) \tag{4-6}$$

Based on classical heterogeneous nucleation theory[7,8], the nucleation rate, I, can be calculated using the following equation:

$$I = NS\frac{kT}{h}\exp\left(-\frac{\Delta G^* + \Delta G_a}{kT}\right) \tag{4-7}$$

Where, N the number of potential nucleation sites per unit area of the α/β interfaces, S the total area of α/β interface per mole of the powder particles, h

Planck's constant, k is the Boltzmann's constant, T temperature and ΔG_a the activation energy of growth of the new phase. N varies during the course of a reaction by (a) the consumption of available preferred sites as the nucleation proceeds, (b) the sweeping out of such sites through the volume occupied by the γ phase.[9] This variation can be described using the following equation,

$$N = N_0(1 - X_i) \tag{4-8}$$

Where N_0 is the potential nucleation sites before the nucleation process started. X_i is the area fraction of the interface that has been transformed to product phase.

The spherical cap will grow three dimensionally in the interface region to form a cylinder with a thickness of Z_0. Due to the high diffusivity of atoms in the interface region, the three dimensional growth of γ phase in the interface region is interface-limited. Therefore, the growth rate (*dr/dt* and *dZ/dt*) is given by: [10]

$$U = K_{i,0} \exp(-\frac{Q_i}{kT}) \tag{4-9}$$

Where, Q_i and $K_{i,0}$ are the activation energy and exponential prefactor for nuclei growth at interface respectively. The radius, r, and the thickness, Z, of the disk nucleated at time τ will be given by

$$r_\tau(t,\tau) = r^* + \int_\tau^t U d\tau \tag{4-10}$$

$$Z_\tau(t,\tau) = Z^* + \int_\tau^t U d\tau, \quad when \quad Z \le Z_0 \tag{4-11}$$

where, $r^* = R^* Sin\theta$ and $Z^* = R^*(1 - Cos\theta)$, and $r_\tau(t,\tau)$ and $Z_\tau(t,\tau)$ are the radius and thickness of the disk nucleated at time τ. Equation (4-10) and (4-11) can be calculated numerically. At time t, the volume of the cylindrical disk that nucleated at time τ is equal to $\pi r_\tau^2 Z_\tau$. The total volume transformed is then given by

$$V_{ex} = \int_0^t \pi r_\tau(t,\tau)^2 Z_\tau(t,\tau) I(\tau) d\tau \tag{4-12}$$

Equation (12) can be solved numerically as well. The subscript "*ex*" stands for "*extended*", and denotes that the transformed volume is not yet corrected for impingement. Taking impingement effect into consideration, the volume fraction of the product at interface region will be given by[11]

$$X_i = 1 - \exp(-\frac{V_{ex}}{Z_0 S}) \tag{4-13}$$

Where S is the interface area per mole of the powder, and Z_0 is the thickness of the interface region. By differentiating Equation (4-13) with respect to time, we have

$$\frac{dX_i}{dt} = \frac{1}{Z_0 S}\frac{dV_{ex}}{dt}\exp(-\frac{V_{ex}}{Z_0 S}) \tag{4-14}$$

dV_{ex}/dt can be obtained by differentiating Equation (4-12) as follows*

$$\begin{aligned}\frac{dV_{ex}}{dt} &= \pi r^{*2} Z^* I(t) + \int_0^t 2\pi r_\tau(t,\tau) U(t) Z_\tau(t,\tau) I(\tau) d\tau + \int_0^t \pi r_\tau(t,\tau)^2 \frac{\partial Z}{\partial t} I(\tau) d\tau \\ &= \pi r^{*2} Z^* I(t) + 2\pi U(t) \int_0^t r_\tau(t,\tau) Z_\tau(t,\tau) I(\tau) d\tau + \pi \int_0^t r_\tau(t,\tau)^2 \frac{\partial Z}{\partial t} I(\tau) d\tau\end{aligned} \tag{4-15}$$

Where, $\frac{\partial Z}{\partial t} = \begin{cases} U(t), & when \quad Z_\tau \le Z_0 \\ 0, & when \quad Z_\tau > Z_0 \end{cases}$. Equation (4-15) can be solved numerically.

4.2.3 Model for Transverse Growth

In this stage the product layer formed during previous stage grows perpendicular to the original interface.[12] The growth of the product at this stage is controlled by

---

* According to Leibniz' formula, if $A(t) = \int_{f(t)}^{g(t)} F(x,t) dx$,

then, $$A'(t) = F(g(t),t)g'(t) - F(f(t),t)f'(t) + \int_{f(t)}^{g(t)} \frac{\partial F(x,t)}{\partial t} dx$$

bulk diffusion of A and B atoms through the γ phase. The growth rate is given by the following equation, the typical one dimensional diffusion equation,

$$\frac{dZ}{dt} = \frac{D_0}{Z}\exp(-\frac{Q_d}{kT}) \tag{4-16}$$

where, D_0 and Q_d are the diffusion prefactor and bulk diffusion activation energy respectively.

By integrating the above equation, we have

$$\frac{Z^2}{2} - \frac{Z_0^2}{2} = \frac{D_0}{R_t}\int_{T_0}^{T}\exp(-\frac{Q_d}{kT})dT \tag{4-17}$$

where, R_t is the constant heating rate.

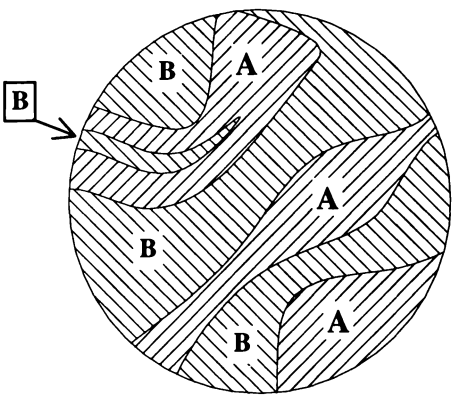

Figure 4-4. Schematic drawing of the as milled powder particles with a wide range of layer thickness.

Assuming a product layer of an area of SX_i and of a thickness of Z, the volume of the product will be SX_iZ. As the layer thickness varies widely, as shown schematically in Figure 4-4, the reactant thickness distribution is likely to follow a normal distribution function in the high energy milled powders, as shown in Chapter three, which is similar to that of cold rolled multi layer Ni/Al foils.[13] When the product layers grow perpendicular to the original interface, some of the thinner reactant layers will be consumed first while some of the thicker reactant layers later. To simplify the mathematical treatment, we adapt the impingement

concept to handle this situation. Therefore, the volume fraction of the product can then be given by

$$X_v = 1 - \exp(-\frac{SX_iZ}{V_m}) \tag{4-18}$$

Where, V_m is the molar volume of the product.

4.2.4 Reaction Rate and Heat Release During Reaction

Now we can obtain the reaction rate in terms of the volume fraction of γphase as

$$\frac{dX_v}{dt} = \frac{SZ_0}{V_m}\frac{dX_i}{dt} + \frac{SX_i}{V_m}\frac{dZ}{dt}\exp(-\frac{SX_iZ}{V_m}) \tag{4-19}$$

The first term in the right hand side of Equation (4-19) corresponds to the first step, nucleation and lateral growth of γ phase, and the second term in the right hand side of Equation (4-19) corresponds to the second step, transverse growth of γphase.

When nucleation and growth of γ phase occurs, heat is released and the rate of heat release is assumed to be proportional to the rate of product volume increase and this gives

$$\begin{aligned}\frac{dH}{dt} &= \Delta H\frac{dX_v}{dt} \\ &= \Delta H\left(\frac{SZ_0}{V_m}\frac{dX_i}{dt} + \frac{SX_i}{V_m}\frac{dZ}{dt}\exp(-\frac{SX_iZ}{V_m})\right)\end{aligned} \tag{4-20}$$

Where, ΔH is the heat of formation of γphase per unit weight (J/g), dX_i/dt is given by Equation (4-14) and dZ/dt is given by Equation (4-16).

4.3 Results and Discussions

The parameters used in the model for predicting dH/dt as a function of temperature during heating Al-25at%Ni powder are listed in Table 4-1. The value of the free energy change ΔG_v (5 kJ/mol) for formation of Al_3Ni was determined

based on reference 3. The strain energy, ΔG_{ε}, was taken to be 0.1 kJ/mol because the molar volume change is not very big from Ni/Al to Al_3Ni. The stored energy accumulated from milling, ΔG_d, was taken to be 0.6 kJ/mol, based on general observation of the stored energy obtained by ball milling.[14] The interfacial energies between the intermediate phases and the supersaturated solution are not known, but a typical value for an incoherent interface is 0.5 J/m^2 [15] and can be as high as 2 J/m^2 [16] Here a value of 1 J/m^2 was taken. The exponential prefactor for bulk diffusion, D_0, was selected to be 0.6 cm^2/s based on the experimental work of Ma *et al.*[12]

Table 4-1. Parameters used in the model.

Symbol	ΔG_v	ΔG_ε	ΔG_d	$\sigma_{\alpha\gamma}$	$K_{i,o}$	D_0	V_m	θ
Unit	kJ/mol	kJ/mol	kJ/mol	J/m^2	cm/s	cm^2/s	cm^3/mol	Deg.
Value	5	0.1	0.6	1	$1.5x10^5$	0.6	9.15	60

The Ni/Al interface area, S, or the average Ni layer thickness, δ_{Ni} (in nm), was obtained by the image analysis of SEM and TEM micrographs of the as milled powders [17]. The relationship between the interface area and the Ni layer thickness was assumed to follow the following equation.

$$\delta_{Ni} = \frac{2V_{Ni}}{S} \tag{4-21}$$

Where, V_{Ni} is the volume of Ni phase per mole atom of Al-25at%Ni powder mixture. The potential nucleation site density, N_0 (in $1/cm^2$), which was assumed to be the triple junction of the Al grain boundary at Al/Ni interfaces, was estimated according to the average grain size, d_{Al}, as

$$N_0 = \frac{1}{d_{Al}^{\,2}} \tag{4-22}$$

Where, d_{Al} is the average Al grain size estimated from the broadening of the XRD peak of the composite powders.

The contact angle, θ, was unknown. In order to obtain a reasonable value, the effect of θ value on the shape and peak position of the calculated DSC curve was examined by varying the θ value from 5° to 80°, as shown in Figure 4-5. It can be seen that the θ value only affected the shape and position of the first peak slightly. With the increase of contact angle from 5° to 80°, the onset and peak temperatures of the first peak shifted to lower temperatures slightly, and meanwhile, the height of the first peak decreased slightly. For a reasonable value, the θ was taken as 60 degree for the model calculation here afterwards.

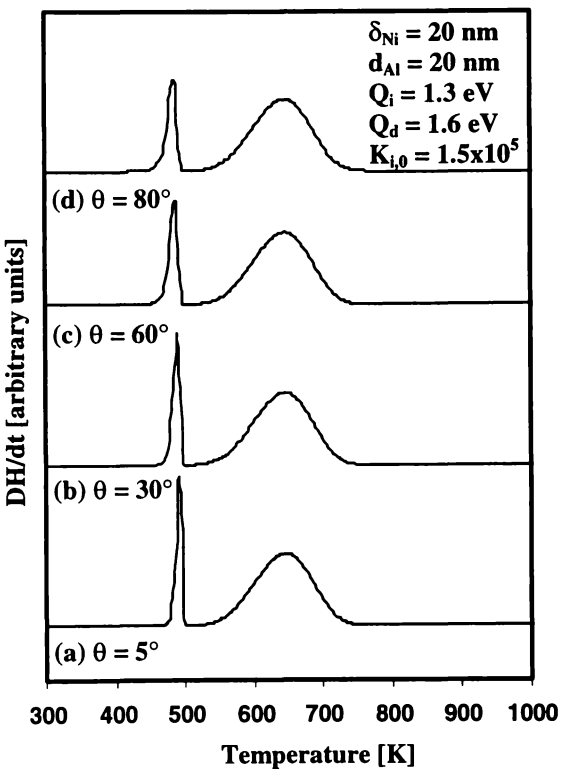

Figure 4-5. The effect of contact angle θ on the shape and position of the calculated DSC curves with a heating rate of 20°C/min. (a) θ = 5°, (b) θ = 30°, (c) θ = 60° and (d) θ = 80°,

The exponential prefactor, $K_{i,0}$, was a measure of interface limited growth rate. Figure 4-6 shows the effect of the value of $K_{i,0}$ on the shape and peak position of the calculated DSC curves with a heating rate of 20°C/min. It can also be seen that the value of $K_{i,0}$ only affected the shape and the position of the first peak of the calculated DSC curves. With the increase of the value of $K_{i,0}$, the first peak shifted to lower temperatures, and in the mean time, the peak became sharper. By best

fitting the calculated DSC curves with experimental DSC trace of the 20 hours milled Al-25at%Ni powder, a $K_{i,0}$ value of $1.5x10^5$ was believed to be reasonable.

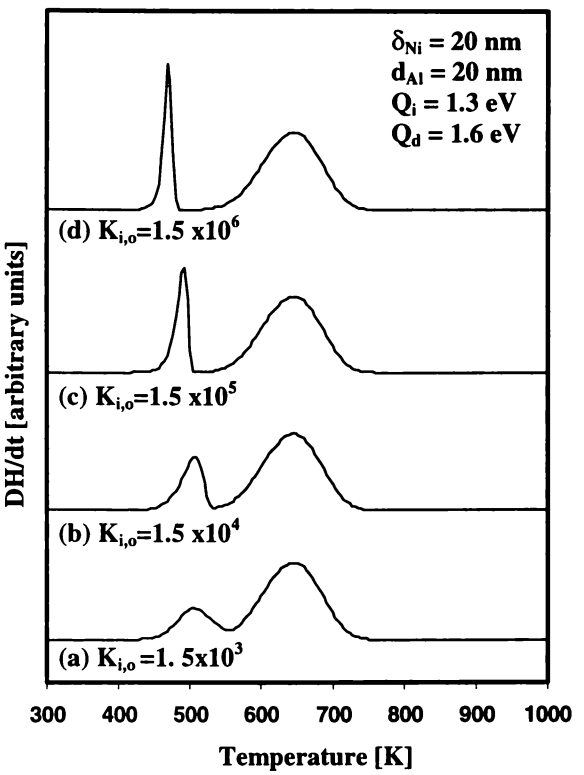

Figure 4-6. The effect of $K_{i,0}$ on the shape and peak position of the calculated DSC curves with a heating rate of 20°C/min. (a) $K_{i,0} = 1.5x10^3$, (b) $K_{i,0} = 1.5x10^4$, (c) $K_{i,0} = 1.5x10^5$ and (d) $K_{i,0} = 1.5x10^6$.

Table 4-2. Parameters used in the calculation.

Parameters	Grain size, d_{Al}	Ni layer thickness, δ_{Ni}	Q_i	Q_d
Milling time\Unit	nm	nm	eV	eV
4 h	52.6	200	1.32	1.63
8 h	40.0	66	1.32	1.63
15 h	15.6	20	1.32	1.63
20 h	11.7	13	1.32	1.62

The values of Q_i (1.3 ~ 1.35 eV) and Q_d (1.6 ~ 2.0 eV) were obtained experimentally by using Kissinger's method as described in Chapter 3. The

activation energy for growth of γphase at interface region, ΔG_a, was taken to have the same value as Q_i. The values of δ_{Ni}, d_{Al}, Q_i and Q_d were summarised in Table 4-2. The thickness of the interface region, Z_0, was assumed to be 10 nm,[12] which is different from the thickness, Z^*, derived from the critical nucleus size R^*. Z^* usually has a value of 1 nm in the case of Al_3Ni forming at Ni/Al interface [15].

Figure 4-7 shows some dH/dt – T curves obtained by calculation and by DSC experiments with a heating rate of 20°C/min. The parameters used in the calculation were listed in Tables 4-1 and 4-2.

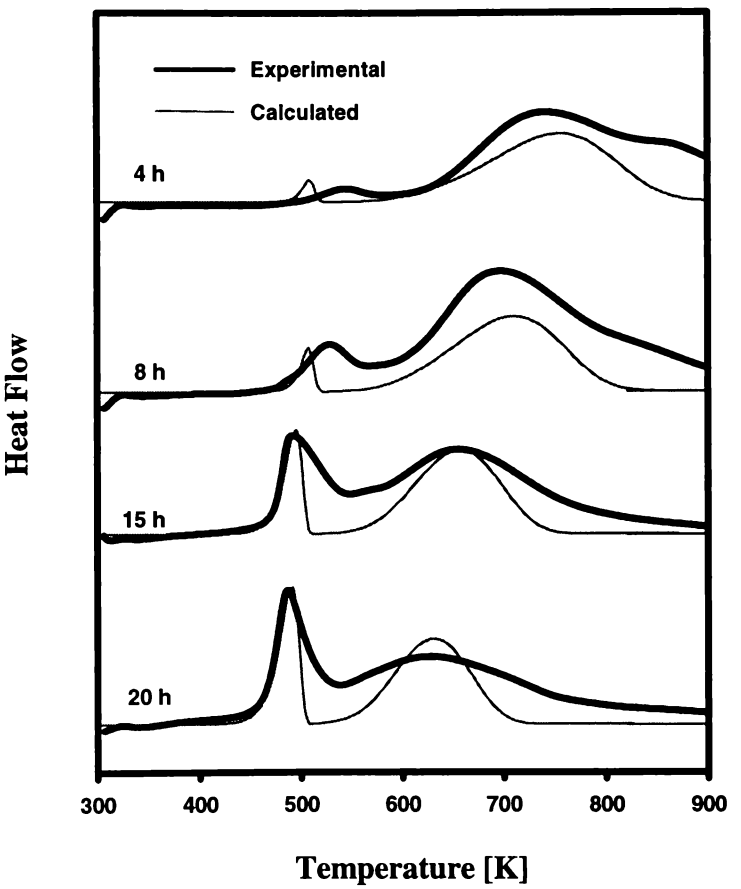

Figure 4-7. Experimental and calculated DSC traces with a heating rate of 20°C/min.

By comparing the calculated and experimental traces one can see that the first peak positions of the model calculation and that of the experiments were not matched well for the 4 and 8 hours milled powders. This indicated that there must be some factors other than activation energy for interfacial growth affecting the peak position. It can also be seen that the second exothermic peak of the

experimental DSC trace is broader than that of the calculated DSC trace. This discrepancy might be attributed to two reasons. The first reason might be the fact that the thickness of Ni layers distribute across a range as shown in Figures 3-1 (e) and (f), but the model is unable to fully incorporate this effect. The second reason might be the high diffusivity in grain boundary regions. The activation energy value for growth of the γ phase in these regions lies between the activation energy value for lateral growth along the interface and that for the transverse growth. Therefore, the second reaction started earlier than solely bulk diffusion controlled reaction as employed in the model calculation.

With the model available, we are able to examine the influence of some of the factors individually. Figure 4-8 shows four predicted DSC traces with the Ni layer thickness of 500, 100, 20 and 2 nm respectively. The peak heights have been scaled to fit the chart.

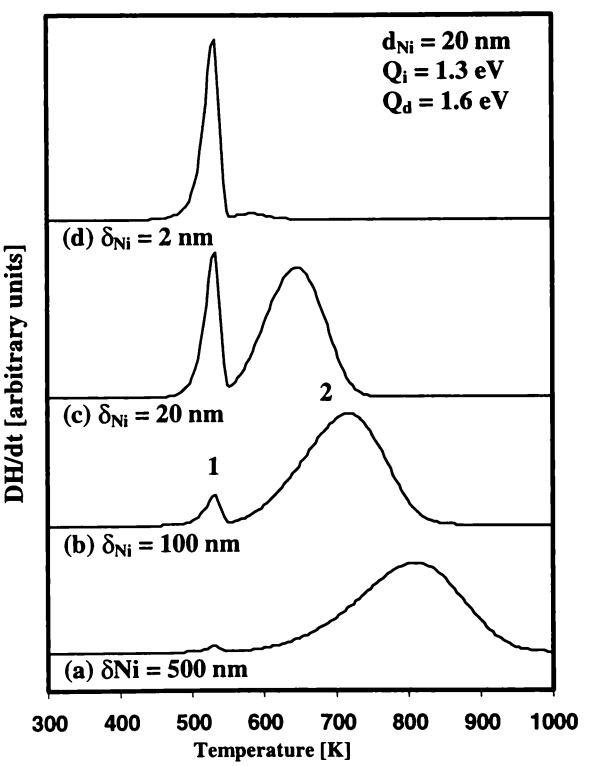

Figure 4-8. Predicted DSC traces as a function of the thickness of Ni layers.

When the Ni layer thickness is 500 nm, the first peak is hardly noticeable, as shown in Figure 4-8 (a). When the thickness of Ni layer reduced to 100 nm, both the peak 1 and the peak 2 are clearly shown, as shown in Figure 4-8 (b). While,

when the thickness of Ni reduces to 20 nm, the peak 1 gets stronger and the peak 2 gets slightly smaller, as shown in Figure 4-8 (c). When Ni thickness reduces to 2 nm, the peak1 becomes very strong and the peak 2 nearly disappeared, as shown in Figure 4-8 (d). In the course of the reduction of the Ni layer thickness, the first peak temperature decreases slightly, whereas the peak temperature of the second peak decreased about 200 K. It is clearly shown that the thickness of Ni layer, or more precisely, the interface area has a significant influence on the relative ratio of the fraction of reaction product from first and second reactions.

Figure 4-9 shows four predicted DSC traces corresponding to grain sizes of 100, 40, 20 and 10 nm respectively. In reality, the reduction in grain size is normally accompanied with some other effects such as increase in diffusivity, but here, in the calculation, only nucleation density increase is accounted for.

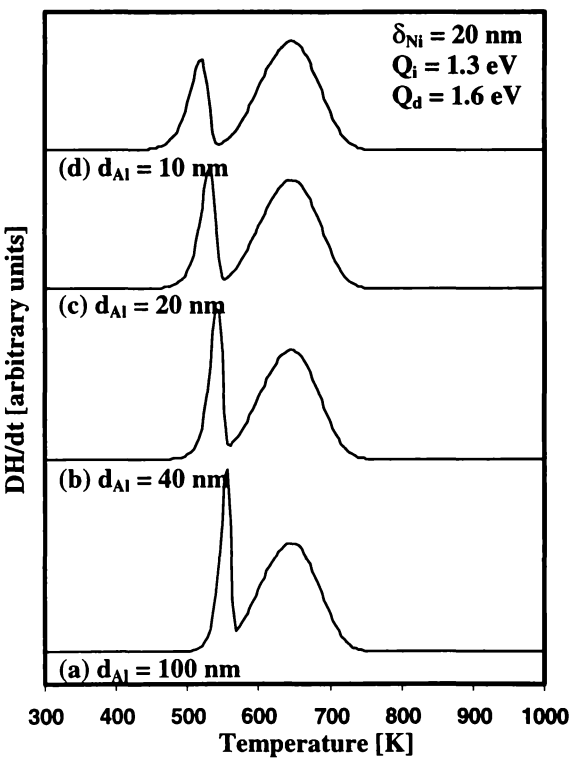

Figure 4-9. Predicted DSC traces as a function of the grain size of Al.

It is shown in Figure 4-9 that with a decrease in grain size, the first peak shifts to lower temperatures and the second peak remains unchanged. With decreasing grain size, i.e. increasing the density of nucleation sites, the initial reaction temperature decreases. In reality, the reduction in grain size is accompanied by

increase in grain boundary area. Consequently, the bulk diffusivity increases and the stored internal energy also increases. This effect can be taken into consideration by adjusting the bulk diffusivity, the activation energy and the ΔG_d terms in the model.

Activation energy is a measure of the barrier of a reaction. With the increase in activation energy for nucleation and lateral growth, Q_i, from 1.3 eV to 1.6 eV, the first peak shifts to higher temperatures, as shown in Figure 4-10. When Q_i increases to a value close to Q_d, the first peak emerges with the second one, as shown in Figure 4-10 (d). Similarly, when the activation energy of the transverse growth, Q_d, decreased from 1.6 eV to 1.3 eV, the second peak shifts to lower temperatures, as shown in Figure 4-11. When Q_d approaches to a value close to Q_i, the second peak emerged to the first one, as shown in Figure 4-11 (d). This suggests that the activation energy difference between lateral growth along interface and transverse growth through the product layer is the dominant factor, which controls whether the reaction kinetics of the two steps can be clearly differentiated.

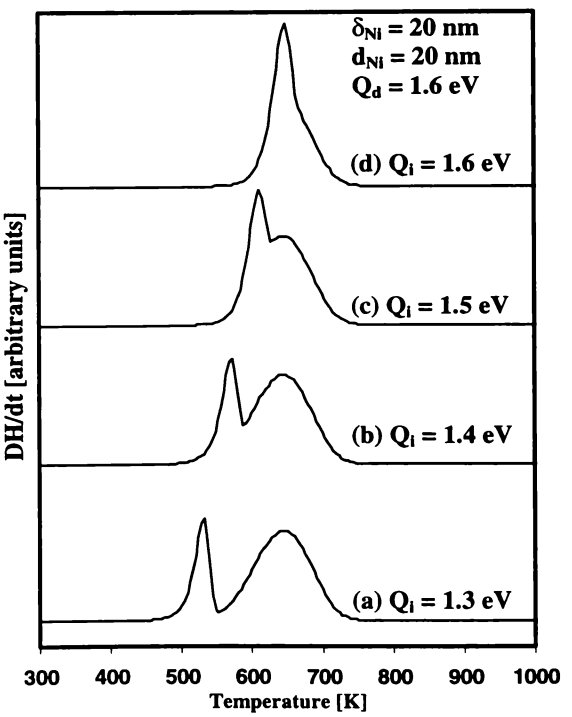

Figure 4-10. Predicted DSC traces as a function of the value of Q_i.

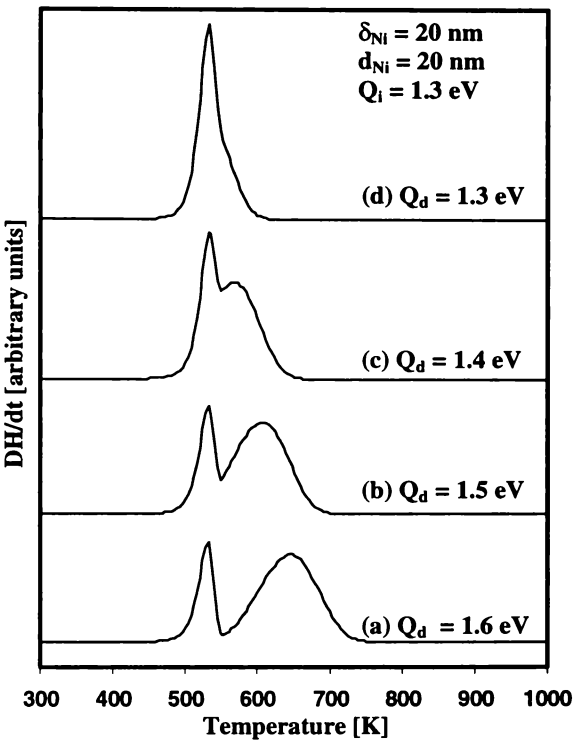

Figure 4-11. Predicted DSC traces as a function of the value of Q_d.

4.4 Summary

A model, which describes the reaction kinetics in high energy milled powders during heat treatment, was developed based on two-step approach: nucleation and lateral growth along interfaces and then transverse growth. Classical heterogeneous nucleation theory was employed to describe nucleation in the first step. Impingement concept was adapted to mathematically treat the layer thickness variation in the high energy mechanically milled powders. The validity of the model was verified against experimental data of high energy ball milled Al-25at%Ni powders and a reasonable agreement between the calculation and experimental data was achieved. It has been demonstrated that the increase of the interface area (or the decreases in multilayer thickness) increases the fraction of reaction product resulting from nucleation and lateral growth. Increasing the density of the potential nucleation sites decreases the reaction initiation temperature. Increasing the activation energies for nucleation, lateral growth and transverse growth increases the corresponding reaction temperatures. When the

values of these activation energies approach to each other, the two reactions occur concurrently.

4.5 References

1 S.K. Pabi, D. Das, T.K. Mahapatra and I. Manna, *Acta Mater.*, 1998, **46(10),** 3501.

2 T.H. Courtney, J.C. Malzahn Kampe, J.K. Lee, D.R. Maurice, *Diffusion Analysis & Applications*, edited by A.D. Roming, Jr. and M.A. Dayananda, *The Minerals, Metals & Materials Siciety*, 1989, pp. 225-253.

3 R. Bormann, in MRS Spring Meeting 1994, Publ. MRS Symp. Proc. 343, 169 1994.

4 D.L. Zhang and D.Y. Ying, Journal of Metastable and Nanocrystalline Materials, 2001, **10**, 323.

5 Coffey, K.R., L.A. Clevenger, K. Barmark, D.A. Rudman and C.V. Thompson, *Appl. Phys. Lett.*, 1989, **55(9)**, 852.

6 D.A. Porter and K.E. Eastering, "*Phase Transformations in Metals and Alloys*", Chapman & Hall, London, UK, 1996.

7 R.D. Doherty, in "*Physical Metallurgy*", R.W. Cahn and P. Haasen (eds.), North-Holland, Amsterdam, 1996, p. 1374.

8 D. Turnbull, and J.C. Fisher, *J. Chem. Phys.*, 1949, **17**, 11.

9 V. Raghavan and M. Cohen, in "*Treatise on Solid State Chemistry*, " (ed. N.B. Hannay), 1975, **5,** p.92.

10 K.R. Coffey, Clevenger, L.A., Barmark, K., Rudman, D.A. and C.V. Thompson, *Appl. Phys. Lett.*, 1989, **55(9),** 852.

11 C.H. Bamford and C.F.H. Tipper (ed.), *Comprehensive Chemical Kinetics*, Vol.22 Reactions in the Solid State, Elsevier Scientific Publishing Company, 1980.

12 E. Ma, C.V. Thompson and L.A. Clevenger, *J. Appl. Phys.*, 1991, **69(4),** 2211.

13 L. Battezzati, P. Pappalepore, F. Durbiano, I. Gallino, *Acta Mater.*, 1999, **47(6)**,1901.

14 H.H. Tian and M. Atzmon, *Acta Mater.* 1999, **47(4)**, 1255.

15 A.S. Edelstein, R.K. Everett, G.Y. Richardson, S.B. Qadri, E.I. Altman, J.C. Foley and J.H. Perepezko, *J. Appl. Phys.*, 1994, **76 (12),** 7850.

16 E. Ma and M. Atzmon, *Mater. Chem. & Phys.*, 1995, **39(4),** 249.

17 D.Y. Ying and D.L. Zhang, *Mater. Sci. and Tech.*, in press.

Chapter Five

Solid State Reactions between Al and TiO_2

5.1 Introduction

The reduction of metal oxide by another active metal has been used in metallurgical industry for very long time. Normally, the reduction reaction is facilitated by heating a mixture of reactants to sufficiently high temperatures. In the last 10 years, it has been demonstrated that many reduction reactions can be realised by high energy milling.[1-6] The Al and TiO_2 is one of the systems in which the reactions are difficult to activate through using high-energy ball milling alone.[7] It has been reported that there were no apparent reactions occurring during 100 hours of high energy ball milling. Subsequent heat treatment was required to activate the reactions in the milled Al/TiO_2 powder mixtures. Milling did enhance the reaction kinetics substantially by establishing the composite microstructure in the powder particles. In the study described in this chapter, the effect of high energy milling on the reaction kinetics of Al and TiO_2 was investigated.

The powders studied had two compositions:

C1 powder: the Al/TiO_2 ratio was determined according to the reaction:

$$3TiO_2 + 13Al = 3Al_3Ti + 2Al_2O_3$$

C2 powder: the Al/TiO_2 ratio was determined according to the reaction:

$$3TiO_2 + 4Al = 3Ti + 2Al_2O_3$$

5.2 Microstructural Evolution During Milling

5.2.1 C1 Powder

Figure 5-1 shows typical SEM micrographs of cross-section of powder particles in C1 powders produced after milling for different times.

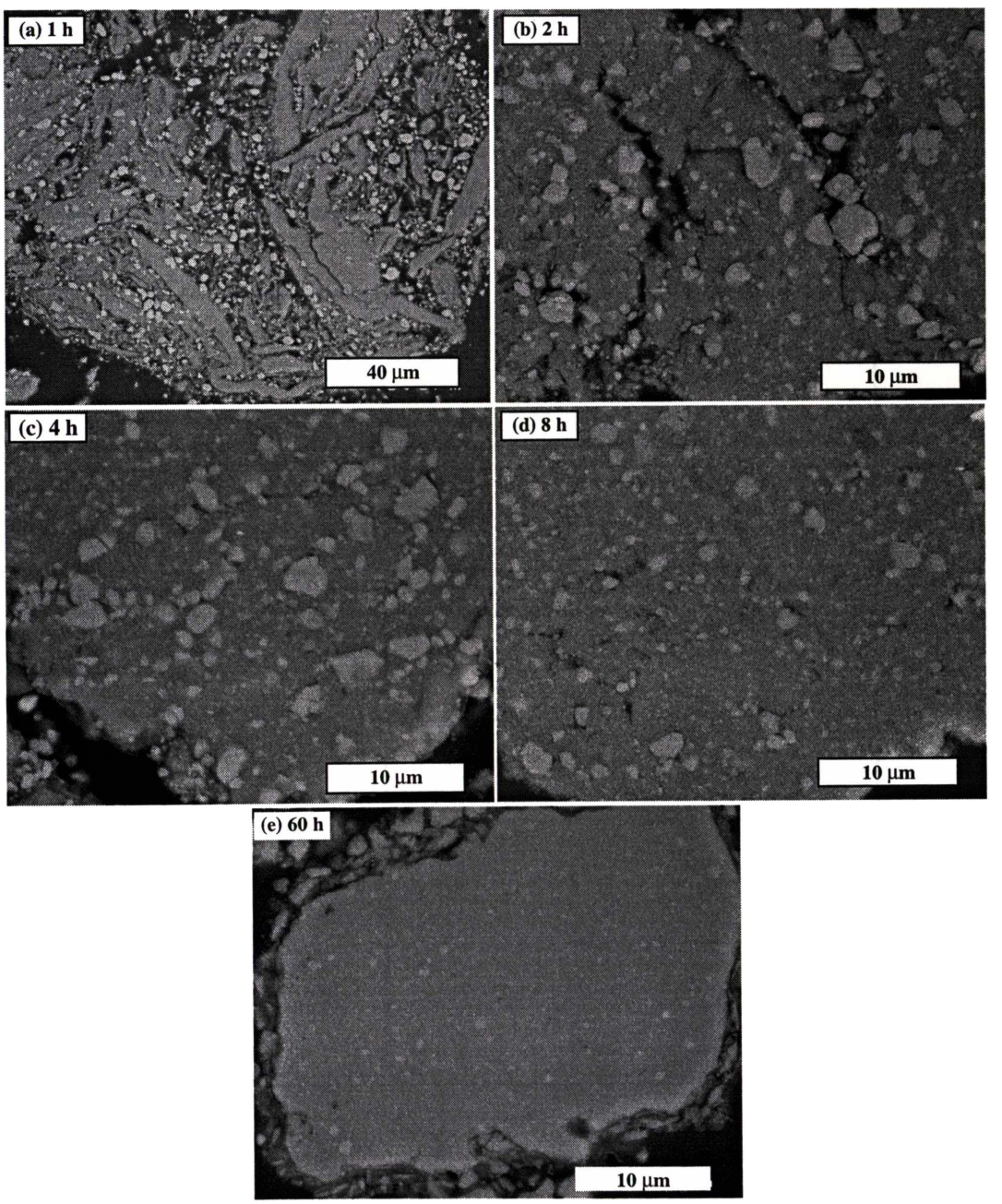

Figure 5-1. SEM micrographs of cross-section of particles in C1 powder produced after being milled for: (a) 1 hour, (b) 2 hours, (c) 4 hours, (d) 8 hours and (e) 60 hours.

After being milled for 1 hour, the Al particles were flattened and cold welded together and the TiO_2 particles were entrapped between the Al particles. After 2 hours of milling, a composite structure formed. Most of the TiO_2 particles were embedded in Al matrix, as shown in Figure 5-1 (b), but the microstructure was inhomogeneous. Some TiO_2 particles had been broken into smaller equiaxed particles and had a diameter around 1 μm. After 4 hours of milling, the composite structure was refined. After 8 hours of milling, the homogeneity increased and the TiO_2 particles were further broken into smaller ones with a diameter less than 1 μm. However there were still some large particles with a diameter up to 3 μm in the Al matrix. After 60 hours of milling, the microstructure was homogenised and some TiO_2 particles with a diameter of 1 to 2 μm still remained, and most of the TiO_2 particles had a diameter of less than 1 μm.

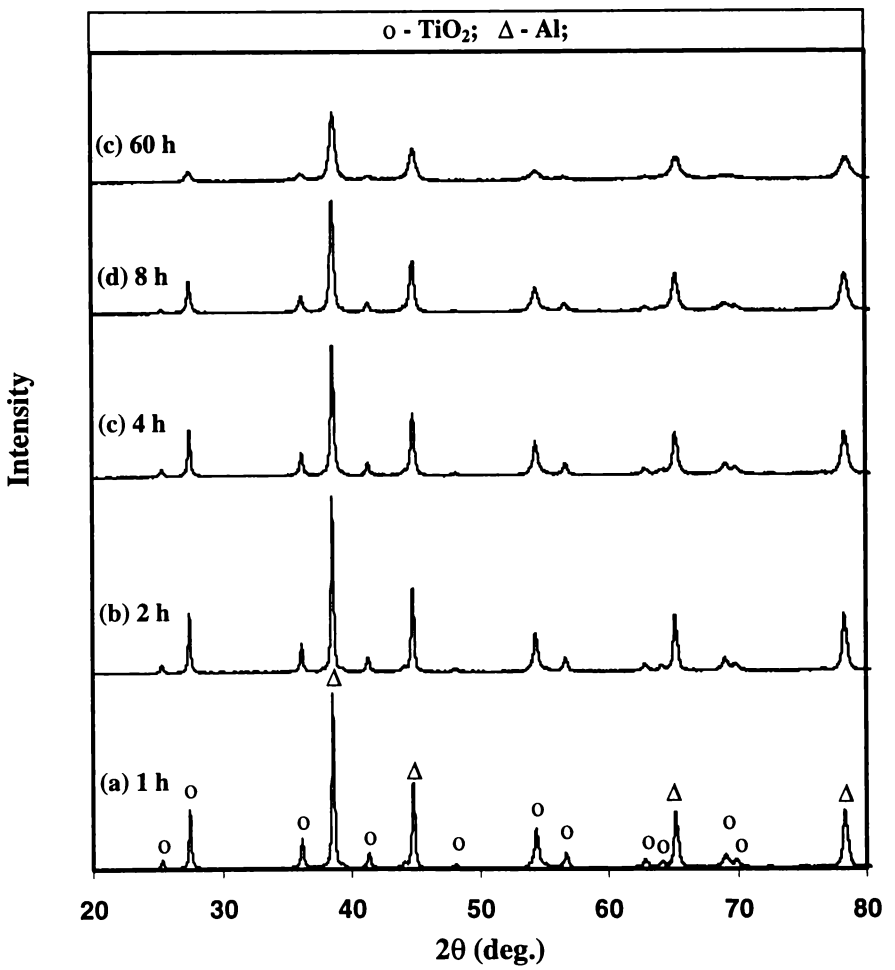

Figure 5-2. XRD patterns of the C1 powder produced after milling for different times: (a) 1 hour, (b) 2 hours, (c) 4 hours, (d) 8 hours and (e) 60 hours.

Figure 5-2 shows the XRD patterns of the C1 powder after being milled for different times. In all the XRD patterns, the only phases observed were Al and TiO_2 phases. With increasing milling time from 1 hour to 60 hours, the peaks were broadened. For TiO_2, this was due to the grain refinement. For Al, this was partly due to grain refinement, and partly due to residual strain. The average grain sizes can be estimated by using Scherrer equation[8] if we ignore the contribution of the residual strain to the broadening of XRD peaks.

Table 5-1. Average grain size estimated from XRD peak broadening.

Ball mill Time [h]	Average Grain Size [nm]	
	C1: $3TiO_2 + 13Al$	
	Al	TiO_2
0	50	51
1	43	46
2	38	43
4	30	36
8	25	27

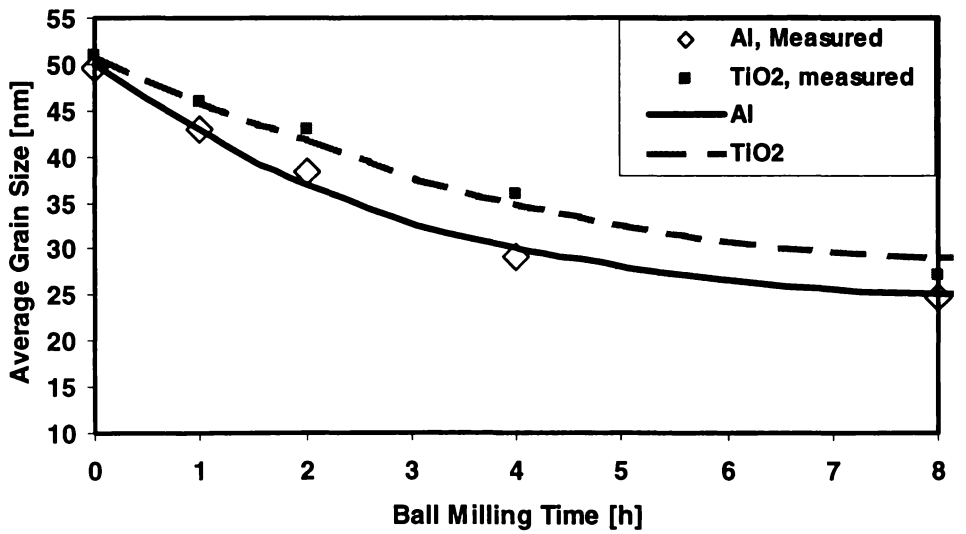

Figure 5-3. Average grain size of the C1 powder as a function of milling time.

Table 5-1 lists the average grain sizes of the Al and TiO_2 phases in the powders produced after being milled for different times. Figure 5-3 shows the average grain size plotted as a function of milling time. It can be seen that during the first 8 hours of milling, the average grain size decreased dramatically from 50 to 25

nm and from 51 to 27 nm for Al and TiO_2 respectively. After this initial period, the average grain size only decreased slowly.

5.2.2 C2 Powder

Figure 5-4 shows typical SEM micrographs of cross-section of powder particles in the C2 powder produced after ball milling for different times.

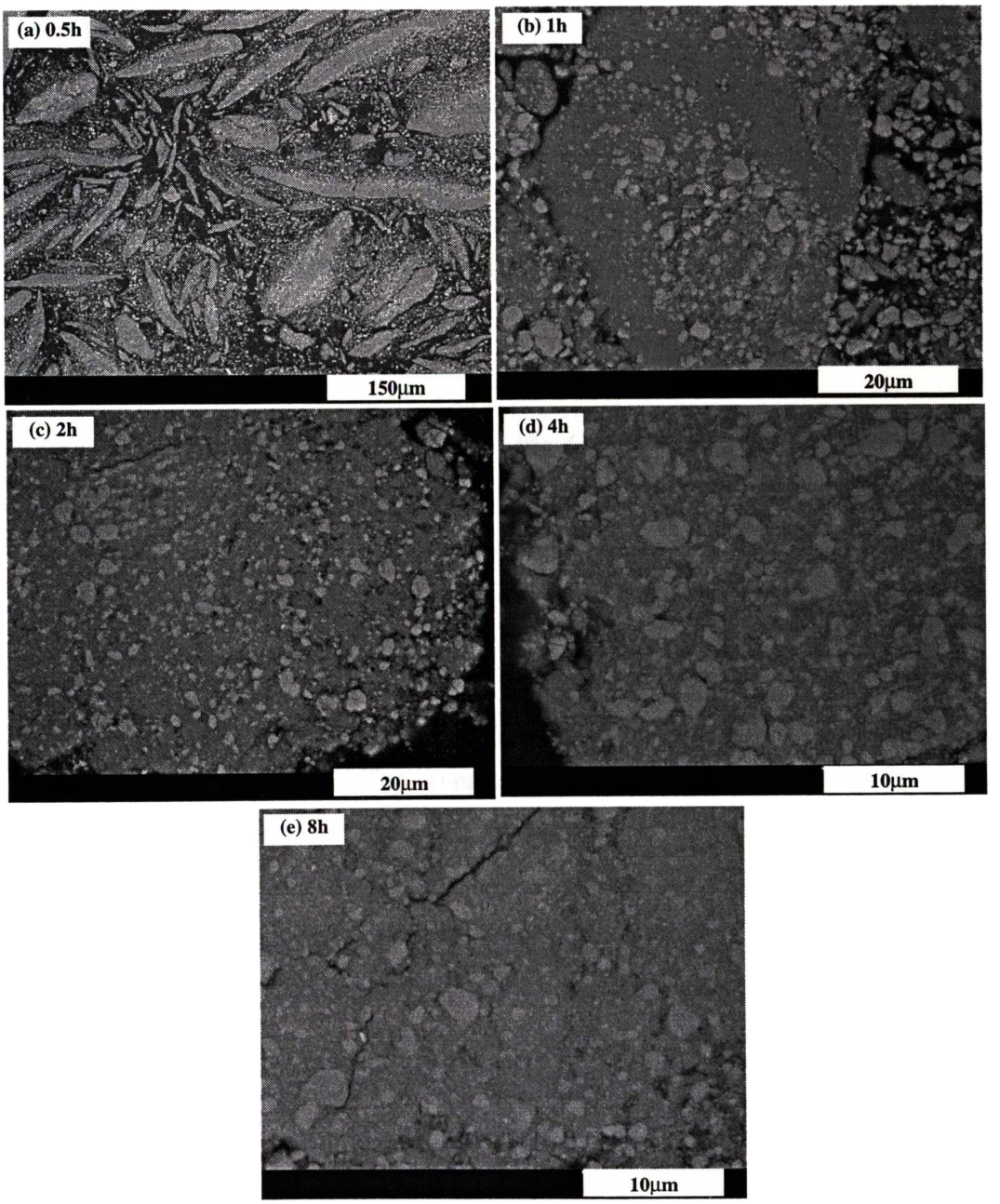

Figure 5-4. SEM micrographs of the cross-section of powder particles in the C2 powder produced after milling for different times: (a) 0.5 hours, (b) 1 hour, (c) 2 hours, (d) 4 hours and (e) 8 hours.

After being milled for 0.5 hours Al particles were elongated, TiO_2 particles were cold welded onto Al particles, as shown in Figure 5-4 (a). Occasionally, a few TiO_2 particles could be found embedded in the Al. After 1 hour of milling, a composite structure formed, with most of the TiO_2 particles being embedded in Al matrix. The microstructure was inhomogeneous and also some TiO_2 particles were found free standing. The size of TiO_2 particles ranged from 2 to 5 μm. Some TiO_2 particles had been broken into smaller particles and had a size around 1 μm. After 2 hours of milling, almost all the TiO_2 particles had been embedded in the Al matrix and the microstructure was more homogeneous. The size of TiO_2 particles still ranged from 1 to 5 μm. After the powder was milled for 4 hours, the composite structure of the powder particles became homogeneous. The size of TiO_2 particles was in the range of 0.5 – 4 μm. After the powder was milled for 8 hours, the range of the size of TiO_2 particles remained unchanged, but the number of small TiO_2 particles increased and the number of the big TiO_2 particles decreased.

Figure 5-5 shows the XRD patterns of the C2 powder after being milled for different times. In all the XRD patterns, the only phases observed were Al and TiO_2 phases. With the milling time increased from 0.5 to 8 hours, the peaks broadened substantially. For TiO_2, this was due to the grain refinement. Again for Al, this was partly due to the grain refinement, and partly due to residual strain.

Figure 5-6 shows the average grain size of Al and TiO_2 in the C2 powder as a function of milling times. The average grain size was determined by using Scherrer's equation and ignoring the contribution of residual strain to the XRD peak broadening. During the first 4 hours of milling, the average grain size of Al and TiO_2 phases decreased significantly from 50 to 26 nm and from 51 to 33 nm respectively. Further milling didn't reduce the average grain size very much. Comparing the data sets in Table 5-1 and Table 5-2, one can find that the grain size reduction for the powders of both composition C1 and C2 has a similar trend with the increase of milling time but it appears that the C1 powder is slightly slower than that of C2 powder. This is likely due to the fact that the former powder contains a larger fraction of soft Al phase than the latter.

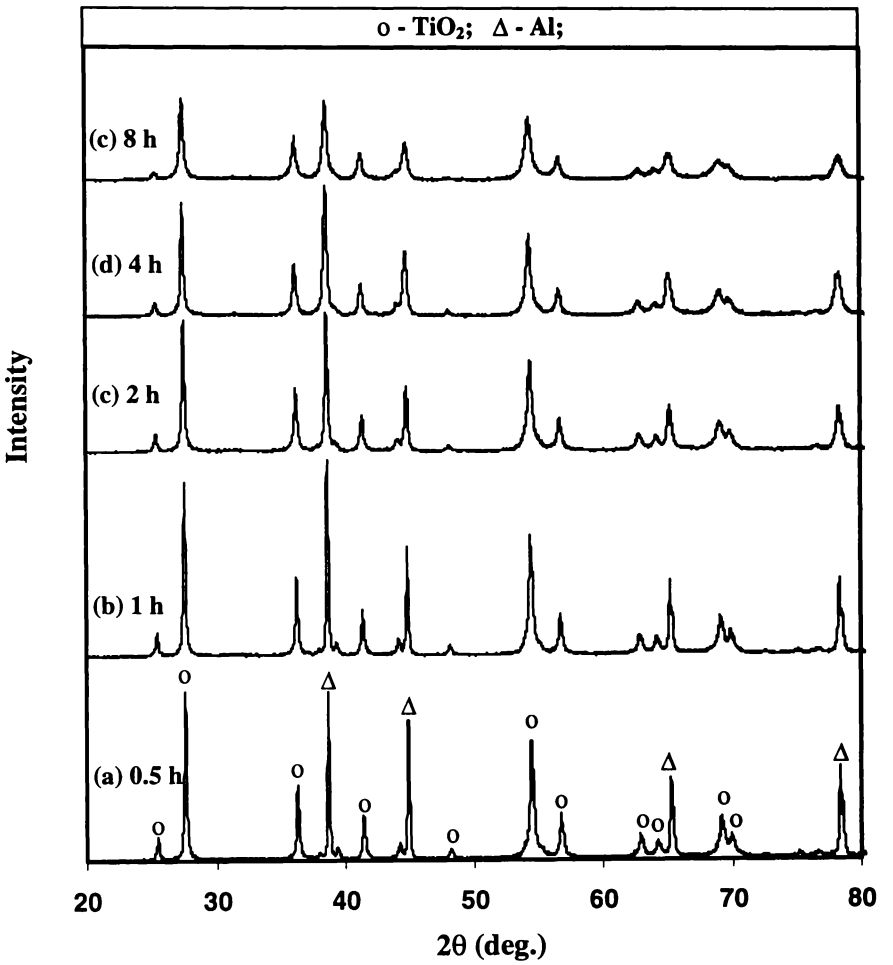

Figure 5-5. XRD patterns of the C2 powder after milling for different times: (a) 0.5 hours, (b) 1 hour, (c) 2 hours, (d) 4 hours and (e) 8 hours.

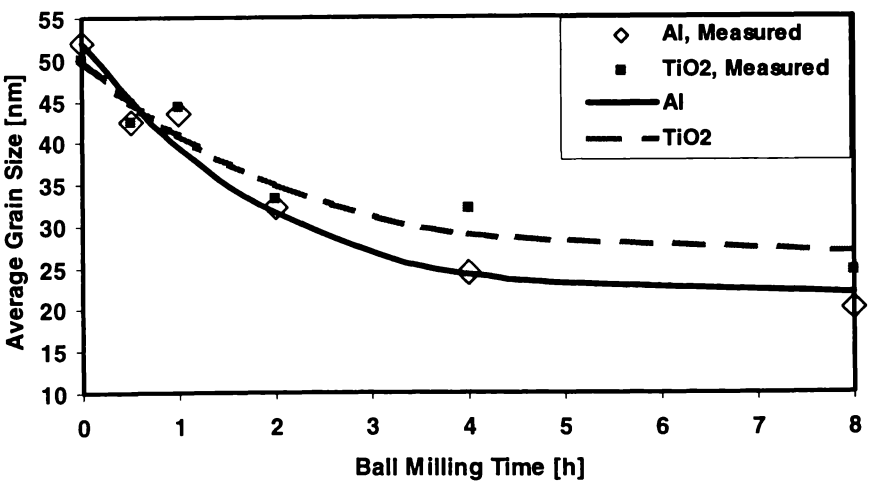

Figure 5-6. Average grain size of Al and TiO_2 phases of the C2 powder as a function of milling time.

Table 5-2 listed the average grain sizes of Al and TiO_2 in the C2 powders after being milled for different times.

Table 5-2. Average grain size estimated from XRD peak broadening.

Ball mill Time [h]	Average Grain Size [nm]	
	C2: $3TiO_2 + 4Al$	
	Al	TiO2
0	50	51
0.5	44	44
1	45	45
2	34	34
4	26	33
8	21	25

5.3 Reactions During Heating

5.3.1 C1 Powder

Figure 5-7 shows the DTA traces of the C1 powder produced after being milled for different times. All the DTA traces showed an endothermic peak with a peak temperature of 660°C, and two exothermic peaks: one was overlapped with the endothermic peak and the other one had a peak temperature of around 890°C. The endothermic peak was caused by melting of the Al phase. After 1 hour of milling, there was a slight exothermic reaction prior to the melting of Al and no evident exothermic reaction followed the melting of Al. The second exothermic reaction started at 800°C, reached peak rate at 870°C. After 2 hours of milling, the first exothermic reaction became stronger, started at 630°C, and continued after the melting of Al. The second exothermic peak became very sharp with onset and peak temperatures being 872°C and 891°C respectively. After 4 hours of milling, the first exothermic reaction became stronger again, and the second exothermic reaction became weaker. The onset and peak temperatures of the second exothermic peak slightly increased to 878°C and 895°C respectively. With further

increase of the milling time to 8 hours, the first exothermic reaction became very strong, whereas the second exothermic reaction became much weaker. The onset and peak temperatures of the second exothermic peak increased slightly to 879°C and 897°C respectively. After the powder was milled for 60 hours, the first exothermic peak became strong and broad and the second exothermic peak disappeared.

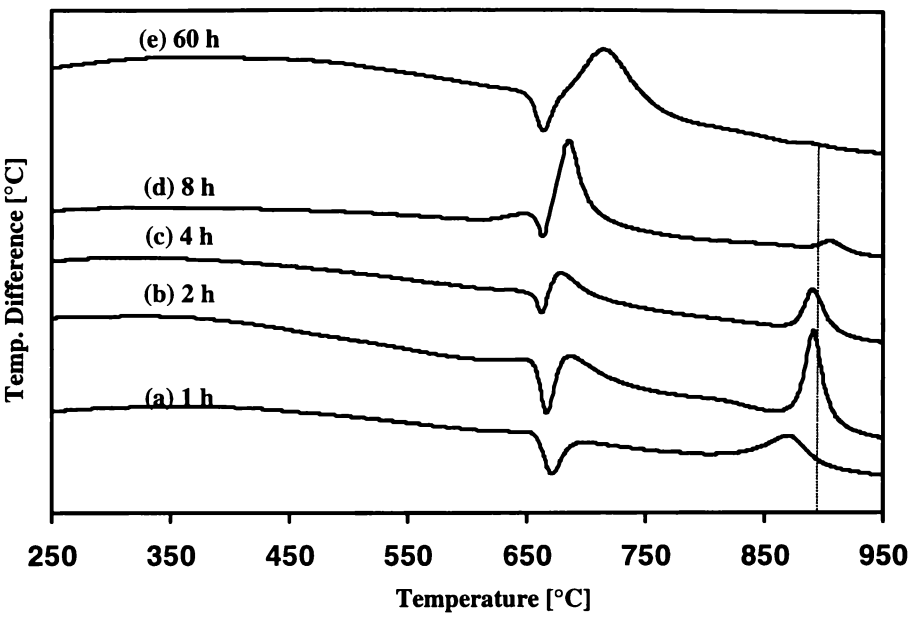

Figure 5-7. DTA traces of C1 powders after milling for different times: (a) 1 hour, (b) 2 hours, (c) 4 hours, (d) 8 hours and (e) 60 hours.

In order to identify the reactions corresponding to each of the exothermic peaks of the DTA traces, the C1 powder was milled for different times and heated to several characteristic temperatures then examined using XRD.

Figure 5-8 shows a group of XRD patterns of the 4 hours milled C1 powder after being heated to different temperatures. When the powder was heated to 500°C, the XRD pattern shows no extra peaks except for those of Al and TiO_2. This suggests that no reaction occurred during heating to 500°C. When the powder was heated to 700°C, Al_3Ti peaks appeared in the XRD pattern. This suggests that the first exothermic peak was caused by the reaction between Al and TiO_2 forming Al_3Ti and another phase(s). Due to lack of clear peaks, it was unable to identify this phase. With further increase in the temperature from 700°C to 800°C, the amount

of Al_3Ti phase increased slightly. When the temperature increased from 800°C to 900°C, the amount of Al_3Ti phase increased significantly and the peaks of α-Al_2O_3 phase appeared. This means that the second exothermic peak of the DTA trace also corresponded to the reaction between Al and TiO_2 forming Al_3Ti and α-Al_2O_3. When the temperature was raised from 900°C to 1000°C, the amount of both Al_3Ti and Al_2O_3 phases increased, but a small amount of residual Al was still left.

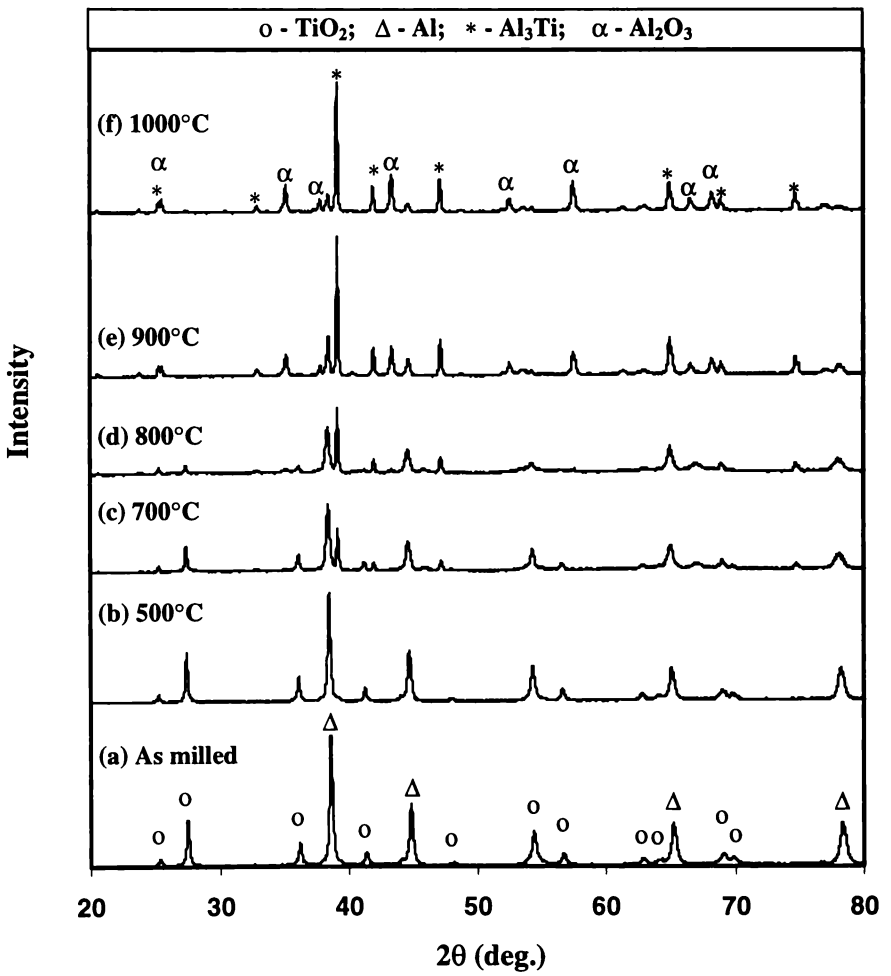

Figure 5-8. XRD patterns of the C1 powder after milling for 4 hours and then heated to different temperatures: (a) as milled, (b) 500°C, (c) 700°C, (d) 800°C, (e) 900°C and (f) 1000°C.

Figure 5-9 shows the XRD patterns of the 8 hours milled C1 powder after being heated to different temperatures. After the powder was heated to 800°C, Al_3Ti phase became the major phase and some Al was still left. TiO_2 phase also almost disappeared. The peaks of α-Al_2O_3 were visible but very weak. After the powder

was heated to 1000°C, the Al peaks also disappeared. This suggests that the reaction between Al and TiO_2 had been completed.

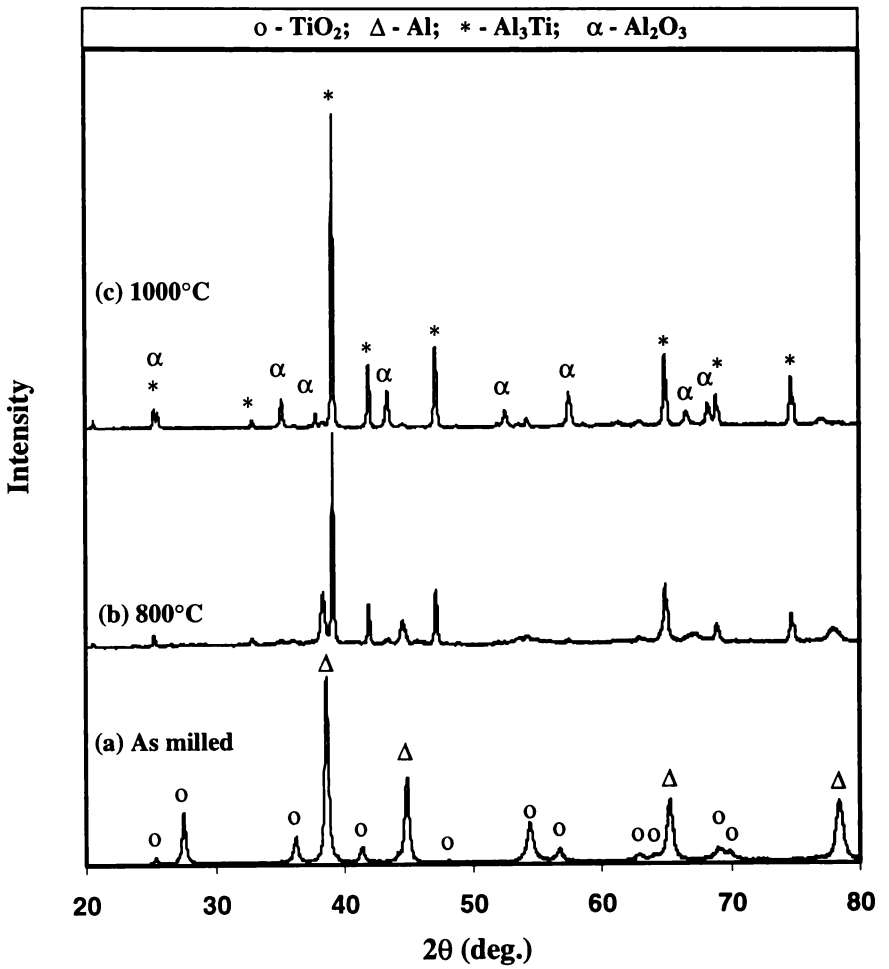

Figure 5-9. XRD patterns of the C1 powders after milling for 8 hours and then heated to different temperatures: (a) as milled, (b) 800°C and (c) 1000°C.

Figure 5-10 shows the XRD patterns of the 60 hours milled C1 powder after being heated to different temperatures. After the powder was heated to 800°C, the XRD pattern showed only Al_3Ti peaks, as shown in Figure 5-10 (b). This means that the reaction between Al and TiO_2 was completed by the time of reaching 800°C. However, the peaks corresponding to the other expected product of the reaction, aluminium oxide, still could not be seen. After the powder was heated to 1000°C, strong peaks of α-Al_2O_3 phase appeared in the XRD pattern, as shown in Figure 5-10 (c).

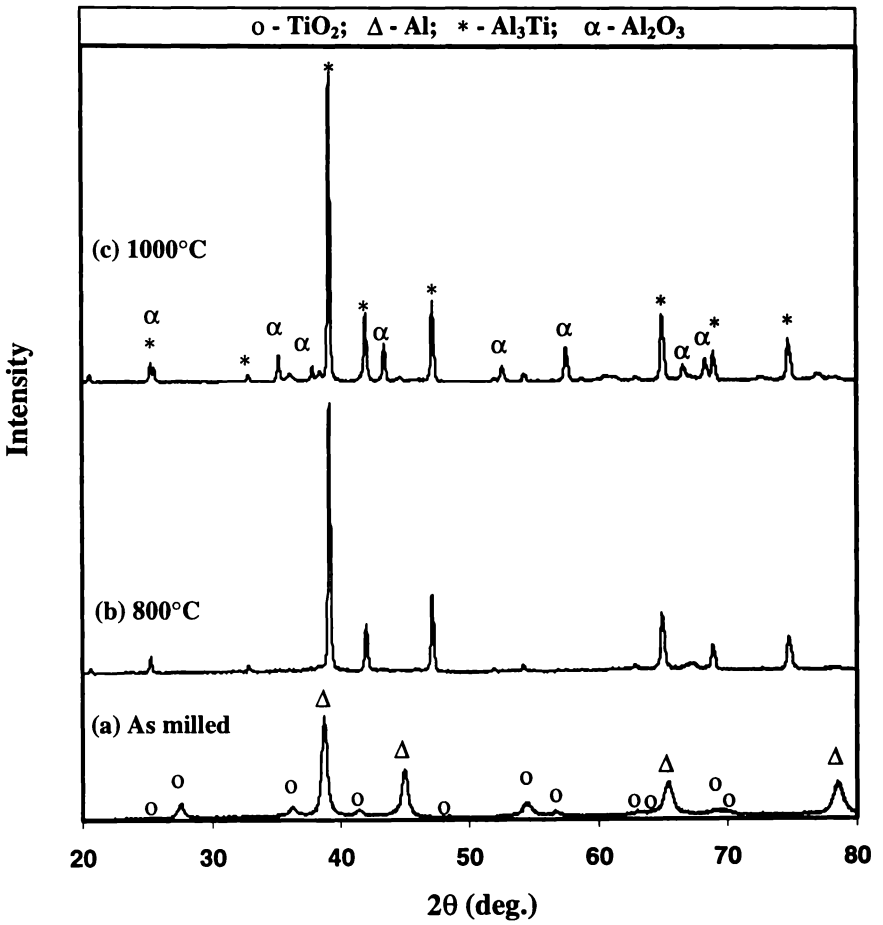

Figure 5-10. XRD patterns C1 powder after milling for 60 hours and then heated to different temperatures: (a) as milled, (b) 800°C and (c) 1000°C.

In order to visualise the influence of the milling on the extent of the reaction between Al and TiO_2 that occurred at low temperatures, the XRD patterns of the C1 powder produced after being milled for different times and then all being heated to 800°C were compared as shown in Figure 5-11. It was clearly observed that the amount of Al_3Ti formed increased and the amount of unreacted Al and TiO_2 decreased with increasing milling time. This was in agreement with the observation that the low temperature exothermic peak became stronger and stronger.

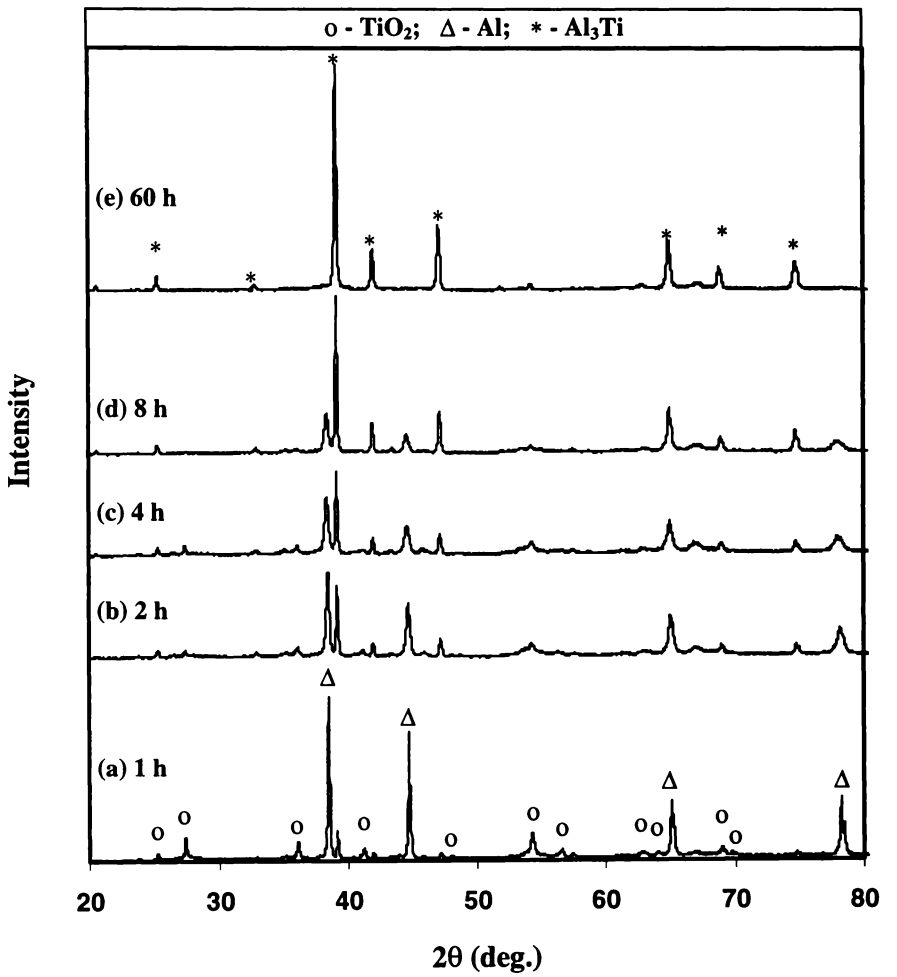

Figure 5-11. XRD patterns of the C1 powder after milling for different times and then heated to 800°C: (a) 1 hour, (b) 2 hours, (c) 4 hours, (d) 8 hours and (e) 60 hours.

The effect of holding time on formation of phases was also investigated. Figure 5-12 compares the XRD patterns of the 4 hours milled C1 powders after being heated to 800°C and held for different times. When the holding time increased from zero to 30 minutes, the amount of Al_3Ti increased slightly, but the amount of α-Al_2O_3 increased dramatically, judging from the relative intensity of the α-Al_2O_3 peaks.

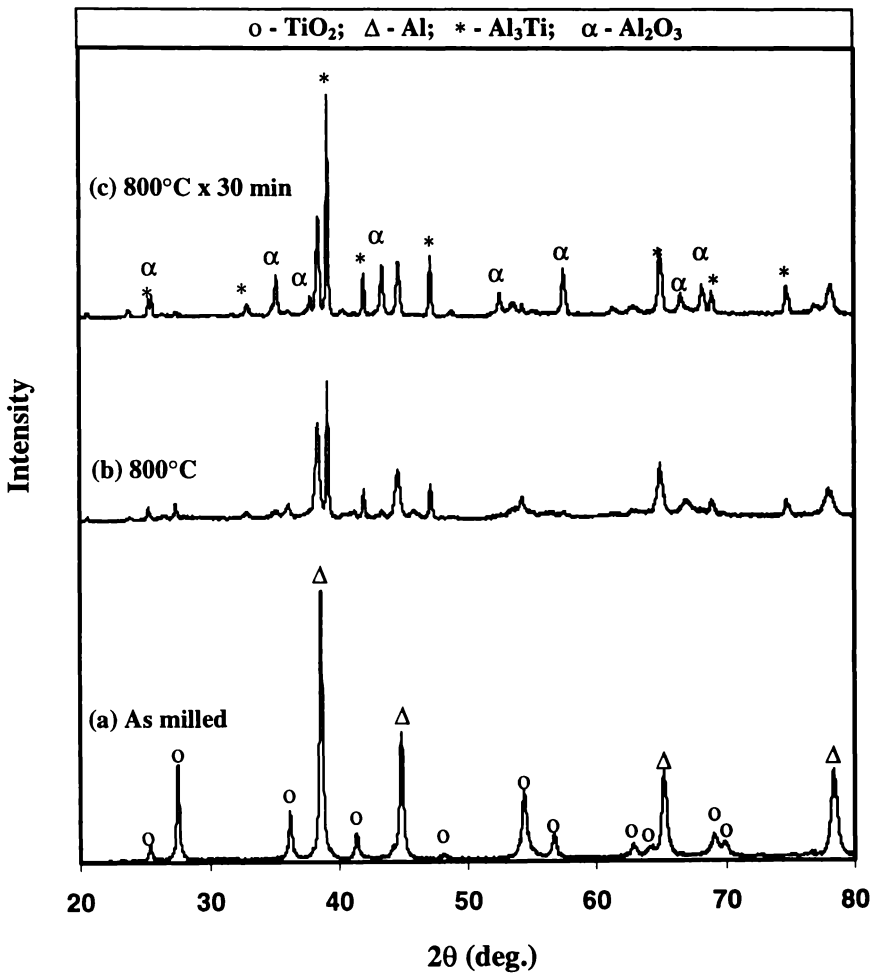

Figure 5-12. XRD patterns of the C1 powder after milling for 4 hours and then heated to (a) 800°C, and (b) to 800°C and held for 30 minutes.

5.3.2 C2 powder

Figure 5-13 shows the DTA traces of the C2 powder produced after being milled for different times. All the DTA traces exhibited an endothermic peak with a peak temperature of 660°C and an exothermic peak at different temperatures. The endothermic peak was due to the melting of Al. With the increase of milling time this peak became smaller. The DTA trace of 1 hour milled powder exhibited one exothermic peak with onset and peak temperatures of 800°C and 850°C respectively. With increase of milling time to 2 hours or more, the high temperature exothermic peak disappeared, and a low temperature exothermic peak started to appear and became stronger with increasing milling time. This exothermic peak had an onset and peak temperatures of 625°C and 675°C respectively.

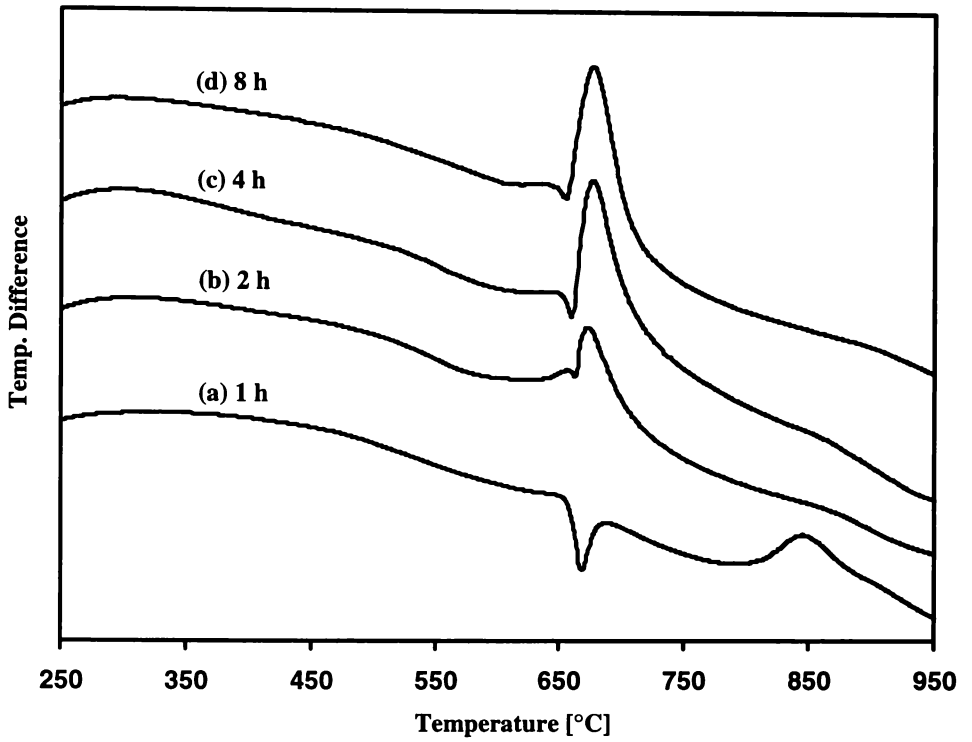

Figure 5-13. DTA traces of C2 powders after milling for (a) 1 hour, (b) 2 hours, (c) 4 hours and (d) 8 hours.

Figure 5-14 shows the XRD patterns of the 4 hour milled C2 powder after being heated to different temperatures. After the powder was heated to 500°C, only peaks of TiO_2 and Al phase were shown in the pattern. After the powder was heated to 700°C, Al_3Ti peaks became the major peaks in the XRD pattern, and the TiO_2 and Al peaks became the minor ones. This suggests that the exothermic peak was caused by reaction between Al and TiO_2, forming Al_3Ti. After the powder was heated to 800°C, the peaks of TiO_2 and Al became very weak, suggesting that most of the TiO_2 and Al had reacted by now. However, there was still no clear peak associated with the aluminium oxide phase. With the powder being further heated to 900°C, TiO_2 and Al peaks disappeared while α-Al_2O_3 peaks started to appear. Some other very weak peaks also appeared, but they could not be identified. Upon further heating to 1000°C, Al_2O_3 peaks became very strong, while the Al_3Ti peaks became weaker. In the mean time, peaks of α-Ti rich phase appeared. This suggests that, during heating from 900°C to 1000°C, the reaction between Al_3Ti and the titanium oxides occurred forming Al_2O_3 and some Ti-rich phases. After the powder was heated to 1200 °C, Al_3Ti phase disappeared, α-Ti rich phase and Al_2O_3 phases became the major phases, and the Ti_3Al and TiO

phases became the minor ones. This indicated that the reaction between Al_3Ti and titanium oxides had completed during heating from 1000°C to 1200°C.

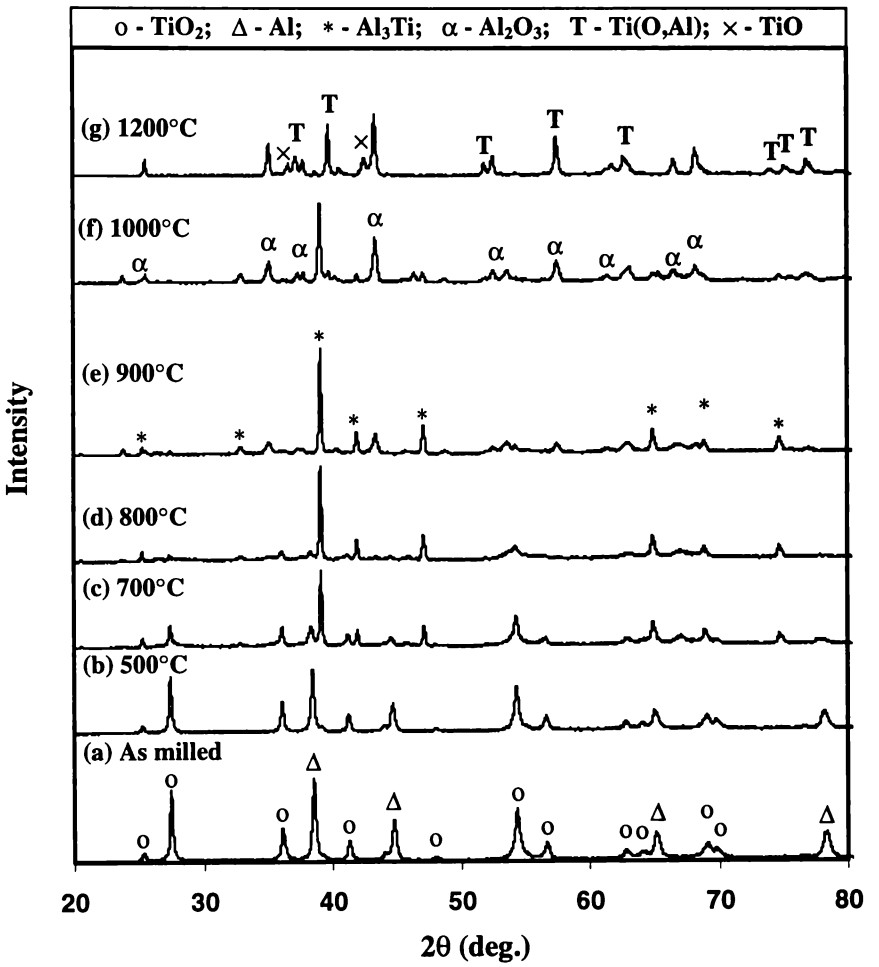

Figure 5-14. XRD patterns of C2 powder after milling for 4 hours and then heated to different temperatures: (a) as milled, (b) 500°C, (c) 700°C, (d) 800°C, (e) 900°C, (f) 1000°C and (g) 1200°C.

Figure 5-15 shows XRD patterns of the C2 powder after being milled for 4 and 8 hours and then heated to 1000°C in DTA. Comparing the two patterns, one can easily find that the amount of Ti-rich phase in the 8 hours milled power was much larger than that in the 4 hours milled powder. This implies that more Al_3Ti was turned into Ti rich phase in the 8 hours milled powder.

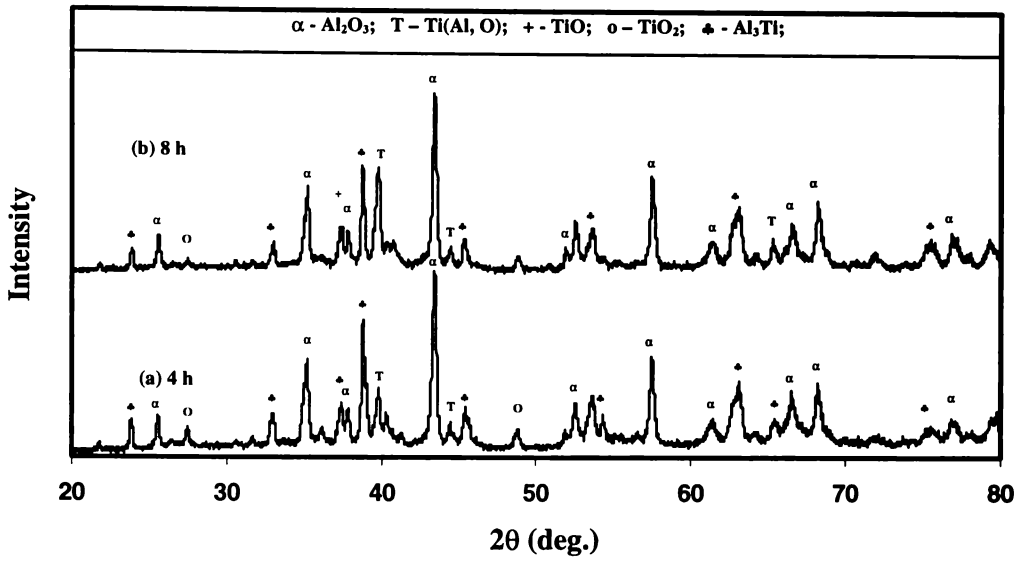

Figure 5-15. XRD patterns of the C2 powder produced after being milled for (a) 4 hours and (b) 8 hours, and then heated to 1000°C.

Figure 5-16 shows the XRD patterns of the 4 hours milled C2 powder after being heated to 900°C and then held for different times. It can be seen that with increasing holding time at 900°C, Al_3Ti was turned into α-Ti phase. While TiO and TiO_2 also formed. This was because the Ti rich phase was oxidised during holding in the DTA furnace.

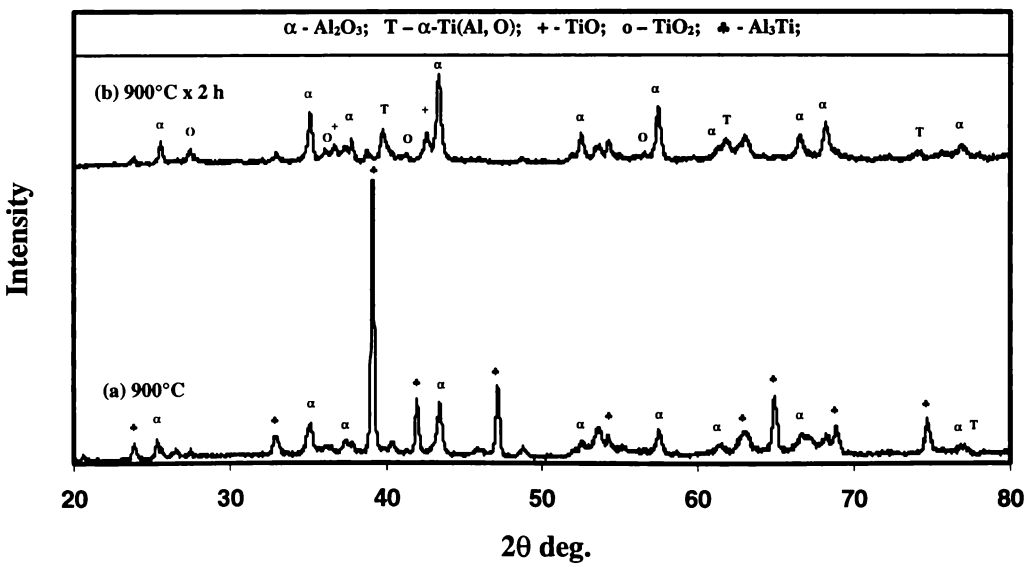

Figure 5-16. XRD patterns of the C2 powder after being milled for 4 hours and then (a) heated to 900°C, and (b) heated to 900°C and held for 2 hours.

Figure 5-17 shows the microstructures of powder particles of the 4 hours milled C2 powder under different heat treatment conditions. Under as-milled condition, the microstructure consisted of two phases: the Al phase (dark) and the TiO_2 phase (light). After the powder was heated to 900°C, the microstructure of the powder shows similar microstructure, but less contrast between the matrix and embedded particles, as shown in Figure 5-17 (b). EDAX examination showed that the matrix contained high percentage of Al and moderate amount of Ti, and the ratio between the Al and Ti was close to 3:1. Combining this information with the XRD analysis, it was certain that this phase was the Al_3Ti phase. The light particles contained high percentage of oxygen and less amount of Ti, and they were likely to be the titanium oxide phases. The darker regions surrounding the light particles contained high percentage of oxygen and a fair amount of Al, indicating they were likely to be the Al_2O_3 phase.

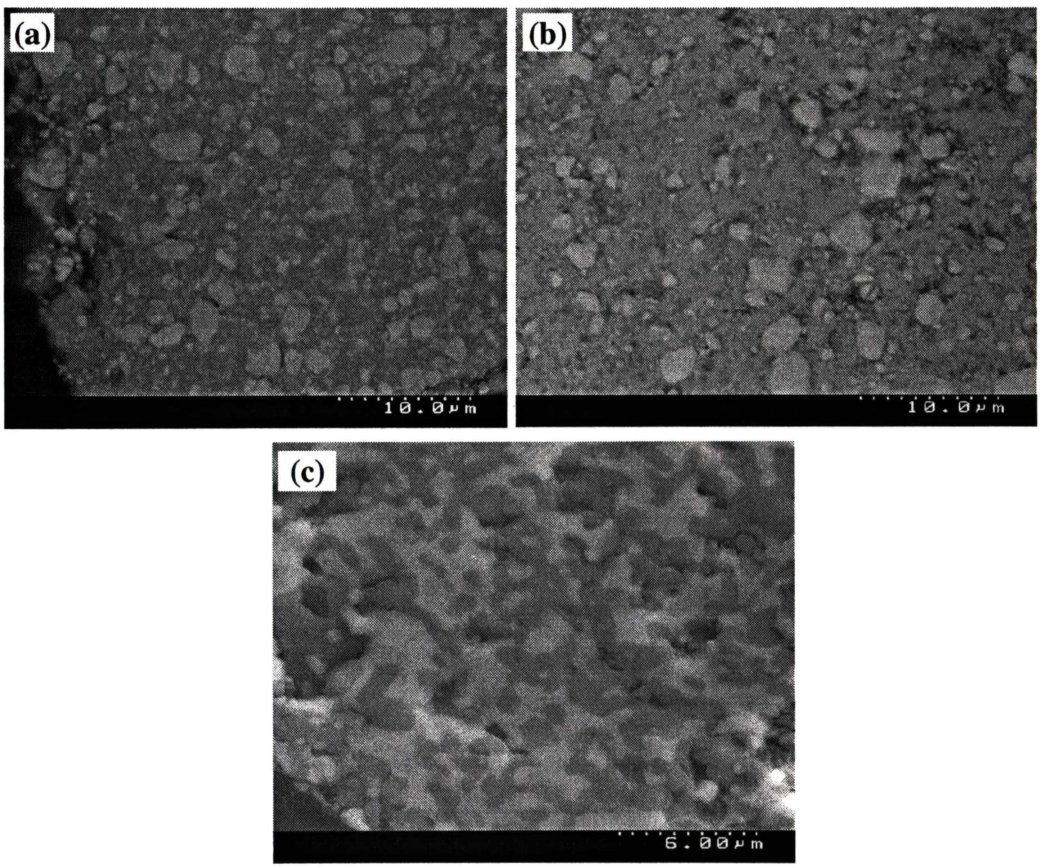

Figure 5-17. SEM backscattered images of the cross-sections of the particles produced after being milled for 4 hours and then heated to different temperatures: (a) as milled, (b) 900°C, and (c) 1200°C.

After the powder was heat treated to 1200°C, the microstructure changed dramatically, as shown in Figure 5-17 (c). EDAX analysis showed that the light phase had a high percentage of Ti and a low percentage of Al while the dark phase had a high percentage of Al and a very low percentage of Ti. Combining the XRD analysis and this EDAX result, it was fairly certain that the light phase was a Ti-rich phase (Ti(O,Al) or $Ti_3Al(O)$) and the dark phase was α-Al_2O_3 phase.

5.3.3 Reactions During Heat Treatment in Furnace

Two quite different reaction behaviours were observed when the mechanically milled powders were heated in a furnace.

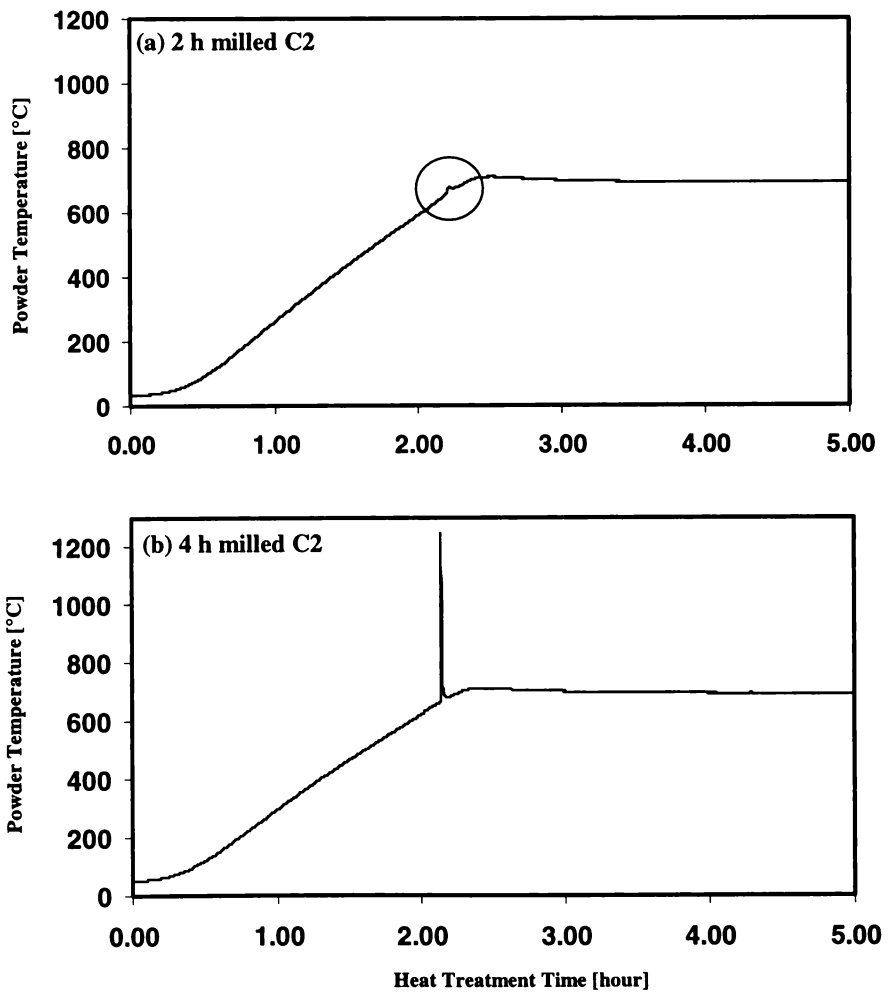

Figure 5-18. Powder temperature as a function of time recorded during heat treatment. (a) 2 hours milled C2 powder and (b) 4 hours milled C2 powder

When the powder with a coarse composite microstructure was heated, the reaction between Al and TiO_2 progressed slowly and did not cause a sharp increase in temperature, as shown in Figure 5-18 (a). However, when the powder with a fine composite microstructure was heated, the reaction between Al and TiO_2 was combustive as long as the powder was packed reasonably densely. The combustion reaction caused a sharp increase of temperature as shown in Figure 5-18 (b). As shown in Figure 5-18, the temperature increase occurred at about 670°C, which was close to the peak temperature of the exothermic peak of the DTA traces, as shown in Figure 5-13.

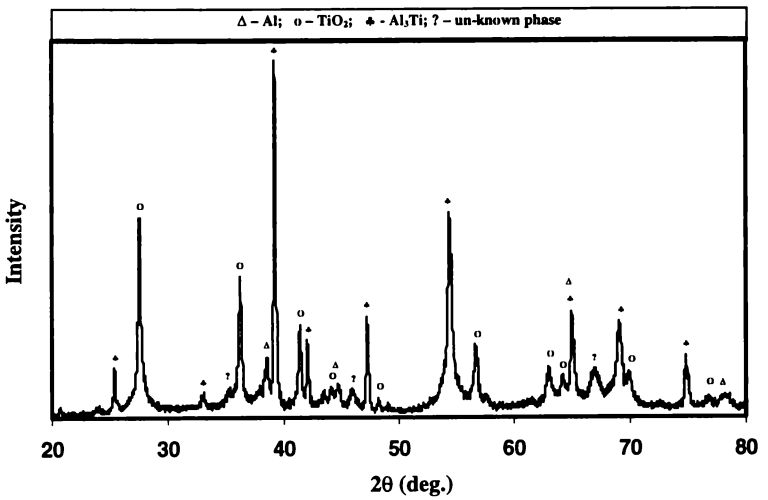

Figure 5-19. XRD pattern of the 2 hours milled C2 powder after being heated to 700°C and then held for 10 minutes. The reaction was slow.

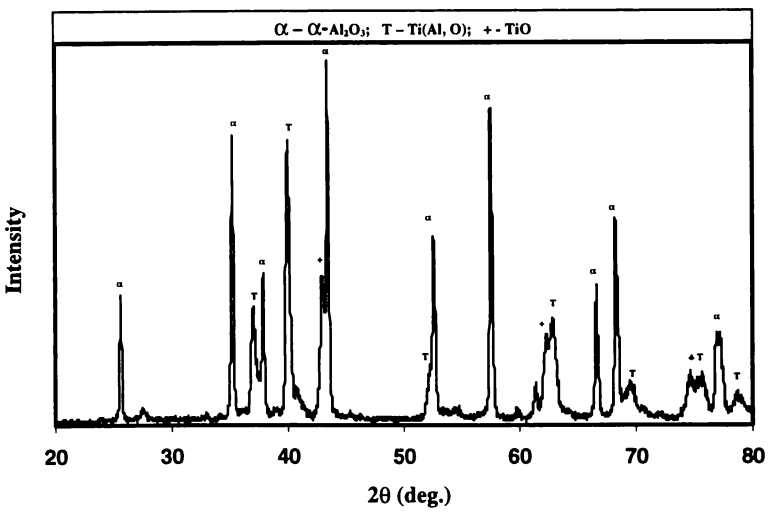

Figure 5-20. XRD pattern of the 4 hours milled C2 powder shortly after a combustive reaction during furnace heat treatment.

The slow reaction resulted in the formation of Al_3Ti and other unknown phases, as shown in Figure 5-19. The combustive reaction caused the powder temperature to rise up to 1250°C in a very short time, and the dramatic increase in powder temperature caused formation of a Ti-rich phase and α-Al_2O_3, as shown in Figure 5-20.

5.4 Discussions

5.4.1 Reaction Mechanism

Two exothermic peaks appeared in the DTA traces of milled C1 powders, as shown in Figure 5-7. The XRD analysis showed that (Figure 5-8), both exothermic peaks were due to the reaction between Al and TiO_2, forming Al_3Ti. With increase of milling time, the first exothermic peak became stronger, and the second exothermic peak became weaker. This indicates that the fraction of the reaction product from the first reaction increased with the increase of milling time. It also shows that the fraction of the reaction product from the first reaction increases with the refinement of composite microstructure and the increase of interface areas.

In the 1 hour milled powder, the direct contact between Al and TiO_2 was limited, and only a small amount of Al and TiO_2 reacted forming Al_3Ti. This was evidenced by the XRD examination of the powders produced by heating the 1 hour milled powder to 800°C in DTA, which showed very weak Al_3Ti peaks, as shown in Figure 5-7 (a). With further increase of temperature, the reaction between the molten Al and solid TiO_2 proceeded gradually and reached the maximum at the peak temperature of 870°C, the reaction continued until TiO_2 was consumed. This reaction led to formation of mainly Al_3Ti, Al_2O_3 and some titanium sub-oxide, with some Al remained. In the case of longer time milled powders, the area of Al/TiO_2 interface increased. As a result, the reaction between Al and TiO_2, enhanced by the melting of Al, resulted in formation of more Al_3Ti and Al_2O_3, as indicated by the increased strength of the first exothermic peaks in Figure 5-7 (b) to (d). Overall, it is clear that with an increase of milling time, the reaction becomes more complete when the powder is heated to a given

temperature above 700°C. It also becomes very clear that both exothermic peaks of the DTA trace of the milled C1 powder are caused by the reaction between Al and TiO_2, forming Al_3Ti and Al_2O_3.

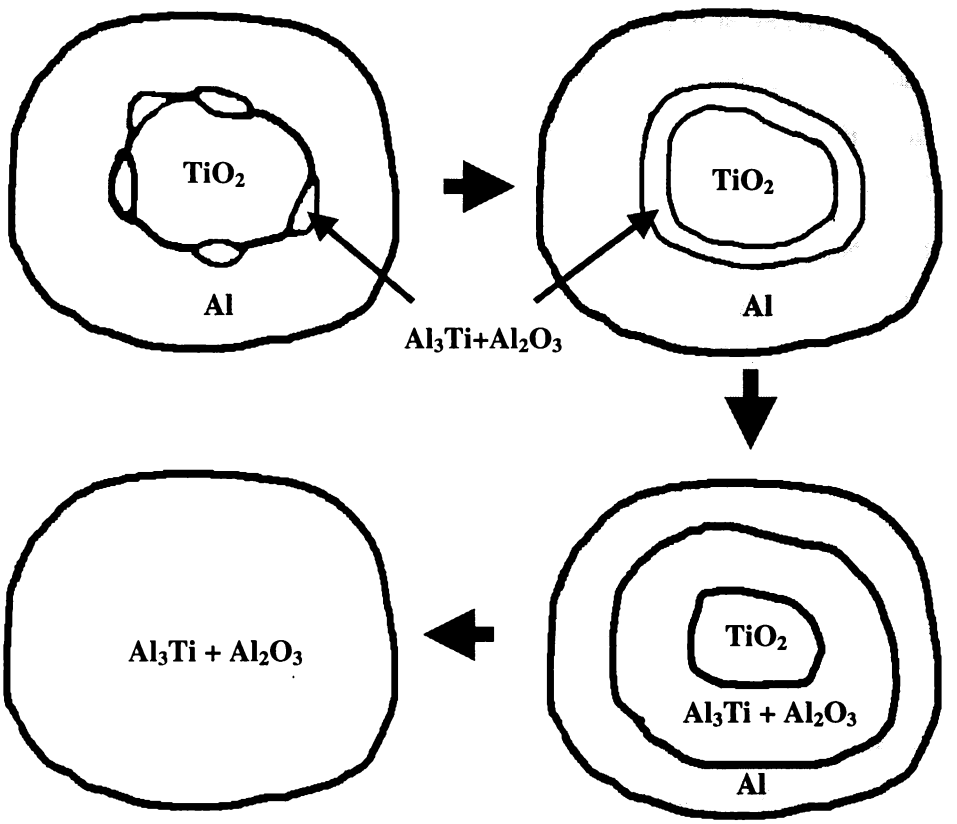

Figure 5-21. Schematic diagram showing the proposed mechanism of the Reactions between TiO_2 and Al in C1 Powders.

Figure 5-21 shows a schematic diagram for the proposed reaction mechanisms. The reaction between Al and TiO_2 firstly occurs at the Al/TiO_2 interface region. Due to the melting of Al, it is easier for Ti atoms to diffuse into Al and forming Al_3Ti solid. The formation of solid Al_3Ti causes a barrier between non-reacted Al and TiO_2. The subsequent reaction between the remaining Al and TiO_2 relies on the bulk diffusion through the product layer. The activation of this diffusion-controlled process requires a higher temperature, as reflected by the second exothermic peak of the DTA traces. With further refinement of the composite microstructure, the fraction of the reactants consumed by the interfacial reaction significantly increases, leaving less reactants to react at high temperatures.

In the C2 powder, the low temperature interface reaction also occurred at around 650°C for the powders with a well established composite particle microstructures. This reaction results in the formation of Al_3Ti and some other phases. Due to the abundence of TiO_2 phase and relatively less Al, the Al phase is quickly consumed by the low temperature interface reaction. Further reaction between Al_3Ti and TiO_2 or titanium sub-oxides proceeds gradually until forming Ti-rich phases and α-Al_2O_3 by either heating to higher temperatures such as 1200°C or holding at some elevated temperatures for a longer time. The formation of α-Al_2O_3 is largely determined by the growth kinetics. During the heating in the DTA at a constant rate of 20°C/min, it is unlikely to form a detectable amount of α-Al_2O_3 until 900°C. However, by holding for a time at a temperature below 900°C but above 800°C, it is possible to form a substantial amount of α-Al_2O_3.

5.4.2 Formation of First Phase

The formation of the first phase from the reaction between Al and TiO_2 is always Al_3Ti for both the C1 and C2 powders investigated here. It is very likely that the same is also true for other compositions.[7] This may be attributed to the fact that the crystal structure of Al_3Ti, being tetragonal, is very close to that of Al, being cubic. When Ti atoms diffuse into Al (in the state of either solid or liquid), it is easier for Al rich Al_3Ti phase to nucleate.

5.4.3 Formation of α-Al_2O_3

It is clear that α-Al_2O_3 does not form directly from the reaction between Al and TiO_2. Instead, this phase may form as a result of a transition from another form of aluminium oxide to α-Al_2O_3. It is not clear what the other form of aluminium oxide is, although Bruhn *et al.* reported the formation of γ-Al_2O_3 from the reaction between TiO_2 and Al at a temperature below 700°C.[9] Solid state nucleus magnetic resonance spectroscopy might be able to illustrate the nature of the Al-O bonds, and thus provide clues on what form the aluminium oxide is. This is beyond the scope of this study and is recommended for the future work. Formation of α-Al_2O_3 seems to be controlled by both temperature and time. When the 4 hours milled C1 and C2 powders were heated in DTA at a constant rate of

20°C/min, the α-Al_2O_3 only appeared after 900°C, as shown in Figure 5-8 and Figure 5-14. However, when the same powders were heated to 800°C and then held for 30 minutes, strong α-Al_2O_3 peaks appeared in the XRD pattern, as shown in Figure 5-12.

5.4.4 Formation of α-Ti Phase

As has been discussed above, the first phase formed from the reaction between Al and TiO_2 is always Al_3Ti. The formation of α-Ti-rich phases requires either higher temperatures up to 1200°C, as shown in the XRD result in Figure 5-14, or a longer time if it is heated to a lower temperature, as shown in Figure 5-16. It has also been shown in Figure 5-15 that the time taken to finish the reaction is inversely proportional to the milling time, or more precisely, the refinement of the composite microstructure. This suggests that diffusion plays an important role in this reaction.

5.4.5 The Effect of Mechanical Milling on the Reaction Kinetics

For the C1 powder, the significance of the interface reaction peak, relative to the bulk reaction peak, increases with the milling time and the fineness of the Al/TiO_2 microstructure, as shown in Figure 5-7. Further increases in the milling time, only causes the reaction temperature to decrease slightly. This suggests that there is a limit beyond which extended milling cannot cause any further decrease in the reaction temperature. As argued by Welham,[7] there is clearly a step in the reaction mechanism which is unaffected by milling and this is likely to be the rate determining step. Assuming that diffusion had been overcome by milling, then the implication is that the initial chemical reaction is the rate determining step. It is unlikely that milling can change a chemically controlled step and this seems to be the most probable limitation.[7]

For the C2 powder, the increased milling time or the refined composite microstructure only leads to a more thorough interface reaction forming Al_3Ti phase. This reaction consumes the Al phase in the powder. Upon further heating, the reactions between Al_3Ti and the remaining TiO_2 or titanium sub-oxides

proceed gradually, leading to the formation of Ti-rich phases and α-Al_2O_3. This later reaction progresses much more slowly than the first reaction, which causes formation of Al_3Ti. This is very likely due to the much less driving force for later reaction in compare with the first reaction.

5.5 Summary

In this chapter, results of the solid state reactions in two high energy mechanically milled Al/TiO_2 powders with nominal mole ratio between Al and TiO_2 being 13/3 and 4/3 respectively are presented. For both compositions, the microstructure evolves from a microstructure of TiO_2 particles being entrapped between the deformed Al particle to that of the TiO_2 particles being embedded in Al matrix with the progress of milling. No reaction was observed during ball milling. The reactions during subsequent heating of the milled powders were in large extent affected by the microstructure of the as milled powders. The first phase formed from the reaction between Al and TiO_2 is always Al_3Ti for both C1 and C2 powders. The formation of Ti-rich phase proceeded much slower than that of Al_3Ti and requires higher temperature and longer time. The formation of α-Al_2O_3 could not be observed immediately after the reaction between Al and TiO_2. High energy mechanical milling can accelerate the reaction kinetics by minimising diffusion barrier, but there is a clear limit for this effect in the case of reaction between Al and TiO_2.

5.6 References

1 G.B. Schaffer and P.G. McCormick, *Appl. Phys. Lett.*, 1989, **55**, 45.

2 G.B. Schafer and P.G. McCormick, *Scr. Metall.*, 1989, **23**, 835.

3 G.B. Schafer and P.G. McCormick, *J. Mater. Sci. Lett.*, 1990, **9**, 1014.

4 G.B. Schafer and P.G. McCormick, *Metall. Trans. A*, 1990, **A21**, 2789.

5 G.B. Schafer and P.G. McCormick, *Metall. Trans. A*, 1991, **A22**, 3019.

6 G.B. Schafer and P.G. McCormick, *Metall. Trans. A*, 1992, **A23**, 1285.

7 N.J. Welham, *Mater. Sci. & Eng.*, 1998, **A255,** 81.

8 C.S. Barret, and T.B. Massalski, *Structure of Metals*, 3rd ed. (McGraw-Hill, New York, 1996), p.155.

9 J. Bruhn, S. Schicker, D.E. Garcia, R. Janssen, F. Wabner and N. Claussen, *Key Engineering Materials*, 1997, **127-131**, 73.

Chapter Six

Solid State Reactions between CuO and Cu-Al Powders

6.1 Introduction

The solid state reactions between CuO and Cu-Al alloy powders are interesting because they involve Cu-Al alloys instead of Cu or Al elemental powders. Much research has been conducted on combustive reactions between CuO and Al induced by high energy milling.[1,2] However, the combustive reaction between CuO and Al occurs rapidly, leading to the formation of coarse Cu and Al_2O_3 powder particles and separation of these two phases.[1] In order to make Cu matrix composite with fine dispersion of Al_2O_3 particles, the combustive reaction must be suppressed. One of the techniques is to dilute the Al using pure Cu. The route used in this study is to firstly, mechanically alloy the Al and Cu forming Cu(Al) solid solution or Cu-Al intermetallic compound. Then, add CuO into the Cu-Al alloy powder and mill the mixture to form a composite structured powder. Finally, consolidate the composite powder to obtain a Cu/Al_2O_3 metal matrix composite material. In order to optimise the process effectively, it is necessary to understand the effect of different process parameters on reaction kinetics.

The three compositions investigated in this study are listed in Table 0-1.

Table 0-1. Nominal compositions of the three Cu-Al-CuO powders studied

	Composition of Cu-Al alloy powder	Composition of final powder
D1	Cu-6at%Al	Cu(Al)-8mole%CuO
D2	Cu-14at%Al	Cu(Al)-17mole%CuO
D3	Cu-37at%Al	(Cu-37at%Al)-36mole%CuO

6.2 Microstructural Evolution

6.2.1 D1 Powder

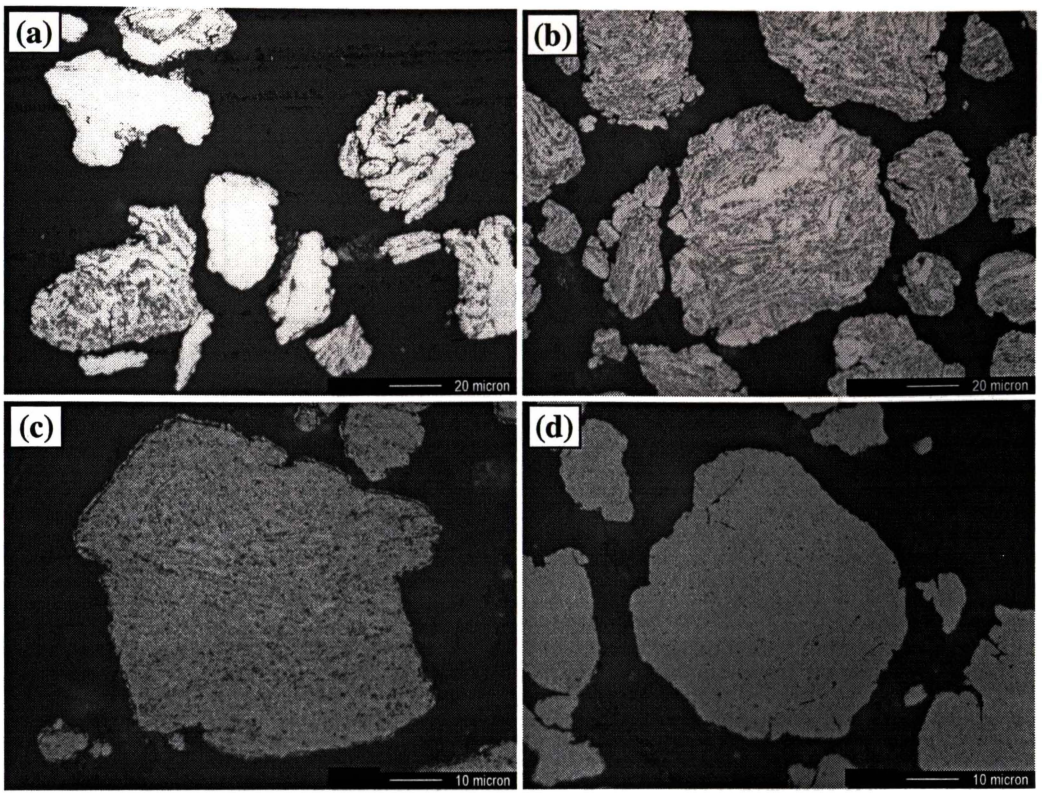

Figure 6-1. Optical micrographs of cross-section of the D1 powder particles produced after being milled for (a) 1 hour, (b) 2 hours, (c) 4 hours, and (d) 8 hours. The light phase is Cu(Al) solid solution and the dark phase is CuO.

Figure 6-1 shows optical micrographs of the cross-section of D1 powder particles produced after being milled for different times. The light phase is Cu(Al) solid solution phase and the dark phase is CuO phase. In the early stage of milling for 1 hour, the microstructure developed very unevenly. Some of the powder particles already had a Cu(Al)/CuO composite structure, but some of the powder particles still mainly consisted of Cu(Al) phase, as shown in Figure 6-1 (a). After 2 hours of milling, most of the powder particles formed a composite structure with the CuO particles being entrapped in a matrix of Cu(Al) phase. The powder particles exhibited a banded structure at this point. After 4 hours of milling, the banded structure disappeared, but the CuO particles were not yet evenly distributed. After 8 hours of milling, the CuO particles were evenly distributed in the Cu(Al) matrix and the microstructure became homogeneous.

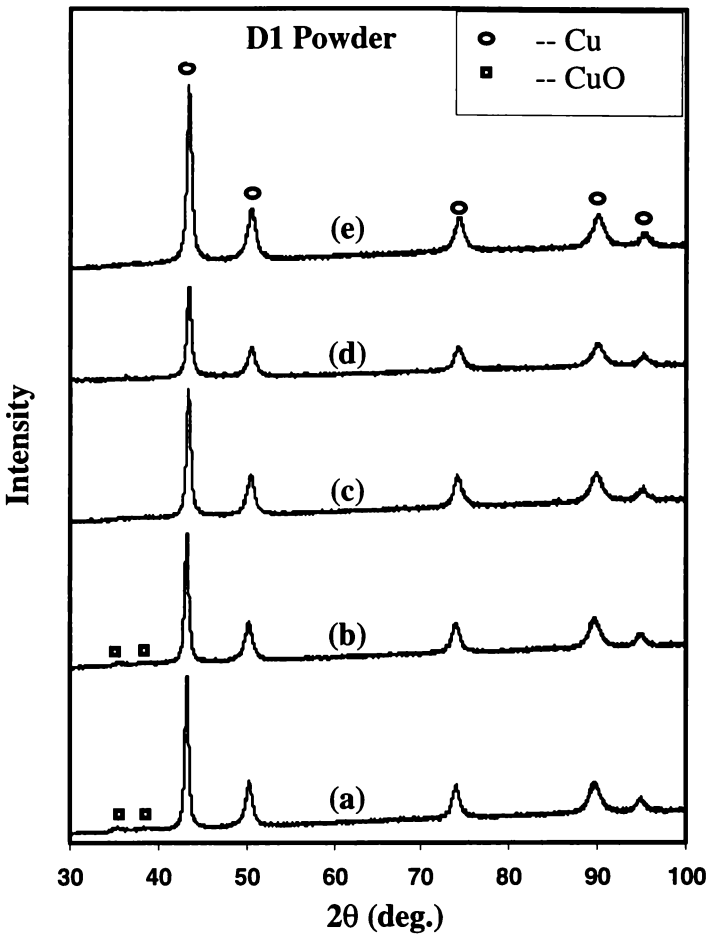

Figure 6-2. XRD patterns of the powders produced after milling D1 powder for (a) 1 hour, (b) 2 hours, (c) 4 hours, (d) 8 hours, and (e) 16 hours.

Figure 6-2 shows the XRD patterns of the powders produced by milling D1 powder for different times. In the XRD patterns, CuO peaks gradually disappeared after 4 hours of milling. The Cu {111} peak shifted to higher angles with the increase of milling time. The Cu {111} peak shifted from $2\theta = 43.27°$ for the 1 hour milled powder to $2\theta = 43.45°$ for the 8 and 16 hours milled powders. This corresponds to a decrease of the lattice parameter from 3.620 to 3.604 Å.

6.2.2 D2 Powder

Figure 6-3 shows typical optical micrographs of the cross-sections of powder particles in the D2 powder after being milled for different times. After 1 hour of milling, CuO powders were entrapped between Cu(Al) layers, forming an alternating multilayer composite structure. The Cu(Al) layer thickness ranged from 1 to 30 μm. The CuO layer was relatively evenly distributed between the

Cu(Al) layers and had a thickness of approximately 0.5 μm. With an increase of milling time to 2 hours, the multilayer structure was destroyed, and the CuO particles were more evenly distributed in Cu(Al) matrix. With a further increase in milling time to 4 hours, the CuO particles became evenly embedded in the metal matrix with particle size ranging from 0.1 to 0.3 μm in diameter. The further increase in milling time to 8 hours rendered the microstructure to become homogeneous. The CuO particle size was slightly reduced to be in a range of 0.1 to 0.2 μm. After the powder was milled for 16 hours, the microstructure was fully homogenised and could not be resolved using SEM.

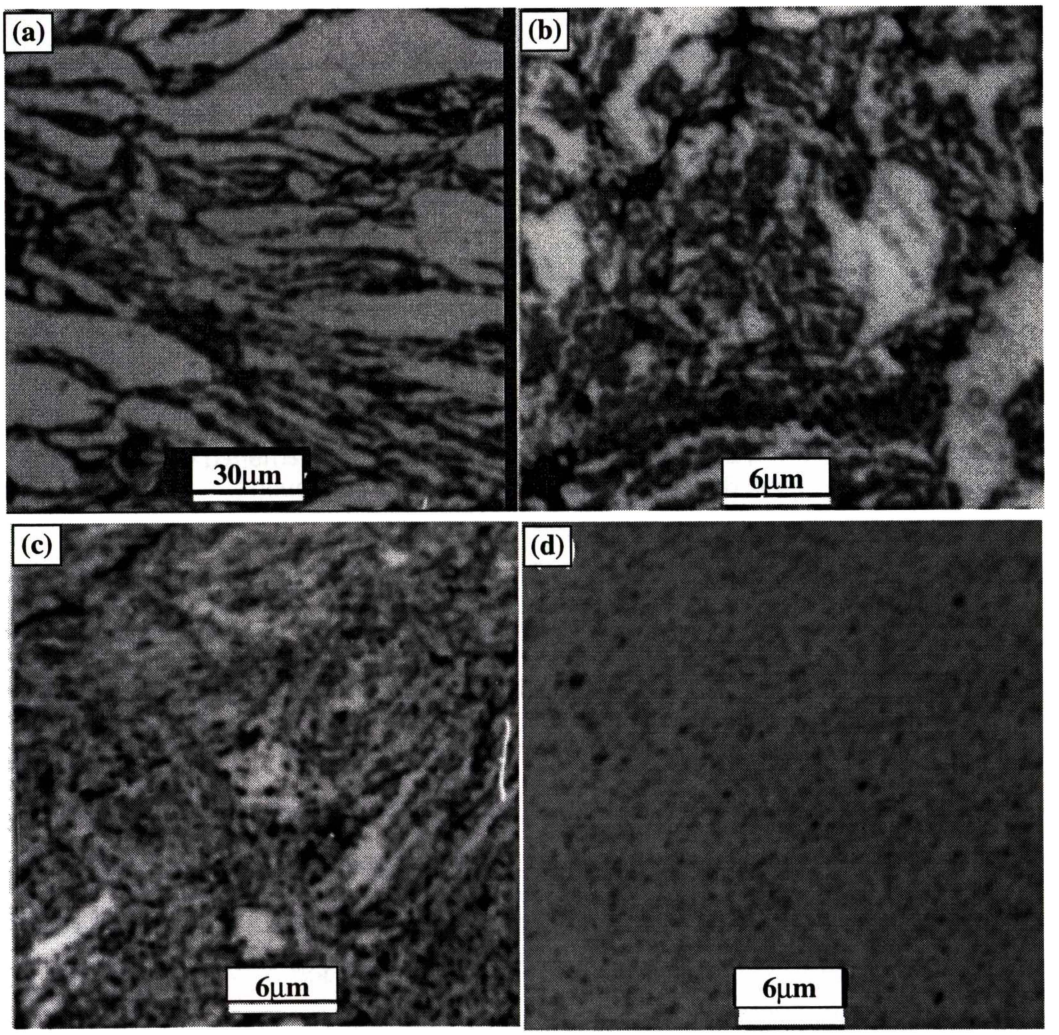

Figure 6-3. Optical micrographs of cross-section of powder particles of D2 powder after being milled for (a) 1 hour, (b) 2 hours, (c) 4 hours, and (d) 8 hours.

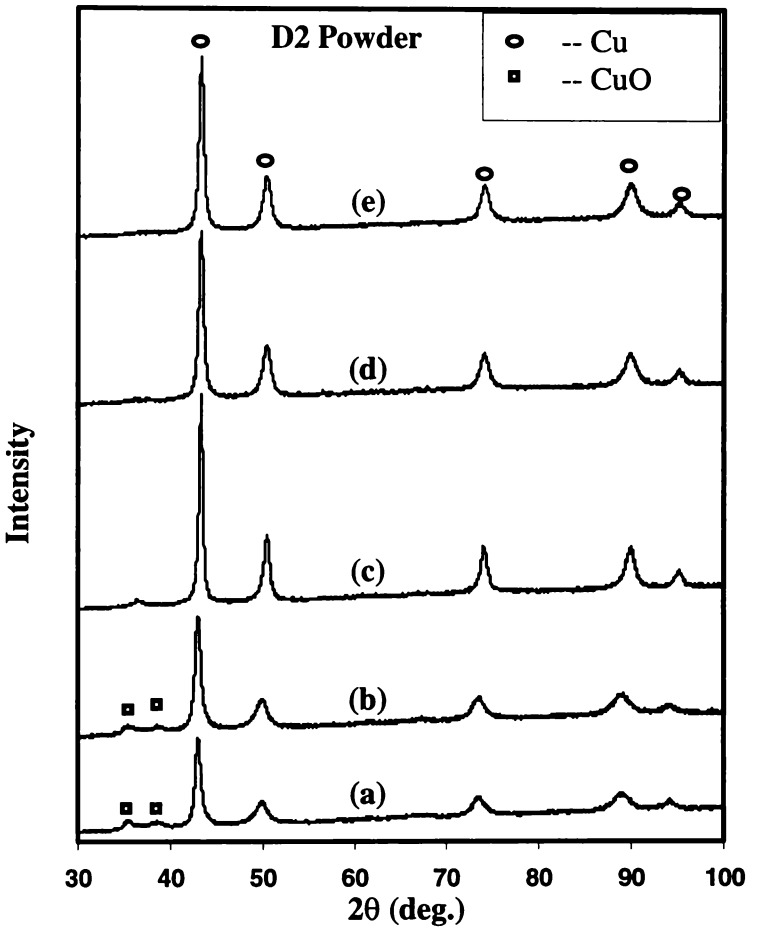

Figure 6-4. XRD patterns of powders produced after milling D2 powder for (a) 1 hour, (b) 2 hours, (c) 4 hours, (d) 8 hours, and (e) 16 hours.

Figure 6-4 showed the XRD patterns of the powders produced by milling D2 powder for different times. In the XRD patterns, CuO peaks gradually disappeared after 4 hours of milling. The Cu(Al){111} peak shifted from 2θ = 43.07° to 2θ = 43.37° after 16 hours of milling. This corresponds to an decrease of the lattice parameter of the Cu(Al) phase from 3.635 to 3.611 Å. This is likely due to the fact that the CuO reacted with the Cu(Al) solid solution forming Al_2O_3 phases and reducing the Al concentration in the Cu(Al) solid solution. However, the Al_2O_3 peaks were not seen in the XRD pattern of the as milled powder. This might be due to the Al_2O_3 particles being too small to be detected using the XRD technique.[3] After the powder was sintered at 900°C for 4 hours the peaks of α-Al_2O_3 phase were clearly observed on the XRD pattern, as will be shown latter.

6.2.3 D3 Powder

Figure 6-5 shows the typical micrographs of the cross-section of powder particles in the D3 powder produced after being milled for different times. The grey phase is CuO and the light phase is γ-Cu_9Al_4 phase.

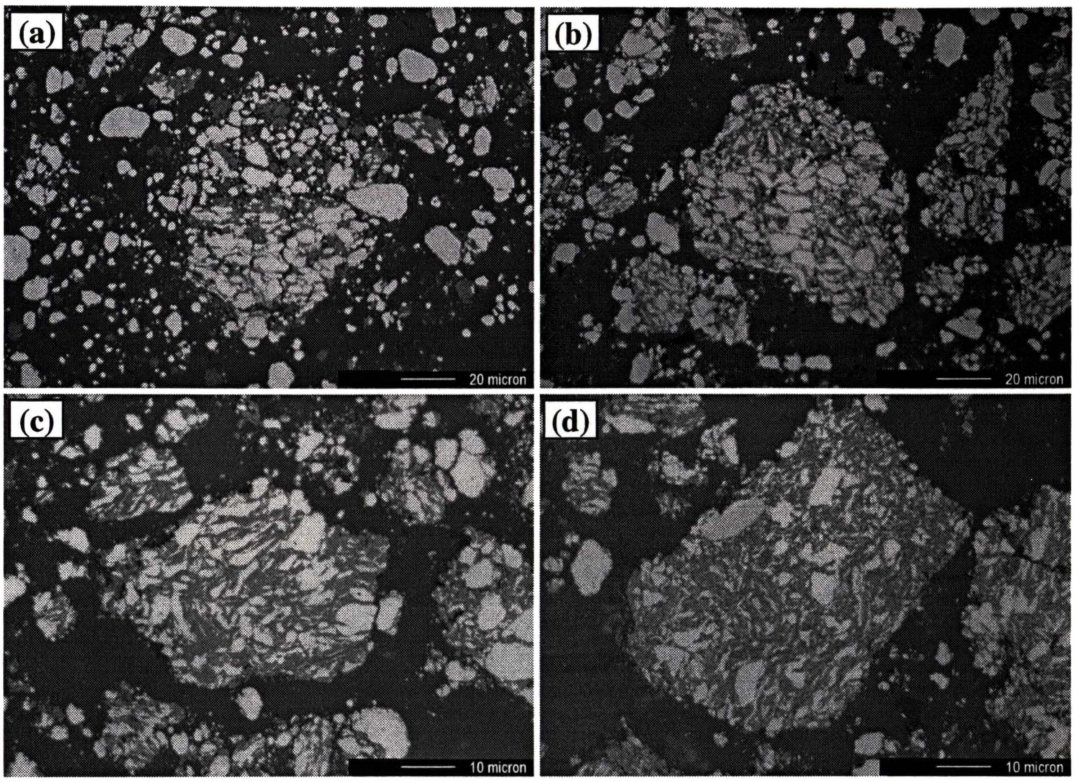

Figure 6-5. Optical micrographs of cross-section of D3 powder particles after being milled for (a) 0.3 hours, (b) 0.66 hours, (c) 1 hour, and (d) 1.33 hours.

After 0.33 hours of milling, some agglomerates formed, and a large fraction of free standing Cu_9Al_4 and CuO particles can still be observed, as shown in Figure 6-5 (a). The particle size of the Cu_9Al_4 phase ranged from a few micrometers to 20 μm and that of the CuO ranged from sub-micrometer to 10 μm. Some Cu_9Al_4 particles in the agglomerates were flattened, and between the flattened Cu_9Al_4 particles were CuO which were distributed unevenly. After 0.66 hours of milling, as shown in Figure 6-5 (b), more Cu_9Al_4 and CuO particles were incorporated into the agglomerates of different sizes. The CuO phase here acted like some kind of binder for the Cu_9Al_4 particles which were deformed. Still some free standing Cu_9Al_4 particles with an equiaxial shape remained. After 1 hour of milling, Cu_9Al_4/CuO composite structured particles were readily formed. Some of the

Cu_9Al_4 particles were severely deformed, forming uneven multilayered composite structures, with thickness ranging from sub-micrometer to 5 μm. There were still some equiaxed Cu_9Al_4 particles with sizes ranging from 1 μm to 10 μm in the powder, either free standing or in the composite particles. After 1.33 hours of milling, the composite structure was substantially refined, but was still inhomogeneous. Some very fine Cu_9Al_4 layers with a thickness from sub-micrometer to a few micrometers co-existed with some big particles with a diameter of 8 μm. Occasionally, free standing equiaxed Cu_9Al_4 particles were still observed.

With an increase of milling time to 1.66 hours, Cu_9Al_4 and CuO reacted during milling, as shown Figure 6-6. The colour of the powder changed from black to brown. The spherical particles in the micrograph are Al_2O_3 particles.

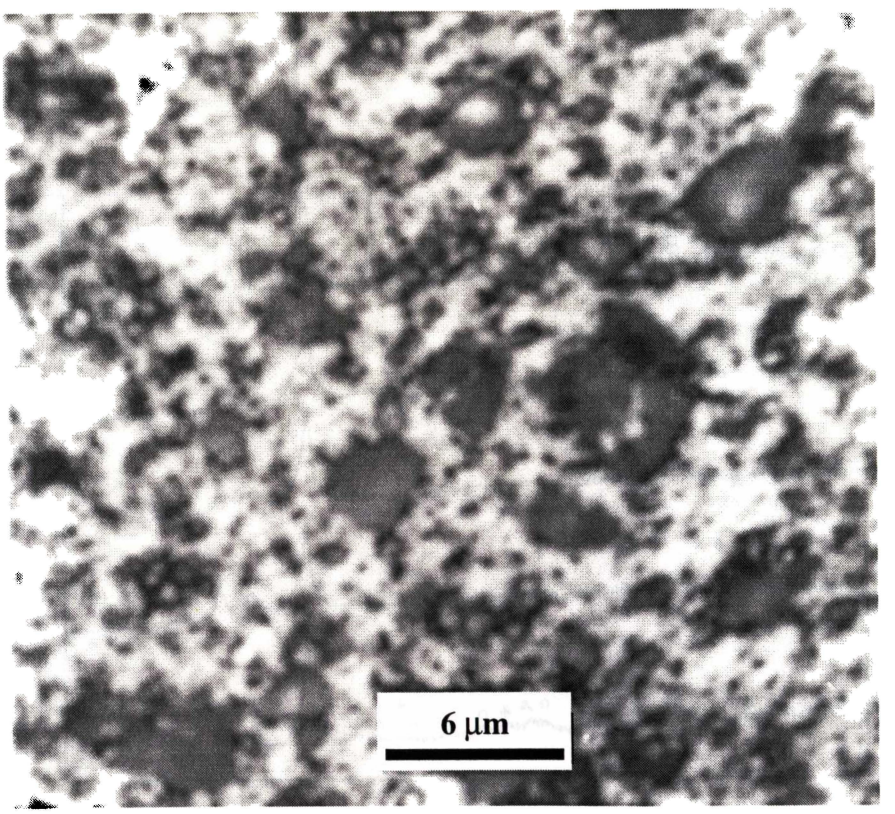

Figure 6-6. Optical micrograph of the D3 powder particles after combustive reaction.

Figure 6-7 shows the XRD patterns of the D3 powder after being milled for different times. The XRD patterns of the powders milled for 0.33, 0.66 and 1 hour, respectively, showed only peaks of Cu_9Al_4 and CuO phases. With increasing milling time to 1 hour, the CuO peaks were slightly broadened. While in the XRD pattern of 1.33 hours milled powder, as shown in Figure 6-7 (d), two extra peaks appeared. These two peaks are very likely to be associated with the Cu_2O phase. After 1.66 hours of milling, the XRD pattern changed dramatically. Pure Cu phase became the major phase and α-Al_2O_3 phase became the second major phase. Cu_2O and Cu_9Al_4 phases became minor phases. The colour of the powder changed from black to dark brown. Some spherical Cu particles could easily be picked up from the powder. This suggests that a combustion reaction had occurred during milling.

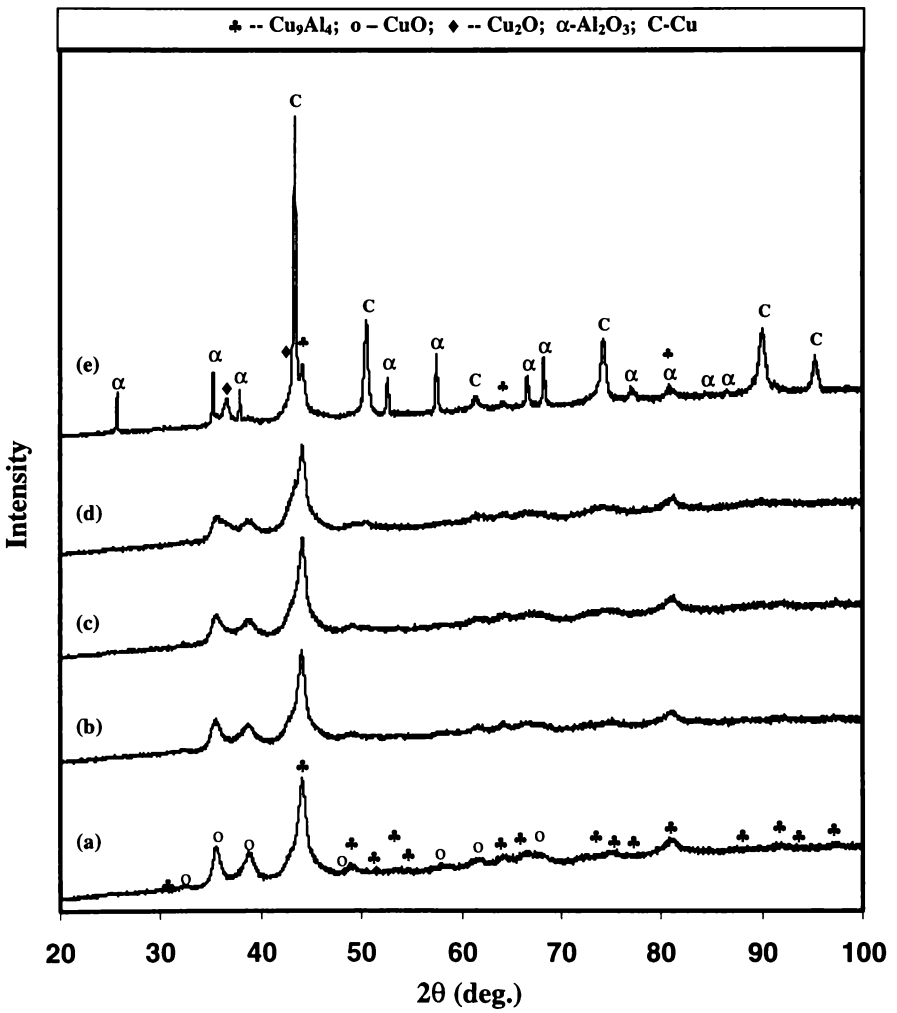

Figure 6-7. XRD patterns of the D3 powders after being milled for (a) 0.33 hours, (b) 0.66 hours, (c) 1 hour, (d) 1.33 hours and (e) 1.66 hours

6.3 Reactions Between CuO and Cu-Al During Heating

6.3.1 D1 Powder

Figure 6-8 shows the DTA traces of the D1 powders after being milled for different times. There were two obvious exothermic peaks in the powder milled for 1 hour, as shown in Figure 6-8 (a). The first exothermic peak started at temperature around 150°C and reached the maximum at temperature of 270°C. This exothermic peak overlapped with the second one. The second exothermic peak started at around 300°C and reached the maximum at about 440°C. The peak tail extended to about 650°C.

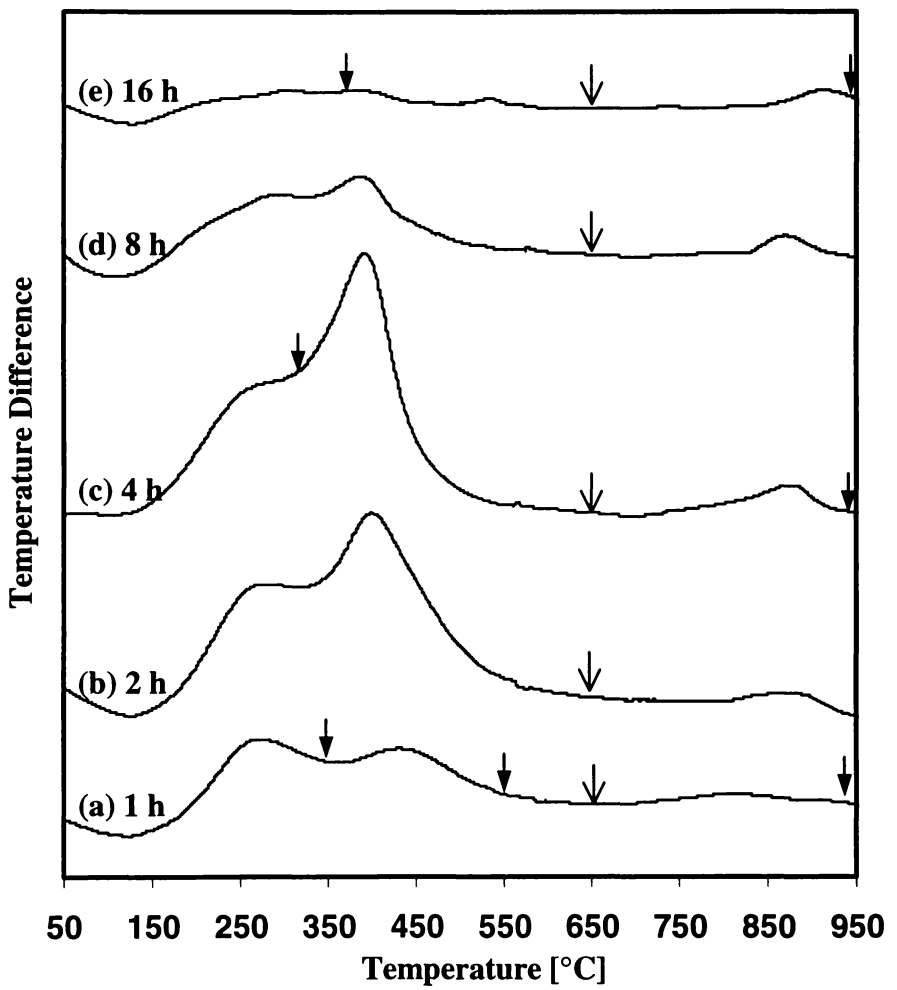

Figure 6-8. DTA traces of Cu(Al)/CuO powder mixtures of composition D1 produced after being milled for (a) 1 hour, (b) 2 hours, (c) 4 hours, (d) 8 hours and (e) 16 hours.

The DTA trace of the 2 hours milled D1 powder showed three exothermic peaks. The first exothermic peak had an onset and peak temperatures of 150°C and 270°C respectively. The second peak overlapped with the first one and had onset and peak temperatures of about 300°C and 400°C respectively. The second peak became stronger than the first one. Compared with the DTA trace of 1 hour milled powder, both peaks became stronger. The third peak appeared at higher temperatures with onset and peak temperatures of about 800°C and 900°C respectively. The DTA traces of the powder produced after being milled for 4 hours also had three exothermic peaks. The first one had onset and peak temperatures of about 150°C and 260°C respectively. The second one had onset and peak temperatures of 280°C and 390°C respectively. The second peak became much sharper than the first one. Compared with the DTA trace of the 2 hours milled powder, both peaks became much stronger, with the increase of the intensity of the second peak being more significant. The third peak remained almost unchanged. When the milling time increased to 8 hours, the intensity of the first two exothermic peaks significantly decreased, although their positions remained unchanged. The third exothermic peak had no change. After 16 hours of milling, the low temperature exothermic peak nearly disappeared. While the high temperature peak still remained, as shown in Figure 6-8 (e).

In order to identify the reactions corresponding to each exothermic peak, the D1 powders produced after being milled for different times were heated to some characteristic temperatures as marked in arrows in Figure 6-8, and then the heat treated powders were subjected to XRD examination.

Figure 6-9 showed the XRD patterns of the D1 powder after being milled for 1 hour and then heated to different temperatures. After the powder was heated to 350°C, *i.e.* after the first exothermic peak in the DTA trace, Cu_2O peak appeared in the XRD pattern. This suggests that the first exothermic peak in the DTA trace is partly due to the reaction between CuO and Cu(Al) solid solution forming Cu_2O. This reaction can be written as (Reaction 1): $CuO + Cu(Al) \rightarrow Cu_2O + Cu(Al)$ with higher Al concentration. With the D1 powder being further heated to 550°C, *i.e.* after the second exothermic peak of the DTA trace, the Cu_2O peaks became stronger. This implies that the second

exothermic peak of the DTA trace is also due to the further reaction between the remaining CuO and Cu(Al) forming Cu_2O. With a further increase of the temperature to 1000°C, the XRD pattern showed that the CuO peaks completely disappeared, whereas, the Cu_2O peaks became slightly weaker, as shown in Figure 6-9 (d). This is probably due to the reaction of CuO and part of the Cu_2O with Cu(Al) solid solution to form Cu and Al_2O_3. This reaction can be written as (Reaction 2): $Cu_2O + Cu(Al) \rightarrow Cu + Al_2O_3$. However, Al_2O_3 was not detected by the XRD. This may be due to the possibility that Al_2O_3 was amorphous or had a very small grain size, which made the detection using XRD very difficult.

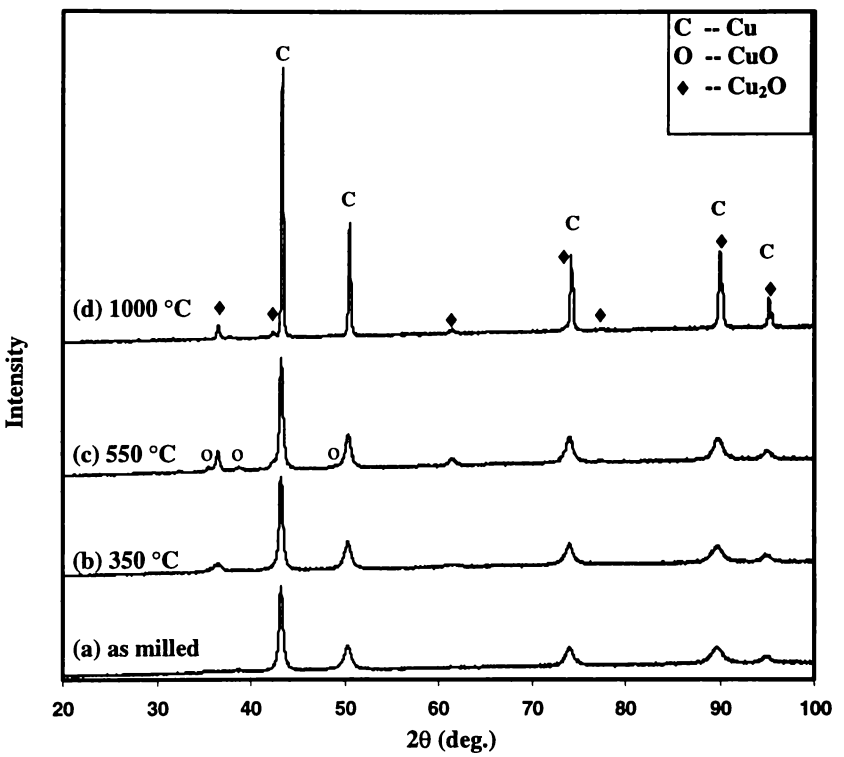

Figure 6-9. XRD patterns of the D1 powder after being milled for 1 hour and then heated to different temperatures: (a) as-milled, (b) 350°C, (c) 550°C and (d) 1000°C.

Figure 6-10 showed the XRD patterns of the D1 powder after being milled for 4 hours and then heated to different temperatures. In the XRD pattern of the powder after being heated to 350°C, Cu_2O peaks appeared. On further heating to 550°C, Cu_2O peaks became very strong. This shows that, during heating to 350°C, the CuO reacted with the Cu(Al) forming Cu_2O and upon further heating, the CuO further reacted with Cu(Al) forming more Cu_2O. Heating the powder further to

1000°C, peaks of CuO and Cu_2O became weaker and disappear, indicating that CuO and Cu_2O reacts with Cu(Al), forming Cu and Al_2O_3. However, again, there were no Al_2O_3 peaks shown in the XRD pattern.

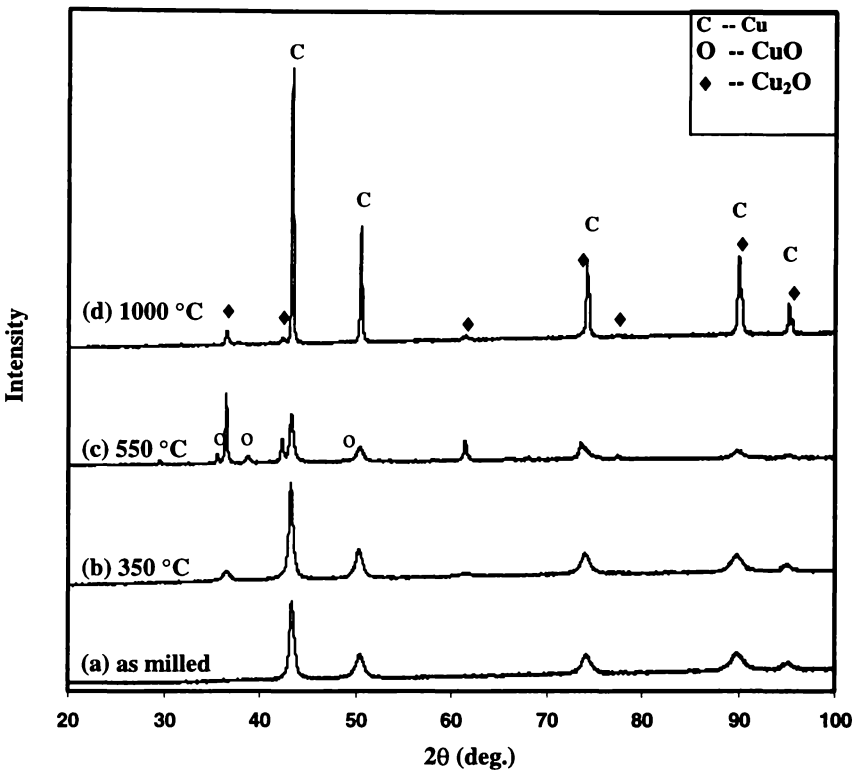

Figure 6-10. XRD patterns of the D1 powder after being milled for 4 hours and then heated to different temperatures: (a) as milled, (b) 350°C, (c) 550°C and (d) 1000°C.

Figure 6-11 compared the XRD patterns of the D1 powder after being milled for 1 hour, 2 hours and 4 hours, respectively, and then heated to 650°C. It can be seen that the Cu_2O peak became stronger with the increase of milling time, and the Cu(Al) {111} shifted from $2\theta = 43.28°$ as in the XRD pattern of 1 hour milled powder to a higher angle, $2\theta = 43.35°$ as in the XRD pattern of the 4 hour milled powder. This suggests that a longer milling time leads to more complete reaction when the powders are heated to a given temperature.

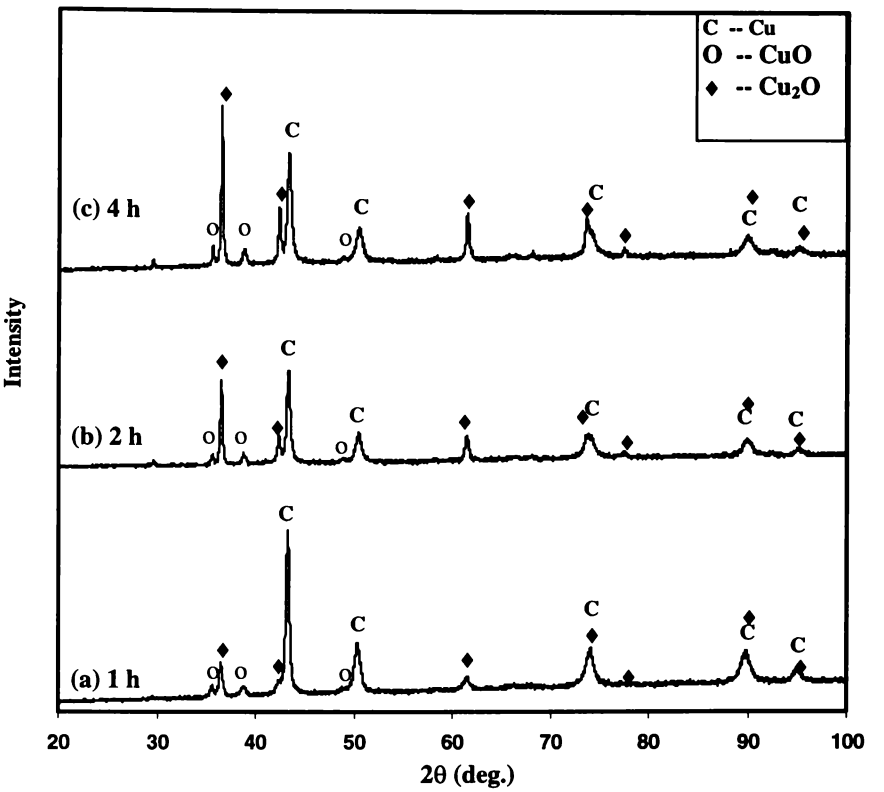

Figure 6-11. XRD patterns of Cu(Al)/CuO powder mixtures of composition D1 produced after milled for (a) 1 hour, (b) 2 hours and (c) 4 hours, and then heated to 650°C in DTA.

6.3.2 D2 powder

Figure 6-12 shows the DTA traces of the D2 powders produced after being milled for different times. The DTA trace of the 1 hour milled powder showed three major exothermic peaks, as shown in Figure 6-12 (a). Two were in the low temperature region of 120°C – 450°C and one was in a high temperature region of 650°C – 950°C. The first exothermic peak had an onset and peak temperature of 130°C and 260°C respectively and the second one had an onset and peak temperature of 250°C and 400°C respectively. The high temperature exothermic peak had onset and peak temperature of about 650°C and 800°C respectively. The DTA trace of the 2 hours milled D2 powder also showed three major exothermic peaks, with the onset and peak temperatures similar to those of exothermic peaks corresponding to 1 hour milled D2 powder.

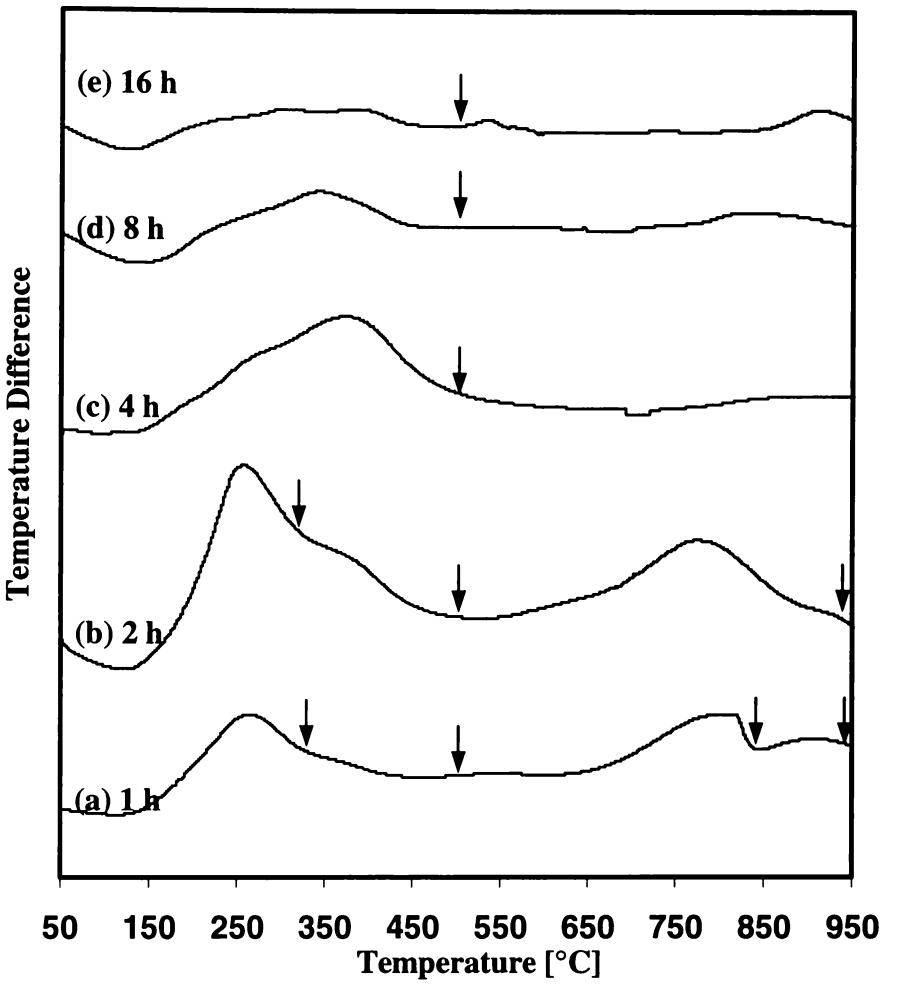

Figure 6-12. DTA traces of the D2 powder produced after being milled for (a) 1 hour, (b) 2 hours, (c) 4 hours, (d) 8 hours and (e) 16 hours.

After 4 hours of milling, only two exothermic peaks were observed in the DTA trace. Two peaks overlapped at the low temperature region. The first exothermic peak had an onset and peak temperature of 150°C and 260°C respectively. The second exothermic peak had an onset and peak temperature of 250°C and 370°C respectively. The second exothermic peak was stronger than the first one. After 8 hours of milling, the low temperature exothermic peaks became weaker and the peak temperatures were shifted to lower temperatures. After 16 hours of milling, no strong exothermic peaks were shown by the DTA trace.

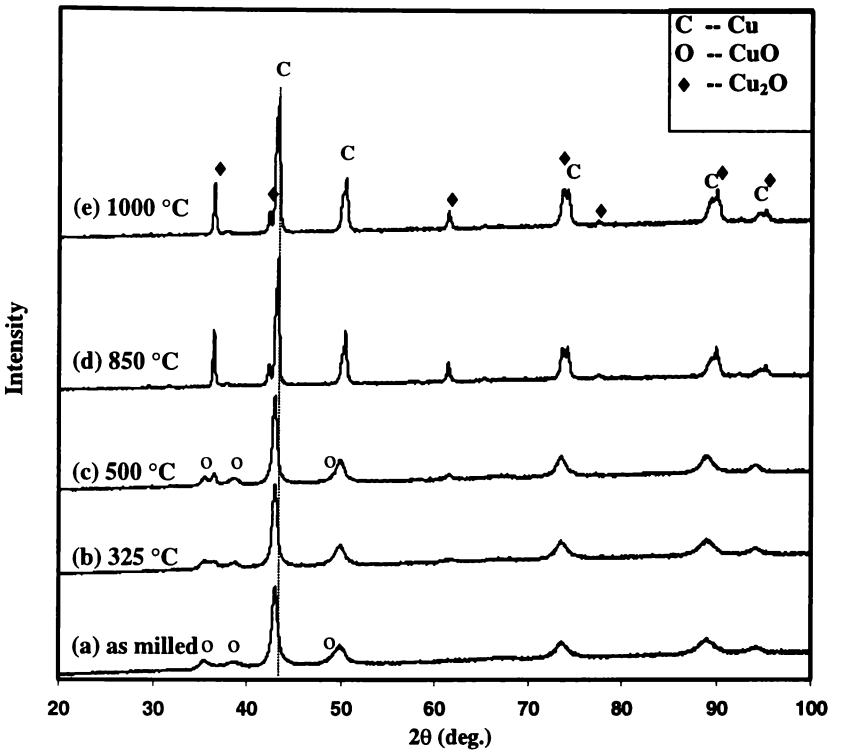

Figure 6-13. XRD patterns of the D2 powder after being milled for 1 hour and then heated to different temperatures: (a) as milled, (b) 325°C, (c) 500°C, (d) 850°C and (e) 1000°C.

Figure 6-13 showed the XRD patterns of the D2 powder after being milled for 1 hour and then heated to different temperatures. After powder was heated to 325C°, i.e. after the first peak in the DTA trace, Cu_2O peaks appeared but the peaks were very weak. After the powder was heated to 500°C, both CuO peak and Cu_2O peaks became slightly sharper and the CuO peaks remained strong. On further heating to 850°C, the Cu_2O peaks became very strong and the CuO peaks disappeared. This suggests that the exothermic peak at 800°C in the DTA trace of the 1 hour milled D2 powder is caused by Reaction 1 forming Cu_2O, whereas, the low temperature exothermic peaks of the DTA trace are not solely due to this reaction. This indicated that Reaction 1 started from low temperature, but only at a high temperature, appreciable reaction rate was achieved. There is no significant difference between the XRD patterns of the powder being heated to 850°C and that heated to 1000°C. There is no clear evidence to show that Al_2O_3 formed during heating.

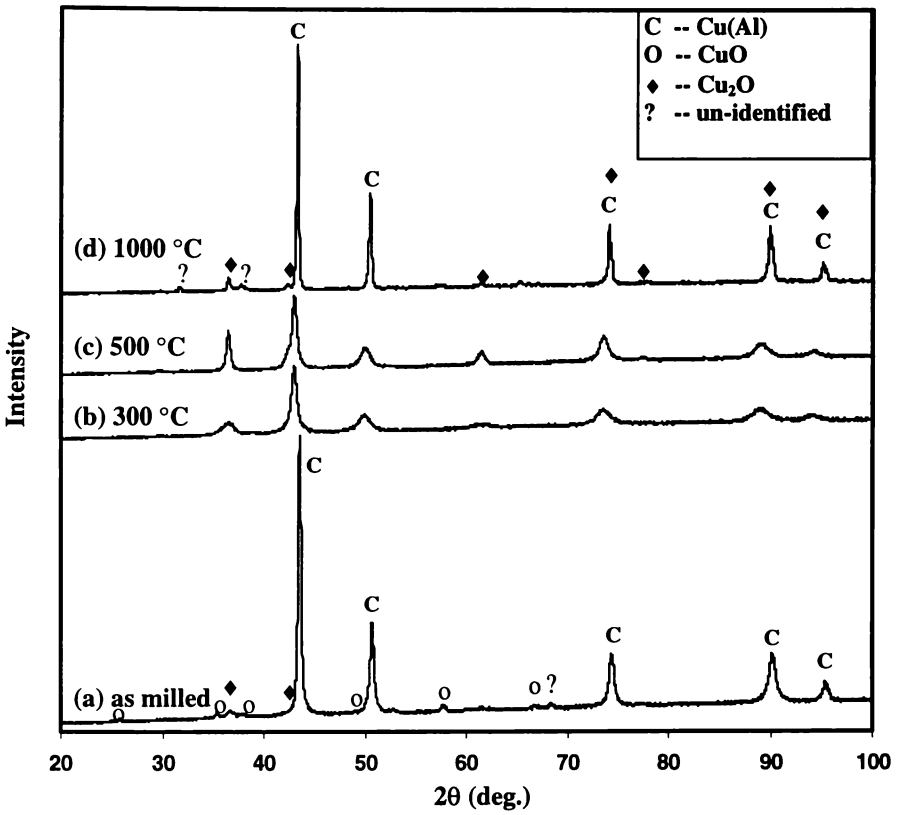

Figure 6-14. XRD patterns of the D2 powder after being milled for 2 hours and then heated to different temperatures: (a) as milled, (b) 300°C, (c) 500°C and (d) 1000°C.

Figure 6-14 shows the XRD patterns of the D2 powder after being milled for 2 hours and then heated to different temperatures. In the as milled powder, Cu(Al), CuO and Cu_2O could be clearly identified. This indicated that the reaction between CuO and Cu(Al) had occurred during the 2 hours of milling. After the powder was heated to 300°C, i.e. after the first peak in the DTA trace, the Cu_2O peaks became slightly stronger and CuO peaks disappeared. This suggests that this first exothermic peak of the DTA trace is partly due to the Reaction 1 forming Cu_2O. After the powder was heated to 500°C, as shown in Figure 6-14 (c), the Cu_2O peaks became very strong. It was also noticed that the Cu(Al) {111} peak shifted to the lower angle slightly. This peak shift is likely to be caused by the increase of Al concentration in Cu(Al) solid solution. The increase of Al concentration in the Cu(Al) solid solution is likely to be due to the fact that some Cu atoms were taken out of Cu(Al) solid solution to be used in the reaction between CuO and Cu. On further heating the powder to 1000°C, i.e. after the high temperature exothermic peak, the intensity of Cu_2O peaks substantially decreased,

and the Cu(Al) {111} peaks shifted back to a higher angle. This is likely due to the reaction between Cu_2O and the Al in the Cu(Al) solid solution, leading to the formation of Al_2O_3 and pure Cu or Cu(Al) solid solution with a lower Al concentration. This reaction was termed as Reaction 2 in the previous section. This suggests that the exothermic peak at 800°C of the DTA trace, as shown in Figure 6-12 (b), is caused by Reaction 2. Again the Al_2O_3 could not be detected.

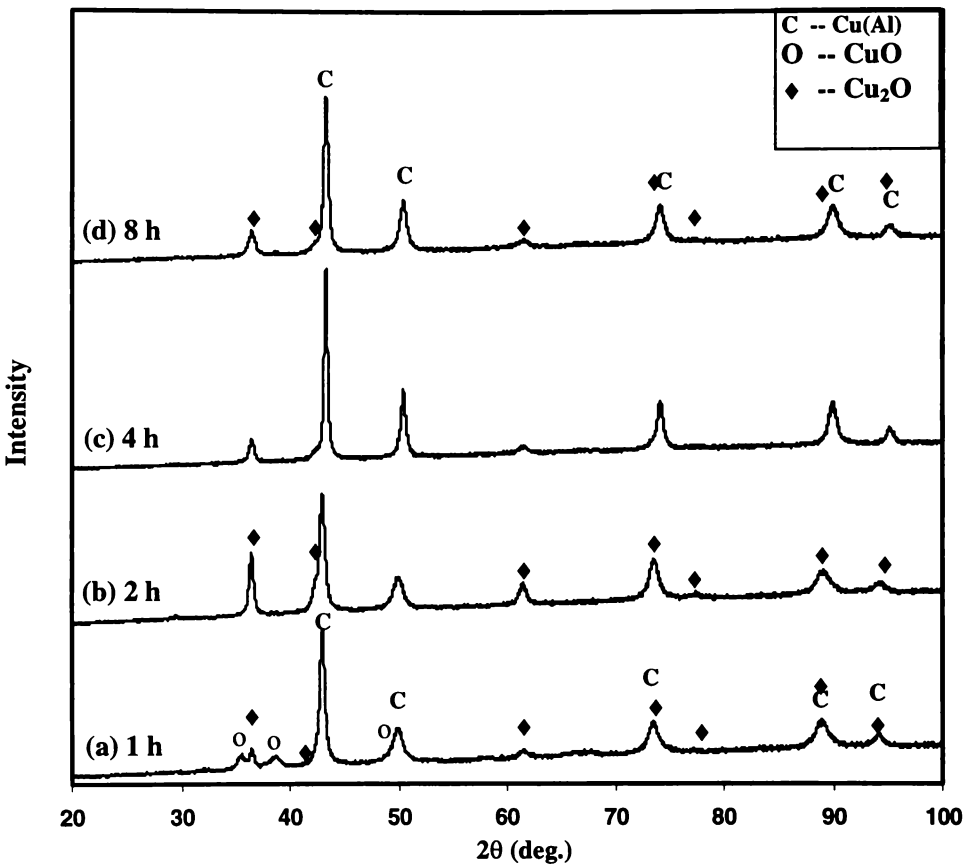

Figure 6-15. XRD patterns of the D2 powder after being milled for (a) 1 hour, (b) 2 hours, (c) 4 hours and (d) 8 hours, and then heated to 500°C in DTA.

Figure 6-15 shows the XRD patterns of the D2 powder after being milled for different times and then heated to 500°C in DTA. The peaks of three phases, CuO, Cu_2O and Cu(Al), co-existed in the XRD pattern of 1 hour milled powder, while in the XRD pattern of the 2 hour milled powder, the CuO peaks disappeared and Cu_2O peaks became much stronger. This suggests that with finer CuO/Cu(Al) composite microstructure, the reaction between CuO and Cu(Al) forming Cu_2O proceeded further during the process of heating the powder to a given

temperature. While in the XRD patterns of the 4 and 8 hours milled powders, the intensity of Cu_2O peaks decreased substantially compared with the XRD pattern of the 2 hours milled powder. This suggests that the reaction between Cu_2O and Al in the Cu(Al) solid solution had occurred during heating to 500°C. In other words, the exothermic peak corresponding to the Reaction 2, had shifted to a temperature below 500°C, as marked by the dotted arrow in Figure 6-12.

6.3.3 D3 Powder

It is much easier for chemical reactions in the D3 powder to be initiated than those in D1 and D2 powders. Milling experiment showed that combustive reactions occurred within 2 hours of milling. Therefore, a shorter milling interval was selected.

Figure 6-16 showed the DTA traces of the D3 powder after being milled for different times. With milling for up to 1.33 hours, all the DTA traces exhibited three exothermic peaks: one in the temperature range of 100°C to 400°C, and the other two in temperature range of 600°C to 1000°C, as shown in Figure 6-16. The onset and peak temperatures of the low temperature exothermic peak remained unchanged with increasing milling time. While the high temperature exothermic peaks were more complicated and overlapped. The peak positions of high temperature peaks shifted to lower temperatures with the increase of milling time. For the powders milled for 0.33 hours and 0.66 hours, the high temperature exothermic peaks started at about 700°C. With the milling time being increased to 1 and 1.33 hours, the shapes of the high temperature peaks changed dramatically. For the 1 hour milled powder, the first high temperature peak had an onset and peak temperatures of around 650°C and 770°C respectively. The second high temperature peak had an onset and peak temperatures of around 800°C and 900°C respectively. With increase of milling time to 1.33 hours, the onset and peak temperatures of the the first high temperature peak had decreased to 600°C and 680°C respectively, and the onset and peak temperatures of the second high temperature peak had decreased to about 700°C and 850°C respectively. After 1.66 hours of milling, no exothermic peaks appeared in the DTA trace. This

suggests that the reaction had occurred during milling in agreement with the XRD results.

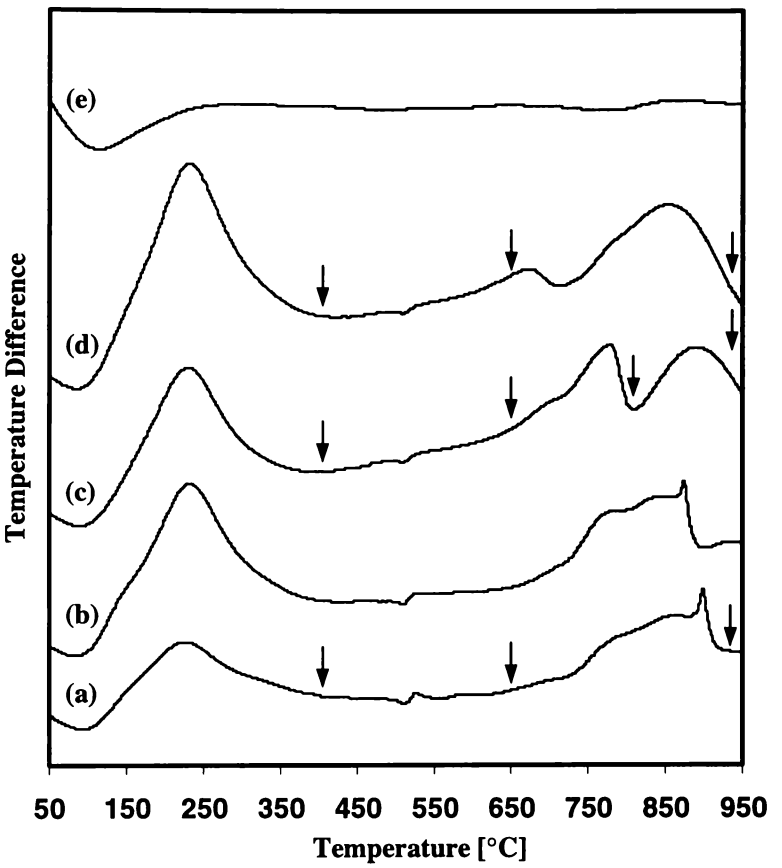

Figure 6-16. DTA traces of D3 powders produced after being milled for (a) 0.33 hours, (b) 0.66 hours, (c) 1 hour, (d) 1.33 hours and (e) 1.66 hours.

Figure 6-17 showed the XRD patterns of the 0.33 hours milled D3 powder after being heated to different temperatures. After the powder was heated to 400°C, *i.e.* after the low temperature peak, the XRD pattern shows mainly two phases: Cu_9Al_4 and CuO. Compared with the XRD pattern of the as milled powder, it can be seen that both Cu_9Al_4 peaks and CuO peaks became much sharper, and no new phases were observed. This suggests that the low temperature peak is not caused by a chemical reaction. Instead, it may be caused by recovery and recrystallisation of Cu_9Al_4 and CuO phases. After the 0.33 hour milled D3 powder was heated to 650°C, a small amount of Cu_2O appeared. After the powder was heated to 1000°C, Cu_2O and Cu peaks became very strong. This implies that the high temperature peak in Figure 6-16 (a) is due to the reactions between CuO and Cu_9Al_4 forming Cu_2O, Cu and Al_2O_3. The reaction can be written as (Reaction 1):

$CuO + Cu_9Al_4 \rightarrow Cu_2O + Cu_9Al_4$ (with a higher Al concentration). Again the Al_2O_3 phase was not observed based on XRD analysis.

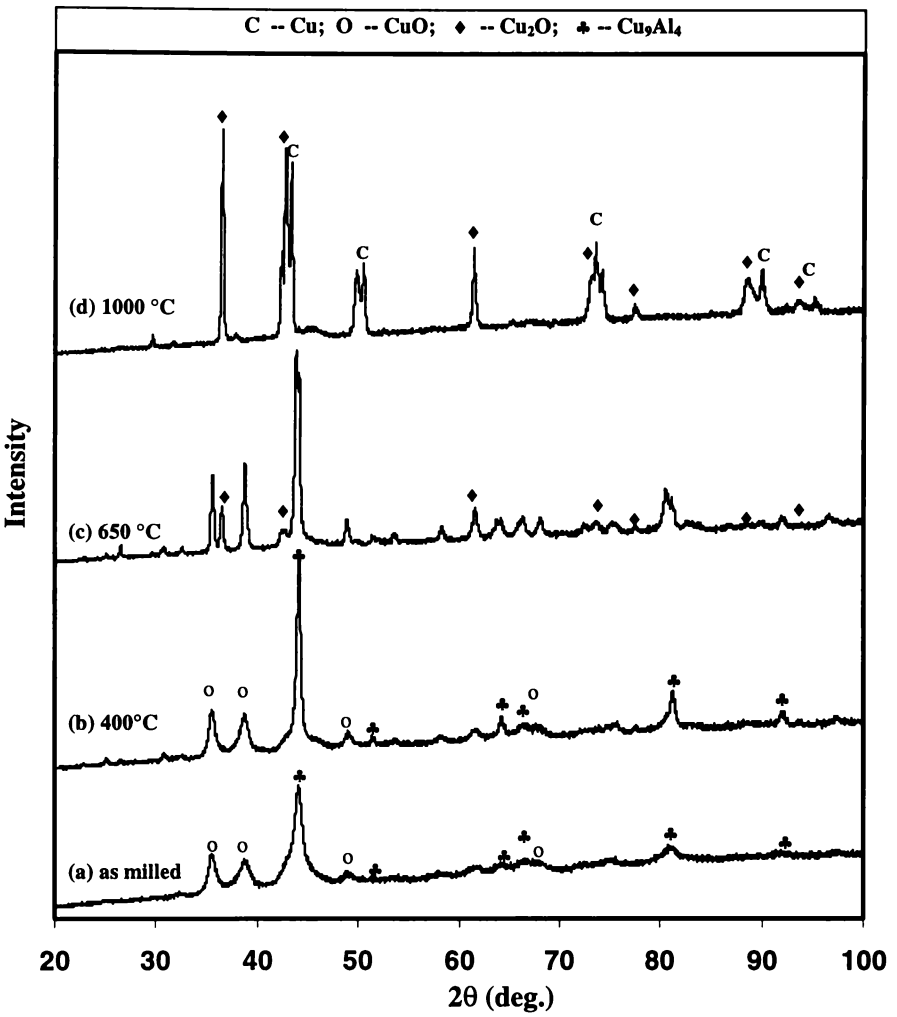

Figure 6-17. XRD patterns of D3 powder after being milled for 0.33 hours and then heated to different temperatures: (a) as milled , (b) 400°C, (c) 650°C and (d) 1000°C.

Figure 6-18 shows the XRD patterns of the 1 hour milled D3 powder after being heated to different temperatures. After the powder was heated to 400°C, CuO and Cu_9Al_4 peaks, became sharper, new Cu_2O peaks also appeared. After the powder was heated to 650°C, the Cu_2O peaks became sharper, and the CuO and Cu_9Al_4 peaks still remained very strong. This suggests that from 100°C to 650°C, the reaction between CuO and Cu_9Al_4 forming Cu_2O proceeded gradually. While after the powder was heated to 820°C, *i.e.* after the first high temperature exothermic peak, a dramatic change in XRD pattern occurred. Peaks of both CuO and Cu_9Al_4 phases disappear and the peaks of Cu_2O phase dominated the XRD

pattern. This indicated that the Reaction 1 had occurred. After the powder was further heated to 1000°C, *i.e.* after the second high temperature peak of the DTA trace, as shown in Figure 6-16 (c), the intensity of Cu_2O decreased substantially and pure Cu phase dominated the XRD pattern. This suggests that a reaction between Cu_2O and Al forming Cu and Al_2O_3 had occurred. This reaction can be written as (Reaction 2): $Cu_2O + Cu_9Al_4 \rightarrow Cu + Al_2O_3$. But the Al_2O_3 phase is hardly observable in the XRD pattern.

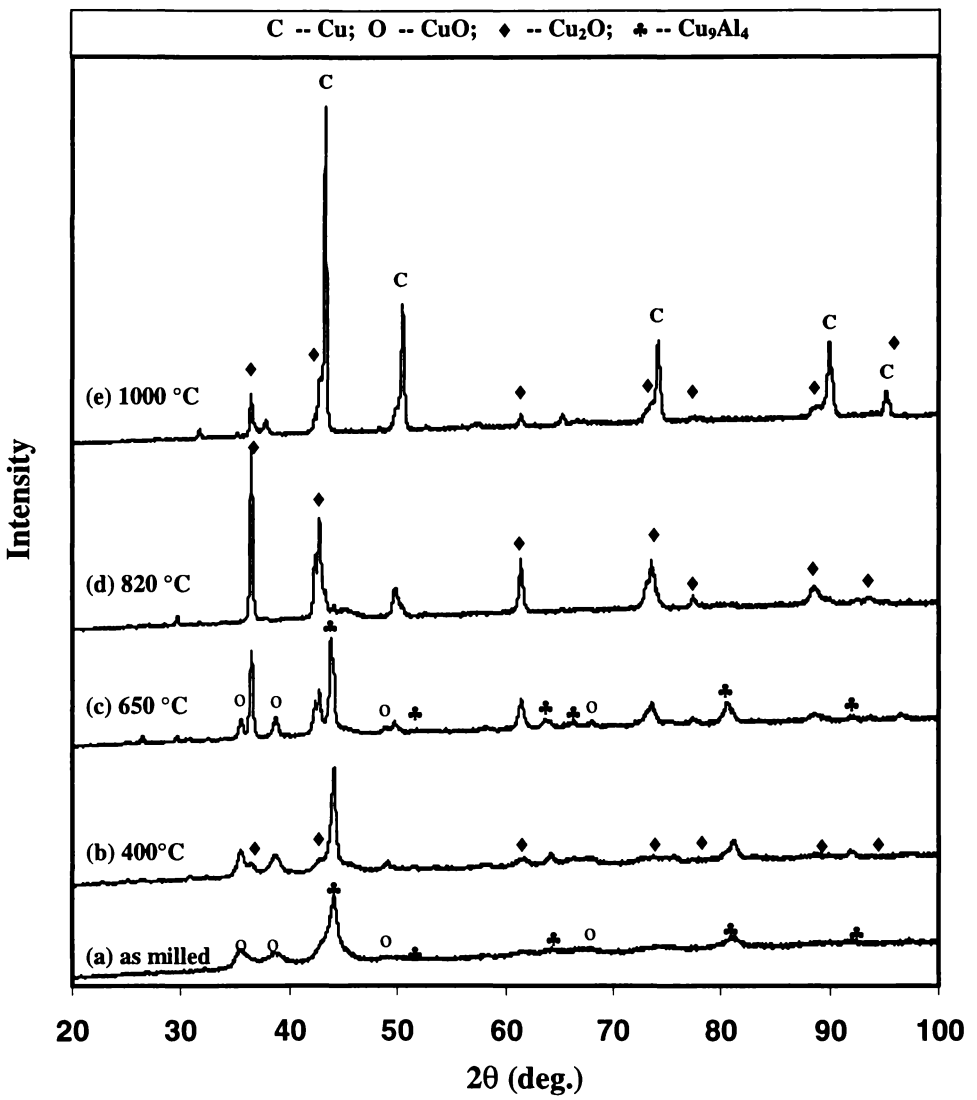

Figure 6-18. XRD patterns of the D3 powder after being milled for 1 hour and then heated to different temperatures: (a) as milled, (b) 400°C, (b) 650°C, (d) 820°C and (e) 1000°C.

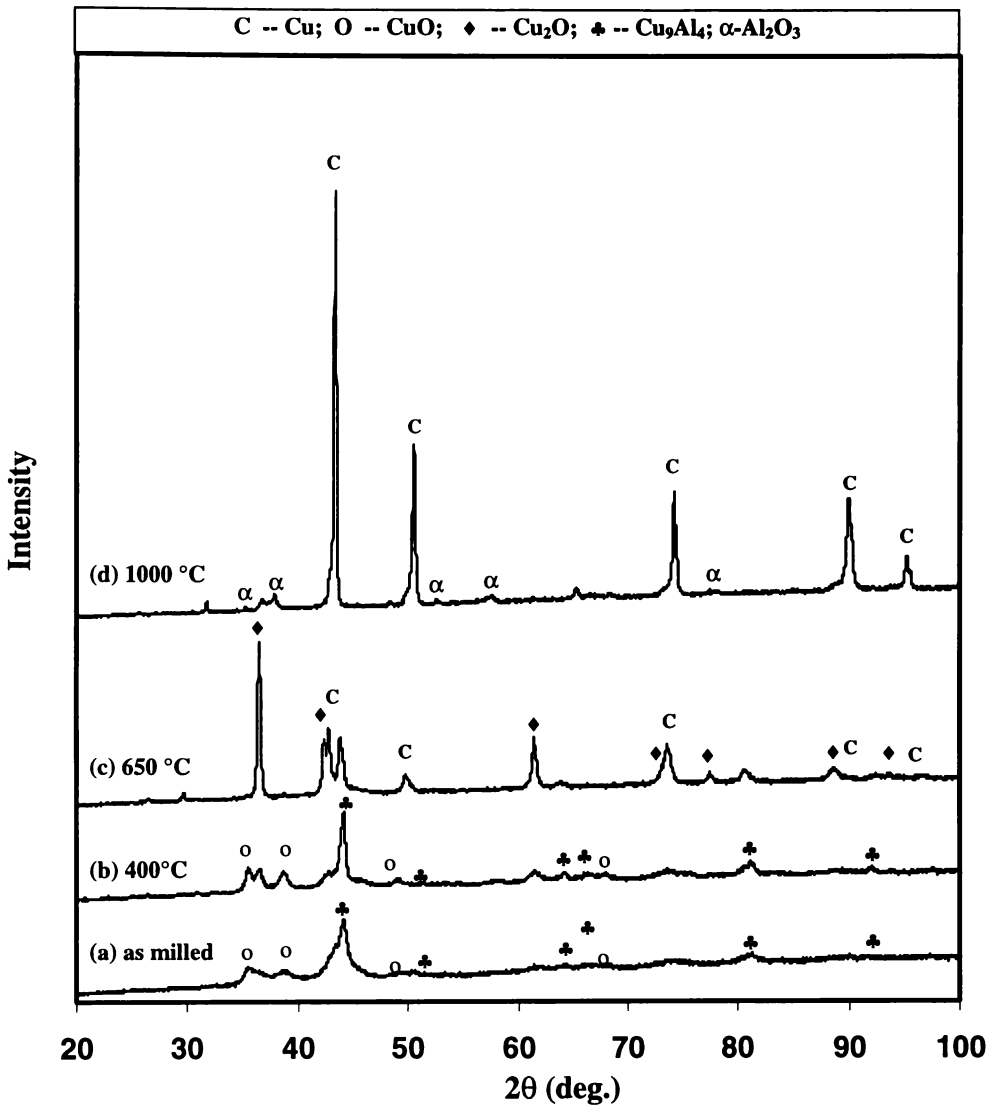

Figure 6-19. XRD patterns of the D3 powder after being milled for 1.33 hours and then heated to different temperatures: (a) as milled, (b) 400°C, (c) 650°C and (d) 1000°C.

Figure 6-19 shows the XRD patterns of the 1.33 hours milled D3 powder after being heated to different temperatures. Again, the Cu_2O phase started to appear in the XRD pattern after the powder was heated to 400°C. After the powder was heated to 650°C, CuO peaks disappeared and Cu_9Al_4 peaks became significantly weaker. In the meantime, strong Cu_2O peaks appeared. This suggests that the Reaction 1 between CuO and Cu_9Al_4 forming Cu_2O and Cu had consumed all the CuO during heating to 650°C. After the powder was heated to 1000°C, the peaks of pure Cu phase dominated the XRD pattern, as shown in Figure 6-19 (d). The α-Al_2O_3 phase was barely observable and Cu_2O peaks nearly disappeared. This

indicates that the Reaction 2 between Cu_2O and Cu_9Al_4 occurred, leading to the formation of pure Cu and Al_2O_3 during heating from 650°C to 1000°C.

Figure 6-20 compared the XRD patterns of the powders produced after being milled for different times and then heated to 400°C. It shows that with the increase of milling time, more Cu_2O forms. This suggests that with the refinement of the CuO/Cu_9Al_4 microstructure, a larger fraction of the Reaction 1 between CuO and Cu_9Al_4 occurs at temperatures below 400°C.

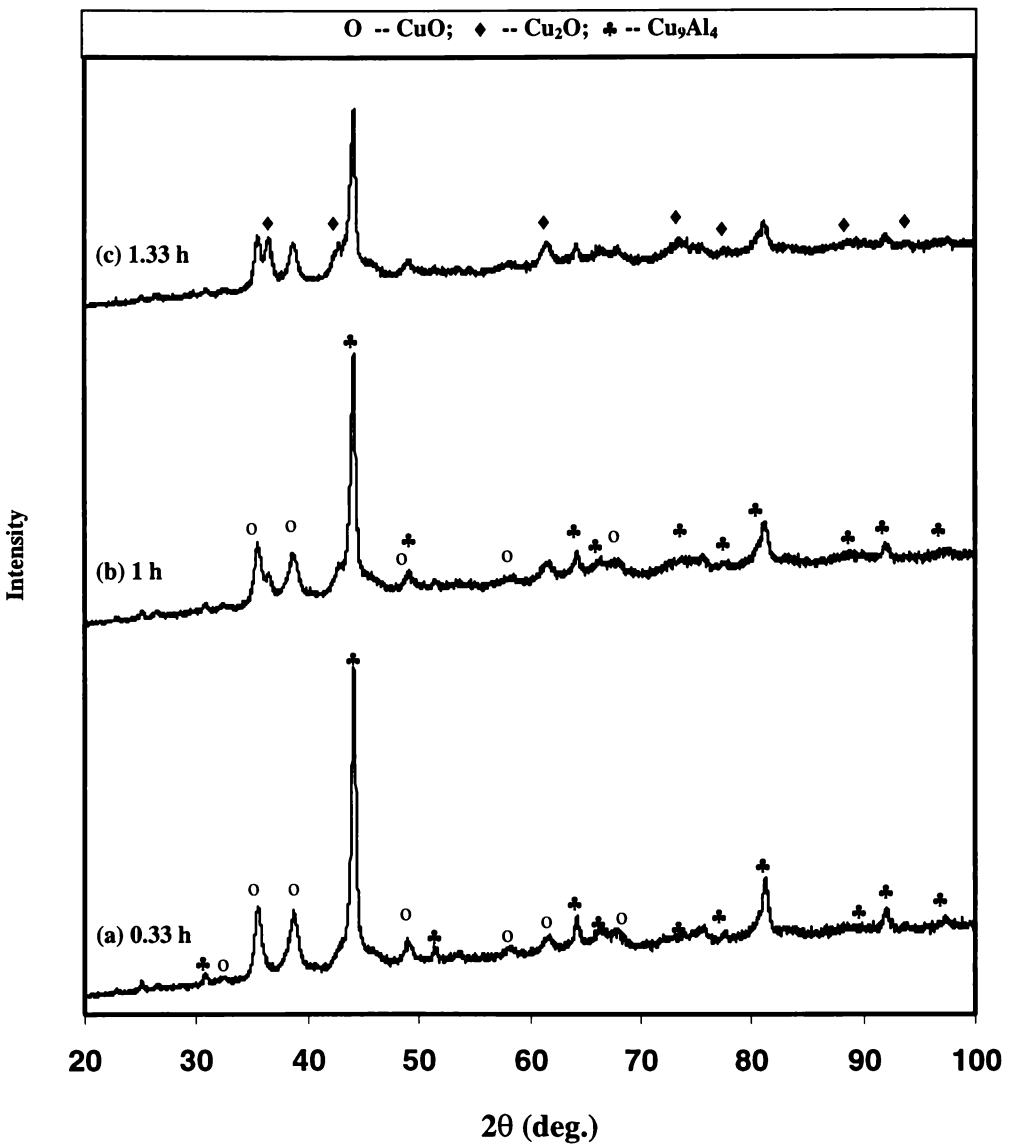

Figure 6-20. XRD pattern for the D3 powder after being milled for (a) 0.33 hours, (b) 1 hour and (c) 1.33 hours, and then heated to 400°C.

Figure 6-21 compared the XRD patterns of the D3 powder after being milled for different times and then heated to 650°C. It can be noticed that with the increase

of milling time, more Cu_2O formed and more CuO and Cu_9Al_4 were consumed. In the pattern of 1.33 hours milled powder, CuO peaks completely disappeared.

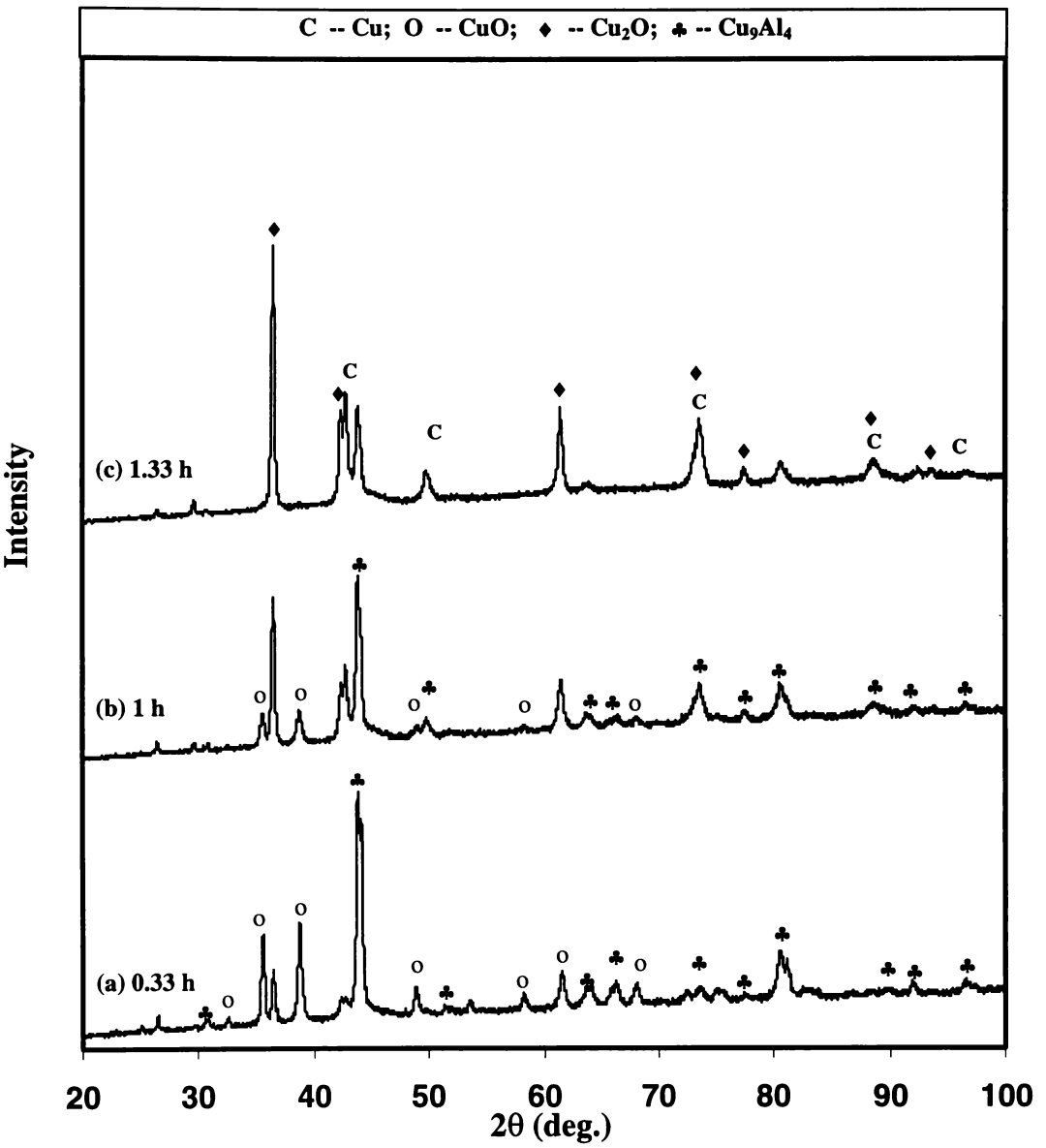

Figure 6-21. XRD patterns of the D3 powder after being milled for (a) 0.33 hours, (b) 1 hour and (c) 1.33 hours, and then heated to 650°C.

Figure 6-22 compared the XRD patterns of the D3 powder after being milled for different times and then heated to 1000°C. It can be seen that with the increase of milling time, the Cu_2O peaks became weaker and weaker, and finally nearly disappeared in the 1.33 hours milled powder, while in the meantime, the pure Cu peaks get stronger and stronger. This indicated that with the refinement of

microstructures, the more of Reaction 2 can be completed within a certain time and temperature.

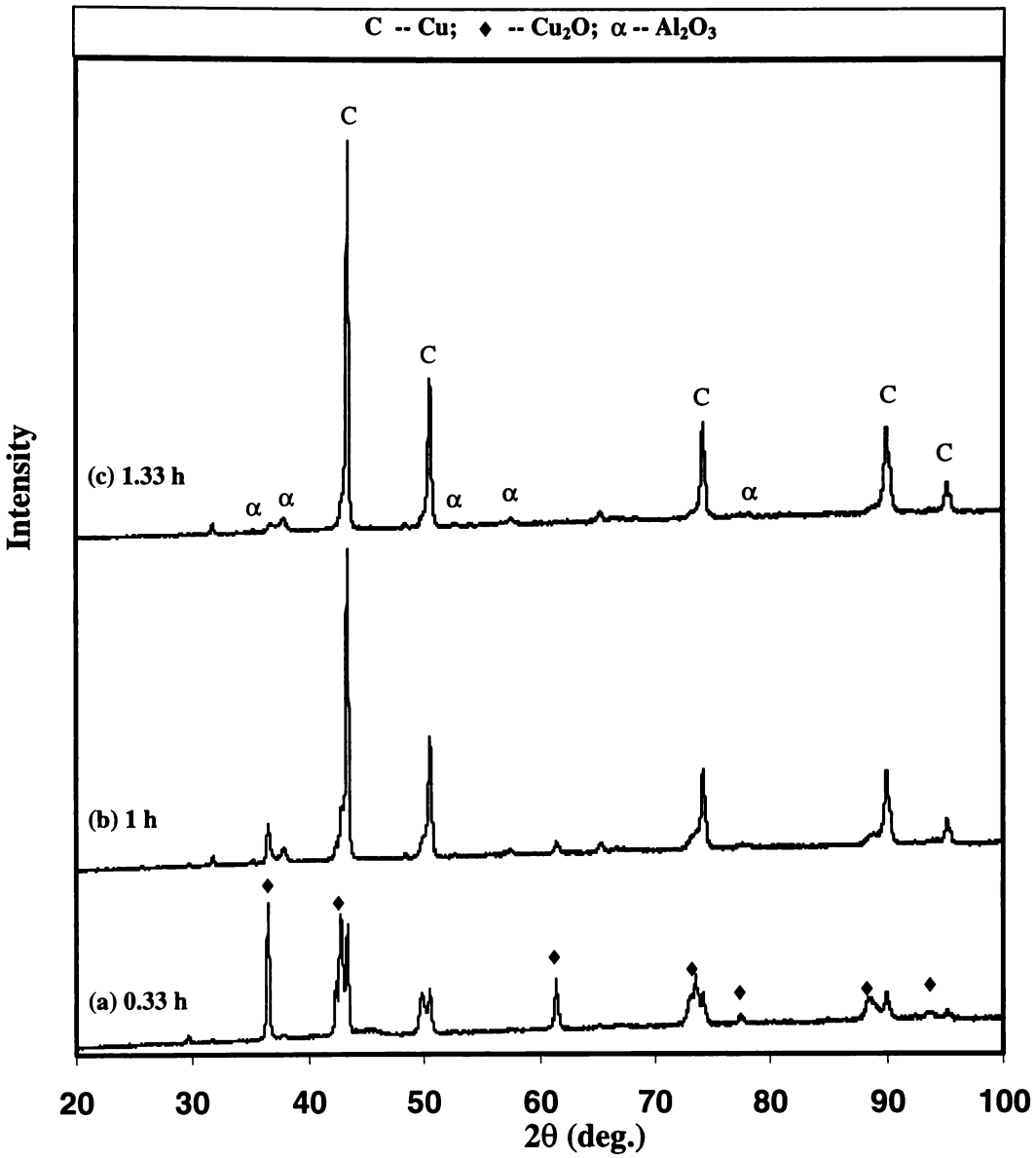

Figure 6-22. XRD patterns of the D3 powder after being milled for (a) 0.33 hours, (b) 1 hour and (c) 1.33 hours, and then heated to 1000°C.

6.3.4 Processing of Cu/Al_2O_3 Metal Matrix Nanocomposite Materials

With the composite powder of D1 or D2, bulk composite materials were produced by pressing and sintering of the powders. Figure 6-23 and Figure 6-24 show typical SEM micrographs of the microstructure of the bulk Cu-10vol%Al_2O_3 and

Cu-20vol%Al_2O_3 composite materials produced by pressing the 16 hours milled D1 and D2 powders and which were then sintered at 900°C for 4 hours.

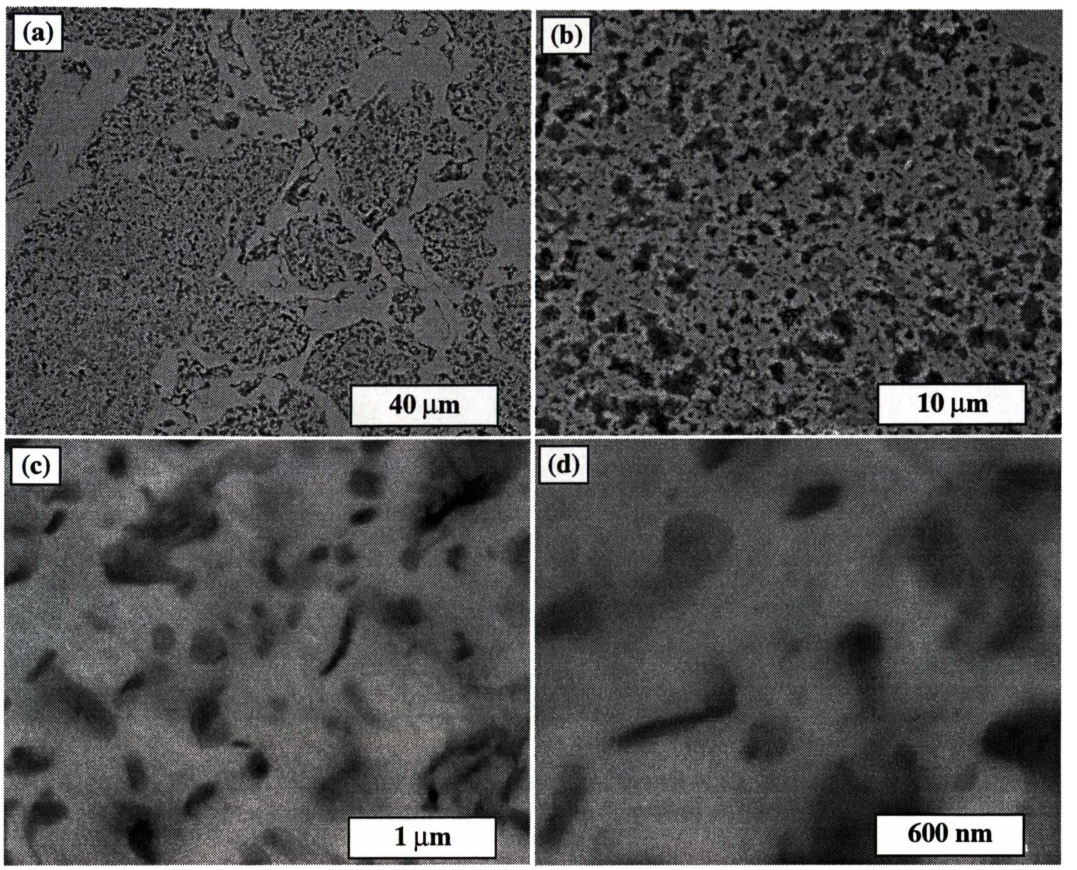

Figure 6-23. SEM micrographs of the bulk Cu-10vol%Al_2O_3 metal matrix nanocomposite material produced by pressing and sintering the 16 hours milled D1 powder.

The dark regions in Figure 6-23 (a) and Figure 6-24 (a) delineate the shape of the composite particles in the starting powder. The light regions are the pure copper phase. It is likely that the monolithic pure copper phase in the gaps between the composite regions was caused by the preferential flow of copper during sintering. Examination of the microstructure of the dark region by using SEM at higher magnifications showed that the microstructure consisted of homogeneously distributed Al_2O_3 particles with size of less than 200nm embedded in a copper matrix. Some of the Al_2O_3 particles are acicular or lenticular with a thickness of about 100 nm and length of about 500 nm as shown in Figure 6-23 (c) and (d), and Figure 6-24 (c) and (d). Occasionally some large Al_2O_3 particles with a diameter of 500 nm can be observed, as shown in Figure 6-24 (c).

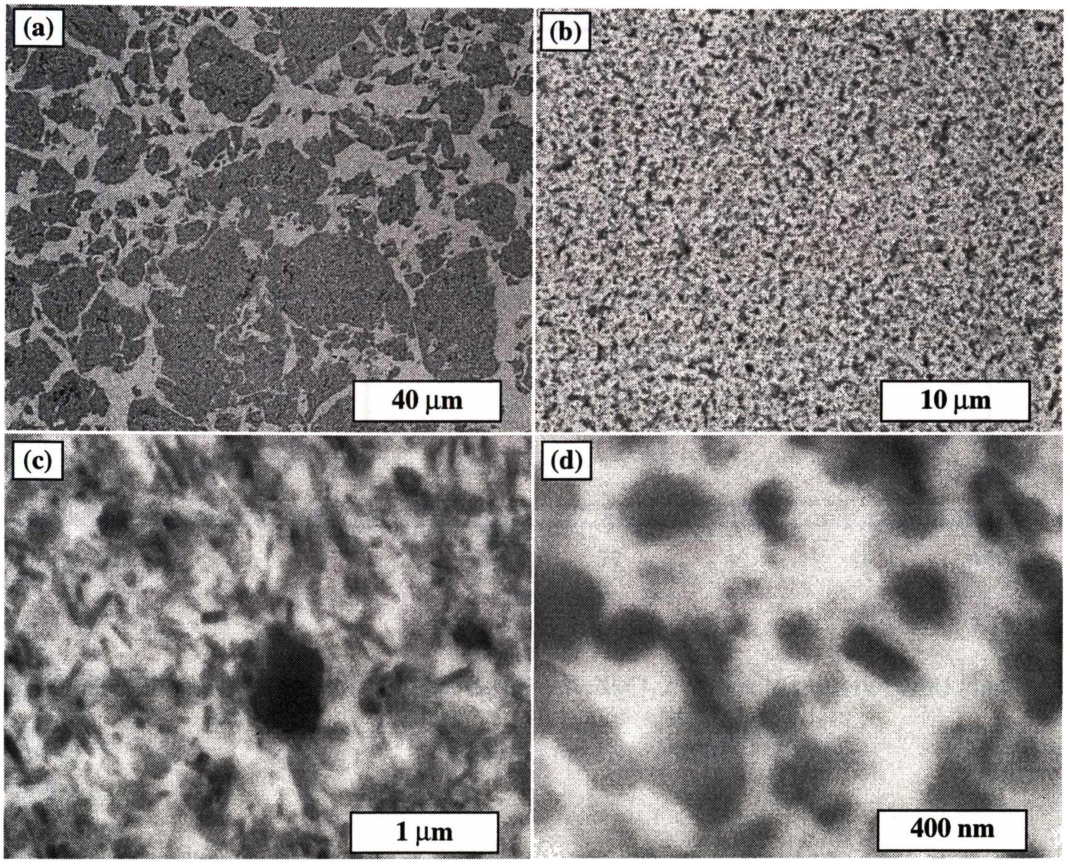

Figure 6-24. SEM Micrographs of the bulk Cu-20vol%Al_2O_3 material produced by pressing and sintering the 16 hours milled D2 powders.

Figure 6-25 shows the XRD pattern of the bulk Cu-20vol%Al_2O_3 composite material produced by pressing and then sintering the 16 hours milled D2 powders at 900°C for 4 hours. α-Al_2O_3 peaks were clearly shown in the pattern, confirming the formation of α-Al_2O_3. However the intensity of the Al_2O_3 peaks is very low and not up to the proportion of the 20vol%Al_2O_3. The reason for this may be attributed to the facts that the Al_2O_3 particles are very small and that they are embedded in a Cu matrix which has high density. Based on the position of the Cu peaks in the XRD pattern of the composite, the lattice parameter of the Cu phase was calculated to be 3.613 Å, the same as that of pure Cu. This proves that the matrix is pure Cu.

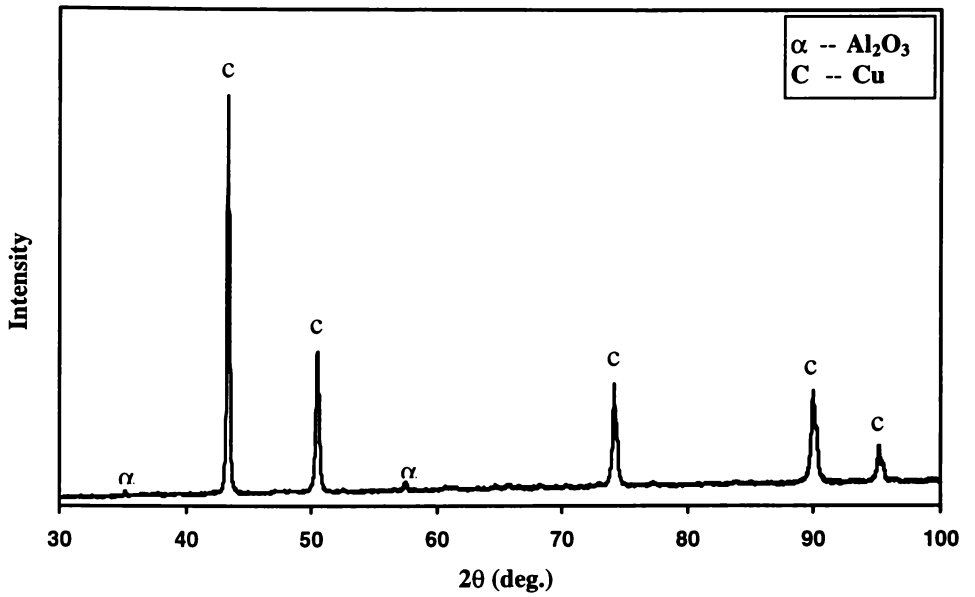

Figure 6-25. XRD pattern of the bulk Cu-20vol%Al_2O_3 composite material produced by pressing and sintering the 16 hours milled D2 powders.

6.4 Discussions

6.4.1 Reaction Sequence During Heating

It is clear that the Cu_2O phase is easy to form in the CuO/ Cu-Al system. In all the three compositions studied, the initial reactions between CuO and Cu-Al causes formation of Cu_2O. This is independent of whether the Cu containing reactant is Cu(Al) solid solution or Cu_9Al_4 intermetallic compound. The reaction can be written as (Reaction 1):

$$CuO + Cu(Al) \rightarrow Cu_2O + Cu(Al) \text{ (with a higher Al concentration)}$$

$$CuO + Cu_9Al_4 \rightarrow Cu_2O + Cu_9Al_4 \text{ (with a higher Al concentration)}$$

Following the Reaction 1 is the reaction between Cu_2O and Cu(Al) or Cu_9Al_4 forming Cu and Al_2O_3 as Reaction 2:

$$Cu_2O + Cu(Al)\,(or\ Cu_9Al_4) \rightarrow Cu + Al_2O_3$$

Similar observation was made by Shen *et al.*[4] in the study of the reaction between CuO and Fe. The reaction between CuO and Fe forming Cu_2O and Fe_3O_4 occurred

at 275°C, whereas further reduction of Cu_2O to form Cu occurred at a higher temperature of 460°C.

6.4.2 Effect of Milling on the Reaction Kinetics

It is obvious that mechanical milling enhances the solid state reactions by establishing and further refining the composite microstructure. In CuO/Cu-Al system, Reaction 1 started at a very low temperature of about 150°C irrespective of compositions and the microstructures. This indicated that this reaction is easily initiated at the interface of CuO/Cu(Al) or CuO/Cu_9Al_4. If we assume that there are interfacial reaction and diffusional reaction in the CuO/Cu-Al system, as the reaction couples studied in the previous chapters, an increased reaction intensity with the increase of milling time or refinement of the powder particle microstructures was not observed from the DTA traces. This is likely due to the fact that the interfacial reaction occurred at a low temperature as such this reaction had already occurred during milling. Whereas, the enhanced diffusional reaction was clearly shown by the DTA traces, as shown in Figure 6-8, Figure 6-12 and Figure 6-16.

Figure 6-7 showed that the second low temperature exothermic peak of the DTA traces of the 1, 2 and 4 hours milled D1 powders increases in intensity and decreases in peak temperature with an increase of milling time. This is attributed to the increased reaction area and decreased diffusion pathway.

The exothermic peaks corresponding to the Reaction 1 and Reaction 2 in the DTA traces of the D2 and D3 powders shifted from high temperatures to much lower temperatures with increasing milling time. For the D2 powder, as shown in Figure 6-11, the peak temperature of Reaction 1 shifted from 800°C to about 400°C with the milling time increased from 1 hour to 2 hours. The exothermic peak temperatures for Reaction 2 shifted from above 900°C to 400°C with the milling time increased from 1 hour to 4 hours. For the D3 powder, as shown in Figure 6-15, the exothermic peak temperature for the Reaction 1 shifted from about 900°C to about 700°C with the milling time increased from 0.33 hours to 1.33 hours. The exothermic peak temperature for Reaction 2 shifted from above 1000°C to about

950°C with the milling time increased from 0.33 hours to 1.33 hours. So, mechanical milling enhances both Reaction 1 and Reaction 2 in the CuO/Cu-Al system.

6.4.3 Phase Formation during Heating

It is clear that Cu_2O is easy to form from either the reduction reaction from CuO using other active metal, or the reaction between CuO and Cu. This reaction starts from low temperature of about 150°C and the phase formed is easy to be detected by XRD technique. The reason why Cu_2O forms first is likely to be that its crystal structure is very simple (cubic) and close to that of Cu. This simple crystal structure makes the nucleation of Cu_2O easy. Comparatively, the Al_2O_3 phase is more complicated. Although the DTA in combination of XRD technique, plus mass balance confirmed that the oxygen has to form some forms of aluminium oxides, no Al_2O_3 peaks could be observed in the XRD patterns of the powders heated to low temperatures. Further investigation using TEM is necessary.

6.4.4 Effect of Compositions

It seems that the composition has no effect on the phase formation sequence. All the three powders start with the Reaction 1 forming Cu_2O and followed by Reaction 2 forming Cu and Al_2O_3. However, the composition does affect the intensity and reaction temperatures. With increasing CuO content, the reaction became more exothermic. Such that a combustive reaction could easily be initiated with 2 hours of milling the D3 powder. This is due to that the more CuO in the powder mixture, the more Cu_2O and Al_2O_3 could be produced. Therefore, more energy could be released from the reaction.

On the other hand, the peak temperatures of both Reaction 1 and Reaction 2 are also affected by the composition. For the D1 powder, the peak temperature of Reaction 1 decreased slightly from 450°C to 400°C with the milling time increased from 1 to 2 hours. For the D2 powder, the peak temperature of Reaction 1 decreased dramatically from 800°C to 400°C with the milling time increased from 1 to 2 hours. This suggests that the higher CuO content in the powder mixture, the higher the reaction temperature is required. The refinement of the

microstructure made the powder with higher CuO concentration more effective in the reduction of reaction peak temperatures. This is likely due to the fact that the diffusion through CuO is more difficult than that through Cu-Al metal phase. Therefore, the thicker layers of CuO existing in the powder with the higher CuO concentration makes the diffusion more difficult, and as a consequence, requires higher temperatures for the reaction.

6.5 Summary

The reactions between CuO and Cu-Al with three nominal compositions, (Cu-6at%Al)-8mole%CuO, (Cu-14at%Al)-17mole%CuO, (Cu-37at%Al)-36mole%CuO, were studied. A Cu-Al/CuO composite powder structure was established and refined through high energy milling. The reaction between CuO and Cu-Al proceeded in two separate steps: Reaction 1, the reaction between CuO and Cu-Al forming Cu_2O and Reaction 2, the reaction between Cu_2O and Cu-Al forming Al_2O_3 and pure Cu. The Reaction 1 is easier to occur than Reaction 2. The high energy milling enhanced the kinetics of both reactions by increasing the interface area and reducing the length of diffusion pathway. Finally the processing of Cu/Al_2O_3 nanocomposite materials was demonstrated by pressing and sintering the 16 hours milled D1 and D2 powders.

6.6 References

1 D.L. Zhang and J.J. Richmond, *J. Mater. Sci.*, 1999, **34**, 701.

2 J.M. Wu and Z.Z. Li, *J. Alloys & Comp.*, 2000, **299(1-2)**, 9.

3 P. Schumacher, M.H. Enayati and B. Cantor, Mater. Sci. Forum, 1999, **312-314**, 351.

4 T.D. Shen, K.Y. Wang, J.T. Wang and M.X. Quan, *Mater. Sci. Eng.*, 1992, **A151**, 189.

Chapter Seven

General Discussions

7.1 Introduction

Further to the results presented in the previous chapters, in this chapter, some general issues will be discussed. These issues include: the effect of high energy milling on initial reaction temperature, the relationship between reaction temperature and phase formation, and the correlation between mechanical alloying and thermally activated solid state reactions.

7.2 Effect of High Energy Milling on the Reaction Temperatures

The results presented in the previous chapters have demonstrated (1) that mechanical milling of powder mixtures produce refined composite powder particle microstructures; (2) The fine composite powders react at substantially lower temperatures (T_c, reaction initiation temperature) than powders that were mixed but not milled. This is summarised in Table 0-1, which lists reaction temperatures and products of the high energy milled powders from this work and from literature including results of experiments with multilayer thin films for comparison. There is a strong correlation between T_c and the change of powder particle microstructure. This can be explained by the following mechanisms.[1]

The first mechanism is the establishment of intimate and contaminant free contact between the reactant phases. In the initial stage of milling, one reactant is incorporated into the other and the incorporated particle is not severely deformed. Therefore, the thin layer of oxide coated on the outside surface of the metal particle is not fully broken. As a consequence, a higher temperature is required to facilitate the diffusion through the interface and drive the reaction. With further

milling, metal particles such as Ni particles, are heavily deformed and fractured together with the other metallic phase. This plastic deformation and fracturing produces a large area of contaminant free interface. It is not too difficult to imagine that it is easier for the reactant phases to diffuse across these interfaces. The effect of this factor is reflected by the substantial decrease of T_c.

The second mechanism which contributes to the decrease of T_c is the significant increase of the total area of reactant interfaces. With establishment of composite structure, be it the multilayered structure or oxide particles embedded in metal matrix structure, the interface area is many times larger. As suggested by Bormann[2] and Zhang *et al.*[1], nucleation of a new phase during the solid state reaction between two phases often occurs heterogeneously at the interfaces between the two phases.

The effect of the increase in area can be estimated by classical heterogeneous nucleation theory, the nucleation rate, I, can be calculated using the following equation:

$$I = NS\frac{kT}{h}\exp\left(-\frac{\Delta G^* + \Delta G_a}{kT}\right) \tag{7-1}$$

The free energy barrier of nucleation, ΔG^*, is determined by the following equation:

$$\Delta G^* = \frac{16\pi\sigma_{\alpha\gamma}^3}{3(\Delta G_v - \Delta G_\varepsilon + \Delta G_d)^2} f(\theta) \tag{7-2}$$

The critical reaction temperature, T_c, is determined by the temperature at which the nucleation rate is sufficiently high that the reaction can be observed within a practical time frame. This nucleation rate is taken as I_c. Accordingly, Equation (7-1) can be re-written as:

$$\frac{1}{T_c} - \frac{k}{\Delta G^* + \Delta G_a}\ln(kT_c) = \frac{k}{\Delta G^* + \Delta G_a}\left(\ln(NS) + \ln\left(\frac{1}{hI_c}\right)\right) \tag{7-3}$$

I_c is dependent on the technique used to detect the start of solid state reaction. For a given technique such as continuous heating in a DSC or DTA, I_c is very much a

constant. The second term at the left hand side of the equation is one and two orders smaller in value compared with the first term at the left hand side. Therefore, Equation (7-3) can be simplified to the following equation:

$$\frac{1}{T_c} = \frac{k}{\Delta G^* + \Delta G_a}\left(\ln(NS) + \ln\left(\frac{1}{hI_c}\right)\right) \qquad (7\text{-}4)$$

Therefore, Equation (7-4) shows that T_c decreases with increasing total area of the interfaces and the potential nucleation sites per unit volume of the powder particles. This is in agreement with the observation that T_c decreases substantially as the composite structure is established and further refined.

The third mechanism which contributes to the decrease of T_c is the fact that plastic deformation and fracturing during milling cause a significant increase of dislocations, vacancies and the total area of grain boundaries. This enhances the diffusivity of reactants, and thus reduces ΔG_a. From Equation (7-4), it is clear that the decrease of the value of ΔG_a also leads to a decrease of T_c.

7.3 Reaction Temperature and Phase Formation

The present work shows a correlation between the reaction temperature and the phase formed. When Cu/Al reaction occurs at high temperatures (>450°C), Cu(Al) solid solution formed in the Cu-14at%Al powder and Cu_9Al_4 formed in the Cu-37at%Al powder. The phases formed are very close to the stoichiometric equilibrium phases. While at low temperatures, the phases formed are more likely controlled by the kinetics of the reaction. Cu_9Al_4 and $CuAl_2$ were the first phase observed during heating the high energy ball milled Cu-14at%Al and Cu-37at%Al powders respectively. Similar results were shown in the Cu-Al/CuO system and the Al/TiO_2 system. At high temperatures, Cu-Al_2O_3 and Ti_3Al-Al_2O_3 phases formed, while at low temperatures, Cu_2O and Al_3Ti formed.

Similar observations have also been made by Zhang and Ying[1], and Klassen *et al.*[3] in the Al/Ti system. At high temperatures (>500°C), tetragonal Al_3Ti with DO_{22} ordering forms directly from the reaction, while when the reaction occurs at low temperatures (<400°C), Al(Ti) solid solution with partial $L1_2$ ordering forms.

The crystal structures of $L1_2$ and DO_{22} are illustrated in Figure 7-1. With further decrease in reaction temperature, the solid solution formed may be fully disordered. This is due to the similarity in the crystal structure of partially ordered $L1_2$ Al_3Ti and that of fcc Al phase, the nucleation barrier, ΔG^*, of this metastable phase may be substantially lower than that of the equilibrium tetragonal Al_3Ti with DO_{22} ordering, even though the latter has a large ΔG_v.[1] It is also true in the case of Cu-Al system, the activation energy for the formation of $CuAl_2$ is 0.54 eV while that for the Al(Cu) solid solution is 1.37 eV.[4] Therefore, at a given temperature, the nucleation rate of the partially ordered $L1_2$ Al_3Ti in the Al/Ti system and of the $CuAl_2$ in the Cu/Al system is likely to be higher than that of DO_{22} Al_3Ti and Al(Cu) solid solution respectively.

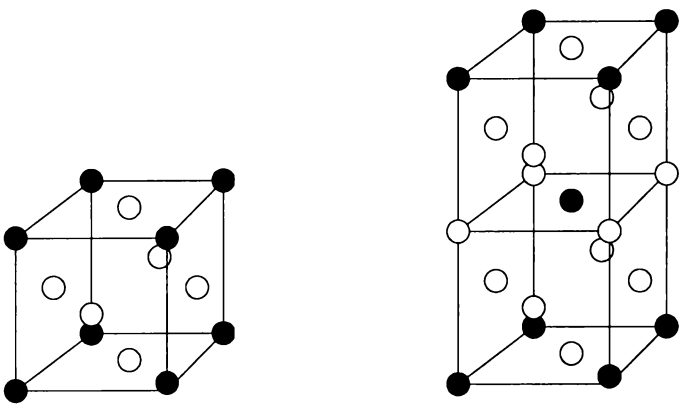

(a) $L1_2$ (b) DO_{22}

Figure 7-1. Unit cell of (a) $L1_2$ crystal structure and (b) DO_{22} crystal structure. (•) Ti, (o) Al

With a small interface area per unit volume of Al/Ti or Al/Cu powder particles, the amount of new phase formed after nucleation might be too small to be detected. The new phase has to grow. When the powder is milled for short time and before the multilayer composite structure is formed, the diffusivity is not significantly enhanced. This means that the powder has to be heated to a high temperature to activate the growth process. However, at high temperatures, the kinetic constrains on nucleation of the equilibrium DO_{22} Al_3Ti phase in the Al/Ti system and on the formation of Al(Cu) solid solution in Al/Cu system is relaxed, and thus the larger thermodynamic driving force for its formation starts to play a dominant role. Once this is the case, formation of DO_{22} Al_3Ti or the Al(Cu) solid

solution can effectively compete with formation of the metastable phase, and become the only observable outcome of the reaction between Al and Ti or between Al and Cu.

When the area of Al/Ti or Al/Cu interfaces is very large, the amount of the partially ordered $L1_2$ Al_3Ti or the $CuAl_2$ formed after the nucleation process may be quite large. While, the activation energy for diffusion of Al, Ti and Cu is reduced to a sufficiently low level for reaction. The metastable phase can also grow to a limited scale at low temperatures without being transformed into equilibrium phase.[5,6] In this case the formation of partially ordered $L1_2$ Al_3Ti or $CuAl_2$ would become observable outcome of the reaction between Al and Ti or between Al and Cu.

As the composite structure is further refined, the much enhanced diffusivity of Al and Ti and enlarged interfacial area may allow all the powder to be converted to the metastable partially ordered $L1_2$ Al_3Ti at low temperatures without giving a chance for the formation of equilibrium DO_{22} Al_3Ti.

The same phenomenon appears in the metal/oxide systems studied in this thesis. At lower temperatures, Al_3Ti and Cu_2O were the major phases formed in the Al/TiO_2 and Cu-Al/CuO powders respectively. While at higher temperatures, Ti_3Al-Al_2O_3 phases and Cu-Al_2O_3 phases formed respectively.

7.4 Mechanical Alloying and Thermally Activated Solid State Reactions

The present study shows that heat treatment of high energy mechanically milled powder with fine Al/Cu and Al/Ni multilayer composite structure and with fine Al/TiO_2 and Cu-Al/CuO composite structure produces a series of metastable or stable phases. Some of these phases are quite similar to those produced after prolonged milling. This strongly suggests that mechanical alloying is achieved through two steps.[1] In the first step, a composite structure is formed in each of the powder particles and diffusivity is enhanced through plastic deformation, fracturing and welding. In the second step, the composite structure is sufficiently refined and the diffusivity is sufficiently enhanced, such that the critical

temperature required to activate the solid state reactions between two phases is lowered to a level that can be achieved through mechanical impacts. It has been proven that the mechanical impact can cause the temperature of the trapped powder to increase by up to 300°C.[7,8] This means that the critical temperature needs to be lowered to a level below 300°C through pre-milling. Each of the impacts only activates the reaction in a very small fraction of the powder particles, and the reaction is maintained for a very short time (a few milliseconds[9]). This makes it necessary to accumulate millions of impacts in order to bring the reaction to completion. This accumulation can only be achieved by dramatically extending the milling process. The present work demonstrates that this extension could be replaced by heat treating the milled powder at a suitable point of milling. In this way, the same product can be attained, but with a much shorter processing time as well as a lower cost. This certainly has important technological implications.

This phenomenon has also been shown in the formation of amorphous phase in Fe/Nb,[10] in that amorphous Fe/Nb alloy was obtained both by prolonged MM and low temperature heat treating the briefly milled powders. The same phenomenon has been shown in some binary systems such as Ni-Ti[11], Al-TM (TM: Ti, Zr, Hf, Nb and Ta)[12, 13, 14, 15, 16]. This process takes place in the same manner as the solid state amorphization in metallic multilayer thin films.[17, 18]

It is true that prolonged high energy mechanical milling can not only change solid state reaction kinetics but can also change thermodynamics of the system.[19] Many examples are available showing that thermodynamically impossible reactions were realised through high energy ball milling.[20] This is due to the introduction of the excess Gibbs free energy by creating large grain boundary areas making certain reactions thermodynamically favourable. Even so, the prolonged mechanical milling process can still be substantially reduced by combining the heat treatment with briefer milling as indicated by Shen *et al.*[19] in the reactions of Fe and SiC. Low temperature (310°C) heat treatment of the 16, 24 and 40 hours milled Fe/SiC powder mixture could obtain Fe_3C phases, the same as those obtained by prolonged milling for 60 and 100 hours.

High energy mechanical milling has its limitation.[21,22] It can eliminate the diffusion barrier by creating large contact area and enhancing the diffusivity, but it

is unlikely for it to alter the chemical reactivity. The reaction temperature of Al/TiO_2 system can be substantially reduced from around 1000°C for the unmilled powder mixture to 650°C for the extensively milled powder. Further milling does not seem to be able to reduce the reaction temperature further. No reactions occurred after prolonged milling (up to 100 hours), although this reaction is thermodynamically favourable. This is quite likely due to the insufficient temperature rise. It was reported that the maximum temperature rise induced by the ball powder impact is 300°C in the high energy ball mill.[7] However, some local reaction spots had been observed in the as milled Al/TiO_2 powder particles produced using a Split Discus mill on which the bowl temperature was up to 200°C. Therefore, the powder temperature at the point of impact could well be over the temperature required for local reactions. A very similar observation has been reported by Yang and McCormick[22] in the study of mechanically activated reduction of nickel oxide with graphite. Although the milling significantly reduced the reaction temperature from 1077°C to 377°C for the 12 hours milled powder, no reduction of nickel oxide to nickel has been observed during ambient temperature milling. The temperature increase was insufficient to drive the reaction even though this reaction is thermodynamically favourable. However, the reaction did occur when milling at the elevated temperatures of 250°C and 350°C.

Overall, it is very likely that the mechanical alloying process is a unique process for establishing a composite microstructure of the powder particles by repeated deformation, fracturing and cold welding. However the true alloying is achieved by the impact induced low temperature thermally activated reaction. Therefore, the prolonged mechanical alloying process could be replaced by a substantially shorter milling to establish the composite powder particle microstructure and raise the internal energy if required followed by a wisely controlled thermal treatment.

7.5 Summary

High energy mechanical milling can substantially reduce solid state reaction temperatures by bringing the reactants into intimate contact, establishing large interfacial area through the formation of composite microstructures of the powder particles and reducing the activation energy for nucleation and diffusion. The low

temperature solid state reaction is favourable to the formation of metastable phases. Prolonged mechanical alloying process can be replaced by a short duration milling used to establish composite microstructure of powder particles, plus a well controlled heat treatment, leading to the formation of the same outcome.

Table 7-1. Reaction temperatures and products of high energy milled powders and multilayer thin films

Reactants	Method	Milling Time	Thickness	T_{on}	T_p	Activation Energy	Reaction Product	Ref
		[hours]	[nm]	[°C]	[°C]	kJ/mol		
$Al_{75}Ni_{25}$	MM+HT	0.5h		650	671		Al_3Ni	
$Al_{75}Ni_{25}$	MM+HT	2h		650	697		Al_3Ni	
$Al_{75}Ni_{25}$	MM+HT	4h		230	265		Al_3Ni	
$Al_{75}Ni_{25}$	MM+HT	8h		206	258		Al_3Ni	
$Al_{75}Ni_{25}$	MM+HT	15h		194	218		Al_3Ni	
$Al_{75}Ni_{25}$	MM+HT	20h		185	215		Al_3Ni	
$Al_{75}Ni_{25}$	MM+HT	25h		185	210		Al_3Ni	
$Al_{75}Ni_{25}$	MM+HT	30h		-	-		Al_3Ni	
$Cu_{85}Al_{15}$	MM+HT	2h	50-200	125	150		Cu_9Al_4	
$Cu_{63}Al_{37}$	MM+HT	2h	50-200	105	150		$CuAl_2$	
Al/TiO2	MM+HT	1h		820	880		Al_3Ti	
Al/TiO2	MM+HT	8h		650	680		Al_3Ti	
Cu-Al/CuO	MM+HT	1h		150	250		Cu_2O	
Cu-Al/CuO	MM+HT	1h		100	25		Cu_2O	
$Al_{75}Ti_{25}$	TFlm			400 ~450			$L1_2$ ->DO_{22}	3
$Al_{75}Ti_{25}$	MM+HT			410			$L1_2$ ->DO_{22}	3
$Al_{75}Ti_{25}$	MM+HT		30,000	605	695		Al_3Ti (DO_{22})	1
$Al_{75}Ti_{25}$	MM+HT		20,000	560	660		Al_3Ti (DO_{22})	1
$Al_{75}Ti_{25}$	MM+HT		300	267	350		Al(Ti)SS Partial $L1_2$ Ordering	1
$Al_{75}Ti_{25}$	MM+HT		<200	150	-		Al(Ti)SS	1
CuO+Si	MM		C/R low				Cu2O	23
CuO+Si	MM		C/R high				Cu	23
CuO+C	MM						Cu_2O	24
Cu_2+C	MM						Cu	24
$Al_{75}Ni_{25}$	Ion-beam		11.4	150	250		Al_3Ni	25
$Al_{75}Ni_{25}$	Ion-beam		110	240			Al_9Ni_2	25
				290			Al_3Ni	25
				320			Al_3Ni	25
$Al_{40}Ni_{60}$	Ion-beam		10	100	175		NiAl	25
			80	210	230		Al_9Ni_2	25
				270	300		Al_9Ni_2	25

				310	375		Al_3Ni_2	25
			400	300	325		Al_9Ni_2 Al_3Ni	25
				320	350		Al_3Ni	25
$Al_{75}Ni_{25}$	TFlm		10	200	210		Al_3Ni	26
	TFlm		15	205	220		Al_3Ni	26
	TFlm		50	225	250		Al_3Ni	26
	TFlm		75	230	252		Al_3Ni	26
	TFlm		150	250	260		Al_3Ni	26
Al-Cu	MM+HT			200	270	0.54	Al_2Cu	27
Al_2Cu	MM+HT			300	400	1.37	Al(Cu)SS	27
$Cu_{67}Al_{33}$	MM	100h					I-43M	28
$Al_{75}Fe_{25}$	MM	Long Time					Al_5Cu_2	29
	MM+HT				400		Al_5Cu_2	29
$Al_{80}Fe_{20}$	MM						n 1~2nm	29
	MM+HT				430		Al_5Cu_2	29
	MM+HT				700		Al_3Cu	29
CuO+Fe	Compact				350		Cu_2O, Fe_3O_4	30
	MM				200		Cu_2O, Fe_3O_4	30
ZnO+Mg	MM				367		Zn+MgO	31
Ni-48~88at% Al	Sputtering		10, 20	87		0.8	B2 NiAl	32
					227		$NiAl_3$	32
Fe+SiC	MM	60h, 100h					Fe_3C+ Fe(Si)	19
	MM+HT	16h- 40h			310		Fe_3C+ Fe(Si)	19
	MM+HT	16h- 40h		750	800		Fe_3Si, Fe_2Si	19
Fe_{52}-Nb_{48}	MM	24-40h					Amorph.	33
	MM+HT	5-18h		270	452		Amorph.	33

7.6 References

1 D.L. Zhang and D.Y. Ying, *Mater. Sci. Eng.*, in press.

2 R. Bormann, *in Mater. Res. Soc. Symp. Proc.*, 1994, **344**, 169.

3 T. Klassen, M. Qehring and R. Bormann, *J. Mater. Res.*, 1994, **6(1)**,

4 M.A. Marcus and J.E. Bower, *J. App. Phys.*, 1997, **82(8)**, 3821.

5 W.J. Meng, C.W. Nieh and W.L. Johnson, *Appl. Phys. Lett.*, 1987, **51**, 1693.

6 W. Johnson, *Prog. Mater. Sci.*, 1986, **30**, 81.

7 R.M. Davis, B. McDermott and C.C. Koch, *Metall. Trans. A*, 1988, **19A**, 2867.

8 D.L. Zhang, T.B. Massalski, and M.R. Paruchuri, *Met. Trans. A*, 1994, **25A**, 73.

9 H. Huang, M.P. Dallimore, J.Pan and P.G. McCormick, *Mater. Sci. Eng. A*, 1998, **A241**, 38.

10 M.S. El-Eskandarany, A.A. Bahgat, N.S. Gomaa, N.A. Eissa, *J. Alloys & Comp.*, 1999, **290(1-2)**, 181.

11 R.B. Schwarz, R.R. Petrich, J. Less-Comm., *Met.*, 1988, **140**, 171.

12 M. Sherif El-Eskandarany, *J. Alloys Comp.*, 1996, **234**, 67.

13 M. Sherif El-Eskandarany, K. Aoki, K. Suzuki, *Appl. Phys. Lett.*, 1992, 60, 1562.

14 M. Sherif El-Eskandarany, *J. Alloys Comp.*,1999, **284**, 295.

15 M. Sherif El-Eskandarany, K. Aoki, K. Suzuki, *Scri. Metall.*, 1991, **25**, 1695.

16 M. Sherif El-Eskandarany, K. Aoki, K. Suzuki, *J. Appl. Phys.*, 1992, **71**, 2924.

17 M. Van Rossum, M.-A. Nicolet, W.L. Johnson, *Phys. Rev.*, 1984, **29B**, 5498.

18 E.J. Cotts, G.C. Wong, W.L. Johnson, *Phys. Rev.*, 1988, **37B**, 9049.

19 T.D. Shen, C.C. Koch, K.Y. Wang, M.X. Quan, J.T. Wang, *J. Mater. Sci.*, 1997, **32(14)**, 3835.

20 E. Ma, M. Atzmon and F. Pinkerton, *J. appl. Phys.*, 1993, **74**, 955.

21 N.J. Welham, Mater. Sci. & Eng., 1998, **A255**, 81.

22 H. Yang, P.G. Mccormick, *Metall. & Mater. Trans. B*, 1998, 29(2), 449.

23 S.Q. Xi, J.E. Zhou, X.T. Wang and D.W. Zhang, J. Mater. Sci. Lett., 1996, **15**, 634.

24 H. Yang, G. Nhuyen and P.G. McCormick, Scr. Metall. Mater., 1995, 32(5), 681.

25 A.S. Edelstein, R.K. Everett, G.Y. Richardson, S.B. Qadri, E.I. Altman, J.C. Foley and J.H. Perepezko, *J. Appl. Phys.*, 1994, **76(12)**, 7850.

26 E. Ma, C.V. Thompson and L.A. Clevenger, *J. Appl. Phys.*, 1991, **69 (4)**, 2211.

27 M.A. Marcus, J.E. Bower, *J. Appl. Phys.*, 1997, 82(8), 3821.

28 J.C. de Lima, D.M. Triches, V.H.F. dos Santos and T.A. Grandi, *J. Alloys & Comp.*, 1999, **282(1-2)**, 258.

29 F.Cardellini, V. Contini, R. Gupta, G. Mazzone, A. Montone, A. Perin and G. Principi, *J. Mater. Sci.*, 1998, **33**, 2519.

30 T.D. Shen, K.Y. Wang, J.T. Wang and M.X. Quan, Mater. Sci. Eng., 1992, **A151**, 189.

31 Yang, H. and P.G. McCormick, J. Solid State Chem., 1993, **107**, 258.

32 C. Michaelsen, G. Lucadamo and K. Barmak, *J. Appl. Phys.*, 1996, **80(12)**, 6689.

33 M.S. El-Eskandarany, A.A. Bahgat, N.S. Gomaa and N.A. Eissa, J. Alloys & Comp., 1999, **290(1-2)**, 181.

Chapter Eight

Conclusions and Recommendations

8.1 Conclusions

- High energy mechanical milling enhances solid state reactions in Ni-Al powders by establishing and refining multilayer composite powder particle microstructure. With the refinement of the Ni/Al composite structure, the interface area increases causing the reaction temperature to decrease from above the Al melting temperature, 660°C, to about 200°C.

- It is confirmed that the reaction of ni and Al proceeds in two steps during heating the mechanically milled powders in the same way as Ni/Al multilayer thin films. The first step is nucleation and lateral growth of Al_3Ni phase along the Ni/Al interface. The second step is the transverse growth of Al_3Ni perpendicular to the interface. With the composite structure being refined, i.e. the interfacial reaction increases, the fraction of the interfacial reaction increases until it is complete.

- In the Cu-Al system, heating the milled Cu/Al powder results in the formation of Cu(Al) solid solution or Cu_9Al_4 intermetallic compound depending on the composition of the starting powder mixture. The reaction products obtained from the short time milling plus heat treatment are the same as those obtained from prolonged mechanical alloying.

- The phase formation sequence during heating the short time milled Cu/Al powders varies from compositions. For Cu-14at%Al powder, γ-Cu_9Al_4 forms first and the γ-Cu_9Al_4 then dissolves into Cu forming Cu(Al) solid solution at higher temperatures; while for Cu-37at%Al powder, θ-$CuAl_2$

forms first and the θ-$CuAl_2$ then reacted with Cu forming γ-Cu_9Al_4 at higher temperatures.

- It was found that in the Al-TiO_2 system, no reaction occurred during high energy mechanical milling. The intensity of the reaction during heating of the mechanically milled powders is to a large extent affected by the microstructures of the powder particles. However, the first phase formed is always Al_3Ti irrespective to the composition of the powder mixture.

- Formation of α-Al_2O_3 phase was controlled by temperature and time. α-Al_2O_3 could form only above 900°C during heating with a constant rate of 20°C/min. However, α-Al_2O_3 phase could also form by heating the powder to 800°C and then holding the temperature constant for 0.5 hours.

- With a high TiO_2/Al mole ratio, the reactions proceed in two steps: Al_3Ti forms first and quickly, then α-Ti(Al, O) phase forms gradually after the powder is heated to a sufficiently high temperature up to 1200°C. The formation α-Ti(Al, O) phase was controlled by the reaction kinetics. It could be formed either by heating the powder to 1200°C at a constant rate of 20°C/min or by heating to a temperature above 800°C and then holding at this temperature for a substantial amount of time.

- The reaction between Cu-Al and CuO proceeded in two steps. The first step is the reaction between Cu-Al and CuO forming Cu_2O, and the second step is the reaction between Cu_2O and Cu-Al forming Cu and Al_2O_3.

- Massive combustive reactions can be suppressed by embedding Al in Cu forming Cu(Al) solid solution. Cu/Al_2O_3 metal matrix nanocomposite materials were produced by consolidation of the composite powders.

- Classical heterogeneous nucleation theory and one-dimensional bulk diffusion with proper treatment of layer thickness variation can be employed to simulate the nucleation at interfaces and in the bulk during heating of high energy mechanically milled powders with a composite powder particle structures.

- The interface area, grain size, activation energy for nucleation and the activation energy for diffusion, are the major parameters affecting the reaction behaviours in the high energy mechanically milled powders during heating. High energy mechanical milling enhances the solid state reactions by increasing the interfacial area, refining grain size and reducing the activation energies for nucleation and diffusion.

- Prolonged mechanical alloying can be replaced by brief milling to establish a composite powder particle microstructure, plus a well controlled heat treatment.

- Overall, it is established that refining the composite structure of powders consisting of reactants is a very effective way of enhancing the reaction kinetics for both metal-metal and metal-oxide systems. Also for both types of systems, the first phase formed at the interface is determined by which phase is easy to nucleate.

8.2 Recommendations for Future Work

- Apply nuclear magnetic resonance (NMR) spectroscopy in combination with TEM to investigate the evolution of the Al_2O_3 phase.

- Extend the kinetic model to the dynamic milling process by incorporating heat transfer equations into the kinetic model to simulate each individual collision events and the accumulation during the milling process.

- Apply the kinetic model to phase selection criteria by systematically analysing the influence of each individual parameter in the model.

- Apply the kinetic model to the systems with positive heat of mixing to check that whether the reaction could only be able to be realised if there is no requirement of growth (only nucleation).

- Apply the kinetic model to TiO_2/Al and CuO/Cu-Al system.

- Attempt low temperature phase diagram Ti-O-Al by using high energy milling to prepare the sample to reduce the diffusion distance.

Appendix A Publications and Award

Journal Publications:

1. D.Y. Ying and D.L. Zhang, "The Impact of Microstructures on the Reaction Kinetics of High Energy Ball Milled Powders." *Journal of Metastable and Nanocrystalline Materials*, Vol.10 (2001) 211-216.
2. D.L. Zhang and D.Y. Ying, "The role of Nucleation in Solid State Reactions during Mechanical Alloying and Heat Treatment of High Energy Mechanically Milled Powders." *Journal of Metastable and Nanocrystalline Materials*, Vol.10 (2001) 323-328.
3. D.L. Zhang and D.Y. Ying, "Solid State Reactions in Nanometer Scaled Diffusion Couples Prepared Using High Energy Ball Milling," *Materials Science and Engineering*, A301 (2001) 90-96.
4. D.Y. Ying and D.L. Zhang, "Solid-state Reactions between Cu and Al during Mechanical Alloying and Heat Treatment." *Journal of Alloys and Compounds*, 311 (2000) 275-282.
5. D.Y. Ying and D.L. Zhang, "Processing of Cu/Al_2O_3 Metal Matrix Nanocomposite Materials by Using High Energy Ball Milling." *Materials Science and Engineering*, A286 (2000) 152-156.
6. D.Y. Ying and D.L. Zhang, "Effect of High Energy Ball Milling on the Solid State Reactions in Al-25at%Ni Powders." *Materials Science and Technology*, in press.

Conference Proceedings:

7. D.Y. Ying and D.L. Zhang, "Modelling of Solid State Reactions in High Energy Ball Milled Powders." In Proc. of *1st International Conference on Advanced Materials Processing*, Nov. 2000, New Zealand.

8. D.L. Zhang and D.Y. Ying, "Solid State Reaction during Heating Mechanically Milled Al-Ti Powders," In Proc. of *1st International Conference on Advanced Materials Processing*, Nov. 2000, New Zealand.

9. D.Y Ying. and D.L. Zhang, "Solid State Reactions between Al and Ni in High Energy Ball Milled Powders." In Proc. of the 6th Annual New Zealand Engineering and Technology Postgraduate Conference, Dec. 1999, Auckland, New Zealand.

10. D.Y. Ying, D.L. Zhang and A.G. Langdon, "Phase Formation During Mechanical Alloying and Heat Treatment of Cu/Al/CuO Powders." In Proc. of 1st New Zealand Korea Seminar on Engineering Materials, Feb. 1999, Hamilton, New Zealand.

11. D.L. Zhang, D.Y. Ying and J.R. Richmond, "Processing of Metal Matrix Nanocomposite Materials by Using a Combination of High Energy Ball Milling and Heat Treatment." in Proc. of 1st New Zealand Korea Seminar on Engineering Materials, Feb. 1999, Hamilton, New Zealand.

12. D.Y. Ying and D.L. Zhang, "Cu/Al_2O_3 Metal Matrix Nanocomposites Produced by High Energy Ball Milling." in Proc. of 5th New Zealand Technology and Engineering Graduate Conference, Nov. 1998, Palmerston North, New Zealand.

13. D.L. Zhang, J.J. Richmond and D.Y. Ying, "High Energy Ball Milling of Copper Oxide and Aluminium Powder Mixtures." in Proc. of "Materials 98", Institute of Materials Engineering, Australia, Jul. 1998, Wollongong.

Award:

Shared Best Paper Award at 6^{th} Annual New Zealand Engineering and Technology Postgraduate Conference, Dec. 1999, Auckland, New Zealand.